EXPERIMENTAL STUDY OF THE IMPACT OF PORT AND DIRECT FUEL INJECTION STRATEGIES ON THE EFFICIENCY, PERFORMANCE AND EMISSIONS OF A DOWNSIZED GDI ENGINE

A thesis submitted for the degree of
Doctor of Philosophy

by

Reza Golzari

Department of Mechanical and, Aerospace Engineering
College of Engineering, Design and Physical Sciences
Brunel University London
United Kingdom

November 2018

Abstract

In recent years after the introduction of gasoline direct injection (GDI) engines, gasoline engine downsizing has been widely adopted to reduce fleet CO_2 emissions of passenger cars. These engines are typically boosted direct injection gasoline engines equipped with variable valve timing systems for both intake and exhaust valves. Fuel consumption reduction in these downsized engines is achieved by operating more at higher brake mean effective pressure (BMEP) area of the engine map in order to reduce pumping losses and through reducing cylinder numbers to decrease total friction losses. However, the degree of downsizing and compression ratio (CR) of these engines are constrained by thermal stresses and knocking combustion as well as the low speed pre-ignition phenomena. In addition, combustion efficiency and emissions in these GDI engines can be improved further by better in-cylinder mixture preparation (in terms of homogeneity and temperature). To overcome these limitations, technologies such as dual injection systems, cooled external exhaust gas recalculation (EGR), Atkinson and Miller cycle, variable compression ratio (VCR) and water injection have been found to be highly effective in improving the combustion processes and reducing pollutant emissions.

The present work investigates the impact of port and in-cylinder fuel injection strategies as well as intake port injection of water on boosted downsized GDI engine combustion, efficiency and emissions. A single cylinder direct injection gasoline engine and its testing facilities were used for extensive engine experiments. Various PFI / DI injection strategies were tested, and the results compared to the baseline PFI only and DI only strategies. Intake port injection of

water also was investigated at different water/fuel ratios and with gasoline with three different research octane numbers (RON). The experiments were performed at several steady state points to determine the optimal strategy for improved engine fuel economy in real applications.

The results show that PFI / late DI and early DI / late DI strategies can reduce the net indicated specific fuel consumption (NISFC) significantly by a maximum of 9% at low speed / mid-high load compared to the baseline due to the reduction of end of compression temperature and therefore advancement in knock limited spark timing. Smoke emissions were also lower under PFI / late DI, PFI / early DI, and PFI only operations compared to early DI / late DI, and DI only operations due to the improvement in mixture preparation. In addition, the results showed that PFI / late DI and early DI / late DI extend the lean limit from 1.5 to 1.7 at 1000 rpm / 8.83 bar net indicated mean effective pressure (NIMEP) due to a more advanced combustion phasing and shorter combustion duration compared to the baseline PFI only and DI only operations.

Water injection results show net indicated efficiency improved significantly by a maximum of around 5% at medium load and around 15% at high load when increasing the injected water mass. Improvement in efficiency was mainly due to the increased heat capacity of charge (higher specific heats of water and increased in-cylinder mass) and the cooling effect of the injected water evaporation which reduced the in-cylinder pressure and temperature. Thus, knock sensitivity was reduced and more advance spark timings could be used which shifted the combustion phasing closer to the optimum point. However, increasing the water ratio further (more than 1 at medium load and more than 1.5 at high load) deteriorated the combustion efficiency, prolonged the flame development angle

and combustion duration, and caused a reduction in the net integrated area of the P-V diagram. Comparison of fuels of different RON also reveals that water injection can virtually increase the RON of fuel, therefore makes it possible to run on a low octane number fuel and achieve higher efficiency by adjusting the water mass. In terms of other, harmful, non-CO_2 emissions, water injection was effective in reducing the NO_x (by a maximum of around 60%) and particle emissions significantly but increased the HC emissions as the water/fuel ratio increased. In addition, water injection also reduced the exhaust gas temperature by around 80 °C and 180 °C at medium and high loads, respectively.

Acknowledgment

I would firstly like to express my thanks and upmost respect to my supervisor, Professor Hua Zhao, for giving me the vital guidance and support in the last four years and the opportunity to work in one of the most renowned engine research groups in the UK (Centre for Advanced Powertrain and Fuels Research).

I am deeply grateful to the assistance and technical support of the technicians Andy Selway and Eamon Wyse. Their commitment and perfectionism were simply exceptional.

I would like to extend my special thanks to Justin Mape, Tony Cains, Jonathan Hall and Dr Mike Basset from Mahle Powertrain, and Dr John Williams from BP Technology Centre for giving me advice and support on many occasions.

To all my friends and colleagues, you not only helped me in my studies but were also valuable companies and a source of motivation.

Finally, and perhaps the most important, is the love and support of my family and my girlfriend which greatly helped me and kept me motivated during my PhD and all the years of my education. Without this support, I could not have coped, I owe you so much.

Nomenclature

Abbreviations

ABDC	After Bottom Dead Centre
AFR	Air Fuel Ratio
APV	Alternatively-Powered Vehicles
ATDC	After Top Dead Centre
BBDC	Before Bottom Dead Centre
BDC	Bottom Dead Centre
BLD	Borderline Detonation
BMEP	Brake Mean Effective Pressure
BSFC	Brake Specific Fuel Consumption
BTDC	Before Top Dead Centre
BTDCF	Before Top Dead Centre Firing
BTDCNF	Before Top Dead Centre Non-firing
CA	Crank Angle
CA10	Crank Angle at 10% Mass Fraction of Mixture Burned
CA50	Crank Angle at 50% Mass Fraction of Mixture Burned
CA90	Crank Angle at 90% Mass Fraction of Mixture Burned
CAD	Crank Angle Degrees
CAFE	Corporate Average Fuel Economy
CAI	Controlled Autoignition
CFD	Computational Fluid Dynamics
CI	Compression Ignition

COV	Coefficient of Variation
CR	Compression Ratio
DAQ	Data Acquisition
DI	Direct Injection
eBoost	Electrical Boosting
ECU	Electronic Control Unit
ECV	Electrically-Chargeable Vehicles
EGR	Exhaust Gas Recirculation
EMOP	Exhaust Maximum Opening Point
EMS	Engine Management System
EOI	End of Injection
EOI2	End of Second Injection
EPA	Environmental Protection Agency
EVC	Exhaust Valve Closing
FID	Flame Ionization Detector
GDI	Gasoline Direct Injection
GIMEP	Gross indicated Mean Effective Pressure
HCCI	Homogeneous Charge Compression Ignition
HEV	Hybrid Electric Vehicle
ICE	Internal Combustion Engine
IEffg	Gross Indicated Fuel Conversion Efficiency
IEffn	Net Indicated Fuel Conversion Efficiency
IEffp	Pumping Indicated Fuel Conversion Efficiency
IMEP	Indicated Mean Effective Pressure
IMOP	Intake Maximum Opening Point
ISFC	Indicated Specific Fuel Consumption

IVC	Intake Valve Closing
IVO	Intake Valve Opening
KI	Knock Intensity
LIVC	Late Intake Valve Closing
LIVO	Late Intake Valve Open
LSPI	Low Speed Pre-ignition
MBT	Minimum spark advance for Best Torque
MFB	Mass Fraction burn
NA	Naturally Aspirated
NEDC	New European Driving Cycle
NI	National Instruments
NIMEP	Net Indicated Mean Effective Pressure
NISFC	Net Indicated Specific Fuel Consumption
NO_x	Nitrogen Oxides
PFI	Port Fuel Injection
PID	Proportional Integral Derivative
PM	Particulate Matter
PMEP	Pumping Mean Effective Pressure
PN	Particulate Number
PRT	Platinum Resistance Thermometer
RON	Research Octane Number
rpm	revolutions per minute
SI	Spark Ignition
SOI	Start Of Injection
TDC	Top Dead Centre
UEGO	Universal Exhaust Gas Oxygen

ULG	Unleaded Gasoline
US	United States
VVA	Variable Valve Actuation
VVT	Variable Valve Timing
WOT	Wide Open Throttle

Symbols

M	Molecular weight
n	Polytropic exponent/specific heat ratio
RON	Research octane number
p	In-cylinder pressure, pressure
pf	Pressure feedback
pn	Predicted pressure
Δp	Change in pressure
ΔT	Temperature difference
V	Volume

Chemical Abbreviations

CO	Carbon Monoxide
CO_2	Carbon dioxide
H	Hydrogen atom
N	Nitrogen atom
N_2	Nitrogen
NO	Nitric oxide
NO_2	Nitrogen dioxide
O	Oxygen atom
O_2	Oxygen

THC	Total hydrocarbons

Contents

List of figures

List of tables

Chapter One

Introduction

Chapter 1 Introduction

1.1 Introduction

Invention of Internal combustion engine (ICE) represents an important breakthrough in the modern world due to its role in the development of mobility and power generation. The history of ICEs goes back to 1876 when Otto first developed the spark ignition (SI) engine followed by the invention of compression ignition (CI) engine by Diesel in 1892. Since then there has been a great deal of research and development on these engines as the issues such as environmental constraints, cost of fuel, increasing demand for more efficient and powerful engines and the competition in the market have become ever more important. ICEs, their manufacturers and related industries are now the main part of the propulsion, power and energy sector. The reciprocating ICEs provide a very high power-to-weight ratio compared to steam engines, this make ICEs suitable for various applications. These engines are by far the most common form of engine and prime mover of land and water vehicles today. Thus, regarded as a main enabler of globalisation [1].

Since the early years the main motivation for development and optimization of these engines was to improve the fuel consumption and increase the power output. Therefore, technologies such as boosting (supercharging and turbocharging), direct injection and water injection were developed to fulfil those requirements for power and fuel economy. Most of these technologies were first developed and used in aircraft engines during the war and then adapted to automotive applications [2]. For example, water injection which recently has attracted lots of attention in automotive industry, initially was used to increase the

power output of military aviation engines. This technology was used during World War II in military aircrafts with petrol piston engines purely to increase the power for short durations such as dogfights or take-off. Technologies like this are being reintroduced today not only to increase power but also to reduce fuel consumption and most importantly engine out exhaust emissions.

Significant increase in demand for ICE powered vehicles in the last century led to increasing concerns about the impact of exhaust emissions on the environment and human health. Therefore, the discussion about the adoption of a new system to control the exhaust emissions of ICEs began. United States introduced emissions standards for automobiles in the early 1960s after conducting extensive studies on different sources of air pollution which ultimately attributed a substantial part of air pollution to automobiles. Initially California Air Resources Board in California then United States Environmental Protection Agency (EPA) nationwide start to create and enforce emission regulations for automobiles in the US which then followed by Europe, Japan and Australia and for other engine applications as well. In the UK “Clean Air Act 1956” was introduced by parliament in order to reduce air pollution and photochemical smog [3].

In addition, the demand for fossil fuels also increased massively due to popularity of ICEs in automotive sector in global markets. This meant greater efficiencies are required from those engines to achieve significant reduction in fuel consumption. Concerns about fuel consumption, impact of carbon dioxide (CO_2) on the environment and the penalties applied for cars with higher CO_2 emissions than a certain quantity has led to an extensive research into more environmentally friendly and fuel efficiency engines.

As a result, emissions from spark ignition and diesel engines have been reduced significantly. Introduction of catalysts in the exhaust system of SI engines and the adoption of the unleaded gasoline due to the toxicity problem of the lead additives in leaded gasoline were the major changes to achieve the emission targets. The way IC engines are designed and operated today have changed considerably due to these emission control requirements and fuel consumption reduction.

Advanced and expensive technologies such as variable valve timing (VVT), direct injection of gasoline (GDI), variable valve lift (VVL), one stage and two stage boosting (turbocharging, supercharging and electrical boosting (eBoost)), external gas recirculation (EGR), variable compression ratio (VCR), dual injection systems and many other technologies are being used by manufacturers to increase efficiency and reduce exhaust emissions.

Greater degree of freedom in controlling the engine parameters can be achieved with these technologies. Parameters such as injection timing, duration and pressure, valve timing, duration and lift, intake pressure and EGR rate can be flexibly changed in order to optimise fuel consumption and reduce harmful emissions. Therefore, different engine concepts can be realised.

Engine downsizing is one of the main engine technologies that can provide both high fuel economy and low exhaust emissions. It has been adopted by many automotive manufacturers over the last decade due to its ability in CO_2 reduction and improved fuel economy.

Dual injection concepts have been investigated by industry and academia after the introduction of GDI engines and engine downsizing. With this system each cylinder is equipped with two injectors, one conventional port fuel injector and one direct

injector. Therefore, part of the fuel can be injected with PFI and the other part with DI. This can be beneficial as it can affect the mixture preparation in terms of both homogeneity and temperature. In addition, with dual injection systems, two different fuels or water can be introduced from each injector. There has been a great deal of research over the last decade about dual fuel engines. Gasoline/ethanol, diesel/ethanol, gasoline/diesel, gasoline/CNG are the most common fuels used in dual fuel engines. Recently, water injection in highly downsized turbocharged gasoline engines also has regained interest due to the higher chance of knocking combustion in these engines. In this case one injector can be utilised to inject water and the other can be used for gasoline delivery.

Boosting system is the crucial part of a downsized engine as the power output of the engine across the speed range heavily relies on the capabilities of the boosting system. Turbocharging is usually used in downsized engines to compensate for the decrease in displacement volume. In downsized engines, the turbocharger needs to provide enough boost pressure to accelerate adequately at low engine speeds without a large lag time. In addition, it must work well at high speeds as well to provide a high-power output without compromising reliability (turbocharger reliability in terms of turbine temperature and power limit, and shaft speed limit).

Downsized turbocharged engines usually operate with higher intake manifold pressure for an equivalent load point in comparison to a larger naturally aspirated engine. As a result, in-cylinder pressure and temperature are higher at the end of compression stroke which increases the chance of knocking combustion. This is more probable at low engine speeds as compression process is slower and the in-cylinder charge motion is weaker compare to the high engine speeds. This results in a relatively long combustion duration. The slower combustion increases the time

available for autoignition reactions to take place in the end gas region and ultimately increases the chance of knocking combustion.

Knock mitigation in downsized gasoline engines is being investigated by many researchers and techniques such as dual injection, water injection and split injection are effective methods which can be used for this purpose. With dual injection two different fuels or fuel and water can be delivered into the engine which gives the flexibility of using a high-octane fuel and a low-octane fuel or one type of fuel and water. In addition, the proportion of each can be also altered according to the operating point. This is highly effective in reducing knock sensitivity of the engine by using fuels with higher heat of vaporisation compared to conventional fuels. Therefore, the resulted cooling effect will be higher which reduces the end of compression pressure and temperature.

Moreover, in dual injection systems the DI injection can take place during the compression stroke which can also decrease the charge temperature at the end of compression stroke and reduces the chance of knocking combustion.

1.2 Research Objectives

The objective of this study is to investigate the impact of port and direct fuel injection strategies on a downsized GDI engine. In addition, the benefits of intake port injection of water are also assessed at medium and high loads and different engine speeds.

Dual injection was employed by means of an intake port and direct injection. Gasoline was injected from both injectors. Injection timing and duration of the direct injection were varied to improve the mixture preparation at each test point.

Water injection was also employed by injecting water through the PFI and varying the amount of water injected. In this case gasoline was injected directly into the cylinder. Gasoline with three different octane numbers were employed to investigate the impact of water injection on research octane number (RON) of gasoline. In addition, another objective of this work was to determine the impact of water injection on particle emissions.

1.3 Outline of Thesis

The literature review is presented in Chapter 2 and summarises all the relevant research work of gasoline engine downsizing, mixture preparation and knock suppression through dual injection, split injection and water injection strategies. In addition, a discussion about the current and future emission regulations is provided, including CO_2 and non-CO_2 emissions legislations. The latest technologies for internal combustion engines are also described.

In the third chapter, experimental facility and methodology used for this project are explained in detail. These include the engine and its condition systems, sensors and analysers. In addition, the engine management system, data acquisition system and the combustion analyser used to record the data are also described thoroughly. Calculation of the main engine parameters such as net indicated mean effective pressure, indicated power, net indicated specific fuel consumption and a few other parameters are also discussed. Finally, this chapter outlines the methods used for making sure that the results were obtained with accurate engine instrumentation setup and installation.

Chapter 4 and 5 consists of an experimental investigation of combined PFI and DI injection strategies under lean and stoichiometric conditions at different speed and

loads. Efficiency, combustion characteristics and emissions are the focus on this chapter.

Chapter 6 comprises an experimental investigation into the impact of intake port water injection on efficiency, combustion characteristic and emissions of the engine. The results are compared to the baseline without water injection to understand the anti-knock characteristics of water.

Chapter 7 consists of the results of intake port water injection and using gasoline with different octane-numbers. Water injection tests were performed for all three fuels and the results were compared to the baseline in order to find out the effect RON (research octane number) of water. Efficiency, combustion characteristics and emissions are all presented and discussed for all three fuels.

Chapter 8 provides the major conclusions from this experimental study as well as a recommendation section for the future works and studies in this field.

Chapter Two

Literature Review

Chapter 2 Literature review

2.1 Introduction

Increasing concerns about climate change and human health have led to an increased focus on powertrain development in order to reduce fuel consumption and exhaust emissions. As a result, in the last two decades, there have been a significant improvement in performance and emissions of internal combustion engines mainly due to the mandatory limits on CO_2 and non-CO_2 emissions imposed through a set of strict emissions legislations.

Initially emission regulations were stablished in California in the US during 1960s with an aim to reduce automobile tailpipe emissions using a technology focused approach [4]. Since then, different organisations related to government have been stablished all around the world to setup emission regulations which can protect the environment and human health. Emission standards have been revised updated every year since the early years they were stablished in order to decrease the limit for toxic exhaust gas emissions and improve fuel consumption. Figure 2-1 shows the timeline of the passenger car emission regulations in the main regions of the world [5]. This timeline covers the evolution of emission legislations from 2015 up to 2025 and how they became more and more stringent to protect environment and human health.

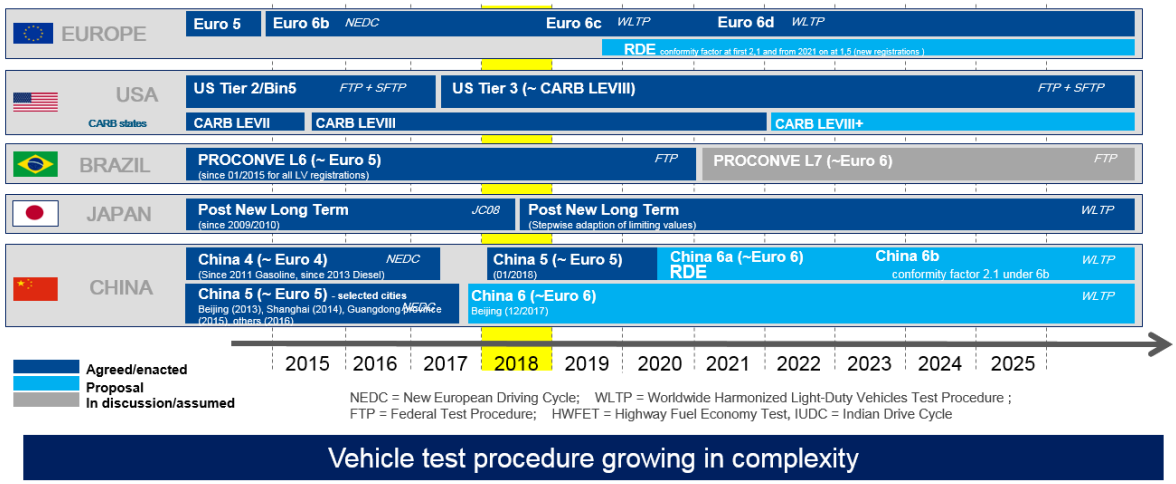

Figure 2-1 Timeline of emission legislations for passenger cars around the world [5]

Table 2.1 shows the European emission standards for passenger cars [6] which have been upgraded from Euro 1 in July 1992 to Euro 6 in September 2014. As can be seen in this figure, there is a significant decrease in the limit of all the emissions when comparing the early regulations to the latest ones. Main changes in recent years were the limit on particle mass or PM for gasoline engines from Euro 5 which was announced after introduction of conventional GDI engines and the limits on particle number (PN) for diesel engines which were added to the regulations since Euro 5b. PN limits were also introduced for gasoline engines in Euro 6 standards. The New European Driving Cycle (NEDC) which is currently used in Europe to assess the emissions levels and fuel economy of passenger cars and light duty commercial vehicles is being replaced by a new test procedure called WLTP (World Harmonized Light Vehicle Test Procedure). WLTP has been developed to achieve results which are as close as possible to the Real Driving Emission (RDE) test results. This replacement started gradually from September 2017.

Table 2.1 EU emission standards for passenger cars (Category M1*) [6]

Stage	Date	CO	HC	HC+NOx	NOx	PM	PN
		g/km					*#/km*
Positive Ignition (Gasoline)							
Euro 1†	1992.07	2.72 (3.16)	-	0.97 (1.13)	-	-	-
Euro 2	1996.01	2.2	-	0.5	-	-	-
Euro 3	2000.01	2.30	0.20	-	0.15	-	-
Euro 4	2005.01	1.0	0.10	-	0.08	-	-
Euro 5	2009.09[b]	1.0	0.10[d]	-	0.06	0.005[e,f]	-
Euro 6	2014.09	1.0	0.10[d]	-	0.06	0.005[e,f]	6.0×10^{11} [e,g]
Compression Ignition (Diesel)							
Euro 1†	1992.07	2.72 (3.16)	-	0.97 (1.13)	-	0.14 (0.18)	-
Euro 2, IDI	1996.01	1.0	-	0.7	-	0.08	-
Euro 2, DI	1996.01[a]	1.0	-	0.9	-	0.10	-
Euro 3	2000.01	0.64	-	0.56	0.50	0.05	-
Euro 4	2005.01	0.50	-	0.30	0.25	0.025	-
Euro 5a	2009.09[b]	0.50	-	0.23	0.18	0.005[f]	-
Euro 5b	2011.09[c]	0.50	-	0.23	0.18	0.005[f]	6.0×10^{11}
Euro 6	2014.09	0.50	-	0.17	0.08	0.005[f]	6.0×10^{11}

* At the Euro 1..4 stages, passenger vehicles > 2,500 kg were type approved as Category N_1 vehicles
† Values in brackets are conformity of production (COP) limits
a. until 1999.09.30 (after that date DI engines must meet the IDI limits)
b. 2011.01 for all models
c. 2013.01 for all models
d. and NMHC = 0.068 g/km
e. applicable only to vehicles using DI engines
f. 0.0045 g/km using the PMP measurement procedure
g. 6.0×10^{12} 1/km within first three years from Euro 6 effective dates

Harmful emissions are believed to be considerably lower by introduction of emissions standards. Figure 2-2 shows the effect of stricter emission regulations on unburned hydrocarbon (HC) and nitrogen oxides (NO_x) emissions reduction [7]. These emission standards also promote the development of new engine technologies such as fuel injection systems, precision electronic control, advanced combustion and aftertreatment systems.

Increasing levels of CO_2 emissions mainly due to human activities all around the world has raised concerns specially during the last decade as CO_2 is the main contributor to the greenhouse effect which has a direct impact on global temperature and climate change [7]. Figure 2-3 shows the different sources of CO_2 emission on a pie chart. As can be seen in this figure, different transport sectors and energy supply are the largest sources of CO_2. Cars are responsible 18.4% of

the total CO_2 emissions which is not the largest source, but it is a substantial part of the emissions.

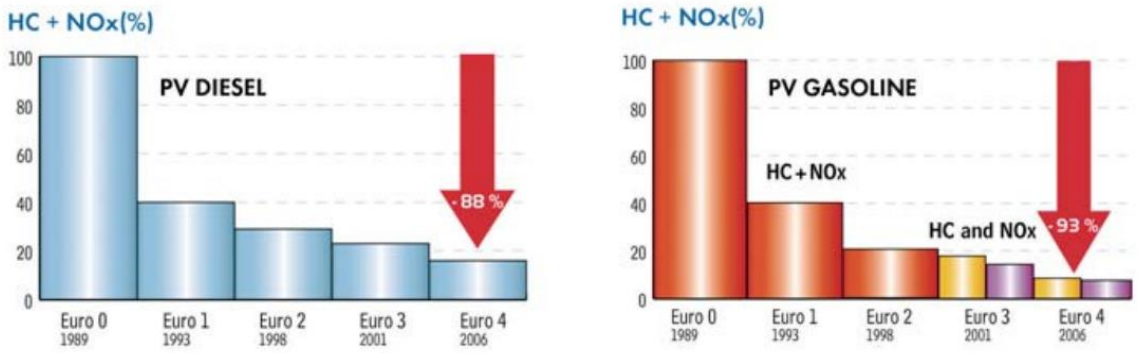

Figure 2-2 Effect of emission standards on reduction of HC and NO_x emissions for passenger cars [7]

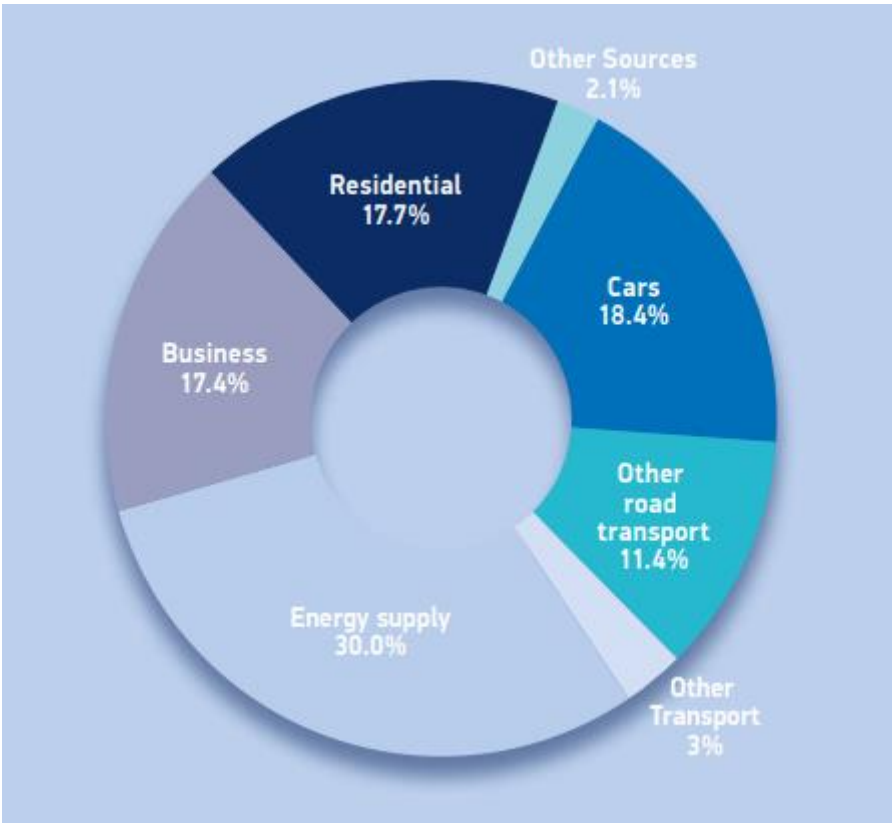

Figure 2-3 Different sources of CO_2 emissions [8]

CO_2 is the product of the complete combustion of a carbon-based fuel in the car engine. There is no aftertreatment system in the car exhaust system to filter CO_2 emissions out. Therefore, using less fuel is the most attractive way to reduce these emissions with the help of the new CO_2 emission standards or fuel economy standards.

As can be seen in Figure 2-4, the governments in major automobile markets worldwide have set mandatory CO_2 emission targets for passenger cars which has become more and more strict [9]. This is done in response to the concerns about the global warming and climate change which was mentioned earlier. In addition, this ensures the development and implementation of new technologies by car manufacturers in order to comply with the new standards and legislations.

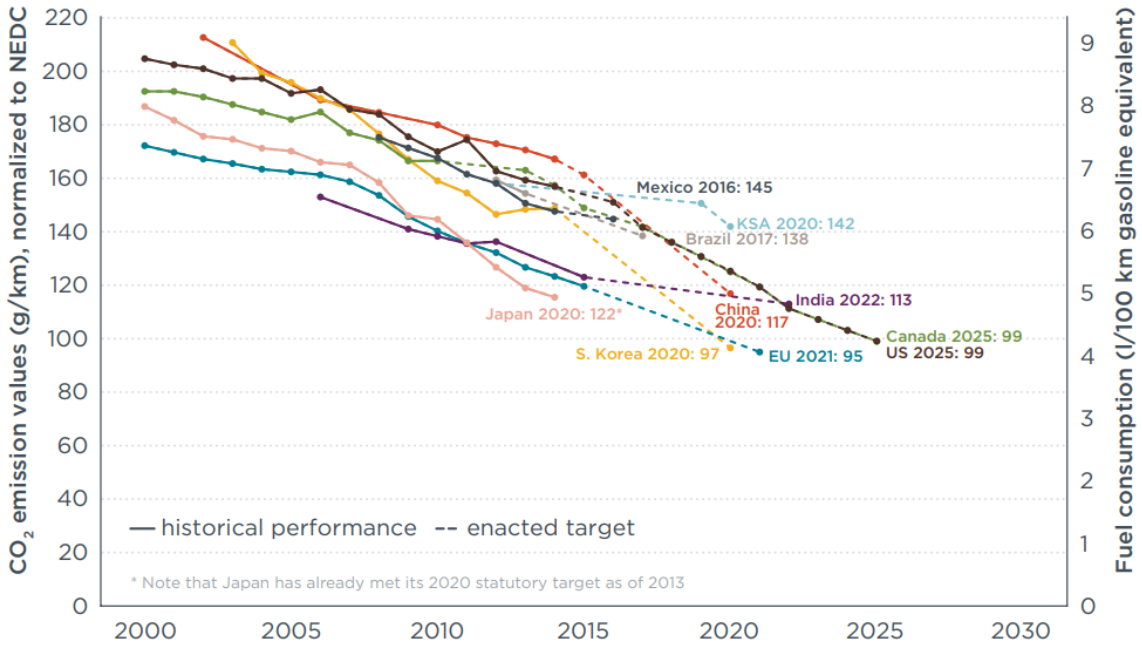

Figure 2-4 Historical fleet CO2 emissions performance and current standards (gCO2/km normalized to NEDC) for passenger cars [9]

CO_2 emissions performance, current standards and future targets for Europe are also shown in Figure 2-5. this graph shows the target for 2030 which was predicted by MAHLE Powertrain and explains how the targets are driving the manufacturers towards the zero CO_2 emissions and electrification [5].

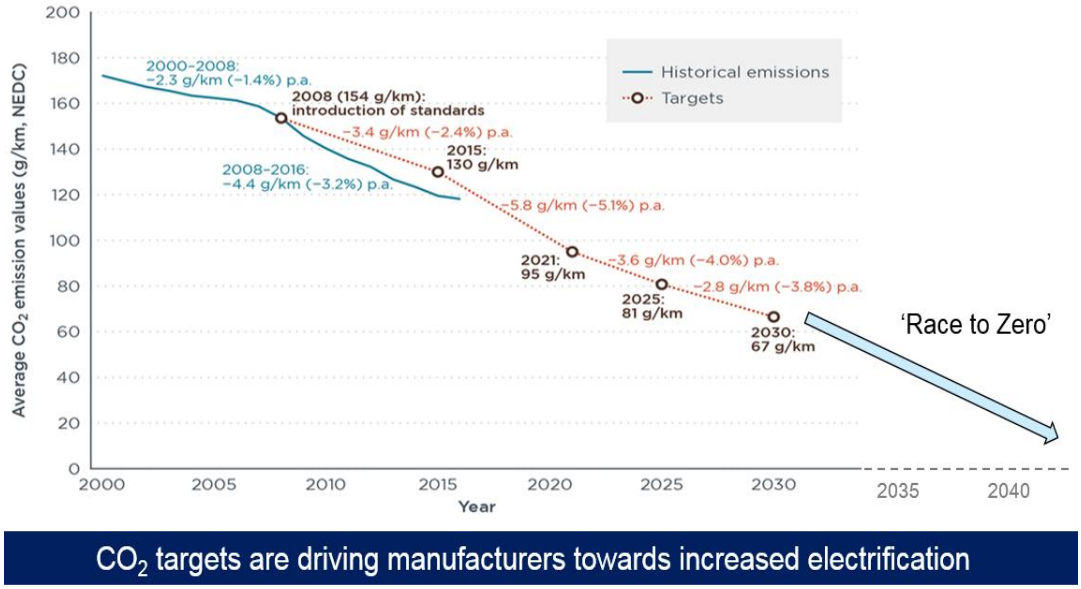

Figure 2-5 Historical fleet CO2 emissions performance and current standards (gCO2/km normalized to NEDC) for passenger cars by MAHLE Powertrain [5]

Electric vehicles could be an alternative to change this dependency on ICEs and fossil fuels but despite the recent advancements in electric motors and batteries, electric vehicles cannot fully replace ICE powered vehicles yet due to issues such as limited range, higher initial cost, time for the recharge, higher particle emissions (due to the weight of the batteries and higher wear on brake discs and tyres), the issue of recycling batteries, infrastructure for power generation and emissions produced by the power generation itself [10]. Therefore, still lots of improvements are required for electric vehicles to be used as a replacement for ICE powered vehicles. Furthermore, alternative fuels such as ethanol, biodiesel and hydrogen

have shown their potential to be used as automobile fuels, however production of these fuels is not sufficient now to cover the demand of large-scale shift towards them and the cost is also not comparable to the conventional fuels. Hence, lots of effort has been put into the improvement of ICEs to achieve the necessary emission reduction imposed by the stringent regulations beyond 2020 [2,10–15].

2.2 ICEs Efficiency and Emissions

Technical development and improvement as well as design optimisation of all different systems and parts is necessary in order to meet the stringent emission legislation and fuel economy standards. The followings are the areas of improvement [16,17]:

- Improve fuel consumption of ICEs
- Efficient thermal management
- Improve transmission efficiency and powertrain integration
- Use of brake / kinetic energy recovery
- Use of exhaust / heat energy recovery
- Alternative fuels
- Hybrid and electric propulsion
- Weight reduction (materials and design)
- Reduce rolling resistance and improve aerodynamics

As can be seen in Figure 2-6, in order to meet the future CO_2 emissions regulations, automobile manufacturers focus mainly on weight reduction and efficiency improvement of their engines [18]. This study aims to investigate fuel

consumption reduction through combustion improvement in direct injection spark ignition (DISI) gasoline engines.

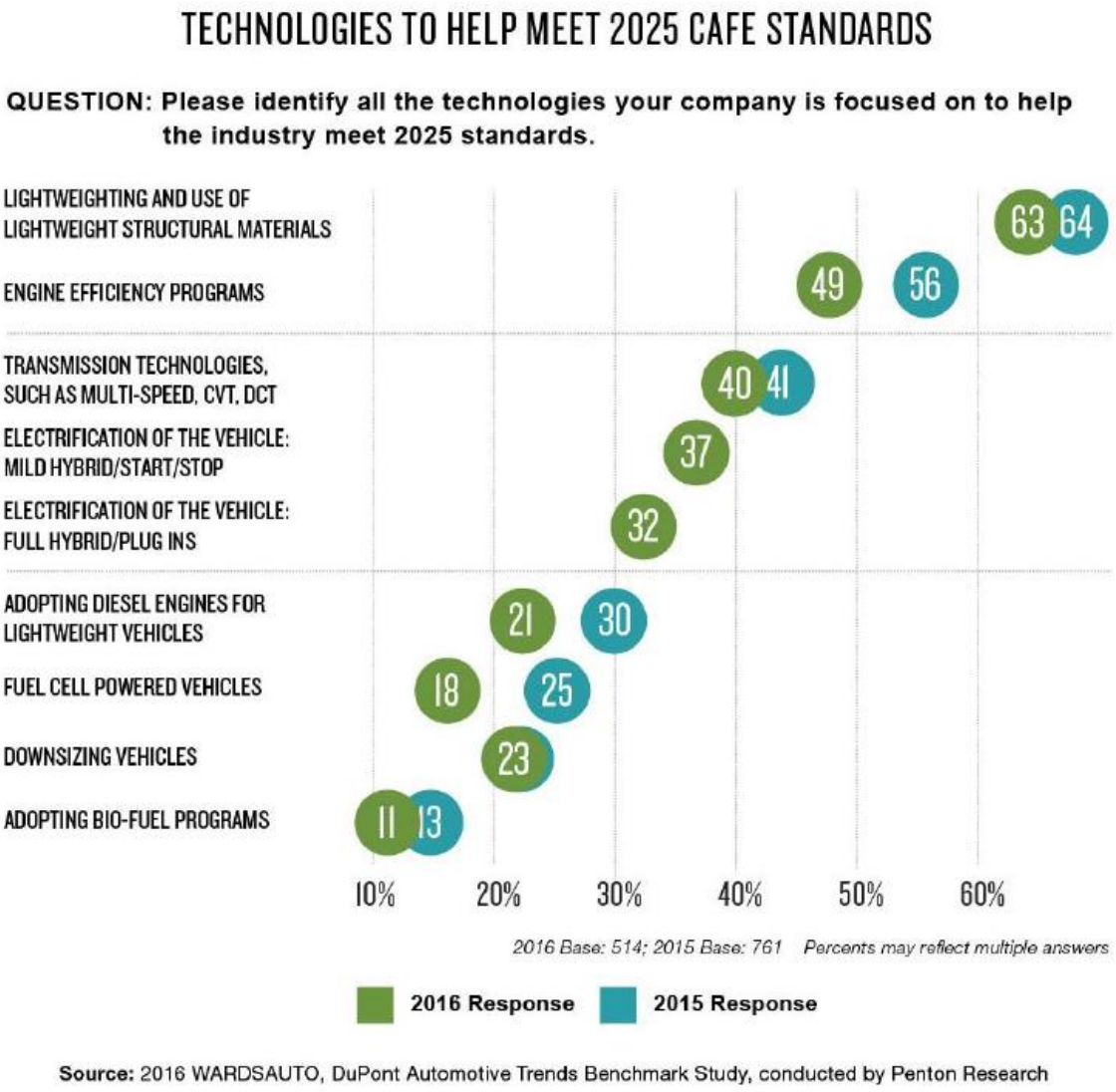

Figure 2-6 Technologies which help to meet 2025 CAFE standards [18]

Fuel conversion efficiency is defined as the ratio of the work produced per cycle to the amount of fuel energy supplied per cycle that can be released in the combustion process [19]. Therefore, improving fuel conversion efficiency is essential for reducing fuel consumption and CO_2 emissions of the ICE powered vehicles. Several complicated processes such as fluid dynamics, thermodynamics, combustion and mechanical movement are involved in

converting the chemical energy of the fuel to mechanical power in an engine. Thus, energy losses in each of these processes are inevitable. A comprehensive discussion about energy conversion process and efficiencies can be found in the literature [2,19–23]. Figure 2-7 shows a summary of energy conversion and efficiencies in ICEs.

It is reported that gasoline engines have the highest share in the passenger cars propulsion market in the world. International Energy Agency (IEA) reported that in 2015, approximately 80% of light-duty vehicles used a gasoline engine [24]. Although diesel engine powered passenger cars had the highest market share in Europe in the past (due to their higher fuel conversion efficiency compared to gasoline engines), this trend has changed since 2017 and passenger cars with gasoline engine currently are dominating the market in Europe (Figure 2-8) [25].

As can be seen in Figure 2-9, approximately 57% of all new passenger cars in Europe have gasoline engine, while diesel cars accounted for 36.3% of the market in the second quarter of 2018 [26]. This figure also shows the percentage of the alternatively-powered vehicles (APV) which are divided into electrically-chargeable vehicles (ECV), hybrid electric vehicles (HEV) and alternatively-powered vehicles other than electric.

Key areas of improvement in fuel economy of gasoline engines are highlighted in Table 2.2.

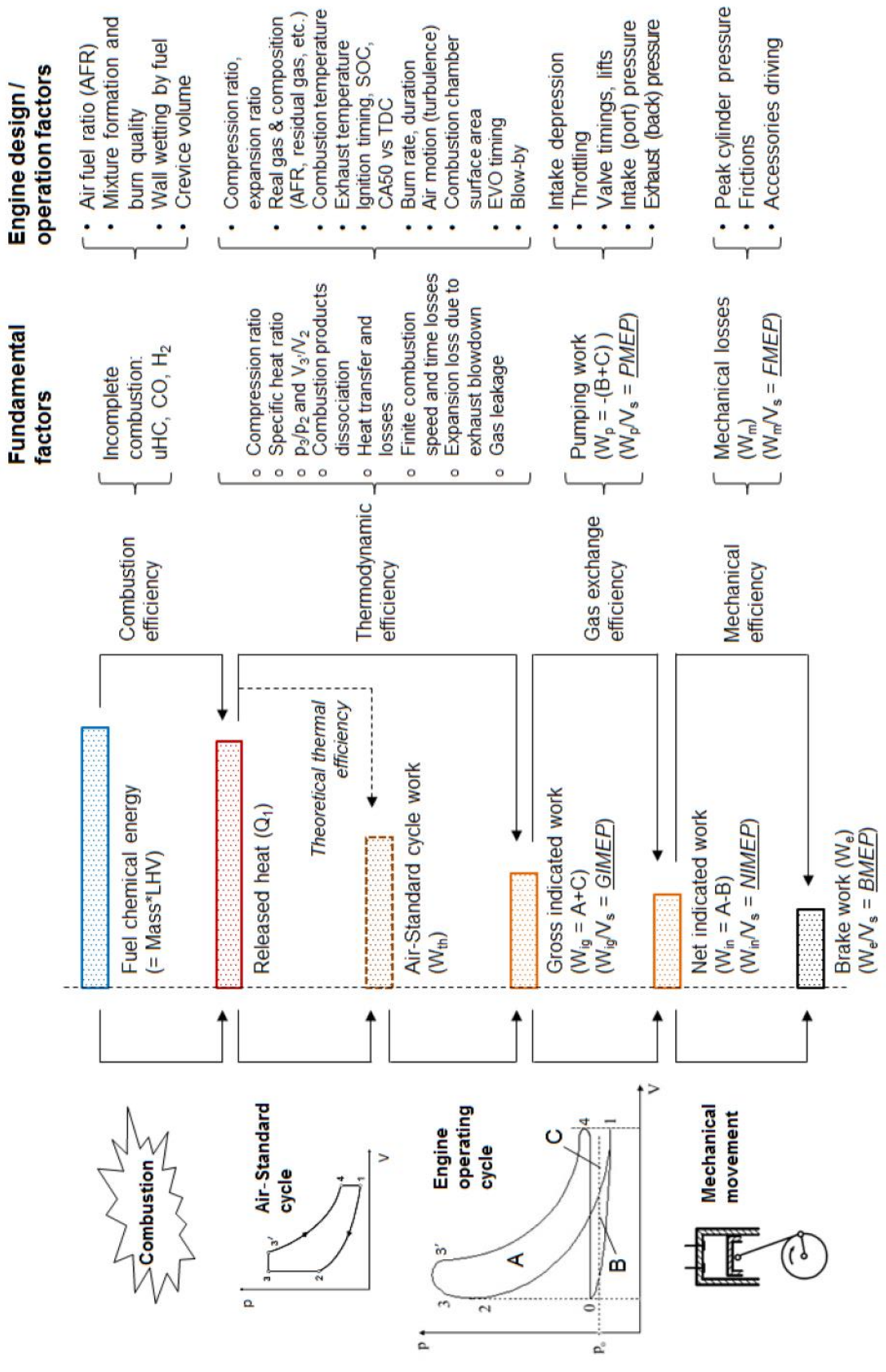

Figure 2-7 Fuel Energy Conversion Process and Efficiencies in Internal Combustion Engines [27]

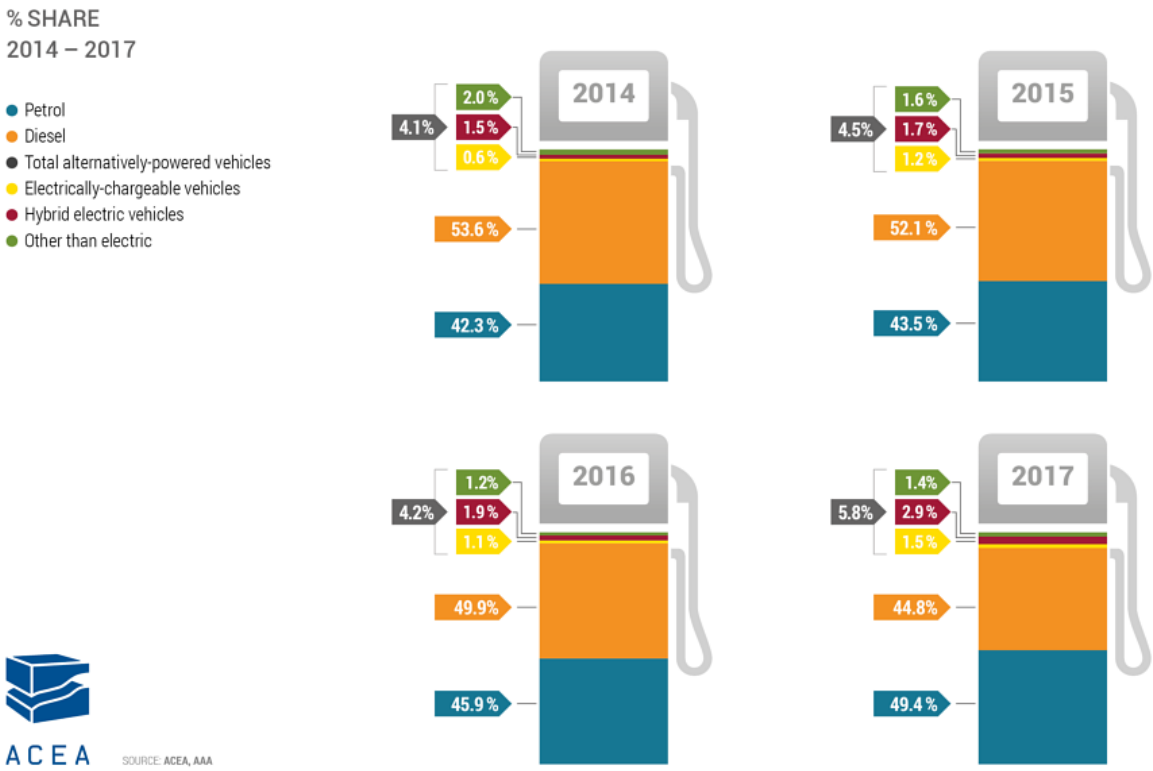

Figure 2-8 New passenger cars market share in Europe by fuel type [25]

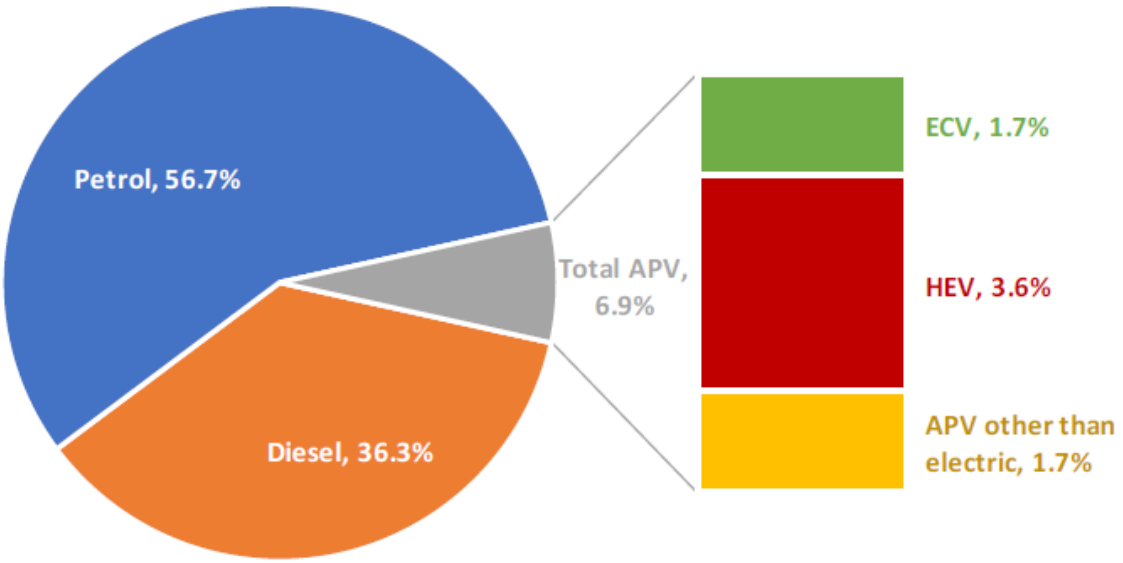

Figure 2-9 New passenger car registrations by fuel type in Europe in the second quarter of 2018 [26]

Table 2.2 Key aspects for improving gasoline engine efficiency [27]

Key objectives	Main obstacles and limitation in (SI) gasoline engine operation
Increase compression ratio	1) Abnormal combustion like knocking, low speed pre-ignition (LSPI); 2) Peak cylinder pressure limit from design side and also for reduction of friction.
Increase specific heat ratio	1) SI engine operates with stoichiometric Air/Fuel Ratio (AFR) mixture (relatively richer than diesel engine), due to the following requirements: i. Spark ignition and flame propagation are essential for gasoline engine combustion, which are greatly influenced by the AFR. AFR should be less than 20 for a typical SI engine; ii. SI engines apply three-way catalyst to reduce CO, HC and NOx emissions in exhaust gas.

	It requires the mixture to be near stoichiometric AFR. 2) Gasoline engine has higher combustion temperature than diesel engine mainly due to its stoichiometric combustion, which decreases specific heat ratio; 3) Gasoline engine has to use enriched mixture at high speed high load area to cool down exhaust temperature for exhaust components protection. It decreases both the combustion efficiency and specific heat ratio.
Reduce pumping loss	Gasoline engine normally uses throttling to reduce air intake mass at part load to control output meanwhile to maintain stoichiometric AFR. It causes decreased intake pressure and high pumping loss.
Optimise combustion time	1) Finite combustion speed causes combustion time losses in the gasoline engine. It will get worse when residual gas fraction increases

	(like at low load) or EGR increases, since they slow down the combustion; 2) Knocking at high load makes spark timing and CA50 retarded. It will make combustion phasing further away from optimum point.

Operating characteristics of an IC engine over its full load and speed range can be presented by plotting BSFC contours on a graph of BMEP against engine speed, as shown in Figure 2-10. As can be seen in this figure, specific fuel consumption changes significantly by changing the load and speed of the gasoline engine. The minimum BSFC is typically achieved at medium load and speed. Increasing or decreasing load and speed from the minimum BSFC point results in an increase BSFC due to various reasons and factors which are described below.

Starting at the minimum BSFC point, increasing speed at constant load (BMEP) increases BSFC mainly due to the increasing friction mean effective pressure (FMEP) at higher speeds which decreases mechanical efficiency. Although at higher speeds gross indicated fuel conversion efficiency ($\eta_{f,ig}$) increases (due to decreasing importance of heat transfer per cycle), increases in friction dominate. Decreasing speed at constant load increases BSFC mainly due to increasing importance of heat transfer which decreases $\eta_{f,ig}$. The effect of lower friction and therefore higher mechanical efficiency is secondary here. Moreover, increasing load at constant speed from the minimum BSFC area increases BSFC due to the knock and mixture enrichment (over-fuelling). At low engine speeds and high loads

knock is the limiting factor in gasoline engines (especially highly downsized GDI engines which can experience low speed pre-ignition (LSPI) at low speed high load conditions) due to high thermal load and high gas temperature and slow combustion. Therefore, combustion timing is retarded to supress knocking which decreases $\eta_{f,ig}$. Over-fuelling or enrichment is mostly used at high load high speeds to decrease the exhaust gas temperature for components protection. Decreasing load at constant speed increases BSFC due the increased pumping losses, increased relative importance of friction and increasing importance of heat transfer which decreases $\eta_{f,ig}$.

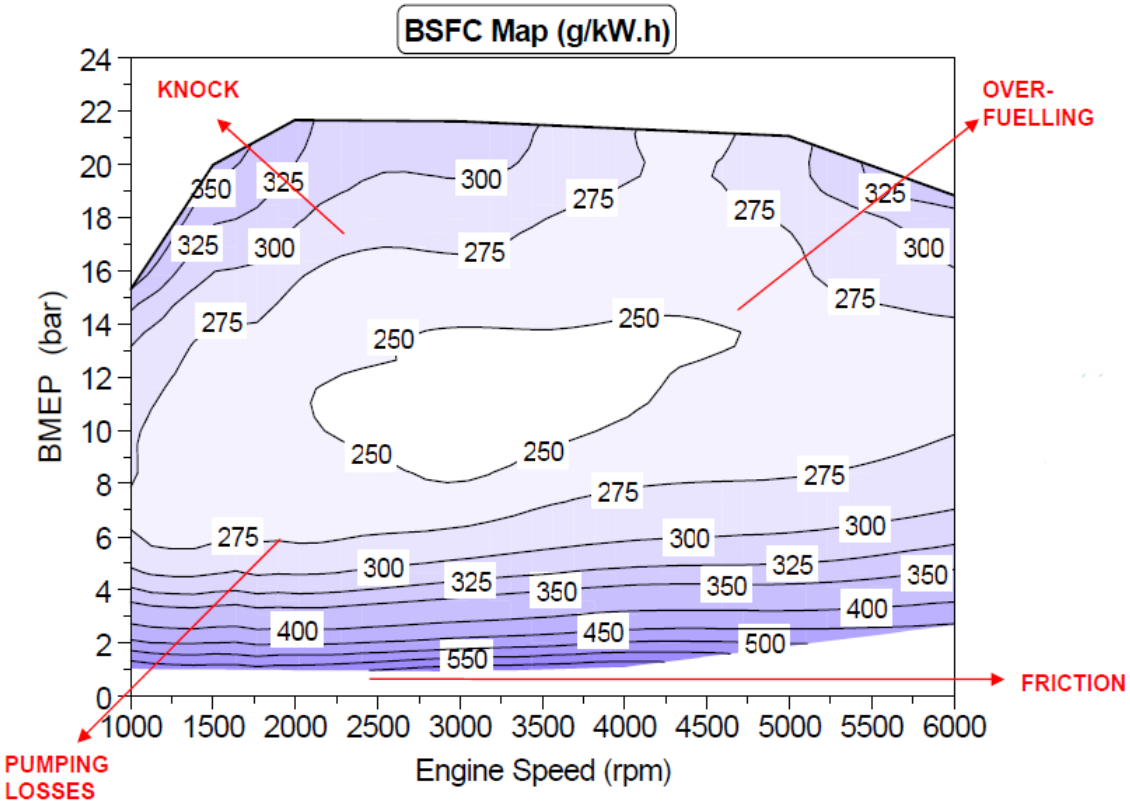

Figure 2-10 Performance map for a fast-burn GDI engine showing contours of constant BSFC [28]

2.3 Latest Automotive Propulsion Systems, Technologies and Trends

Reducing emissions and improving fuel economy are the most important drivers for the internal combustion engines' recent developments. Therefore, many advanced technologies have been developed and used in gasoline engines in the recent years. Some of these technologies are discussed briefly in this section.

2.3.1 Gasoline Direct Injection

Since the introduction of the first modern gasoline direct injection (DI) automotive engine in 1996 by Mitsubishi, direct fuel injection systems have been widely used by automotive manufacturers [2,21,22,29,30]. The main advantages of this technology which makes it revolutionary for gasoline engines are:

- Since the fuel is injected directly into the combustion chamber, it absorbs the heat from the air and evaporates which reduces the air temperature or in other words provides a charge cooling effect, Hence: a) Higher volumetric efficiency by approximately 5% due to the fuel evaporation which only lowers the air temperature, not the intake port and other engine component as is the case in Port Fuel Injection engines, b) Lower compression end temperature (approximately 30 K lower) due to a greater cooling of the air. As a result, higher compression ratio (1 or 2 ratios higher) can be achieved (without inception of combustion knock) which in turn increases the efficiency.
- In addition, this technology allows the precise and accurate control over fuel injection mass as well as providing more flexibility for different injection strategies. AFR can be controlled more accurately with direct injection

during cold start and transient operation which results in significant reduction in fuel consumption and emissions. These advantages allow GDI technology to be utilised in conjunction with other technologies and enable advanced combustion processes.

In general, there are two different operating modes for gasoline direct injection engines: homogeneous and stratified modes (Figure 2-11). Homogeneous mode is usually used at high engine loads. Homogeneous mixture can be created by injecting the fuel into the cylinder during intake stroke which lead to an even distribution of air inside the combustion chamber. This method is fairly similar to the mixture preparation of a port fuel injection engine. On the other hand, stratified mode is used at part load. Stratified charge can be obtained by injecting the fuel during compression stroke just before ignition take place. As a result, an ignitable mixture can be created at the spark plug surrounded by air. This process ideally happens with the wide-open throttle (WOT). Therefore, the load can be controlled by the amount of fuel injected [2].

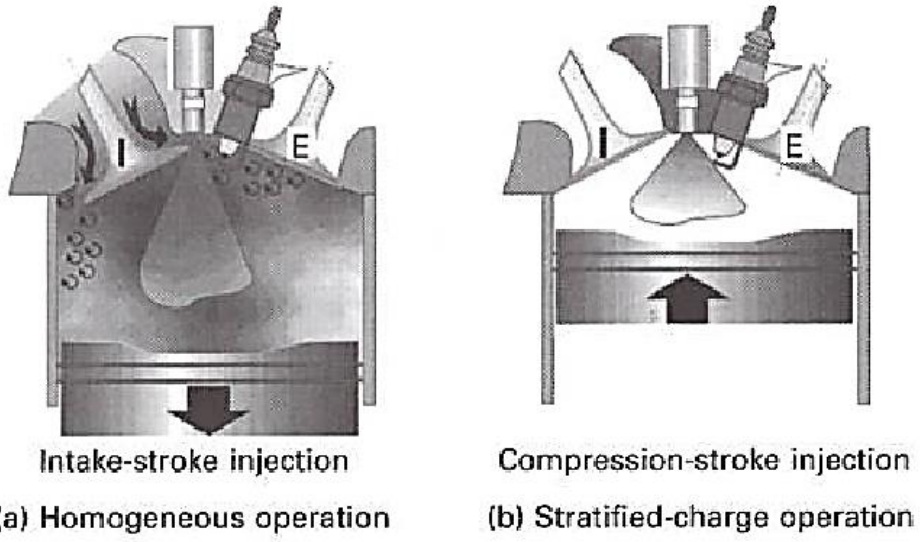

Figure 2-11 GDI engine operating modes [2]

The engine operation map below (Figure 2-12) illustrates the different engine operating modes for GDI engines.

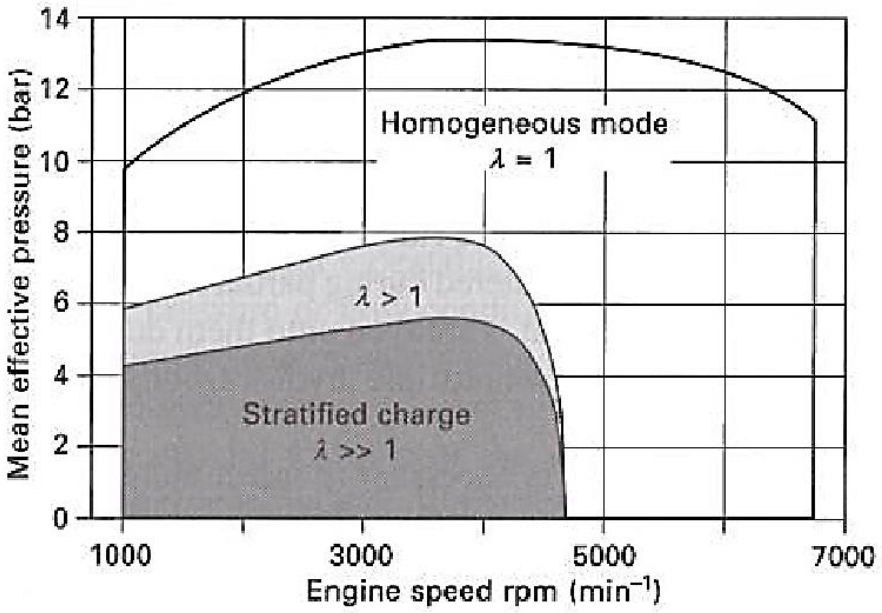

Figure 2-12 Operation map for GDI engines [2]

2.3.2 Stratified charged Lean-burn Combustion

As it was mentioned in the previous section, in addition to lower compression ratio, the main factors contributing to the higher fuel consumption of gasoline engines compared to their diesel counterparts are the pumping losses and lower specific heat ratio. Both factors are related to the stoichiometric air/fuel ratio operation in gasoline engines. Lean combustion has been extensively studied since the invention of ICEs in order to improve fuel economy in gasoline engines [31–35]. Mixture ignitability is usually the challenge in homogeneous lean combustion systems. Thus, an advanced ignition device or other solutions are required to reliably ignite the homogeneous lean mixture [36,37].

On the other hand, stratified lean combustion system reduces the need for such advanced ignition systems due to the rich mixture formation at the vicinity of the spark plug just before the ignition which significantly improves the flame kernel formation and the consequent flame propagation. Engines with this type of combustion system can operate with a wide variety of liquid fuels and are fuel tolerant, since the conventional SI engines requirements for high antiknock quality fuels and the CI engines necessities for high ignition quality fuels are not the case in stratified charge engines [19]. However, stratified fuel-air mixture with an easily ignitable composition near the spark plug at the time of ignition is necessary for a successful charge stratification.

During recent years many types of stratified charge engines have been designed and developed. As can be seen in Figure 2-13, the early stratified charged engines designed with a bowl in piston which can generate a high degree of air swirl during intake stroke. This can result in a rapid air-fuel mixing. In this system fuel is injected into the cylinder tangentially to the bowl during final stages of compression stroke followed by a long duration spark ignition which ignites the fuel-air mixture and ultimately the combustion is completed during expansion when the flame spreads downstream in the combustion chamber and consumes the mixture [19]. In order to increase the power density this engine can also be turbocharged or supercharged.

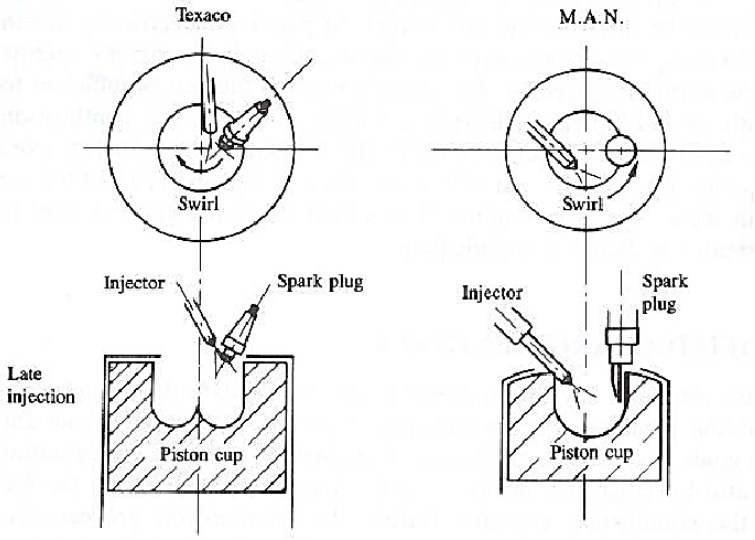

Figure 2-13 The Texaco Controlled Combustion System and the M.A.N.-FM Systems are two types of stratified charge engines which have been used in commercial practice [19]

Figure 2-14 illustrates sectional drawing of the M.A.N multifuel engine, a commercial stratified charge engine in which the fuel injector is positioned in the top left side of the cylinder and therefore can inject the fuel into the piston bowl. The fuel mixes with the air after evaporation by the swirling flow effect created during induction [19]. In this design the spark plug is situated vertically at the top right-hand side of the combustion chamber.

In the 1920s Ricardo developed a new type of stratified charge engine (Figure 2-15) which had an additional small pre-chamber in order to introduce a rich fuel mixture at the spark plug. This pre-chamber fed by a separate intake manifold and carburettor. During intake stroke, both intake valves will open at the same time, therefore the rich mixture is introduced to the pre-chamber and a lean mixture is introduced to the main chamber by the main carburettor and intake manifold. During the compression stroke the lean mixture is compressed into the pre-

chamber. As a result, a slightly rich and easily ignitable mixture is created at the spark plug. Combustion starts by spark plug ignition and burning the rich mixture which acts as a jet for burning the lean mixture [19]. Therefore, this kind of engine is called jet ignition or torch ignition.

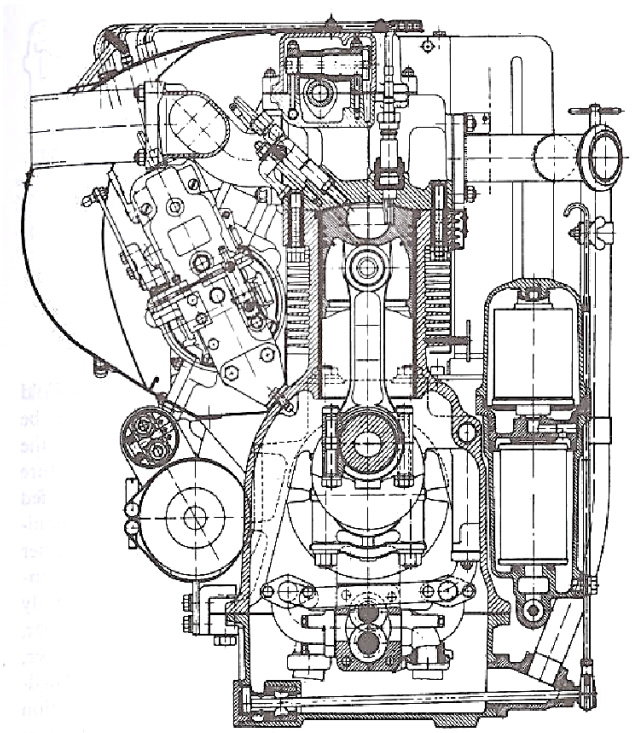

Figure 2-14 Sectional drawing of the M.A.N. high speed multifuel four cylinder direct injection stratified charge engine [19]

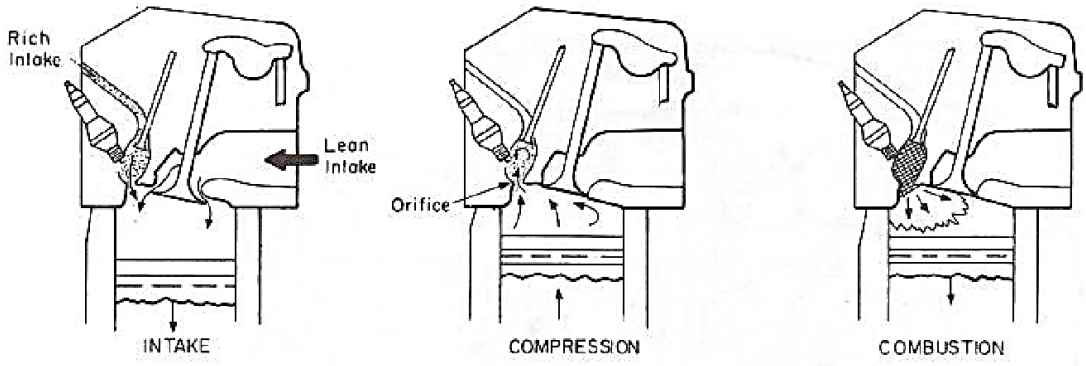

Figure 2-15 Three valve torch ignition stratified charge engine [19]

Before the introduction of DI combustion system achieving an ideal stratification was challenging due to the limitations of port fuel injection (PFI). Direct injection for gasoline engines gives a much higher flexibility in terms of injection configuration and timing, and the number of injection events per cycle which makes it suitable for stratified combustion. Hence, the first generation of mass production GDI engines were all running on lean stratified combustion mode [2,21,38]. Basically, there are three combustion concepts for mixture preparation in GDI engines: wall-guided, air-guided and spray-guided combustion systems (Figure 2-16). The first generation of stratified engines were mostly wall-guided or air-guided. The spray-guided combustion system was introduced later by BMW and Mercedes-Benz as the second generation of these engines which utilized the more expensive outwardly-opening piezo actuated injector mounted next to the spark plug [2].

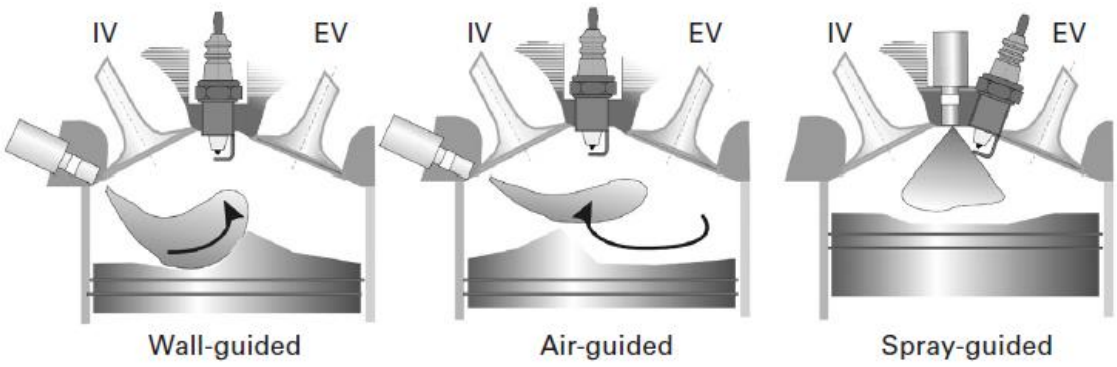

Figure 2-16 Wall-, air- and spray-guided combustion concepts [2]

Wall guided system were used in the first generation of stratified charge engines. In this method fuel is injected towards the piston crown which is designed in order to transport the fuel to the spark plug. The issue with this system is increased fuel

deposits and emissions of unburned hydrocarbons due to the injection of the fuel at the piston.

Figure 2-17 shows a GDI engine which was introduced by Mitsubishi for the first time in a modern car in 1997. This engine comprises spherically bowled pistons which supports the air fuel mixture to move towards the spark plug. In this engine, reverse tumble is used in order to transfer the fuel spray (fuel injector is positioned near the inlet valves to prevent contact with exhaust valves with high temperatures) to the spark plug after impingement on the piston bowl. Therefore, the key element in successful operation of this engine is matching the in-cylinder air flow to the fuel injection. Moreover, in order to reduce the droplet size and therefore easing evaporation, Mitsubishi used an injector with a swirl generating geometry which operates at pressures up to 50 bar [21].

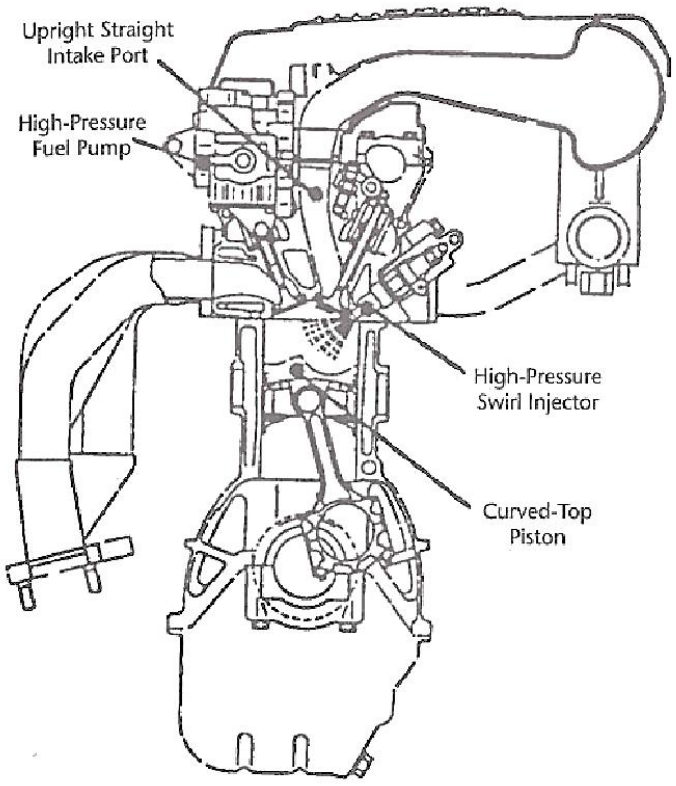

Figure 2-17 GDI engine by Mitsubishi [21]

When this engine operates in stratified charge mode, global air/fuel ratio is in the range of 30 to 40 which reduces the throttling losses. In addition, in stratified charge operation, injection timing is significantly important. Cycle by cycle variations in combustion are very sensitive to the injection timing [21].

Calculations of the fuel spray transport and piston displacements for a gasoline direct injection engine are displayed in Figure 2-18. Start of the fuel injection is 310 CAD ATDC (after top dead centre) on the non-firing revolution. Then the fuel meets the piston bowl at point A and moves toward the piston rim (point B) and ultimately tumbling flow direct it towards the spark plug at point C. as can be seen in this figure, horizontal lines show the amount of time required to transfer the fuel injected to the spark plug. Therefore, a rich mixture is created when this time is too short, or an over diluted mixture is created when this time is too long. However, the best combustion stability can be achieved when the richest mixture is formed at the spark plug [21].

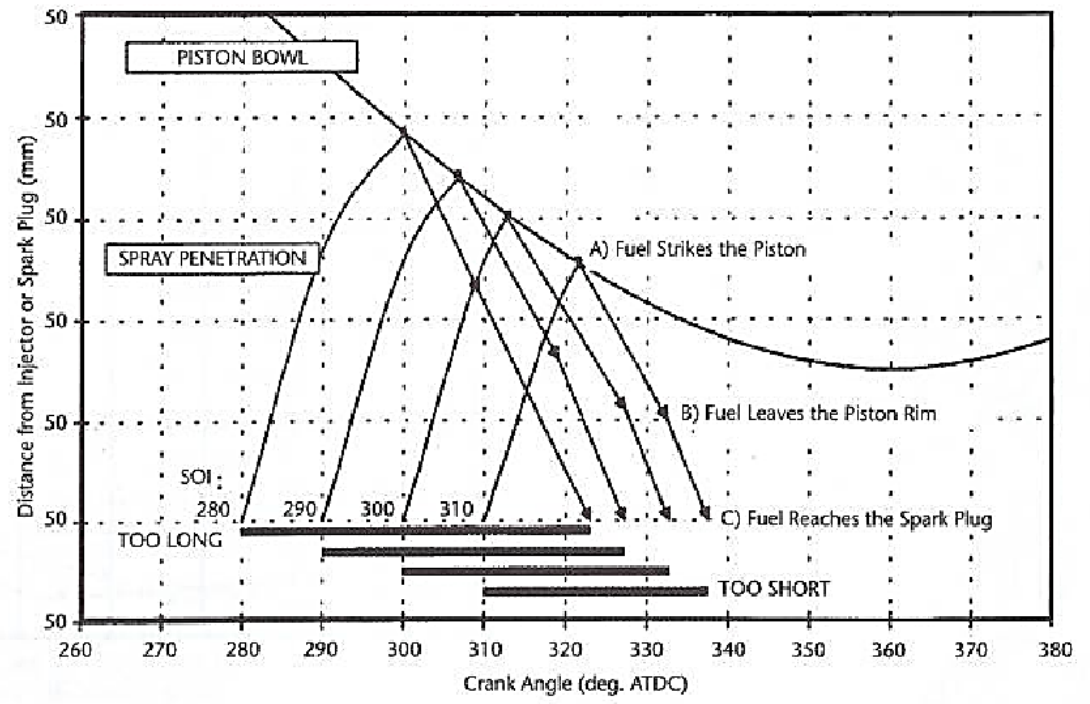

Figure 2-18 Calculations of the fuel spray transport and piston displacements for a GDI engine [21]

In this method of stratification since the injection timing is linked to the piston position in the cylinder, hence it is dependent on engine speed. In addition to injection timing, in-cylinder air flow needs to be optimised in order to form a desirable mixture at the spark plug. This also depends on the engine speed. All these factors make it difficult to coordinate the injection and ignition timings across a wide engine speed and load range. In practice, it was not possible to achieve the theoretical potential of gasoline direct injection for reducing fuel consumption with wall-guided combustion configuration for the following reasons [2]:

- Coordinating the injection and ignition timing over a wide engine operating range is hard due to the dependency of mixture transport to the piston position.

- At high engine loads, swirl or tumble ports which are designed to create the desired flow at intake stroke can have a negative effect on the charge.
- Increased hydrocarbon emissions due to creation of the fuel deposits on the piston and the cylinder wall.
- Special design of the piston crown leads to an increase in size and weight of the piston which in turn increases the mechanical losses.
- Increased unburned hydrocarbon emission due to the fuel entry to the squish gap.

In air-guided combustion systems, the goal is to reduce the harmful hydrocarbon (HC) emissions through avoiding wall wetting of the combustion chamber (liquid fuel contact with the walls of the combustion chamber should be minimised or eliminated). As a result, fuel deposits on the wall of the combustion chamber can be removed. In this method the air fuel mixture is prepared by using the charge movement which is supported by suitably shaped piston crowns. Furthermore, directional orientation of the injection jet and generation of a particular charge movement are the key factors in designing an air-guided combustion system. Swirl and tumble flow are the most common types of charge movement inside the cylinder which have been used extensively to deliver the mixture at the spark plug. However, both of these methods reduce volumetric efficiency and ultimately the performance of the engine [2]. Wall and air-guided combustion systems are known as the first generation of gasoline direct injection (GDI) engines.

In the spray-guided direct injection (SGDI) engines, characteristics of the injector have direct effect on the mixture preparation. A greater control of the spray pattern

is achieved by the recent developments of injectors such as multi-hole or outwardly opening injectors. The benefits of spray-guided systems compare with wall guided systems are:

- Higher volumetric efficiency due to the removal of high velocity in cylinder flows.
- Lower emissions of particulate matter and unburned hydrocarbons due to a more homogeneous mixture which is achieved by a better mixture preparation (reduced piston and wall wetting, higher injection pressures and smaller droplets compared to wall/air-guided combustion systems).

A wider operating range can be achieved when these engines working in stratified charge mode (increased maximum speed from 3000 rpm to 4000 rpm and increased maximum BMEP from 3.5 bar to 5 bar). As can be seen in Figure 2-19, BMW six-cylinder engine is able to operate in a wider range than operating regime for New European Driving Cycle (NEDC) [2]. Stratified-charged in this engine is prepared by an outwardly opening centrally positioned piezoelectric injector which reduces wall wetting of the combustion chamber. Injection pressures of up to 200 bar were used in this engine and 10% lower BSFC (at 2000 rpm and 2 bar BMEP) was achieved compare with the BMW variable valve actuation engine. Small fuel droplets, rapid spray break up and strong spray induced charge motion are the benefits of high injection pressures. Spray guided combustion systems have a potential for 20% lower fuel consumption than conventional throttled gasoline engines in the NEDC [2,21]. In lean homogeneous mode, there is an early injection during intake stroke followed by a late injection just before ignition. This creates a stratified zone near the spark plug which can increase the combustion stability. Multiple injections with very short delays (due to the extremely fast needle

reaction) can also deliver high combustion efficiency with low HC and CO emissions [39].

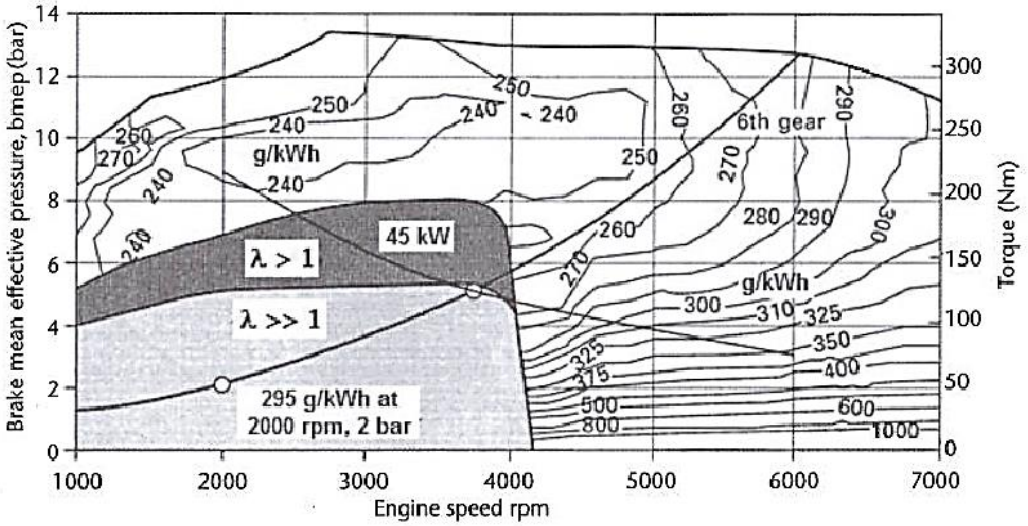

Figure 2-19 Stratified-charge range of BMW 3 litre six-cylinder engine with gasoline direct injection and spray-guided combustion system [2]

As can be seen in Figure 2-20, in homogeneous operating condition the injector produces a hollow cone with high penetration and stable and almost constant cone angle during injection. A very small recirculation area appears far downstream the injector tip because of low backpressure at this condition. During stratified operation, fuel is injected in higher cylinder pressure in compression stroke. Thus, spray penetration is reduced considerably, and a more visible recirculation area is created. In addition, there is no significant change in the cone angle of the spray [39].

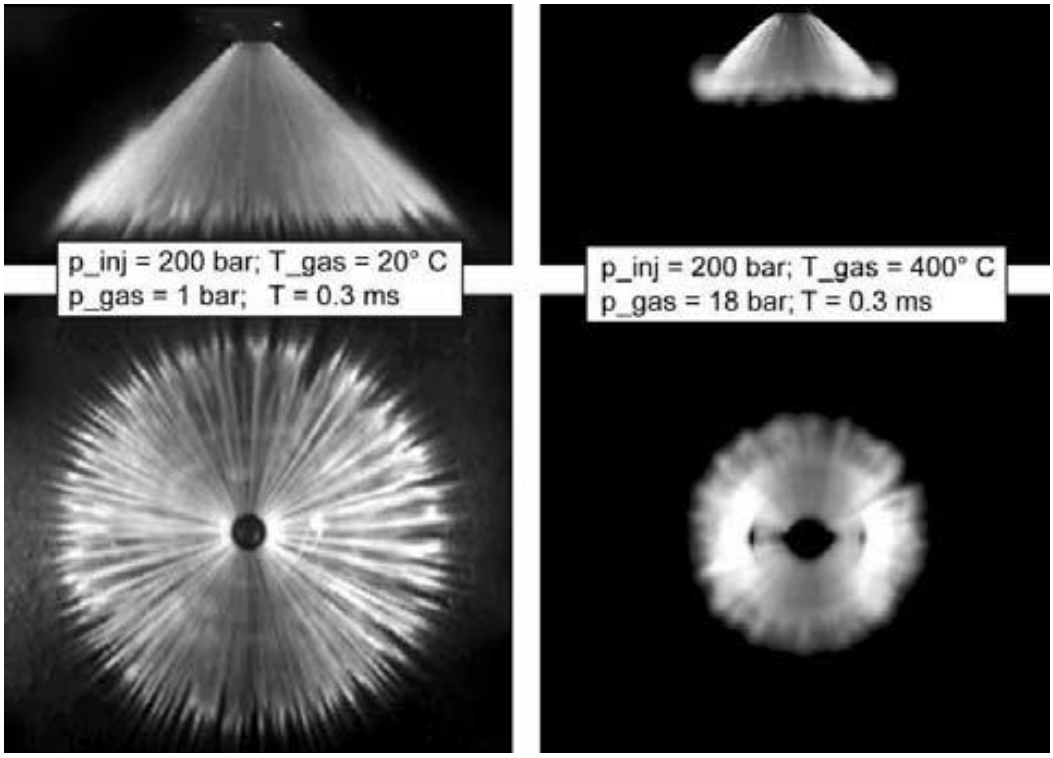

Figure 2-20 Spray formation under Homogeneous (left) and stratified (right) conditions [39]

Spark plug fouling can occur in spray guided direct injection engines because of fuel impinging on the spark plug as well as over rich areas near the spark plug. This can be addressed by using an ignition system with higher energy.

[40] conducted different experiments on the stratified-charged combustion and emission characteristics of a single cylinder direct injection gasoline engine with a spray guided, bowl in piston and high squish combustion chamber layout (Figure 2-21). The outward opening injector is located at the centre of the combustion chamber with a 7-degree inclination from the vertical cylinder axis. Spark plugs with different electrode lengths (3 to 11 mm) were tested to realise the optimum ignition location. In addition, in cylinder air motion was controlled by a variable swirl valve control located in the intake manifold. Two different injectors (low flow rate with 80 degree spray angle and high flow rate with 90 degree spray angle) both

with variable pintle lift control were employed, which allowed a full control over fuel injection rate. In this investigation a series of tests were performed in order to observe the effect of fuel injection pressure, fuel spray duration, in cylinder swirl, spark plug electrode length and spark energy, on the fuel consumption, emissions and combustion characteristics of the engine as well as evaluating the use of multiple injection at part load operating range. The tests were conducted at a part load point in the stratified-charged operating area of the engine (2000 rev/min, manifold absolute pressure of 95 kPa, 10 mg/cycle fuel mass and EGR level was adjusted to maintain NO emissions below 8 g/kg-fuel).

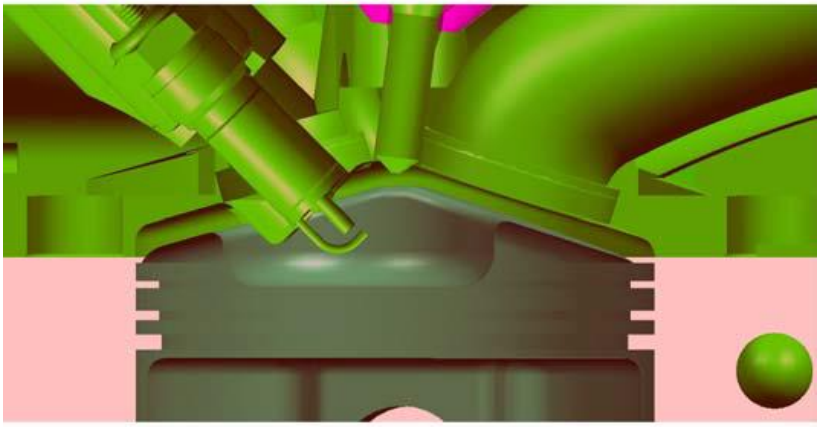

Figure 2-21 Combustion chamber geometry of the engine [40]

The experimental results illustrate, increasing spark plug length, increasing spark energy (ignition energy from 73 to 133 mJ), decreasing air swirl motion and decreasing effective rate of injection significantly improved the fuel consumption of the engine. However, fuel consumption is relatively insensitive to fuel rail pressure in the range of 100 to 200 bar. 30,000 consecutive cycles were examined at optimal injection and ignition timings and no misfires were discovered. Furthermore, no improvement in the part load fuel consumption, emissions and robustness was found in the case of multiple injections (with maximum of 4

injections, different injection timings and dwell times between injections) compare to the single injection strategy. Moreover, there is a direct correlation between how much of the injected fuel is burned in the cycle and the cyclic variations of IMEP.

The thermodynamic benefits of GDI engines can be clearly shown by analysing the losses at part-load operating conditions. As can be seen in Figure 2-22, the positive effect of real gas is clear for the direct injection cases. The increased isentropic exponent results in significant improvements over the PFI engines. When compared to throttled engines with port fuel injection, direct fuel injection also reduces the pumping losses substantially. In terms of efficiency, the advantages of direct injection outweigh the disadvantages such as losses due to incomplete and thermodynamically unfavourable combustion due to lean peripheral areas.

NO_x and particle emissions are the main challenges that lean stratified-charge engines are facing [2,21]. High levels of NO_x emissions mean that these engines need additional lean NO_x aftertreatment systems to pass the stringent emission standards. These aftertreatments systems are usually expensive, complex and sensitive to fuel quality specifically the sulphur content in fuel [2,21,38]. High sulphur concentration in fuel can cause sulphur poisoning of NO_x storage catalysts and increases the fuel consumption [41,42]. Thus, most car manufacturers don't produce this type of engines anymore, although there is still lots of interest from automotive industry and research on this technology due to its superior CO_2 reduction capability.

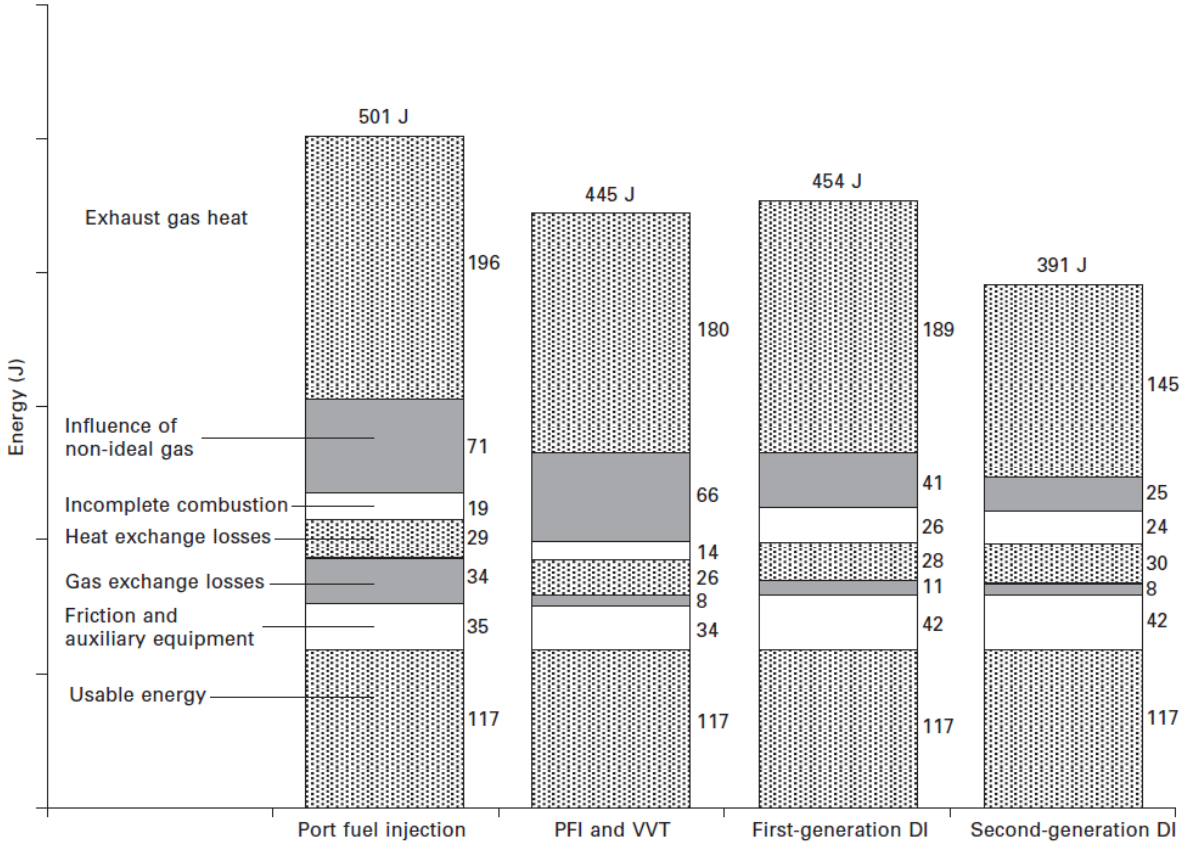

Figure 2-22 Comparison of losses for PFI, VVT, first and second-generation of GDI engines at part-load operating point [2]

2.3.3 Homogeneous charge compression ignition (HCCI) or Controlled Auto Ignition (CAI)

The incapability of conventional stratified charged lean-burn combustion system to produce ultra-low NO_x and particle emission, and also the challenges such as the high ignition energy required and the slow flame speed in homogeneous charged lean-burn combustion system, have led to a considerable research on homogeneous charge compression ignition (HCCI) or Controlled Auto-Ignition (CAI) combustion [2,36,43]. As shown in Figure 2-23, HCCI combustion concept is significantly different from the conventional spark ignition (SI) premixed combustion in gasoline engines and compression ignition (CI) diffusion flame

combustion in diesel engines [44]. In this combustion concept cylinder charge is lean premixed air and fuel mixture highly diluted by the recycled exhaust gases. Compression of this mixture leads to multiple ignition sites in the combustion chamber which leads to a rapid combustion. Therefore, HCCI can eliminate the high combustion temperature zones which leads to producing ultra-low NO_x and particulate emissions. In addition to high compression ratio, the use of lean air/fuel mixture with recycled burned gases allows unthrottled operation of a CAI/HCCI gasoline engine, thus yielding higher engine efficiency and improved fuel economy compared to SI combustion.

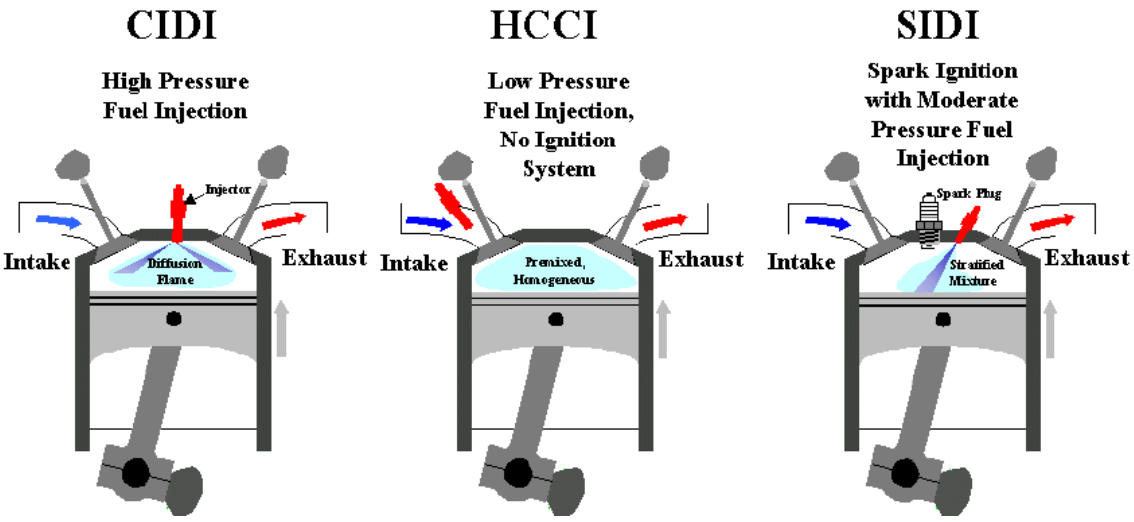

Figure 2-23 HCCI combustion concept in comparison with spark ignition DI and compression ignition DI combustion systems [45]

However, due to factors including the narrowness of the potential operating range and the challenge represented by controllability in response to transient operations, much research and development works are still needed prior to such combustion technologies being incorporated in the mass-produced engines. Major automotive and propulsion companies such as GM, Mercedes-Benz, AVL and VW have all shown their interest in HCCI combustion concept with lunching

demonstrator engines and vehicles [45–48]. Furthermore, Mazda recently announced the debut of their first HCCI gasoline engine will take place in 2019. This engine uses a proprietary combustion system which called Spark Controlled Compression Ignition (SPCCI) [49–51].

2.3.4 Gasoline DI Engines with Variable Cam Timing and Boosting (Downsizing)

Challenges such as complex exhaust aftertreatment system required for stratified combustion system engines and combustion controllability and switching for HCCI combustion system engines has led to development and production of homogeneous-charge stoichiometric GDI engines by automobile and engine manufacturers. Three-way catalysts can be effectively used in these engines in order to control the emissions similar to conventional PFI engines. The cooling effect advantages of direct injection of fuel such as increased compression ratio and higher torque output is still available for these engines but the fuel saving levels are limited due to no improvement in pumping losses and specific heat ratio [2,21,29].

Turbocharging or supercharging the spark ignition engine is conventionally used in order to improve the maximum torque or power output of the engine which also called boosting. However, in recent years, this technology has become more synonymous with fuel saving through the advent of engine downsizing and several manufacturers have recently introduced the new generation of DI gasoline engines called “Downsized GDI” engine. These GDI engines are boosted by a turbocharger or a mechanical supercharger or both (to provide faster response and higher performance at different operating conditions). This allows the use of a smaller

displacement volume turbocharged engine instead of a larger displacement naturally aspirated engine (downsizing) [2,29,52]. Higher inlet manifold pressure produced by the turbocharger leads to a higher BMEP, therefore pumping losses will be lower and ultimately lower fuel consumption can be achieved [21]. In other words, these engines are forced to run at higher BMEP level to produce the same torque or usually higher torque than a larger naturally aspirated engine. As a result, engine operates more in the higher efficiency area of the engine map due to lower pumping work. In addition, this approach also helps to reduce the vehicle CO_2 emission levels by reducing the number of cylinders which reduces the total friction and weight of the engine. Shorter warming up time and therefore improved cold start performance of the engine is also expected [53].

Figure 2-24, shows a good example of engine downsizing in which a significant fuel economy benefit is achieved by changing the engine operation from the least efficient part load condition to the more efficient wide-open throttle (WOT) condition. At part load operating conditions, pumping loss is increased due to the partly closed throttle, but this problem can be solved by using a smaller engine which will be operated more often at wide open throttle and higher load. Therefore, to meet the maximum power and maximum torque requirements, downsized engines need to be boosted. GDI technology facilitates engine downsizing through charge cooling effect which allows higher boost pressure to be used without the risk of knocking combustion. As a result, a turbocharged 1.6 litre engine can produce 130 kW maximum power output which is the same as a 2.5 litre naturally aspirated engine [2].

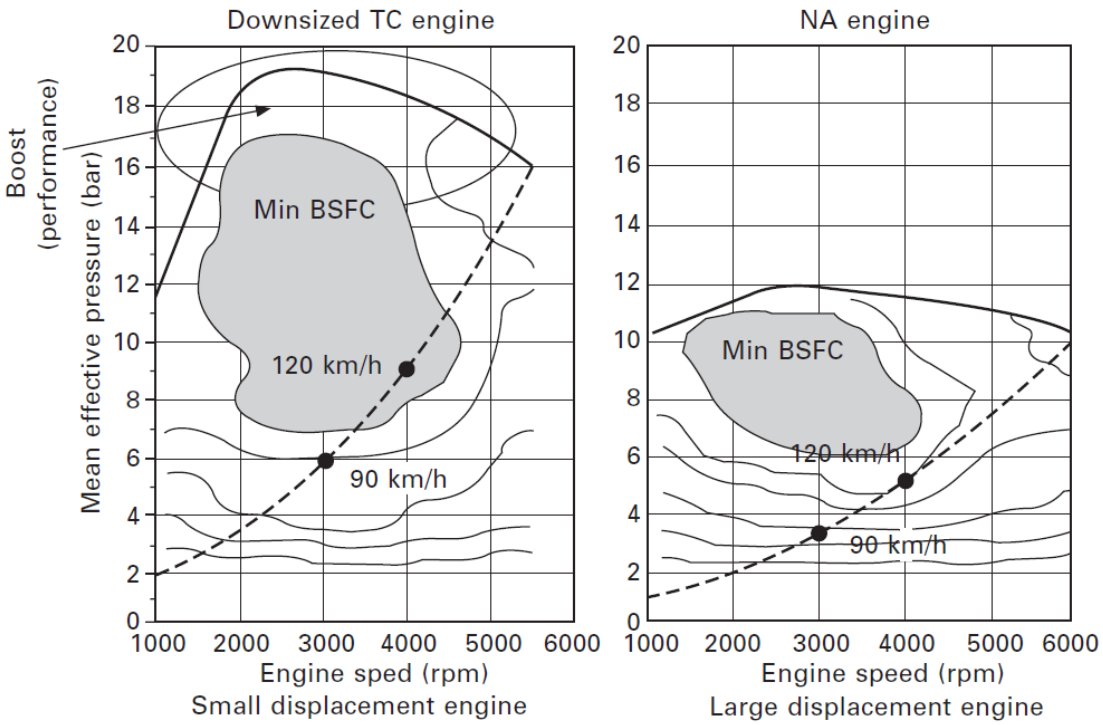

Figure 2-24 Engine Downsizing [2]

As downsized boosted GDI engines are more prone to knocking combustion (due to the elevated intake manifold pressure and therefore end of compression pressure and temperature), compression ratio normally needs to be decreased which results in lower improvements in fuel consumption and performance. However, considerable synergy between GDI engines and boosting can be achieved due to the cooling effect of DI which reduces the charge temperature and the consequent knock tendency. Hence, boosted downsized GDI engines has become a mainstream in the current gasoline engine development and production.

In addition, Variable Cam Timing (VCT) technology has been developed and applied to improve SI engine performance since 1980s. This technology allows engineers to adjust engine cam timings according to engine speed and load in order to reduce pumping loss and improve performance output. This technology has been proven to be essential for boosted gasoline DI engines. It is

advantageous for reducing engine pumping loss at low load and strengthening scavenging effect at low speed high load zone to improve maximum torque. Variable cam timing strategies can be applied more flexibly by GDI approach which separates the intake air from the fuel [21,54,55]. As a result, almost all the GDI engines today are equipped with VCT devices [56].

2.3.5 Variable Valve Actuation and Air Intake

Lots of effort have been put by researchers and automobile manufacturers to develop variable intake air mechanism and devices which can improve the gas exchange processes in gasoline engines. These devices can have a significant impact on pumping and combustion processes by providing a higher level of flexibility for gas exchange process optimization. There are several types of these devices, some of the main ones are listed here: variable cam timing or phaser (VCT or VCP), variable intake manifold, 2-step or 3-step cam profile switching (CPS) / variable valve lift (VVL), continuous variable valve lift (CVVL), camless valvetrain and variable charge motion. Fuel consumption reduction of around 3% to 12% were reported using this technology [21,57].

Using variable intake manifold can improve the engine torque and power in the entire speed range as a result of improvements in volumetric efficiency. With this technology the intake tuning effect is optimized at different engine speeds by step adjusting or continuous adjusting the manifold length [21,58].

Most of modern SI engines are equipped with VCT or VCP devices which allow advancing and retarding the camshaft timing in relative to crank timing. As a result, the valve opening and closing timings during engine operation changes. These products are mostly hydraulically driven and continuously adjustable VCT.

Electronic VCT devices has become more popular recently since they have a faster response capability. Most of the modern gasoline engines use VCT on both intake and exhaust cams, which allows these engines to reduce the pumping losses at part load by optimising intake and exhaust valve opening/closing timings and to enhance the low speed peak torque through scavenging behaviour [54,55,59,60].

There are some limitations with variable cam timing devices. These devices change the camshaft phasing and therefore change both the valve opening and closing times simultaneously. In addition, these devices are incapable of changing the valve lift which makes them less flexible compared to the variable valvetrains with the ability to change the valve event and lift. Honda VTEC system and Audi Valvelift system (AVS) are two examples for variable valvetrains which can provide 2-step or 3-step valve lift adjustment by switching cam profiles. There are also other examples such as BMW Valvetronic, Toyota Valvematic, Mitsubishi MIVEC and Nissan VVEL systems which provide continuous valve lift adjustment in a wide range. Significant reduction in pumping loss can be achieved when utilizing VVL and CVVL devices due to reduced throttling or even un-throttled operation in gasoline engines. In addition, other engine and combustion concepts such as HCCI/CAI combustion, Atkinson and Miller cycle operation and cylinder deactivation can be realized by using these systems [61–67]. Electronic and electro-hydraulic valvetrains have also been explored for camless operation and a more flexible control of valve actions but they are not widely employed on mass production engines because of their complexity, durability and cost.

Furthermore, the intake charge motion also can be adjusted by using devices such as a tumble flap which is fitted to some VW and Audi GDI engines in order to

increase the tumble motion at low loads by blocking the bottom half of the intake ports [68]. Swirl motion also can be increased by deactivating one of the two intake valves or adopting asymmetric intake valve profiles [32,65,69]. These systems can improve the in-cylinder air charge motion and turbulence which can in turn improve the air-fuel mixing and combustion process and ultimately reduce the fuel consumption.

2.3.6 Variable Compression Ratio

Increasing the compression ratio results in improvement of theoretical efficiency. Low compression ratio is one of the key reasons for gasoline engines delivering lower fuel conversion efficiency compared to diesel engines, which is because of the detonation limit at high load operating conditions. This issue can be addressed using variable compression ratio (VCR) technology, which enables the SI engine to benefit from a higher CR at low load area where the engine is not knock limited and reduces CR at high load operation where the engine operation is knock limited. Several types of VCR systems have been developed and 5% to 12% fuel consumption reduction has been reported. The benefits can increase significantly by applying VCR simultaneously with other technologies such as lean burn, CAI/HCCI, VVL, Atkinson/Miller cycle [70–73]. Durability, system complexity and cost are still the main issues of the VCR technology which limit the application of this system on mass production engines. Despite the mentioned challenges, this is a promising technology due to its excellent potential in reducing gasoline engine CO_2 emission. Nissan has introduced the VCR technology in their premium brand vehicles in 2017 [74].

2.3.7 Cooled Exhaust Gas Recirculation

The history of exhaust gas recirculation (EGR) goes back to 1970s when this technology was used in order to reduce emissions and fuel consumption in gasoline engines. EGR is used as a diluent to dilute the cylinder charge while maintaining stoichiometric air/fuel ratio. This can reduce the pumping loss and the in-cylinder gas temperature. Lower in-cylinder gas temperature results in a reduction in thermal losses and dissociation as well as reducing knock tendency [75–78]. Recently, this technology has regained more interest due to the introduction of boosted downsized GDI engines which are more prone to knocking combustion. This technology can help to mitigate knock by reducing the in-cylinder charge temperature, thus there is a potential to increase the compression ratio on the engine for lower fuel consumption [2,79–81]. In addition, EGR is one of the key technologies used in the most efficient production SI engine introduced by Toyota which has the highest thermal efficiency of 41% [82].

2.3.8 Pre-chamber combustion systems

Lean burn combustion technologies have been developed since 1970s in order to reduce fuel consumption and emissions of conventional spark ignition engines. Lean burn combustion refers to burning the fuel inside the combustion chamber with excess air which has several advantages compare with conventional stoichiometric combustion [83]:

- Lower nitrogen oxides emissions due to lower combustion temperatures
- Lower heat loss during combustion which decreases fuel consumption

- Allowing the engine to run less throttled, therefore significantly reducing the pumping losses. In this case the power is controlled by varying the amount of fuel in the cylinder, hence throttling is reduced
- Lower CO_2 emissions due to reduced fuel consumption

By running an engine lean, in addition to emissions reduction, engine thermal efficiency is also increased. This can be explained by Equation 2-1:

$$\eta_{th} = 1 - \frac{1}{CR^{\gamma-1}} = \frac{W_{out}}{Q_{in}}$$

Equation 2-1

Where CR is compression ratio and γ is the specific heat ratio ($^{C_p}/_{C_v}$).

The excess air in lean burn combustion increases the specific heat ratio (γ). Therefore, thermal efficiency can be increased according to the above equation.

Furthermore, lean burn technology has some disadvantages such as compromised combustion stability and three-way catalyst incompatibility. Nitrogen oxides emissions are also another issue in lean burn combustion, since significant improvements in NO_x emissions only begin to appear at the lean limit of conventional spark ignition engines which is approximately $\lambda \sim 1.4$. In addition, efficiency of the three-way catalyst decreases significantly if air/fuel ratio varies from stoichiometric. By running an engine lean, combustion stability decreases, and unburned hydrocarbon emissions increase due to partial burn and misfiring cycles. These problems can be addressed by improving the ignition system to increase ignition energy or intensifying turbulence in combustion chamber to increase flame velocity [84].

One method to produce additional ignition energy is called jet ignition system. This system utilizes a pre-chamber combustion system in order to initiate the combustion of lean air fuel mixture. By using this method, high combustion stability is achievable in a wide range of air fuel ratios. Short combustion duration is possible by using this method and that is due to existence of a large number of distributed ignition sites which ensure the relatively small flame travel distances [84]. In order to achieve fast burn rates in lean burn engines, high ignition energy, long ignition duration and multiple distributed ignition sites are required [85].

A comprehensive review on pre-chamber combustion systems with particular attention to jet ignition system has been done by [84]. This review includes references to patents and SAE papers for pre-chamber systems and is arranged in chronological order.

Using pre-chamber in spark ignition engines was first started in the beginning of the twentieth century with the Ricardo Dolphin engine [84]. In this engine fuel rich mixture entered the pre-chamber via an auxiliary intake valve and is ignited by a spark plug which then ignited the lean mixture in the main chamber. In addition to this design, torch cell combustion chambers deliver a simpler design by eliminating the need for auxiliary pre-chamber fuelling. Instead in torch cell combustion chambers, pre-chamber just contains a spark plug and is filled by the main chamber fresh charge during compression stroke. Therefore, by igniting the charge trapped in the pre-chamber, a turbulent torch is produced which then ignites the main chamber charge. Turbulence Generating Pot (TGP) is an example of this kind of pre-chamber which was developed by Toyota in order to extend the lean misfire limit as well as increase flame propagation velocity [84]. The

experiments show that the configuration of the TGP and the spark plug location has direct effect on the lean misfire limit and the combustion velocity. The results also reveal that the jet flame produced by TGP creates a strong turbulence in the main chamber which increases the flame propagation velocity and reduces the NO_X emissions [84].

Honda's Compound Vortex Controlled Combustion (CVCC) is a successful example of pre-chamber stratified charge engines [84]. In this engine, pre-chamber contains an auxiliary valve in order to draw in the rich mixture which is prepared by carburettor (in modern engines a separate pre-chamber fuel injector is used). By igniting the rich mixture in the small pre-chamber, a regular flame front is produced which exits into the main chamber [84]. Many other pre-chamber combustion systems have been developed since that time in order to increase the lean burn limit of the spark ignition engines. Nilov engine, Broderson Conta engine, Heintz Ram Straticharge engine, Porsche SKS engine and GM Electronic Fuel Injection Pre-chamber Torch Ignition engine are the main examples of the engines with pre-chamber combustion systems [84].

Pre-chamber combustion systems or divided combustion chamber systems can be classified by:

- Pre-chamber volumes (small or large)
- Auxiliary pre-chamber fuelling (stratified charge)
- Size of orifices which connect the pre-chamber to the main chamber (small or large)

Using smaller orifices connecting the pre-chamber and the main chamber, results in faster traveling of the burning mixture through the orifices. Although, this

extinguishes the flame, the reacting active radical species reignite some distance away from the pre-chamber and initiate the combustion in the main chamber. In addition, deeper penetration of the flame jets into the main charge is another advantage of smaller orifice size. These igniters called jet igniters which are a subgroup of the divided chamber stratified charge concept [84,85].

Figure 2-25, shows the LAG (Lavinia Aktivatisia Gorenia or Avalanche Activated Combustion) combustion system which was the first jet ignition engine designed by Gussak [86]. Maximum optimization of the LAG process can be achieved by a pre-chamber size of 2-3 percent of the clearance volume, an orifice area 0.03-0.04 cm^2 per 1 cm^3 of pre-chamber volume and by an orifice length to diameter ratio of ½ [84,86].

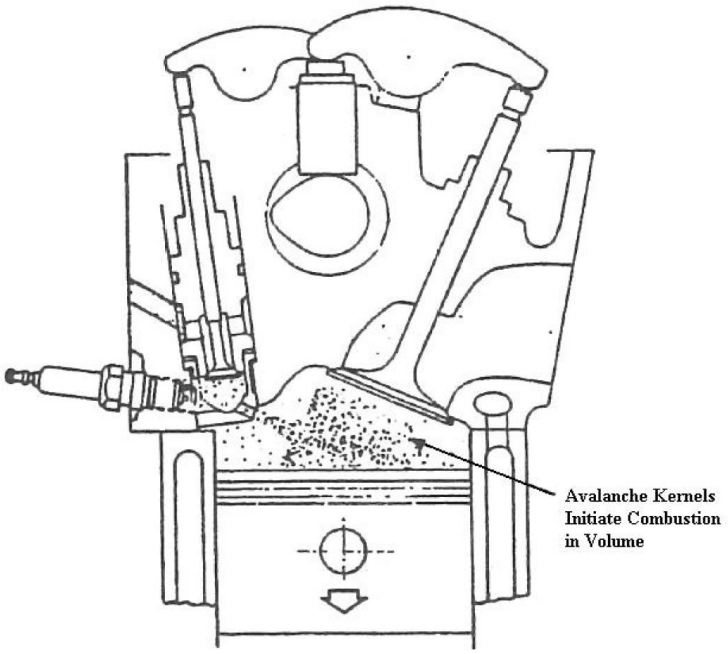

Figure 2-25 The Lag combustion system [84,86]

An experimental investigation which was made by Ford in order to analyse the effect of torch nozzle orientation on power, burn rate, fuel consumption and

exhaust emissions shows that by directing the torch nozzle diametrically across the combustion chamber, the power and the burn rate are maximised, and exhaust emissions are inversely proportional to burn rate and ISFC. In addition, it was found that the torch chamber can be used as a means to increase the turbulence after combustion to improve the mixing of the quench layer and therefore reduce the hydro carbon emissions. This was achieved but at the expense of increased fuel consumption [84].

Bosch also developed a swirl chamber spark plug which was able to reduce fuel consumption and exhaust emissions by increasing the speed and uniformity of the energy conversion process. This system consists of a small chamber houses the spark plug and called ignition chamber. This small chamber has 4 tangential and 1 central orifices. A significant swirl motion of the charge is created in the compression stroke by the 4 tangential orifices and to initiate combustion, the ignition spark moves from a small lateral pin on the electrode across to the wall of the swirl chamber. The swirl motion in the ignition chamber creates a rapid combustion and 5 torch jets which guarantee a fast and uniform energy conversion process in the main chamber [84].

In an investigation, MAHLE Powertrain suggest a new advanced spark-initiated pre-combustion chamber called Turbulent Jet Ignition system (Figure 2-26). This new pre-chamber design can be easily used instead of spark plug in conventional spark ignition engines and has the advantage of very fast burn rates of the main charge because of the ignition system creating multiple, widely distributed ignition sites, which consume the main charge instantly [84,87–91]. Moreover, in this pre-chamber design, partially combusted pre-chamber products initiate combustion in the main chamber which results in a high ignition energy. Therefore, the level of

dilution can be increased due to the fast burn rates compare to combustion in conventional spark ignition engines.

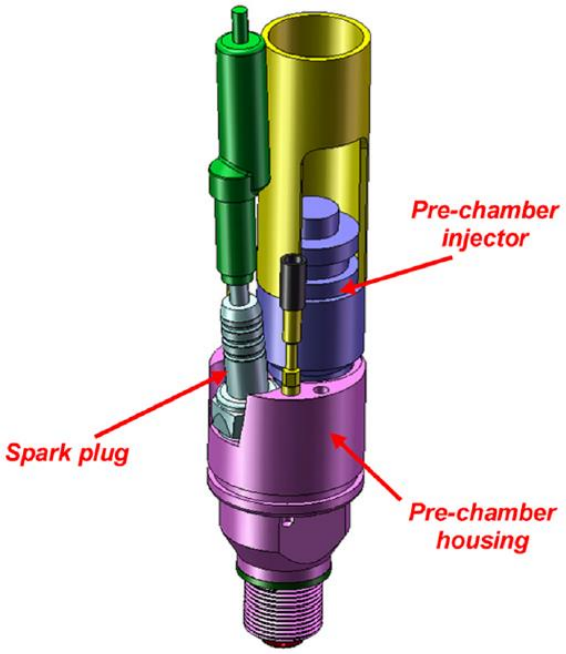

Figure 2-26 The Turbulent Jet Igniter by MAHLE Powertrain [84,91]

Furthermore, peak net indicated thermal efficiency values of 42 percent was achieved for the previous Turbulent Jet Ignition experiment in a standard modern engine platform. In addition, pre chamber combustion system has the ability to tolerate up to 54 percent mass fraction diluent (EGR and excess air) at the world wide mapping point of 1500 rev/min, 3.3 bar NIMEP (~2.62 bar BMEP), which results in an 18 percent improvement in fuel economy and near zero engine out NO_x emissions [89].

The experiments were performed on a single cylinder engine at the world-wide mapping point in order to increase the dilution level by modifying the flame kernel development inside the very small and rich pre-chamber environment. This experiment conducted several tests on different factors such as variations in spark

plug type, orientation, location and electrode gap for the spark plug initiated pre-chamber combustion system which has influence on dilution limits in conventional spark ignition combustions systems.

This specific pre-chamber has a very small volume, auxiliary pre-chamber fuelling and 6 small orifices which connect the pre-chamber to the main chamber. The orifices were selected to be small since this increases the velocity of the turbulent jet through the orifice and then the reacting pre-chamber products cause ignition of the charge in the main chamber through thermal, chemical and turbulent effects with a distance from the pre-chamber, therefore a distributed ignition system is created. Moreover, turbulent jet can penetrate further into the main charge by using smaller orifices. In addition, the reason for using a small pre-chamber volume other than a large one is to have lower HC (hydrocarbon) emissions and a negligible power loss due to the reduced combustion surface area and crevice volume [91].

The main chamber fuel is supplied by a PFI fuel system to achieve a homogeneous lean mixture in the main chamber; however, a DI fuel system is used to provide fuel in the pre-chamber. Under normal operating conditions fuel stratification is achieved in the pre-chamber by injecting a small amount of fuel just before ignition in the vicinity of the spark plug. Hydrocarbon (HC) and CO emissions can be controlled and heat losses can be reduced by locating the spark plug in a small pre-chamber with the volume of roughly 2 percent of the clearance volume [91].

The ignition system in the Turbulent Jet Ignition system produces multiple and distributed ignition sites which burn the main charge rapidly and with minimum combustion variability. Therefore, very fast burn rates can be achieved which is

the main benefit of this ignition system. As a result of fast burn rates, levels of dilution can be increased compare to conventional SI engines. Another advantage for the fast burn rates is that the base compression ratio can be increased compare with conventional SI engines. This is possible as the increased flame propagation (reduced flame front travel path) associated with a distributed ignition system decreases the likelihood of end-gas knock because of the reduced residence time.

The followings are the most important features of the MAHLE Turbulent Jet Ignition system [91]:

- Using very small pre-chamber volume which minimizes heat loss, HC emissions, pre-chamber residual gas, surface to volume ratio effects and crevice volume.
- Connecting the pre-chamber to the main chamber by one or more small orifices which promote flame quenching and penetration into the main chamber.
- Required fuel for the pre-chamber is provided by a separate flush mounted electronically controlled direct injector which gives a rich mixture in the pre-chamber while the main chamber is heavily diluted.
- Required fuel for the main chamber is provided by an electronically controlled PFI injector which allows homogeneous or stratified main chamber mixtures and HC and NO_x emissions control.

Figure 2-27 and Figure 2-28 show the Turbulent Jet Igniter, and the pre-chamber and nozzle assembly respectively.

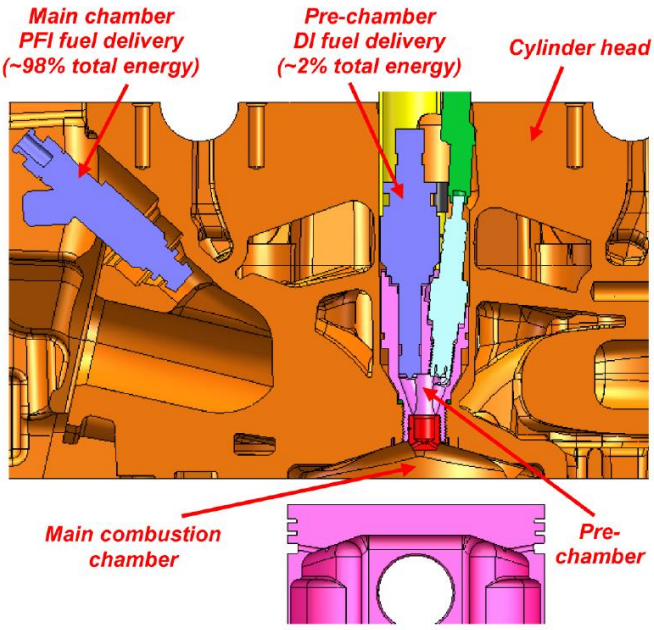

Figure 2-27 The centrally installed Turbulent Jet Igniter in the pent roof combustion system of the test engine [91]

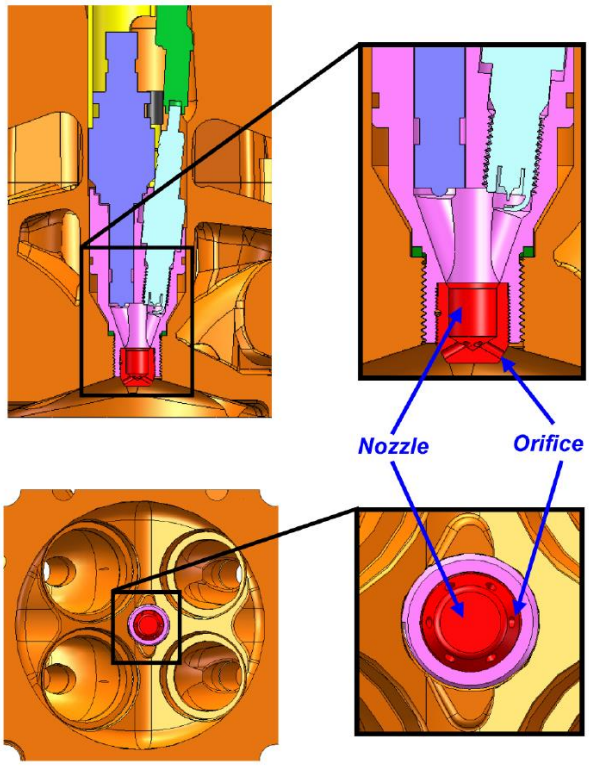

Figure 2-28 The Turbulent Jet Ignition pre-chamber and nozzle [91]

Table 2.3, shows the geometric specifications of the pre-chamber design, which was used in the experiments.

Table 2.3 Turbulent Jet Ignition pre-chamber specifications [91]

Pre-chamber Volume	1.3 cm^3 (2% clearance volume)
Number of Orifices	6
Orifice Diameter	1.25 mm
Orifice Length	3 mm

According to the experimental results, the increased air dilution limit of the Turbulent Jet Ignition compared to spark ignition engine shows that this pre-chamber combustion system can operate with sufficient stability even with exhaust lambda of over 2. Enhanced combustion burn rates leads to this increase in operating range of the engine. In overall, Turbulent Jet Ignition system can tolerate 50% more diluent mass compare to spark ignition combustion and therefore, the fuel consumption is improved by 18% [91].

In this research pre-chamber burning profile was investigated as an important factor to enhance the jet formation and penetration into the main chamber. In order to improve the burning ability inside the pre-chamber, it was proposed to modify the location of the spark plug electrode tip by rotating the spark plug 90 degree and 180 degree. This changes the location of the ignition point from the centre of the pre-chamber to the corner, and therefore minimizes the wall and quench-effects associated with the flame propagation inside the pre-chamber [89]. The results of changing the orientation of the spark plug show that these changes have no effect on extending the dilution limits. Therefore, it can be concluded that the

location of the spark plug electrode and the location of the ignition point inside the pre-chamber have no influence on the combustion inside the pre-chamber [89]. Moreover, the effects of varying the spark plug electrode gap were also investigated and the results show that increasing the spark plug gap extends the excess air and excess fuel dilution limits slightly. In addition, there is a minor improvement in the 0-10% MFB inside the pre-chamber. These minor improvements also can be seen at the lean and rich combustion stability limits which are approximately up to 0.04 lambda. The mixture inside the pre-chamber is always rich hence; the discharge current and duration have a negligible influence on flame kernel development and ultimately combustion in the pre-chamber. As a result, combustion in the pre-chamber is not highly influenced by increasing the spark plug gap [89].

Furthermore, three different spark plugs were also tested to find out the effect of spark plug type on the combustion stability. The results show that there was almost no or very small changes at the combustion stability limits. Therefore, it can be concluded that the spark plug changes have very small or no effect on the Turbulent Jet Ignition system due to the main chamber combustion which is initiated by the pre-chamber ignition jets and produce multiple ignition sites.

Ultimately, the influence of spark plug depth variation inside the pre-chamber was studied and the results show that the spark plug recess has a significant effect on combustion stability limits relative to previous tests. Up to a 0.1 lambda for the lean dilution limit and a 0.04 lambda for the rich stability limit was recorded by changing the spark plug depth. By varying the spark plug depth inside the pre-chamber [89]:

- The volume of the pre-chamber will change slightly

- The quantity of residual gas trapped near the spark plug at the time of ignition also will change

Since the combustion system is unable to scavenge the residual gas in the region of the spark plug, the quantity of residual gas in that region is the key factor in differing diluent limits.

The following are the limitations and potential difficulties associate with this ignition system designed by MAHLE Powertrain:

- The system cannot be applied on all the available engine designs and it is required some modifications on cylinder head and sometimes on the engine block as well since the majority of engines are designed with an specific space and place for the spark plug and a separate place for the fuel injector (sometimes far from each other). Therefore, sometimes it is not possible to accommodate the larger pre-chamber igniter which includes both the spark plug and the fuel injector in a smaller space.
- Results have shown that the current Mahle Turbulent injection jets operation is limited at higher load due to the higher boost required for additional air in the lean-burn mixture and restricted to low and medium engine speeds due to poor scavenging of the prechamber.
- Combustion initiation inside the pre-chamber is really important in this system since the pre-chamber is unable to scavenge the residual gas trapped near the spark plug at the time of ignition. Especially when the spark plug is not flush mounted this increases the quantity of the residual gases inside the pre-chamber. Therefore, combustion initiation inside the pre-chamber becomes much harder.

- Since combustion in the heavily diluted main chamber is produced by the chemical, thermal and turbulence effects of the propagating jets exiting the rich pre-chamber, it is crucial to ensure that these effects are able to start combustion in the main chamber at all the engine operating conditions.
- The combustion of lean-burn mixture would require additional lean-NO_x aftertreatment and sophisticated engine operation controls to meet the transient vehicle operations.

2.4 Dual Injection System Development and Application

The gasoline direct injection (GDI) is a cost-effective option for improving the efficiency and the performance of the gasoline engines and has been introduced by several manufacturers as it was mentioned earlier. These engines initially used lean-burn stratified operation in order to improve the fuel economy. The issue with stratified operation is increased NO_x and smoke emissions due to existence of a relatively rich mixture near the spark plug. Hence, more recently in order to meet the ever so stringent emission regulations, DISI engines have been modified to run under homogeneous stoichiometric operation so that the 3-way catalyst can be used effectively to meet the emission regulations. The main advantages of homogeneous stoichiometric DISI engines over conventional port fuel injection (PFI) engines are higher full load performance (due to higher volumetric efficiency and reduced knocking tendency which enables around 1 to 2 points increase in compression ratio), improved fuel consumption and lower unburned hydrocarbon, NO_x and CO emissions. However, compared to the port-fuel injection, the direct injection engines (even with homogeneous stoichiometric mode) is more likely to produce less homogeneous mixture due to shorter mixing time and sometimes fuel

impingement on cylinder walls. This can lead to the production of soot particles from fuel rich regions and higher cyclic variations. With the introduction of particle number limit in EURO VI, it is imperative to minimize the particle emissions from gasoline DI engines [2,21,38,92].

As it was mentioned earlier, the incapability of conventional stratified charged lean-burn combustion system to produce ultra-low NO_x and particle emission, and also the challenges such as the high ignition energy required and the slow flame speed in homogeneous charged lean-burn combustion system, have led to a considerable research and investigation on HCCI combustion system [2,36,43,44].. Although, fuel consumption and NO_x emissions can be reduced with this combustion mode, much research and development works are still needed prior to such combustion technologies being incorporated in the mass produced engines due to factors including the narrowness of the potential operating range and the challenge represented by controllability in response to transient operations [2,36,37,44].

Because of these complexities and limitations of current lean burn and HCCI/CAI combustion technologies, almost all the current gasoline direct injection engines operate with the homogeneous stoichiometric mode and a 3-way catalyst is used to meet the emission regulations. The fuel economy and power output improvement in typical test cycles is then mainly achieved by the engine downsizing approach using a smaller turbocharged gasoline DI engine in place a larger naturally aspirated PFI engine. However, future emission regulations will focus on real driving conditions which normally result in higher fuel consumption and exhaust emissions compared to the current testing conditions. Hence,

combustion processes have to be optimized significantly in order to meet future emission standards under real driving conditions and/or in the World Harmonized Test Procedure (WLTP) [93,94].

Combustion processes can be improved by means of advanced injection strategies such as split (using direct injector with multiple injections) and dual injections (using port and direct fuel injectors simultaneously to inject one or two fuels) [95–98]. Many studies have revealed that the split injection can increase the high load performance of the GDI engine due to reduced knocking tendency with a late injection and at the same time producing an acceptable volumetric efficiency with an early injection [99,100]. Split double (early and late) injections enables a greater control on the mixture formation and flow field over the early flame development stage of combustion [101–104]. Thus, higher net indicated mean effective pressure (NIMEP), combustion stability and total heat release for the same fuel mass, which is consistent with the increased flame propagation speed can be achieved with split injection [35,105–109]. Furthermore, Split injection also can reduce soot emissions by reducing spray penetration which reduces the piston and wall wetting. UHC can also be reduce by containing the fuel vapor more effectively within the piston bowl with this method [40,110–115].

Dual injection systems which utilize both PFI and DI injectors simultaneously are also used in some production engines and have been assessed by other researchers [95,116]. This system provides a great flexibility in terms of mixture preparation and combines the benefits of direct injection in terms of improving engine performance and benefits of port injection in terms of exhaust emissions. Dual injection systems enable the use of:

- Hybrid combustion (homogeneous-stratified combustion) to improve mixture preparation, increase lean combustion stability and reduce smoke emissions [98]
- Two different fuels (such as biofuels and gasoline or methane/CNG and gasoline) in order to optimize combustion processes and reduce particulate emissions. Also improving the high load efficiency by means of octane on demand concept which utilizes a base low octane fuel and a booster high octane fuel to suppress the knock when necessary [117–132].
- Water injection (through PFI or DI injectors) for knock suppression in GDI turbocharged engines [133–137]

These configurations can greatly affect mixture formation and properties, and combustion processes, hence changing the efficiency, and gaseous and particulate emission formation.

Dual injection systems, combined PFI and DI injection, can improve both combustion efficiency and suppress knocking at load speed high load. Combustion efficiency can be improved by using PFI which can create a more homogeneous mixture compare to the DI due to a more time available for the fuel evaporation. Also, knocking tendency can be reduced by using a late DI injection during compression stroke which can reduce the charge temperature and allow the use of more advanced spark timings (closer to optimum) and consequently better fuel economy can be achieved. In addition to the above benefits, PFI / late DI can be used as an effective method to extend the lean limit of the engine by creating a reliable source of ignition near the spark plug to ignite the overall lean mixture near the periphery of the combustion chamber. In this operation, a lean mixture is

present throughout the combustion chamber by injecting most of the fuel through the PFI injector. Then an ignitable mixture is created at the spark plug through the late direct injection of a small quantity of fuel [98]. This mixture can be ignited easier which increases the combustion stability especially during lean operation.

Toyota introduced simultaneous fuel injections in the intake ports and in the cylinders of their V-6 3.5-liter gasoline engine (2GR-FSE), in order to improve mixture homogeneity at low speeds and part loads in the absence of a large-scale charge motion. Tests showed that using DI and PFI simultaneously (with an optimized DI ratio of 30%) can reduce fuel consumption and torque fluctuations, while increasing the speed of combustion compared to using DI or PFI exclusively [95]. In the case of higher engine speeds (above 2000 rpm) direct injection alone was able to provide a sufficiently homogeneous mixture due to the high piston speed and similar combustion efficiency to PFI/DI operation could be achieved. In addition, it was stated that the PFI / DI operation tended to lead to the formation of deposits on the injector due to higher injector tip temperature with reduced fuel flow rate in the DI injector. Thus, simultaneous PFI / DI injections were not used at high speeds [95].

Zhu et al. [96] conducted a research using a dual (PFI / DI) injection system to study the combustion characteristics of a single-cylinder engine fuelled by gasoline and ethanol. Three different fuelling cases where tested: a) gasoline PFI and DI, b) gasoline PFI and ethanol DI, and c) ethanol PFI and gasoline DI. In the case of PFI/DI gasoline injections operation, the IMEP and peak cylinder pressure were found to decrease with increased DI ratio, accompanied with slower combustion.

In another experimental investigation Kim et al. [120,121] and Cho et al. [122] examined the effect of ethanol/gasoline dual fuel operation. Ethanol was delivered by two port fuel injectors and gasoline was delivered directly into the cylinder by a DI injector. The results showed that knock was suppressed and IMEP was improved. HC and particulate emissions also decreased by using ethanol.

Dual fuel spark ignition (DFSI) combustion is also used as an effective method to reduce the particulate number associated with conventional GDI engines. Alcohol/gasoline with different ratios and injection configurations (PFI/DI) are the most common fuels used in these experiments which can significantly reduce PN [123,124].

An experimental investigation was performed by Di Iorio et al. [97,125,126] and Catapano et al. [127,128] on a single cylinder optical engine in order to study the methane-gasoline dual fuel combustion. In this study methane was injected directly into the cylinder and gasoline was injected in the intake ports. Different methane /gasoline ratios were tested in both stoichiometric and lean conditions. Higher flame front propagation speed and lower exhaust emissions were achieved with dual fuel operation compared to PFI gasoline operation.

Characteristics of SI combustion were also examined by Viollet et al. [130] when operating on three different dual fuel configurations. One low and three high RON fuel were delivered by DI and PFI injectors and the experimental results were compared with the baseline gasoline operation in terms of fuel economy, knock intensity and combustion duration.

Effect of water direct injection and gasoline port fuel injection was experimentally investigated by Kim et al [137] on a 1.6 L naturally aspirated prototype engine with

a compression ratio of 13.5. The engine knock was suppressed at medium load condition therefore the spark was more advanced and as a result lower BSFC was recorded. At full load water injection also helped to reduce the mixture temperature, thus eliminated the need for fuel enrichment. The amount of water injected was optimized since too much water deteriorated the combustion efficiency. In addition, the benefit of water injection was less at higher engine speeds due to reduced tendency to knocking combustion.

In the above works, a side mounted multi-hole DI injector was used and the DI injection timings were limited to mostly early injections during the intake stroke. In this study, experiments have been carried out on a highly downsized DI gasoline engine capable of 120kW/litre with a centrally mounted piezo actuated outward opening injector. The focus is on the effect of the late DI injection timings, ratios and its effect on combustion temperature and knock and lean combustion stability limit with simultaneous PFI / late DI and early DI / late DI injections. The fuel economies, combustion characteristics, gaseous and particulate emissions of the engine under both PFI / late DI and DI / late DI strategies are presented and compared to those of single early DI and PFI-only operations.

2.5 Water Injection Technology

2.5.1 History, development and application of water injection for ICEs

Introduction of the more stringent emission regulation has led to a shift towards boosted downsized GDI engines. Hence, the modern engines will be run more frequently under medium and high loads with greater intake pressures. Under such high intake pressures GDI engines are more prone to abnormal combustion.

Water injection is one of the technologies that recently has regained interest due to its ability to reduce hazardous emissions (particularly NO_x emissions) and increase efficiency simultaneously by mitigating knock in boosted downsized GDI engines [137–141]. Water injection into a combustion chamber is not a new technology. This concept was used in military aircraft piston engines even before the World War II in order to increase power output for short durations when high thrust is required such as during take-off or dogfights [142]. Water injection was mostly used in aviation industry [143] and only a few number of high performance automobiles with supercharger or turbocharger were equipped with water injection system. The 1962 Oldsmobile F85 with its Jetfire engine and Saab 99 Turbo S are among the first few cars with water injection [144]. The interest in water injection nearly vanished by introduction of more powerful engines with new technologies such as the charge-air cooler which could reduce the temperature of the hot compressed charge air to prevent knock. However, more recently due to the introduction of more stringent emission regulations water injection has been reintroduced. BMW M4 GTS is an example of recent developments in water injection which benefits from intake manifold water injection to increase performance [139,145,146]. There are several configurations for water injection systems in ICEs:

- Fumigation or water injection into the intake manifold [133,134,136,147–164]
- Water and fuel emulsion or injection of water-fuel mixture directly into the combustion chamber [159–162,165–173]
- Direct injection of water into the combustion chamber [135,163,174–181]

Fumigation or intake manifold water injection is used in both spark ignition (SI) and compression ignition engines (CI). This method can increase the charge density and therefore volumetric efficiency by decreasing the intake charge temperature. Water is injected in the intake through a fine spray to create a homogeneous mixture of water and air or water, fuel and air and deliver this mixture into the cylinder. A portion of the injected water evaporates in the intake port by the heat from the ports, valves and the intake air and reduces the intake charge temperature during the intake stroke (followed by volumetric efficiency increase). The rest of the injected water ultimately evaporates during the compression stroke due to the compression heat and decreases the mixture temperature. In this case. the cooling effect of water vaporization leads to a lower in-cylinder temperature and pressure which in turn reduces the compression work [147]. Cooling and dilution effect of water injection also results in decreased NO_x emission. In CI engines this method is used mostly for NO_x emissions reduction. Some studies also investigate the effect of ethanol fumigation on NO_x emissions in CI engines as ethanol has a comparable latent heat of vaporization to water.

Water-fuel emulsion is typically used in CI engines particularly for NO_x and smoke reduction. In this case emulsified fuel is injected directly into the cylinder by means of a high-pressure injection equipment. Hybrid injectors can also be utilized for simultaneous injection of water and fuel through the sequential injection of diesel-water-diesel [173]. These injectors are specially designed with separate water and fuel passages which can inject sequentially. Compared to EGR, water injection shows significantly higher performance in NO_x reduction. As the pilot injected emulsified fuel is increased, combustion phasing is retarded due to water evaporation which leads to an increase in pre-mixed combustion. Low O_2

concentration of 15% in this condition makes it possible to simultaneously reduce NO_x and smoke emissions.

Direct injection of water into cylinder can bring additional benefits and flexibility compared to the port injection. Greater charge cooling and higher volumetric efficiency can be achieved with direct injection of water since the water cools down the in-cylinder charge only, and not the intake valves and ports (similar to port fuel and direct fuel injection comparison). In addition, when injecting large amount of water in the intake manifold, the injected water (liquid and vapor) can take up some volume of the intake charge which reduces volumetric efficiency. Thus, the maximum water injection mass can be limited with manifold injection. On the other hand, with direct injection of water the maximum injected water mass, injection timing and pressure can all be controlled with more flexibility as the water is injected directly into the cylinder without any penalty for volumetric efficiency. One of the main advantages of direct injection which led to emergence of GDI engines and their significant increase in market share over PFI (port fuel injection) engines was also such charge cooling effect of the injected fuel inside the cylinder. Water is reported to have a heat of vaporization of 2257 kJ/kg (at vapor or saturation pressure of 1.0142 bar and temperature of 100 °C which is the standard boiling point) which is around six times higher than that of gasoline with 305 kJ/kg, hence a greater charge cooling is expected with direct injection of water [19].

Direct injection of water is also investigated in HCCI (homogeneous charge compression ignition) engines to extend the operating area of the engine map. Several studies reported that water injection could improve the mean effective pressure (MEP) in HCCI engine which was otherwise limited by the fast heat

release rate of the advanced combustion phasing. There are relatively few researches that investigate the effect of port or direct water injection in downsized turbocharged GDI engines. Introduction of boosted downsized GDI engines shifted the operating range of gasoline engines to a higher load conditions which increases the knock tendency of the engine. Thus, technologies such as cooled EGR and water injection are necessary to reduce the charge temperature and therefore knock sensitivity. Injected water acts as an inert gas to decrease the O_2 concentration and increase the heat capacity of the charge [137–141]. Port injection of water has proved to be significantly beneficial due to thermal efficiency gain achieved by increasing the anti-knock characteristics of the fuel [151]. It is reported that the research octane number (RON) of fuel could be boosted from 70 to 93 when the water / fuel ratio was increased to 1.5 in a CFR (cooperative fuel research) engine [147,151].

Thermal efficiency gains can be increased even further with direct injection of water by allowing the use of higher compression ratios [137,141]. Direct injection of water enables the advancement of combustion phasing to the optimum point and results in a significant fuel consumption reduction. Although direct water injection brings several advantages in terms fuel economy and emissions, the risk of cylinder wall wetting by the water spray impingement and the possibility of oil dilution or contamination also has to be considered carefully as it might reduce the life span of the engine [179]. Therefore, there are several studies which investigate the effect of direct water injection timing and pressure using numerical simulation and in-cylinder spray visualization techniques [179].

As it was mentioned earlier, there are few studies that specifically investigate the effect of water injection on GDI engines [136,137,139,141,148,152–157,177]. Efficiency improvements in the range of 3 up to 35% were reported in these studies by utilizing water injection at medium and high loads mainly due to the increased knock resistance of fuel, advancement in combustion phasing and elimination of fuel enrichment. There are several factors such as injection configuration and position, injection timing and pressure, water/fuel ratio, spark timing and fuel octane number that need to be considered carefully when utilizing water injection. The impact of positioning of the intake port water injector was investigated in the literature and found to be critical for water consumption, fuel efficiency and power delivery [139].

Since manifold water injection has already proved to be highly beneficial, direct water injection is also researched and exhibited even higher potential compared to the port injection system. It is reported that direct water injection demonstrates higher efficiency especially when it is combined with high injection pressures. FEV investigated a high pressure separate direct water injection system where water injection was combined with a high compression ratio and Miller cycle in order to exploit the knock suppression potential also at lower engine loads. CO_2 emission reduced by around 5% in the WLTP when compared to an engine that already features variable compression ratio. Further potential was gained when EGR was applied as well [137,139–141,182].

In the above experimental works, direct injection of water is studied mostly without a detailed and clear understanding of port injection of water in modern boosted GDI engines first. In this study, experiments have been carried out on a highly

downsized boosted GDI engine capable of 100-160 kW/liter [183–187]. In this study the engine is equipped with a centrally mounted piezo actuated outward opening injector. Water is injected into the intake ports by means of a PFI injector and gasoline is injected directly into the cylinder. Gasoline with three different octane numbers of 95, 97 and 100 were also tested to find out the effective octane-number of water at different test points. The efficacy of water as an anti-knock is also considered at 6 steady state test points. In addition, water injection was performed during both intake valve close and open to understand the effect of two injection timings on water vaporization. Effect of water injection on gaseous and particulate emissions are also presented and discussed in this thesis.

2.5.2 Limitations and further developments

There are several factors that need to be considered carefully with water injection. The initial work in this study was performed with constant injection timing and pressure for water. Although water was injected in the intake port through a PFI injector, different injection timings (specifically comparing the water injection into the closed intake valves with water injection into the open intake valves) and pressures can lead to slightly different results. This is particularly important in combustion systems with direct injection of water into the cylinder.

In this study fuel was directly injected into the cylinder by DI and water was port injected by PFI. However, direct injection of water can be more effective similar to direct injection of fuel as it is also reported in the literature [188]. With direct injection of water higher cooling effect is expected from the same amount of water compared to port injection. In addition, direct injection of both fuel and water can create a synergy and increase the effectiveness of both systems [139–141,182].

On the other hand, this leads to a more complex control and calibration process to optimize different parameters such as injection quantity, timing and pressure for both fuel and water. The design of the combustion system with two direct injectors also is another issue which makes the optimization more complex.

One of the main concerns of water injection in the engine is the possibility of damage and wear caused by water. Injecting large quantities of water can increase the risk of condensation or can form a water film on the cylinder wall and can result in oil dilution when the piston moves in the cylinder [179]. This can cause problems in long term and can decrease the lifespan of the engine. In-cylinder temperature and pressure play a key role in full vaporization of water droplets especially in direct injection of water as existence of water droplets can potentially increase the risk of unwanted damage to the engine. In this study water was injected into the closed intake valves during the late stages of compression stroke so there was 180 CAD for evaporation to take place in the intake port. However, when water quantity is large, or injection takes place into the opened intake valves, full vaporization of the injected water is unlikely to happen in a low pressure and temperature environment during intake stroke which increases the amount of water droplets. With direct injection of water, the full vaporization of large quantities of water is even less likely as there is less time available for vaporization after injection compared to port injection system.

In addition, distribution of water droplets in the cylinder can be affected by the spray targeting with respect to different injection timings. These water droplets can be a source of flame quenching when they are not fully vaporized before the combustion takes place. Optical visualization and 3D simulation (computational fluid dynamics (CFD)) can be effectively used to better understand the water spray

behaviour (targeting, penetration, distribution and vaporization) in the intake port and inside the cylinder. It is worth noting that an alternative ignition system might be required depending on the water injection system in use.

Improvement in ignition system is another which could also enhance the effectiveness of the water injection concept even further by reliably promoting a fast and safe ignition of the in-cylinder mixture which contains air, fuel, residual gas, EGR and water.

Ultimately, compatibility of the materials used in water injection system needs to be reassessed. Water delivery and injection systems are the main parts to be redesigned due to different properties of water and fuel (for instance lubrication effect of fuel in fuel pump and injector which does not exist for water). Other aspects such as protection against water freezing in the delivery pipes and tank as well as the capacity of the water tank also needs to be evaluated carefully. Water injection enables an increase in load beyond the current production levels, therefore the engine hardware strength needs to be increased in order to withstand higher in-cylinder pressures during full load operation.

2.6 Summary

The latest development and technologies used in passenger car SI gasoline engines were briefly reviewed and presented in this chapter. Strict emission regulations (CO_2 and non-CO_2 emissions) have been the main motivation for technical advancement and development of ICEs. Significant CO_2 emission reduction has been achieved through gasoline engine downsizing in the NEDC previously used for vehicle certification. Fuel consumption reduction potential of downsizing concept however is more by the introduction of more transient WLTC

and RDE in the new European legislation because of the more likelihood of knocking and LSPI occurrence in the downsized GDI engines. Dual injection systems (PFI / DI) and water injection have been developed to improve part load and high load performance of boosted downsized GDI engines. However, there is a lack of detailed and systematic analysis of the individual process and factors contributing to the overall effect observed with the application of PFI / DI and water injection. Water injection has recently regained lots of interest specially after introducing the boosted downsized GDI engines and have been investigated by researchers and automotive industry, but its merits and limitations have never been fully investigated and understood especially for modern GDI engines at extended engine operating conditions. By setting up a single cylinder GDI engine and performing well controlled experiments on such an engine, the current study will lead to much better understanding of the underlying processes and their interactions involved and therefore guide the further development of high efficiency gasoline engines.

Chapter Three

Experimental Facility and Methodology

Chapter 3 Experimental Facility and Methodology

3.1 Introduction

Due to the nature of this project which was based on an experimental research, this chapter is designed to describe the experimental methodology and all the experimental facilities used in this research to gather the data used in this thesis.in addition to the experimental facility and setup, this chapter also explains the data acquisition used in this project to collect the raw data and describes the data processing system used to analyse the raw data.

3.2 Experimental Setup

The single cylinder engine testbed is the main part of this study which is described in detail in this section. Figure 3-1 shows the schematic diagram of the single cylinder engine testbed which comprises a single cylinder engine, a dynamometer, the engine testbed, supply and conditioning systems (fuel, oil, coolant and external boost rig), a data acquisition system and measurement devices and the engine control unit with its INCA software.

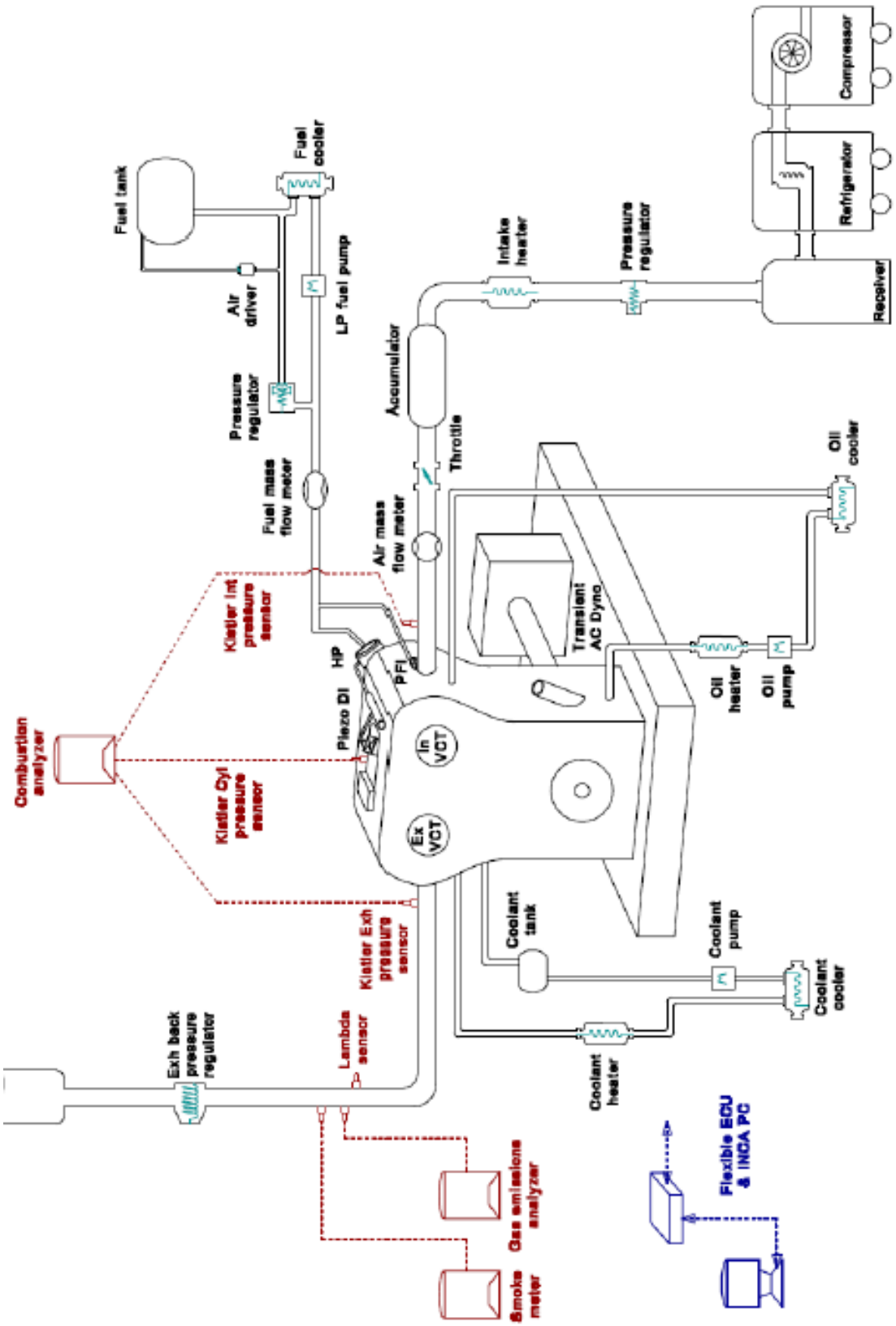

Figure 3-1 Schematic diagram of the single cylinder engine testbed

The dynamometer fitted on the testbed is a transient electrical motor type dynamometer to load the engine, maintain the engine speed during the tests and measure the engine torque output.

3.2.1 The Engine

All the experiments were conducted on the single cylinder engine. The boosted downsized single cylinder DISI engine which was used for this study comprises a high speed single cylinder Ricardo Hydra crankcase, a standard cylinder head from the MAHLE 3 cylinder 1.2l downsizing demonstrator engine [98,183–187,189,190] and a unique cylinder block designed to couple the cylinder head to the crankcase. Figure 3-2 shows the engine on the testbed and Table 3.1 shows the main engine specifications.

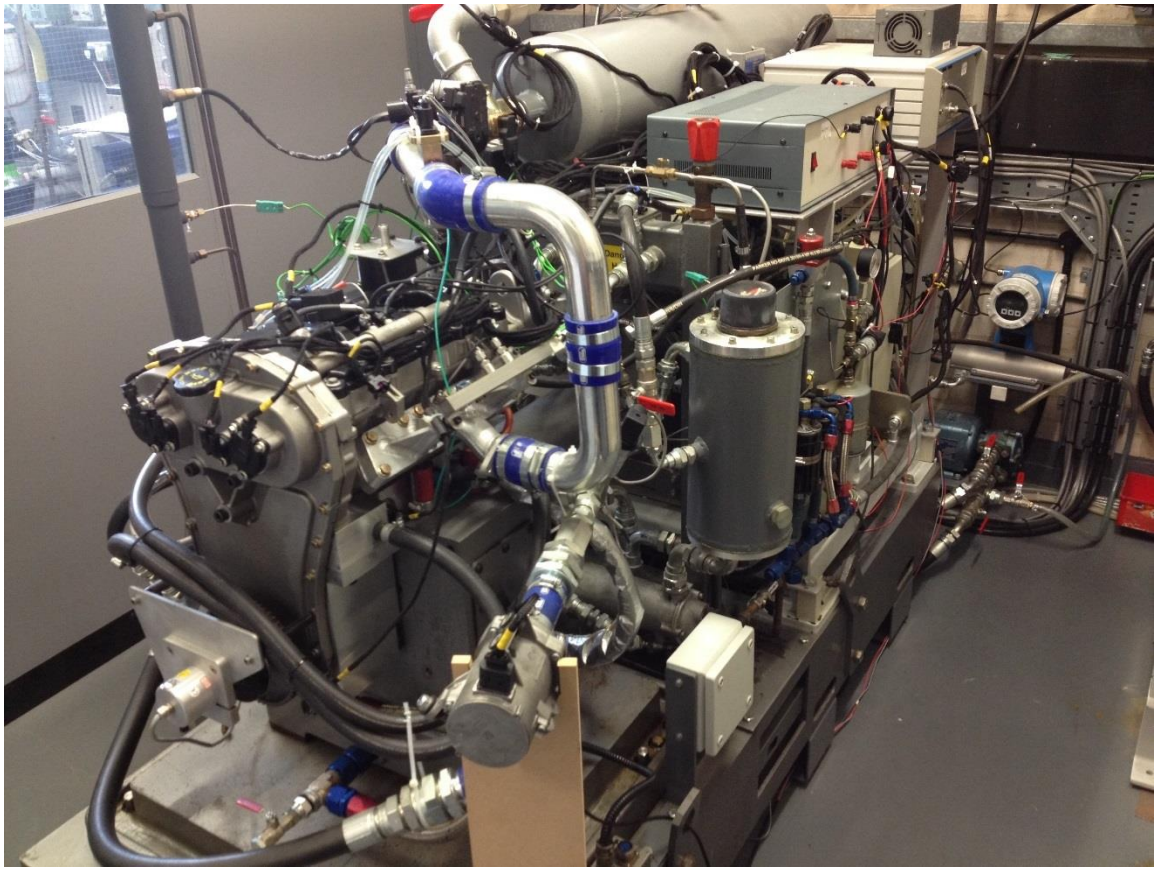

Figure 3-2 Brunel-Mahle Single Cylinder DISI Engine on the testbed

Table 3.1 Engine Specifications

Displacement volume	400 cm^3
Stroke	73.9 mm
Bore	83 mm
Connecting rod length	123 mm
Compression ratio	11.43: 1 / 12.78: 1
Number of Valves	4
Maximum Peak Cylinder pressure	140 bar
Intake Cam Timing (maximum opening point)	80-120 CAD ATDC
Intake cam duration	240 CAD
Exhaust Cam Timing (maximum opening point)	100-140 CAD BTDC
Exhaust cam duration	278 CAD
Direct injection system	Siemens outwardly opening piezo injector with hollow-cone spray, up to 200 bar injection pressure
Intake port injection system	Bosch EV 12 with 4 narrow conical sprays and maximum injection pressure of 8 bar

The engine has a pent-roof combustion chamber with two intake and two exhaust valves. The direct injector is a centrally mounted outwardly-opening piezo injector (Siemens-BMW 13537565138-07) with the spark plug mounted next to it on the cylinder head (Figure 3-3) so that spray guided charge stratification can be achieved. The injector is capable of three injections in a cycle (one early and two late injections, the timing and duration can be adjusted for each injections) with the injection pressures of up to 200 bar which was adjusted according to the operating point of the engine. The minimum pulsewidth for each injection event is 0.15 ms and the interval between the end of one injection and the start of the next must be at least 0.2 ms. The sophisticated MAHLE Flexible ECU was upgraded so that the injector lift could be decreased in order to allow the use of even shorter pulsewithd of 0.11 ms for injecting very small quantities of fuel.

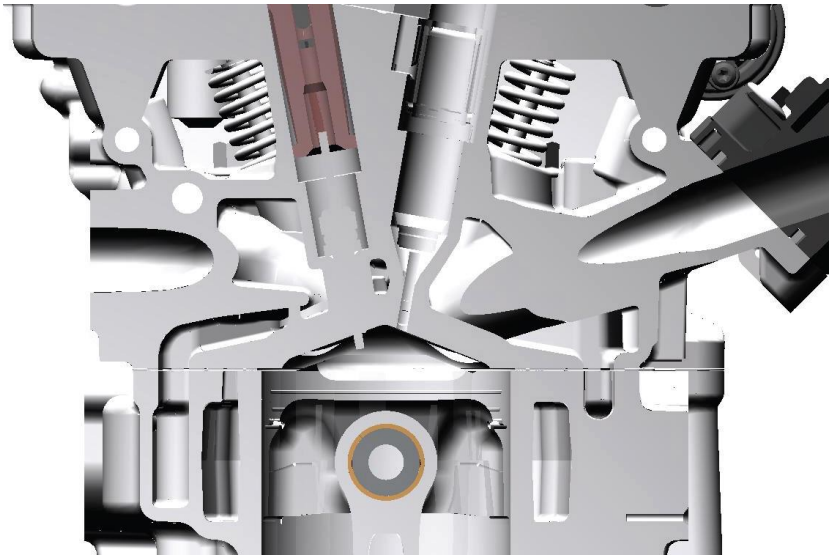

Figure 3-3 Combustion chamber with the injector and the sparkplug [183]

3.2.2 Cam Profiles and Valve Timings

The engine is equipped with two hydraulic variable cam phasers, one for the intake and one for the exhaust cam, which are accommodated in the cylinder head.

Therefore, the cam timings can be adjusted up to 40 crank angle degrees (CAD). In this study, standard intake camshaft with 240 CAD opening duration and exhaust camshaft of 278 CAD opening duration were fitted on the engine both with an 11 mm maximum valve lift which is more relevant to the actual engine operation. Cam profiles and phasing are shown in Figure 3-4 (cam timings are defined by the valve maximum opening point (MOP)). Table 3.2 shows the phasing of the intake and exhaust cams.

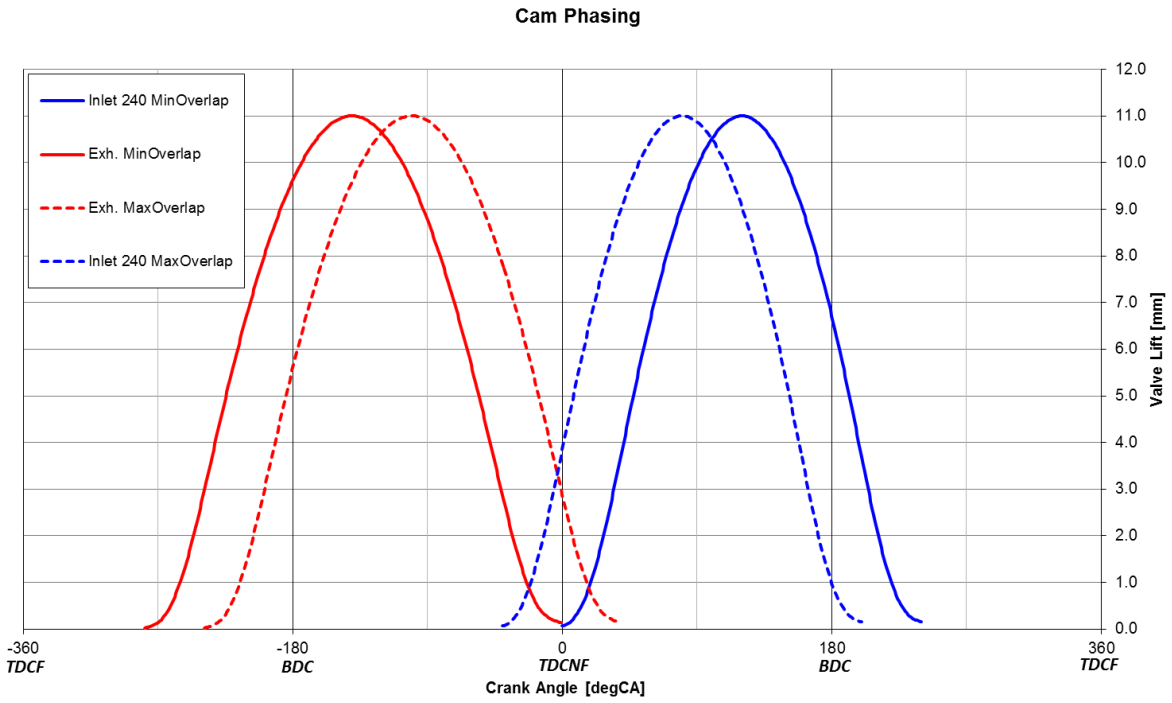

Figure 3-4 Intake and exhaust cam profile and phasing

Table 3.2 Intake and exhaust cam phasing and specifications

Cam	Opening duration CAD (TOR)	Minimum overlap phasing (CAD ATDCNF)			Maximum overlap phasing (CAD ATDCNF)		
		MOP	IVO/EVO (0.5 mm lift)	IVC/EVC (0.5 mm lift)	MOP	IVO/EVO (0.5 mm lift)	IVC/EVC (0.5 mm lift)
Intake	240	120	13	227	80	-27	187
Exhaust	278	-140	-262	-17	-100	-222	23

3.2.3 Oil System

Oil system is responsible for supplying the engine with oil at a desired pressure and maintaining the desired oil temperature. In this engine the oil system mainly includes oil sump, oil filter, oil pump, oil heater and heat exchanger.

The lubrication system used on this engine is a wet sump lubrication system. Standard Mobil1 0W-40 oil is used for all the experiments. The oil pump used in the oil system is an externally located single speed three-phase electric oil pump which circulates the oil in the system at a nominal flow rate of 9.1 l/min. In order to heat up the oil to the desired temperature at low loads and be able to pre heat the oil before running the engine, two 1 kW electric oil heaters are immersed in the oil sump. Oil cooling is performed by using a heat exchanger with the maximum heat rejection rate of 4 kW. It is located upstream of the crankcase oil gallery and cooling is adjusted by a capillary actuator which controls the flow rate of cooling water through the heat exchanger. Oil temperature, therefore, is controlled by both turning on/off the oil heaters and adjusting the cooling capacity of the heat

exchanger (oil cooler). An AC Delco X19 equivalent oil filter is used to filter the oil. This oil filter is mounted next to the oil heat exchanger.

In order to display and track the oil pressure and temperature, several sensors are fitted in different places in the oil circuit. Three pressure sensors are located upstream of crankcase oil gallery. The minimum oil pressure is set to 4.2 barA at this place. Pressure sensors comprise a pressure gauge for quick readings during the startups, a pressure switch for emergency shutdown and a Druck PTX 1400 (0-10 bar, 4.2 mA) pressure sensor which is connected to the low speed data acquisition system for data logging. There are also three temperature sensors in the oil circuit. Oil temperature into the crankcase oil gallery is measured by two Platinum Resistance Thermometers (PRTs), one for the testbed high oil temperature emergency shutdown set at 100 °C and the other one feeds the low speed data acquisition system for data logging. The last PRT is also used for data acquisition and is located at the outlet of oil sump for temperature measurement.

3.2.4 Coolant System

The coolant system is responsible for supplying coolant to the engine at a desired flowrate as well as maintaining the desired coolant temperature. Coolant tank, coolant pump, coolant heater, coolant cooler and ball valves are the main parts of this coolant system.

A mixture of 50% de-ionized water and 50% ethylene glycol is used as coolant for all the experimental work. A coolant tank in the coolant system is used in order to firstly store the additional coolant in the coolant circuit and secondly to allow the expansion of coolant at high temperatures. In order to ensure that the engine cooling jacket is fully submerged in coolant, the coolant tank is located 120 mm

higher than the highest point of the engine cylinder head cooling jacket. An external single speed three-phase electric pump is used in order to circulate the coolant in the system with a nominal flowrate of 32 l/min. A bypass ball valve installed upstream of engine inlet allows the entire flowrate of coolant into the engine to be varied, which is typically set to 13 l/min to limit the delta coolant temperature between engine outlet and inlet within 6°C. Since the engine is equipped with split cooling circuits for cylinder head and cylinder block, two ball valves are fitted at the coolant outlets of cylinder head and block respectively in order to control the coolant flowrate independently.

Coolant temperature is controlled using a 3 kW immersion heater in the circuit to heat up the coolant when it is required and a heat exchanger with the maximum heat rejection rate of 53 kW which works as the coolant cooler, similar to the oil system. Thus, engine out coolant temperature is controlled by adjusting the heating and cooling of the coolant heater and cooler.

There are several sensors in the coolant circuit for pressure, temperature and flowrate measurements. A Druck PTX 1400 (0-4 bar, 4.2 mA) pressure sensor is used to monitor the coolant pressure and is located upstream of the engine coolant inlets. Coolant flowrate is measured using two Apollo turbine type flowmeters. One flowmeter measures the coolant supply to the whole engine and the other measures the coolant flowrate supplied to the cylinder block. In total five temperature sensors are used in the coolant system. One PRT is located upstream of the engine coolant inlets, where the Druck pressure sensor is also placed, in order to monitor the coolant temperature into engine. Two other PRTs are used to measure and monitor the coolant temperature at the outlet of cylinder head and cylinder block. The last PRT is used to measure the coolant temperature in the

coolant tank for the testbed emergency shutdown. Finally, the last temperature sensor is an automotive type coolant temperature sensor which is mounted at the cylinder block outlet side.

3.2.5 Fuel System

Fuel was delivered to the engine through a low-pressure fuel supply and conditioning system connected to a high-pressure system. The low-pressure system is responsible for supplying fuel to the engine at a desired pressure and temperature, and it also contains a fuel flow meter for fuel consumption measurements. The high-pressure system mainly comprises of the high-pressure fuel pump, high pressure rail and the injector.

Regular unleaded gasoline with Research Octane Number (RON) of 95 from pump is used for PFI / DI experiments. For water injection tests in addition to RON 95, RON 97 and 100 are also used for comparison. The fuel tank used to store the fuel is a stainless-steel motorsport type fuel tank and it is positioned higher than all the other components in the fuel system. A heat exchanger (cooler) is located downstream of the fuel tank in order to control the fuel temperature by adjusting the cooling water flowrate through it. A Bosch 12 V automotive type fuel pump then pumps the fuel to the rest of the fuel line where there is a fuel filter and a mechanical pressure regulator downstream of the pump. The pressure regulator regulates the fuel pressure to 5 bar. There is a return line which returns all the extra fuel released by the regulator to the inlet of the fuel heat exchanger. There is a pipe connected to this loop with another top end connected to the entrance of fuel tank at atmospheric pressure. This pipe goes upwards, and the top end is

higher than all other pipes and parts in the system, which helps to remove any air bubbles in the low-pressure fuel circuit.

A Druck PTX 1400 (0-10 bar, 4.2 mA) pressure sensor and a PRT temperature sensor are located downstream of the pressure regulator in order to measure the fuel supply pressure and temperature. Figure 3-5 shows the Coriolis type mass flow meter which was used in this project for fuel consumption measurement. This flowmeter is manufactured by Endress+Hauser and has a DN01 1/24” sensor size which makes it suitable for accurate measurement even with very small mass flowrates.

Figure 3-5 Coriolis mass flow meter by Endress+Hauser

Downstream of the flowmeter the fuel line is split into two lines. One fuel line supplies fuel directly to the low-pressure fuel rail which is connected to the PFI injector. The other fuel line supplies fuel to the high-pressure fuel pump which is a cam driven type pump and it is driven by the intake camshaft. High pressure fuel pump then feeds the high-pressure common rail with the required volume of fuel.

The high-pressure pump is capable of increasing the fuel pressure in the rail up to 200 bar. The rail pressure is controlled by the ECU through a close-loop control function. This is done by a high-pressure automotive type pressure sensor which is located on the common rail. The pressure sensor provides feedback of the actual rail pressure for ECU, then the ECU compares the actual rail pressure to the desired rail pressure and reacts accordingly by increasing or decreasing the fuel volume fed into the common rail. The common rail then supplies the injector with the high-pressure fuel through a short stainless-steel pipe.

The PFI injector used in this study is an EV 12 type Bosch Motorsport injection valve designed to inject the fuel as efficiently as possible into the intake port to achieve a homogeneous distribution of fuel in air. This injector produces 4 narrow sprays and the flow rate at 3 bar is 269 g/min n-heptane. In this experiment the PFI injection pressure was set at 5 bar which is the minimum inlet pressure for the high-pressure pump. Figure 3-6 shows the PFI injector location in the intake manifold and its spray configuration.

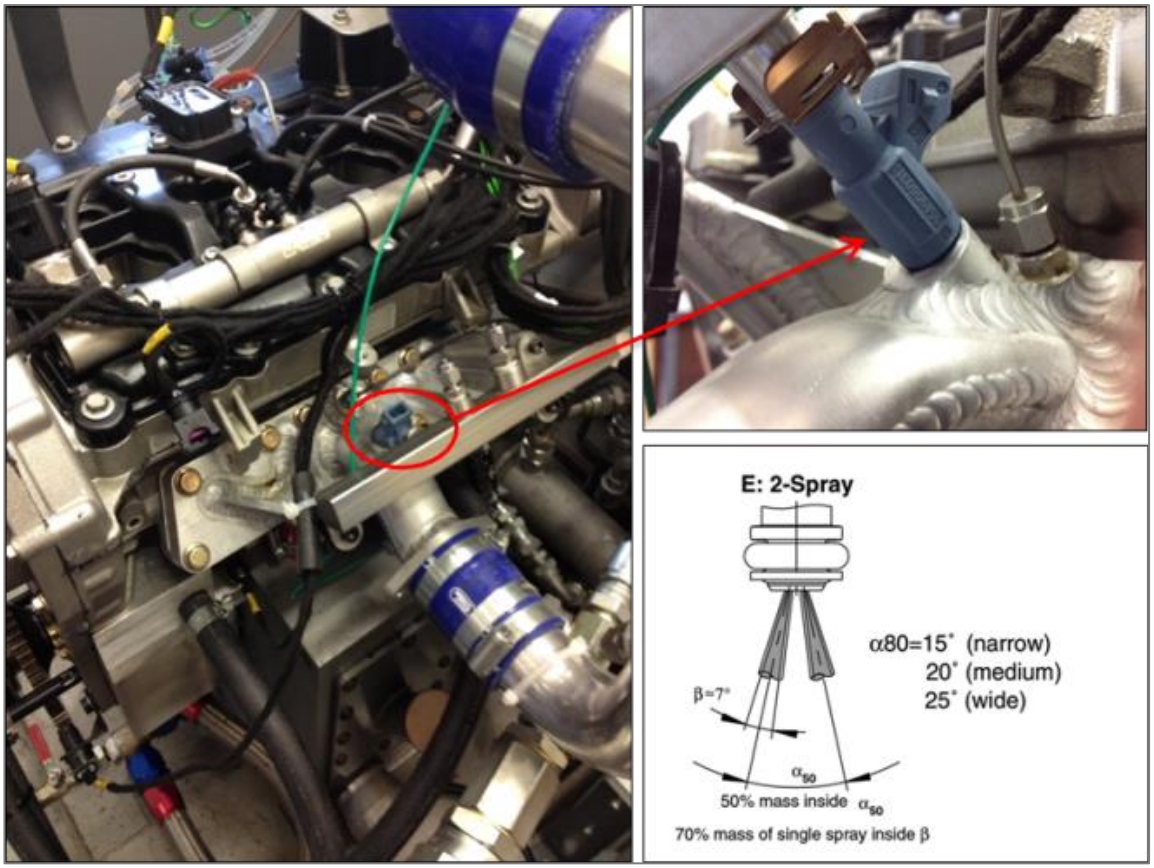

Figure 3-6 PFI injector and its spray configuration

3.2.6 Intake System

The external boost rig is the main part of the intake system in this engine as boosted downsized GDI engines require elevated intake pressures compared to their naturally aspirated (NA) counterparts to compensate for the lack of power imposed by a smaller displacement volume. Therefore, enough pressurized air is required for the single cylinder engine to operate at high loads.

Dried compressed air is supplied to the engine by means of an external boost rig at a pre-set pressure and temperature. The rig consists of a compressor (CompAir HV22RS AERD hydrovane type compressor) which is driven by a 22kW electric motor, a refrigerator (dryer unit), a five micron oil filter and a 272 litres receiver.

The compressor has a nominal flowrate of 3.53 m^3/min at 6 bar absolute pressure. The minimum pressure at which the compressor can deliver air is 6 bar. The refrigerator is located downstream of the compressor and it is connected to the outlet of the compressor to provide air with less than 3% humidity (according to the manufacturer manual). The refrigerator also cools down the air to approximately 3 °C. In order to store and keep the pressure of the compressed dried air delivered by the compressor stable, a 272 litres receiver is fitted downstream of the refrigerator. Air pressure in the receiver is maintained between 6.5 to 7 bar by the rig controller which automatically turns the compressor on/off when required. Then a Parker Hannifin EPDN4 type pressure regulator is used to regulate the air pressure to the required pressure for engine consumption and has a precision of ± 0.15 bar. This pressure regulator is closed-loop controlled by the ECU and is fitted downstream of the receiver.

In order to increase the dried compressed air temperature which was cooled by the refrigerator (dryer) to a desired temperature that represents the charge temperature after the inter-cooler in boosted GDI engines, an electrical 3 kW Secomak 632 type heater is used downstream of the pressure regulator. This heater is closed-loop controlled with the precision of ± 1 °C. The intake air temperature for all the experiments in this thesis was set at 40 °C.

Intake system also contains a large volume plenum (accumulator) which basically is a 40 litre stainless steel cylindrical pressure vessel equipped with a k-type thermocouple. The thermocouple measures the temperature inside the accumulator. This feedback is then used by a Eurotherm PID controller to control the heater. Pressure fluctuations are minimized by using this large volume accumulator upstream of the Bosch DV-E5 40mm automotive type electronic

throttle. This throttle is controlled by the ECU. There is a Bosch automotive type boost pressure and temperature sensor between the accumulator and the throttle body in order to provide feedback for the ECU. The feedback is then used to adjust the pressure regulator for desired boost pressure before the throttle body.

In order to achieve the desired and stable intake port pressure required at each load, a large diameter and long intake pipe is used between the throttle body and the engine intake ports. This helps to mitigate the pressure wave after the throttle body. There is a Bosch 1-way hot wire automotive type mass air flow meter downstream of the throttle body to measure the air mass flow and send feedback to the ECU. Air pressure and temperature are also measured post throttle using a pressure and temperature sensor which send feedback to the ECU.

Furthermore, there is a Kistler 4005B piezoresistive absolute pressure sensor (Figure 3-7) installed in the intake port just before the intake valves to measure the transient intake port pressure for the combustion analyzer software and further analysis. A PRT is also fitted in the same place for intake port air temperature measurement.

3.2.7 Exhaust System

The main part of the exhaust system comprises an austenitic stainless steel pipe which has no sudden changes in the pipe diameter to keep the exhaust gas flow as smooth as possible. This pipe is able to withstand high exhaust gas temperatures of up to 980 °C and pressures up to 4 bar. A large automotive type exhaust muffler is installed at the exit of the exhaust system which minimises the exhaust back pressure due to its large size. In addition, a servo motor actuated butterfly valve is fitted upstream of the muffler in order to control the exhaust back

pressure. This valve can be remotely adjusted by the testbed computer to achieve the desired back pressure to simulate the presence of a turbocharger turbine when required.

In order to measure the exhaust port temperature, a K-type thermocouple is installed close to the exhaust valves. PRT is not used for the exhaust port temperature measurements despite higher accuracy compared to the thermocouple since it cannot withstand the high exhaust temperature. There are two pressure sensors in the exhaust system. The first one is a Kistler 4005B type piezoresistive absolute pressure sensor (Figure 3-7) with a cooling water adaptor fitted 100 mm downstream of the exhaust ports. This sensor is used for transient exhaust pressure measurement required for gas exchange analysis. Figure 3-7 shows Kistler sensor with its specification.

Kistler 4005BA10FA0

Range	0 - 10 bar abs
Pressure range	0 - 10 bar abs
Temperature range	-20 - 125 degC (1100deg C w/cooling adapter)
Linearity	± 0.2%
Size	M5 (M10 w/cooling adapter)
Construction	316 Stainless Steel
Warm up	30 mins
Output	0 - 10V

Figure 3-7 Kistler 4005B type Piezoresistive Absolute Pressure Sensor

The second pressure sensor is a Druck PTX 1400 (0-10 bar) type low speed pressure sensor and it is installed to measure the mean exhaust pressure. This sensor is located downstream of the first pressure sensor. Moreover, there are two automotive type Universal Exhaust Gas Oxygen (UEGO) lambda sensors on the exhaust pipe. The first lambda sensor is used for the closed-loop control of lambda and the second one is only used to double check the reading of the first lambda sensor. In addition to the sensors, there are a few sampling ports on the exhaust pipe for gaseous and particulate emissions measurements. Gaseous emissions are measured by means of a Signal Ambitech Model 443 Chemiluminescent NO/NOx Analyser, a Signal Rotork Model 523 FID HC Analyser and a Horiba MEXA-554JE analyser for measuring the CO, CO2 and O2 concentration. For particle measurements a AVL 415SE Smoke Meter is used to record the smoke number and a Cambustion fast response DMS 500 particle analyser is also used to measure the particles concentration.

3.2.8 Dynamometer

An electrical motor dynamometer (CPEngineering 48kW AC motor with a 4 quadrant AC regenerative inverter drive) is coupled with the engine crankshaft for torque measurements and load adjustments. The dynamometer is capable of transient operation with the maximum speed of 6000 rpm and the maximum torque of 140 Nm. This dynamometer is also capable of motoring and absorbing 48 kW and is equipped with CP CADET V14 dynamometer control system to adjust the speed, load and the exhaust back pressure valve position when required. Figure 3-8 shows the operating envelope of the dynamometer. The highly downsized boosted GDI engine used in this experimental study was capable of 120 kW/liter.

This is equal to 48 kW of power for the single cylinder engine which has the capacity of 0.4 liter.

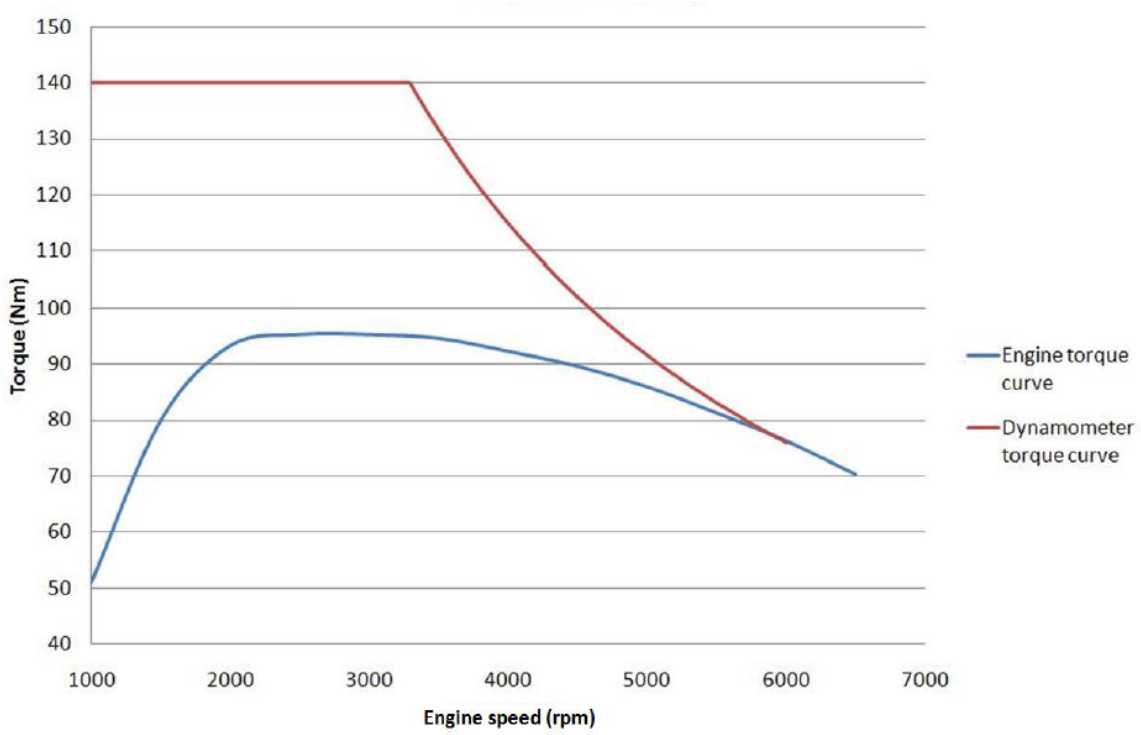

Figure 3-8 Comparison of the dynamometer torque curve and the engine torque curve

Figure 3-9 shows the schematic diagram of the dynamometer system.

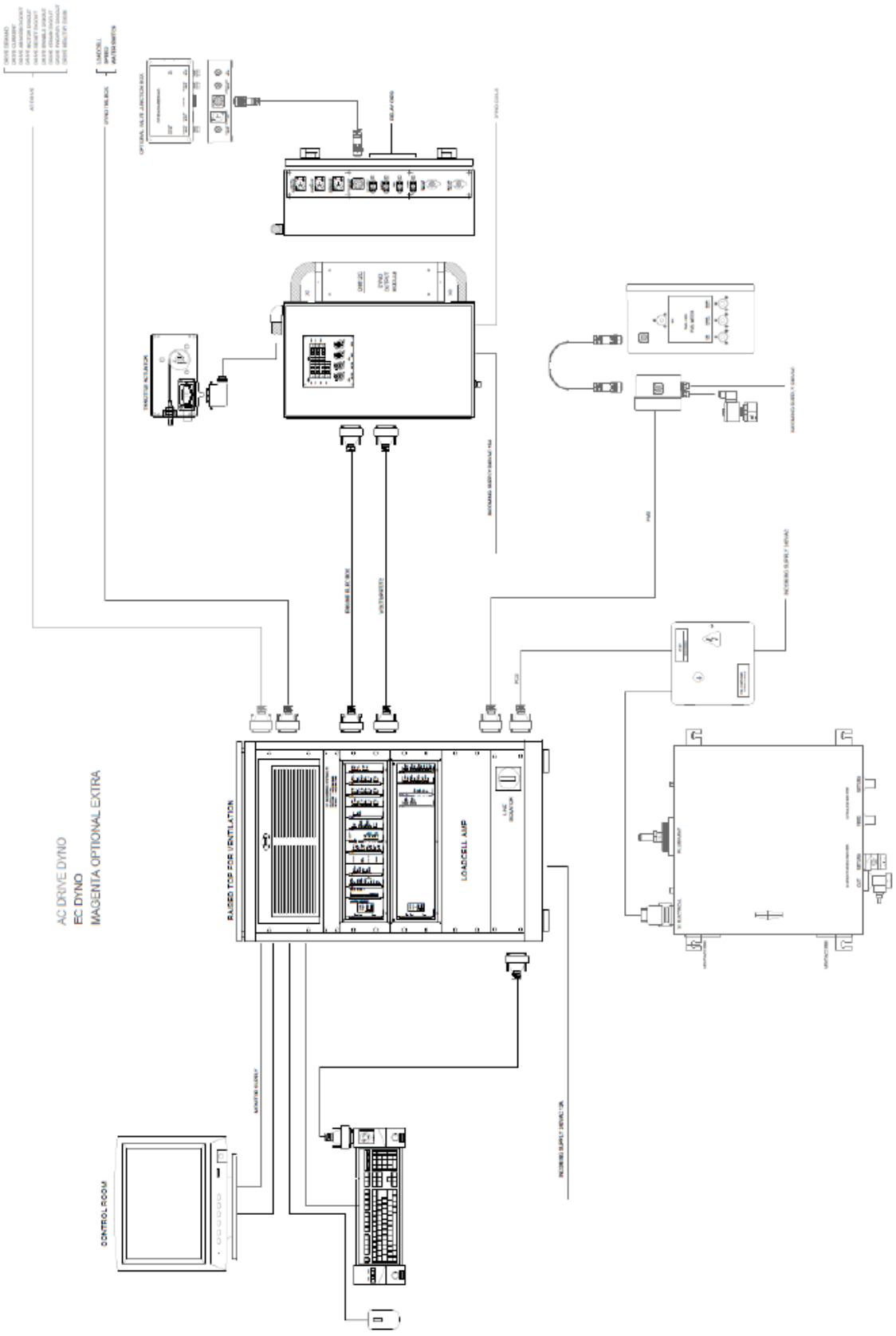

Figure 3-9 Schematic diagram of the dynamometer

3.2.9 Water injection system

Since the engine is equipped with both port and direct fuel injection, it gives flexibility to introduce different fuels or water through each injector. In this study fuel was injected directly into the cylinder and water was injected into the intake port through the PFI injector. The water injection system (Figure 3-10) comprises a pressurized stainless-steel water tank (Figure 3-11) to store water, several ball valves to control the water flow, a pressure relief valve, pressure regulators and gauges, water filter and a gas bottle to apply pressure. In this system pressure is applied on the water by using an external gas cylinder which contains pure nitrogen. Cylinder pressure is controlled by a pressure regulator and is set in a way that the water pressure at the PFI rail is equal to 5 bar gauge. The water tank can be easily refilled by first releasing the pressure inside the tank and then using a small electric pump to fill up the tank with water again.

A new injector (EV 12 type Bosch Motorsport injection valve) with the same specifications as the one used for PFI / DI experiments is used for the water injection experiments as well. In all experiments the injection pressure of water was set at 5 bar. The PFI injector which was used for water injection experiments was calibrated before the experiments. Figure 3-12 shows the calibration curve of the water injector. Furthermore, there was no sign of damage to the injector during these tests due to use of water.

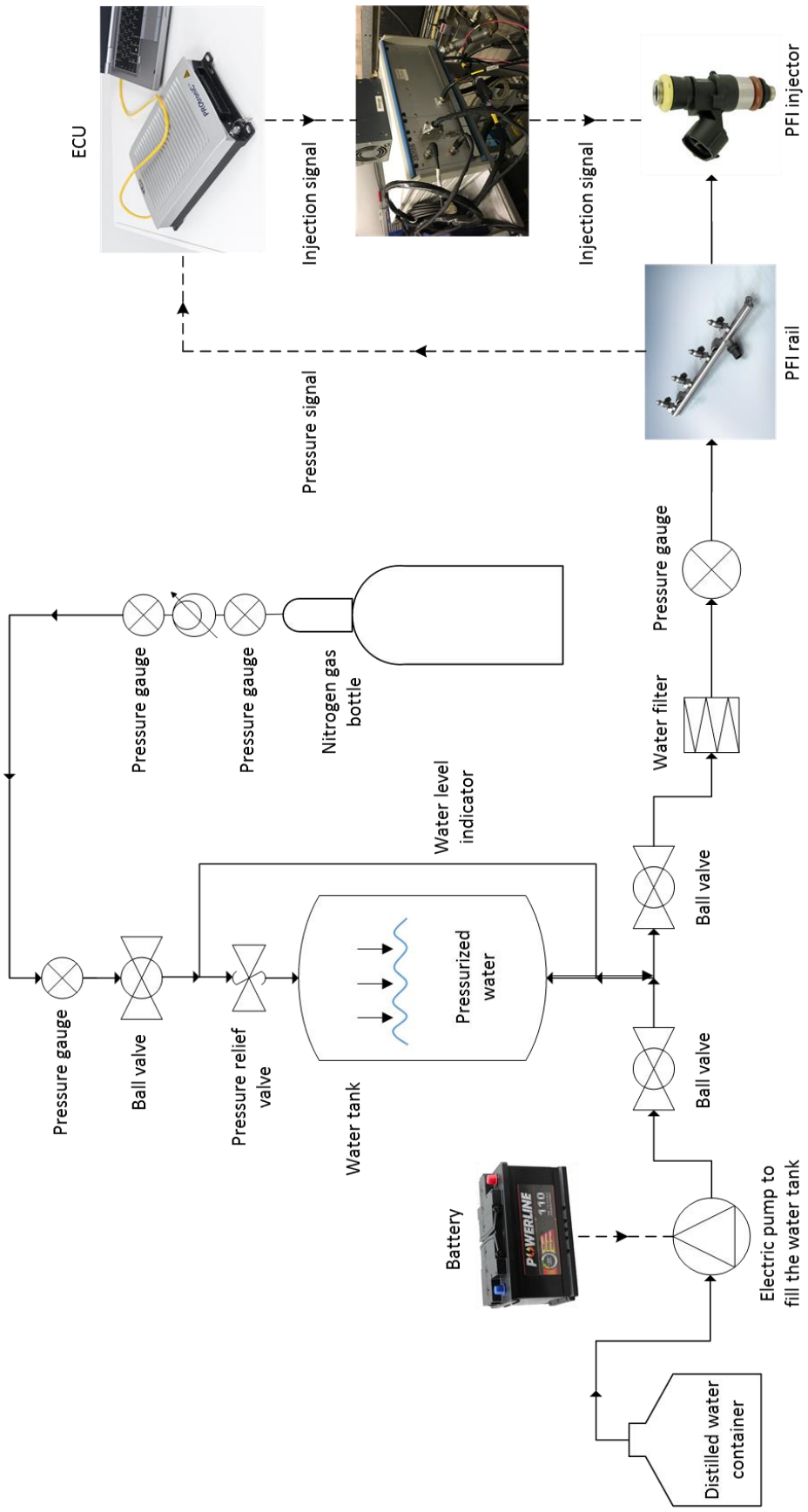

Figure 3-10 Water injection system schematic diagram

Figure 3-11 Pressurized water tank and some other components of the water injection system in the test cell

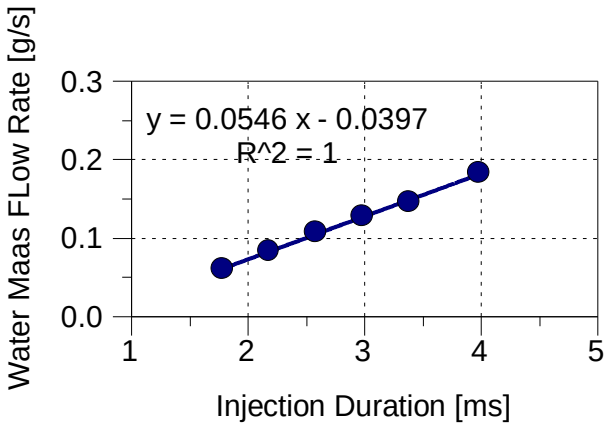

Figure 3-12 Water flow rate against injection duration at 1000 rpm and 5 bar injection pressure

3.3 Engine Control Unit and Management System

To ensure a smooth and flexible engine operation for testing, an advanced engine management system (EMS) is employed. This system allows a flexible control of the engine and some other actuators in the testbed and comprises a flexible engine control unit (ECU), several sensors, actuators, a wiring harness with two looms and a computer to control the ETAS INCA V7.0 software for the ECU communication.

Figure 3-13 shows the main part of the engine management system which is the flexible ECU developed by Mahle Powertrain (The ECU is based on the AFT PROtroniC platform). The ECU hardware provides enough processing power and supports sufficient I/O channels (input and output channels) to control all the required components. In addition, all the functions for a modern engine operation are included in its software as well as the capability of adding extra codes for additional control when required.

Figure 3-13 Mahle Flexible engine control unit

Table 3.3 shows the main channels used in this experimental work to control the main engine parameters. All of these feedbacks also were logged through ETAS INCA software for data analysis purposes.

Table 3.3 The main ECU inputs and outputs used during the experiments

Inputs (sensors)	Outputs (actuators)
Throttle position	Electronic throttle body
Manifold pressure and temperature	
Intake cam position	Intake cam phaser
Exhaust cam position	Exhaust cam phaser
Exhaust lambda	PFI injector
Boost pressure and temperature	Boost pressure regulator
Air mass flow meter	DI injector
High pressure fuel rail pressure	High pressure fuel pump
Crank angle sensor	
Knock sensor	Ignition coil
Coolant temperature	
Battery voltage	

A Vemac injector driver is used to control the GDI injector and is coupled to the flexible ECU to control different injection parameters. A Controller Area Network (CAN) connection is used to control the ECU remotely. This is connected to an ETAS 571.3 interface card which itself is connected to the testbed computer with

ETAS INCA V7.0 to communicate with the ECU. There are some inputs which are controlled by the dynamometer control system not the ECU in order to have some control over the engine in the event that the ECU or its computer should malfunction. These inputs include the ignition, the accelerator pedal and the low-pressure fuel pump.

The Mahle flexible ECU also offers the closed loop control of exhaust lambda which was used in this project. Closed loop control of boost pressure and exhaust back pressure (EBP) also could be set to have closed loop control as well. Spark timings were dictated by a map of intake manifold pressure (MAP) and engine speed. The knock sensor was used with an oscilloscope purely to help the operator for knock indication and it was never used for spark timing control. However, the cylinder pressure was used almost exclusively for knock detection as the knock sensor was located at the end of the cylinder head and therefore its feedback was never completely accurate.

3.4 Data Acquisition System and Instrumentation

In order to display and record the key information and data received from the different sensors and devices on the engine a data acquisition (DAQ) system was developed in house in Brunel University London. This system consists of two main parts; first is the DAQ hardware which receives signals from sensors, actuators and devices on the engine and the second is the DAQ software which process the signals, performs combustion analysis live and can also log the data when required.

3.4.1 Data Acquisition Hardware

Three logging systems were used in this experimental work to save the data. A data card for high speed data acquisition, a data card for low speed data acquisition and the last data card used for the PRTs. Figure 3-14 shows the DAQ hardware.

A National Instrument (NI) USB-6353 card was used for the high-speed data logging which logs in-cylinder pressure, intake absolute pressure, exhaust absolute pressure, fuel flow rate, encoder clock and reference and torque channels. This card has a maximum sampling speed of 1MS/s and can record up to 32 channels.

Figure 3-14 High and low speed DAQ cards

An Encoder Technology EB58204040 shaft encoder was used for this experimental work which gives a 0.25 CAD resolution which is required for the in-cylinder pressure analysis.

Another NI USB 6210 card was used for the low-speed data recording which logs signals from thermocouples, low speed pressure transducers and low speed flow meters such as exhaust port temperature, exhaust manifold temperature, total coolant flow, block coolant flow, oil pressure, low pressure fuel pressure, coolant pressure and average exhaust pressure channels. This card is capable of logging 16 channels. The sampling frequency of 0.5 Hz was used in this project.

An eDam-9015 acquisition card is used for the PRT logging system which supports up to 7 PRT inputs. This card connects to the test bed computer by a serial connection.

A great deal of effort was put into reducing the noise from different signals. Signal amplifiers have been placed as close as possible to their corresponding sensors where possible, all sensor cables are screened and ground to a common ground to avoid any ground loop in the instrumentation used. Power cables were also separated from the instrumentation cables and were placed far from each other. In addition, power cables never ran parallel to instrumentation cables in an effort to reduce electrical noise which was present in the initial setups.

3.4.2 Data Acquisition Software (Combustion Analyzer)

All the data gathered by the DAQ cards are transferred to a bespoke software called “Transient Combustion Analyzer” which was developed at Brunel University London by Dr Yan Zhang [191]. Figure 3-15 shows the user interface of this software. This software processes all the signals received from the DAQ cards and

displays the information such as the temperatures, pressures, flowrates, torque and engine speed. Moreover, some online calculations such as engine power output, specific fuel consumption, combustion characteristics and heat release rate are performed based on the engine specifications and displayed by the software. These data can be recorded for several cycles as defined by the user for further analysis. For this project 300 consecutive cycles were recorded at each test point for combustion analysis. Heat release, combustion characteristics and fuel consumption calculations are based on [19,192] sources.

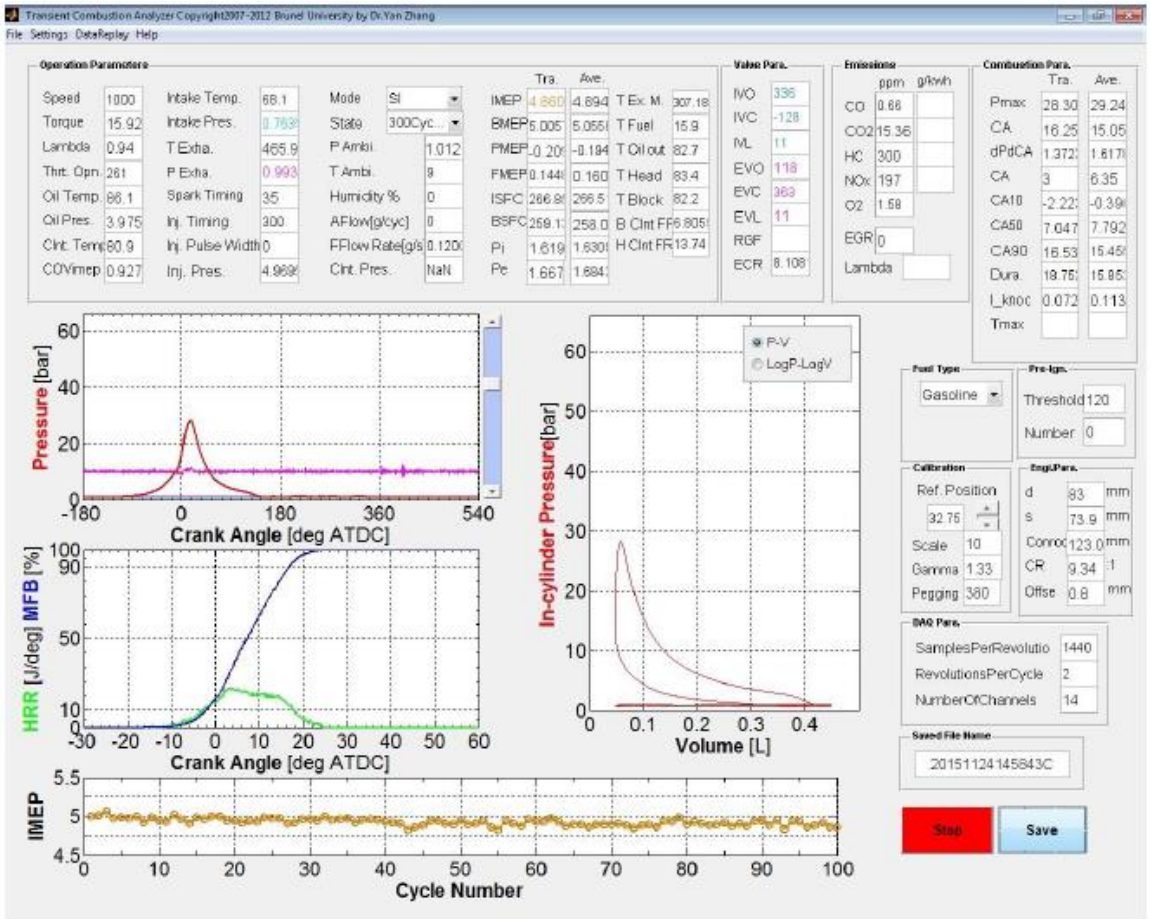

Figure 3-15 Transient Combustion Analyser user interface

Figure 3-16 shows the P-V diagrams of a four-stroke SI engine at full load and part load. Net Indicated Mean Effective Pressure (NIMEP) is calculated using Equation

3-1 which correlates to the work delivered to the piston over the entire four-stroke cycle (area A - area B in Figure 3-16).

$$NIMEP = \int_{-180}^{540} \frac{P}{Vs}\dot{V}(\varphi)d\varphi \quad (4-stroke)$$

Equation 3-1

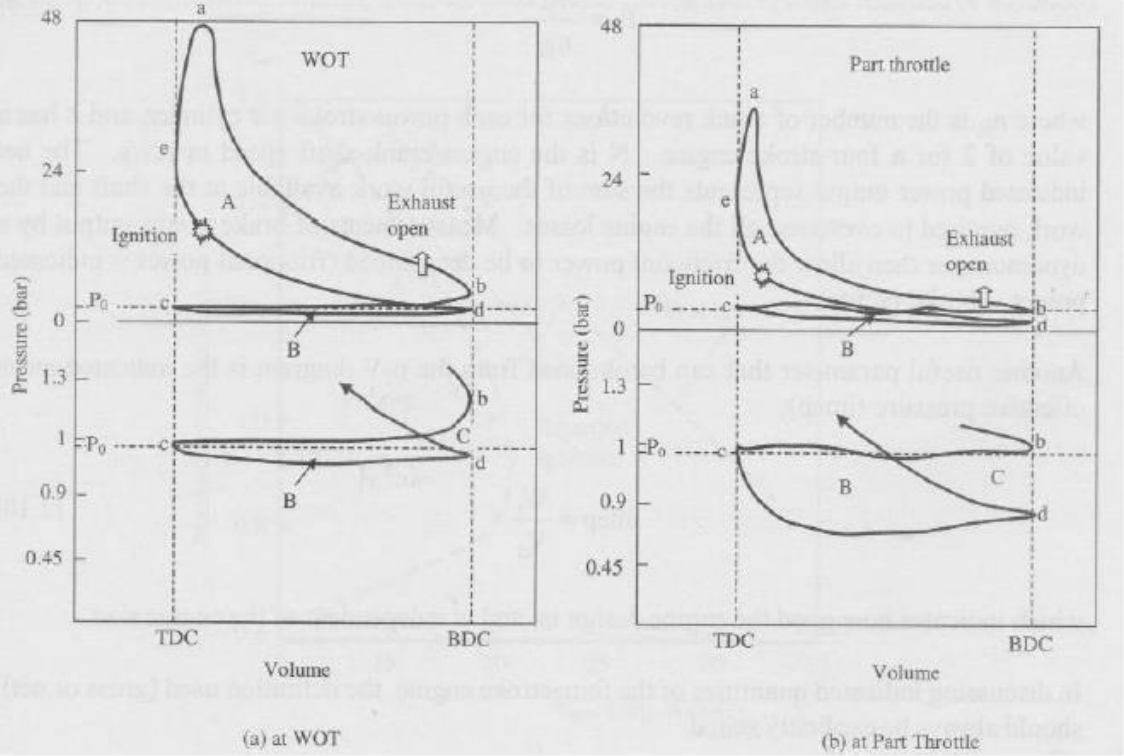

Figure 3-16 P-V diagrams of a four-stroke SI engine at full load and part load [192]

Moreover, Gross Indicated Mean Effective Pressure (GIMEP) is calculate using Equation 3-2 which corelates to the work delivered to the piston over the compression and expansion strokes only (area A + area C in Figure 3-16).

$$GIMEP = \int_{-180}^{180} \frac{P}{Vs}\dot{V}(\varphi)d\varphi$$

Equation 3-2

Where Vs is the displacement volume of the engine, P is the in-cylinder pressure in real time, φ is the crank angle and $\dot{V}(\varphi)$ is the cylinder volume.

Equation 3-3 shows how Pumping Mean Effective Pressure (PMEP) is calculated. This parameter corelates to – (area B + area C).

$$PMEP = NIMEP - GIMEP$$

Equation 3-3

As can be seen in Figure 3-17, NIMEP, GIMEP, PMEP and fuel mass flow is used to calculate Net Indicated Fuel Conversion Efficiency (IEffn), Gross Indicated Fuel Conversion Efficiency (IEffg) and Pumping Indicated Fuel Conversion Efficiency (IEffp).

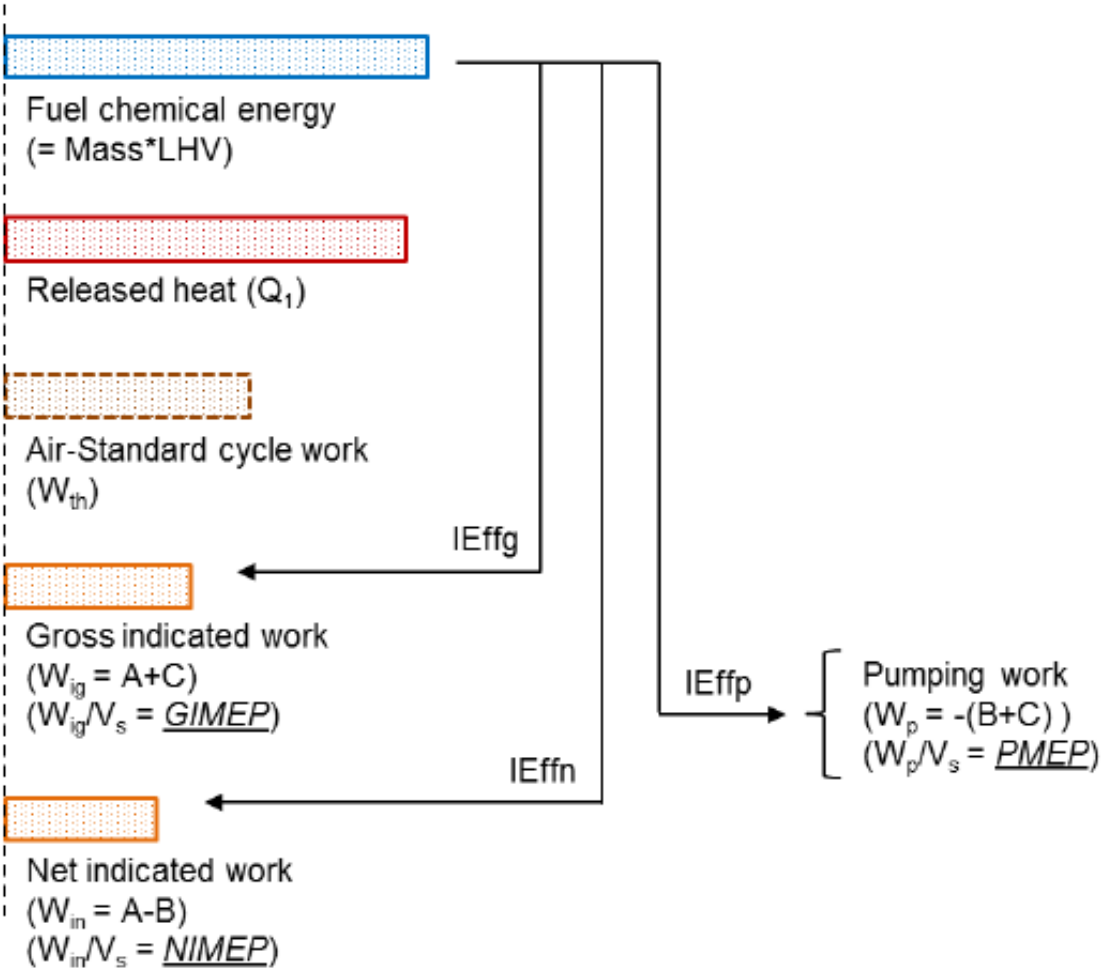

Figure 3-17 Indicated work and fuel conversion efficiencies

According to Equation 3-3, the relation between IEffn, IEffg and IEffp can be written as:

$$IEffn = IEffg + IEffp$$

Equation 3-4

This can be used in efficiency breakdown analysis.

The software also shows in-cylinder pressure and knock intensity which are both updated on a cycle to cycle basis. The cylinder pressure data comes directly from the cylinder pressure transducer. The difference between the actual pressure

obtained by the pressure transducer and the predicted pressure is defined as Knock Intensity (KI). Equation 3-5 shows how the predicted pressure is calculated. This value is obtained by averaging the pressure across the 10 points before and 10 points after the point in question.

$$Pn = \frac{\sum_{n-2.5}^{n+2.5} P}{21}$$

Equation 3-5

As shown in Figure 3-18 , the predicted pressure Pn at crank angle of n is calculated by averaging the points from $(n - 2.5)$ to $(n + 2.5)$ at 0.25 CAD resolution. Cylinder pressure and Knock Intensity are both plotted against the crank angle in this software.

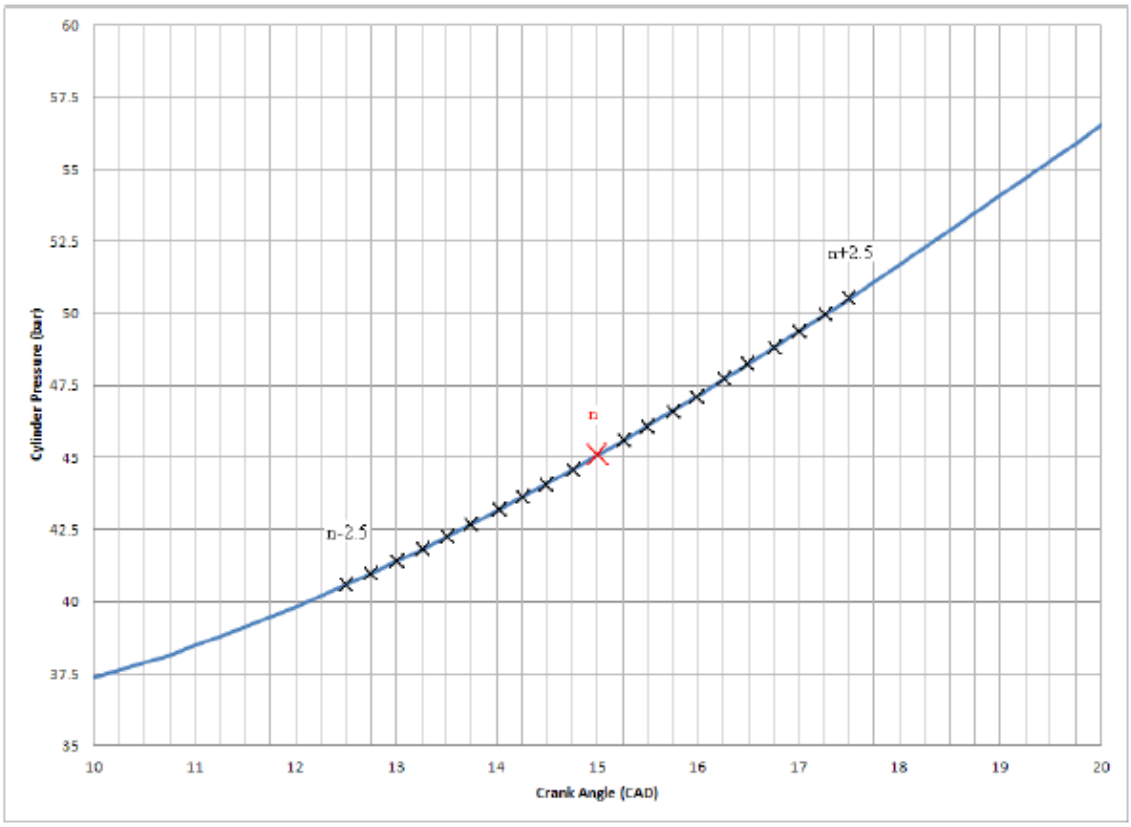

Figure 3-18 Band-Pass filtering calculation [193]

Equation 3-6 then shows how to obtain the knock intensity using the actual pressure (Pf, pressure feedback from the cylinder pressure transducer) and the predicted pressure (Pn) which were explained earlier.

$$KI = Pf - Pn$$

Equation 3-6

This is a very effective method for measuring knock intensity which is also used in industry. Other methods such as using a band-pass filter is computationally more expensive.

3.4.3 Finding Top Dead Centre

A great deal of attention has been paid in this experimental work to increase the accuracy of the recorded data. Correct Top Dead Centre (TDC) determination is essential for achieving highly accurate in-cylinder pressure data which is used for indicated efficiency calculations and combustion analysis. Small errors in TDC position determination can create large errors in various combustion characteristics calculations. Therefore, a Kistler 2629C capacitive type TDC sensor is used in this experimental work for dynamic determination of TDC position. This sensor has an accuracy within 0.1 CAD but since the crank encoder has a resolution of 0.25 CAD, the actual accuracy of the TDC determination system would be 0.125 CAD. Figure 3-19 shows the TDC sensor toolkit.

Figure 3-19 Kistler TDC sensor toolkit

When using the TDC sensor two graphs are generated, Figure 3-20 shows an example of these. Peak of the signal output represents the mechanical TDC position. Initially there is an offset of 20.1 CAD between the piston TDC and zero degree crank angle which is shown in the combustion analyser (Figure 3-20(a)). Figure 3-20 (b) shows the measurement after inputting the offset value of 20 CAD into the combustion analyser. As can be seen, the zero degree crank angle is set to match the piston TDC in combustion analyser.

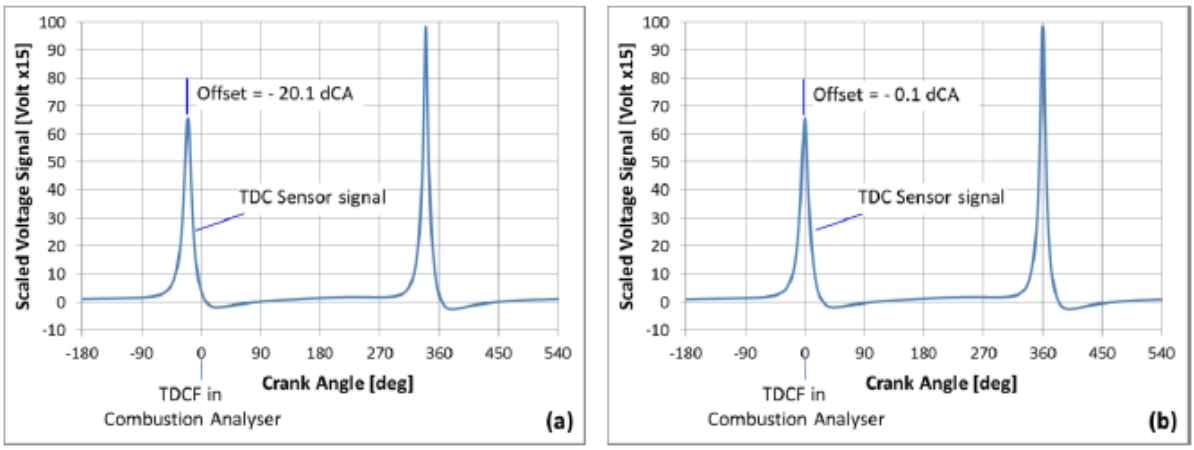

Figure 3-20 TDC determination in combustion analyser

After finding the correct geometric TDC, the engine is motored at 1200 rpm and log P-V diagram is generated as shown in Figure 3-21 (a). Figure 3-21 (b) shows that the peak in-cylinder pressure occurs 1 CAD before TDC due to the heat loss and leakage as it is explained in [192].

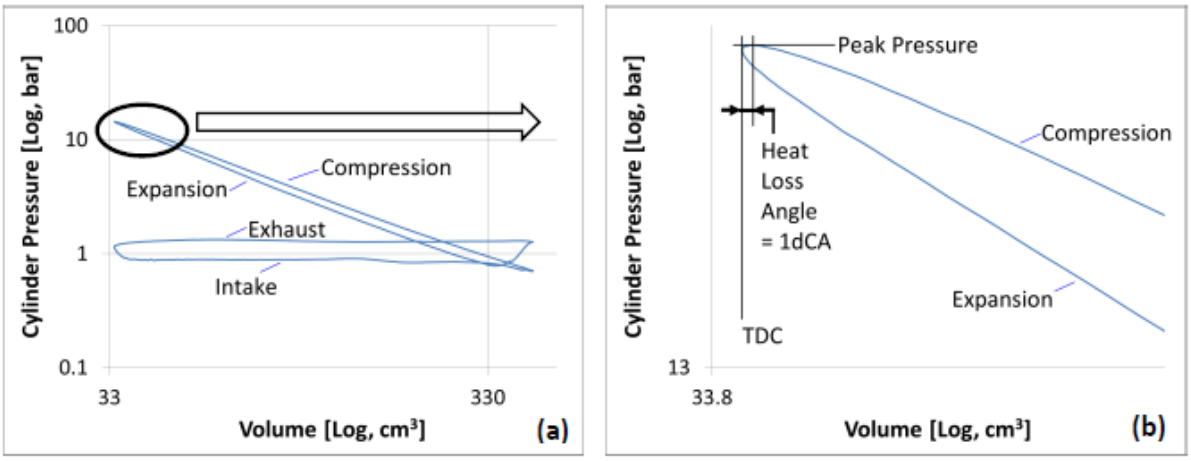

Figure 3-21 Log P-V diagram during engine motoring at 1200 rpm

3.4.4 In-Cylinder Pressure Pegging

Piezoelectric pressure sensors do not provide the absolute in-cylinder pressure directly instead they respond to pressure differences by outputting a charge referenced to an arbitrary ground. Therefore, in order to quantify absolute

pressures, the transducer output must be referenced, or pegged to a known pressure in the cycle [192]. There are several methods for cylinder pressure pegging. Randolph summarized nine methods which can be find in [194].

As shown in Figure 3-22 a revised method for cylinder pressure pegging is used in this experimental work which utilizes both transient intake and exhaust port pressures detected by piezoresistive absolute pressure sensors. The combustion analyzer software includes a variable named as “Pegging” which allows the user to manually select a point on the exhaust port pressure curve for in-cylinder pressure to be pegged to. Adjusting this variable moves the pressure curve upwards or downwards. A suitable value at each test point is achieved when the cylinder pressure is as close as possible to exhaust pressure during exhaust stroke after exhaust valve opened (EVO) and to intake port pressure during intake stroke before intake valve closed (IVC). Intake port pressure is employed as the primary reference.

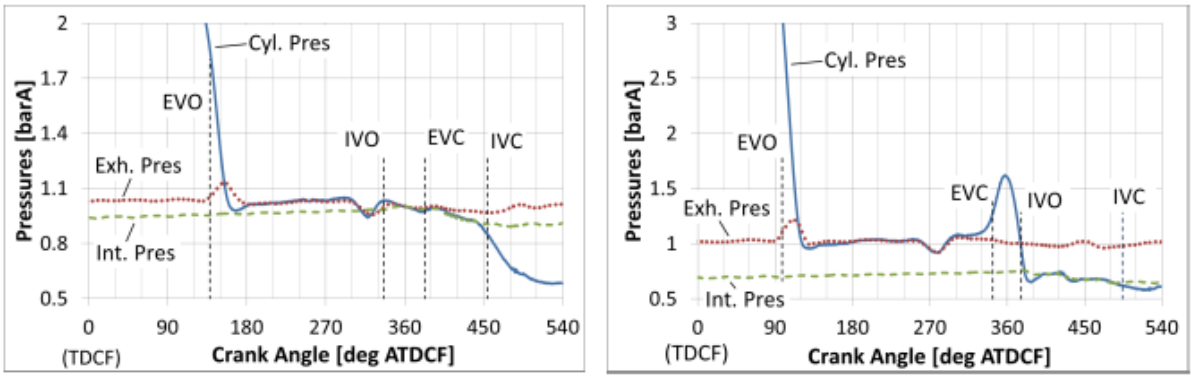

Figure 3-22 Cylinder pressure pegging examples

3.5 Exhaust Emission Measurements

3.5.1 Emission analyzers

Gaseous emissions were measured by means of a Horiba MEXA-554JE analyser (measuring CO, CO_2 and O_2) and two Signal analysers (Ambitech model 443 Chemiluminescent NO/NO_x and a Rotork Analysis model 523 FID HC analyzers). Particle emissions were measured by means of an AVL 415SE smoke meter and a Cambustion DMS 500 fast response particulate analyzer which is capable of measuring particulate size spectral density.

Figure 3-23, Figure 3-24, Figure 3-25 and Figure 3-26 show all the emission analysers used in this experimental work for gaseous and particulate emissions measurement as it was explained in the above paragraph.

Furthermore, Table 3.4, Table 3.5 and Table 3.6 show the detailed specifications (such as the range, repeatability, linearity and sensitivity) of the analysers used in this experimental work.

Figure 3-23 Horiba MEXA-554JE for CO, CO_2 and O_2 measurements

Figure 3-24 Signal Rotork Analysis model 523 FID analyser used for HC measurements (first unit at the top) and Signal Ambitech model 443 Chemiluminescent analyser used for NO/NO_x measurements (bottom three units)

Table 3.4 Rotork Analysis model 523 FID analyser (HC) specifications

Range	0 - 10000 ppm
Pressure range	N/A, 3l/min sample fow
Temperature range	10 - 30 degC
Linearity	± 1%
Repeatability	± 1%
Size	19" rack mount
Construction	316 Stainless Steel
Warm up	40 mins
Output	Analogue display

Table 3.5 Signal Ambitech model 443 Chemiluminescent analyser (NOx) specifications

Range	0 - 10000 ppm
Pressure range	N/A, 1.5l/min sample fow
Temperature range	10 - 30 degC
Linearity	± 1%
Repeatability	± 1%
Size	3 x 19" rack mount
Construction	316 Stainless Steel
Warm up	40 mins
Output	Analogue display

Figure 3-25 AVL 415SE smoke meter used for particle measurement

Figure 3-26 Cambustion DMS 500 fast response particulate analyzer

Table 3.6 Specifications of the Emission analysers

Device	Repeatability	Linearity	Sensitivity	Min detectable concentration / range
NO_x analyser	± 1% FS	± 1% FS		0.2 ppm
HC analyser	± 1% FS	± 1% FS		0.1 ppm
Smoke meter	σ ≤ ± 0.005 FSN			0.002 FSN
DMS 500			1.0 × 103 (dN/dlogDp /cc)	5 nm – 1 µm

3.5.2 Calculation of specific emissions

The gaseous emission analyzers used in this study all measured and recorded the emissions as volume concentration in parts per million (ppm) initially which were later converted to indicated specific emissions following the UN regulation number 49 [11]. All gases measured in dry basis were transformed to wet basis taking in account the air humidity and water-in-fuel content. In addition, no NO_x humidity and temperature corrections were applied.

CO, NO_x and UHC (unburned hydrocarbon) were the main exhaust gases to be converted from ppm to g/kWh following the below equations:

$$ISCO = \frac{u_{CO}[CO]k_w\dot{m}_{exh}}{P_i}$$

Equation 3-7

$$ISNOx = \frac{u_{NOx}[NOx]k_w\dot{m}_{exh}}{P_i}$$

Equation 3-8

$$ISHC = \frac{u_{HC}[UHC]\dot{m}_{exh}}{P_i}$$

Equation 3-9

Where u_i is the molar mass fraction of each gas, $[i]$ is the gas concentration in ppm, k_w is the dry-to-wet correction factor, $\dot{m}_{exh}$ is the exhaust mass flow rate and P_i is the indicated power. These parameters were calculated as:

$$\dot{m}_{exh} = \dot{m}_{air} + \dot{m}_{fuel}$$

Equation 3-10

$$\dot{m}_{air} = \dot{m}_{dry\ air} + \dot{m}_{humidity}$$

Equation 3-11

$$\dot{m}_{fuel} = \dot{m}_{actual\ fuel} + \dot{m}_{water}$$

Equation 3-12

The exhaust mass flow rate was calculated as the sum of wet air mass flow rate $\dot{m}_{air}$ and fuel mass flow rate $\dot{m}_{fuel}$, while the dry air and water (present in air) were calculated taking in account the water saturation pressure polynomial estimation proposed by [195]:

$$SP = 604.8346 + 45.9058(T_a - 273.15) + 1.2444(T_a - 273.15)^2 + 0.03522481(T_a - 273.15)^3 + 0.0009322091(T_a - 273.15)^4 + 0.000004181281(T_a - 273.15)^5$$

Equation 3-13

Where T_a is the ambient temperature. With RH as the relative humidity, and p_a the ambient pressure, air humidity H_a (in grams of water per kilogram of dry air) was calculated as:

$$H_a = \frac{6.211\ RH\ SP}{p_a - \frac{(RH\ SP)}{100}}$$

Equation 3-14

$$\dot{m}_{dry\ air} = \frac{\dot{m}_{air}}{1 + H_a}$$

Equation 3-15

$$\dot{m}_{humidity} = \dot{m}_{dry\ air} H_a$$

Equation 3-16

The molar mass fraction of each gas was calculated according to specified values from the [11] (Table 3.7).

Table 3.7 Raw gas molar mass fraction of the exhaust gases for gasoline [11]

Exhaust Gas	u_i (Gasoline)
CO	0.000966
NO_x	0.001587
UHC	0.000499

The dry-to-wet correction factor k_w applied to CO and NO_x emissions was dependent not only on the ambient conditions, but also on the added water content from the fuel:

$$k_w = 1.008\left(1 - \frac{1.2442H_t + 111.19W_{ALF}\left(\frac{\dot{m}_{fuel}}{\dot{m}_{dry\ air}}\right)}{773.4 + 1.2442H_t + 1000\left(\frac{\dot{m}_{fuel}}{\dot{m}_{dry\ air}}\right)k_f}\right.$$

Equation 3-17

$$k_f = 0.055594W_{ALF} + 0.0070046W_{EPS}$$

Equation 3-18

Where W_{ALF} and W_{EPS} were the hydrogen and oxygen contents in the fuel, respectively. The original air humidity factor was replaced by the total humidity factor H_t to take in account the water-in-fuel added additional content.

$$H_t = H_a + H_f$$

Equation 3-19

$$H_f = \dot{m}_{water}/\dot{m}_{dry\ air}$$

Equation 3-20

After the conversion of all gaseous emissions to mass flow rates, the combustion efficiency was calculated by comparing the fuel energy supplied to the engine to that actually released during the combustion. Therefore, the combustible species found in the exhaust (CO and UHC) and resulted from incomplete combustion were multiplied by their heating values [19]. The LHV values used for CO is 10.1 MJ/kg. The LHV of UHC was assumed to be the same as the fuel which was used in the respective test. Then this value is divided by the fuel energy delivered to the engine:

$$\eta_c = 1 - \frac{\dot{m}_{CO} LHV_{CO} + \dot{m}_{UHC} LHV_{UHC}}{\dot{m}_{fuel} LHV_{fuel}}$$

Equation 3-21

When defining combustion efficiency, it is clear that not all the energy contained in the fuel could be released during the combustion.

Furthermore, lower heating value of the gasoline which was used for PFI / DI tests was 42.66 MJ/kg and the heating value and other properties of the fuels used for water injection tests are reported in Table 3.8.

Table 3.8 Properties of the fuels used for water injection experiment

	BP Gasoline 1	BP Gasoline 2	BP Gasoline 3
Research octane number (RON)	95	97	100
Lower heating value (MJ/kg)	43.63	43.63	42.35
Density @ 15 °C (kg/L)	0.7198	0.7273	0.7377

3.6 Testing and Data Accuracy

Table 3.9 shows the engine operating parameters and boundary conditions which were applied throughout this experimental project.

Table 3.9 Test operation and boundary conditions

Variables	Control criteria
Engine speed	Controlled by dyno (1000-5000)
Engine load (NIMEP)	Set by adjusting throttle opening and boost pressure
Intake cam timing (MOP)	Controlled by ECU (set at the optimized position)
Exhaust cam timing (MOP)	Controlled by ECU (set at the optimized position)
Exhaust lambda	Controlled by ECU (set at 1 unless lambda sweep is performed)

High pressure fuel rail pressure	Controlled by ECU (set at the optimized value for each test point)
Low pressure fuel rail pressure	Set at 5 bar gauge
Injection strategy	Controlled by ECU
Spark timing	Controlled by ECU (optimized at low and part load, BLD at high load when knock limited)
Air humidity	Dried air, humidity < 3%
Boost air temperature	40 ± 3 °C (pre-throttle)
Coolant in temperature	80 ± 3 °C
Oil in temperature	85 ± 3 °C
Low pressure fuel temperature	20 ± 3 °C
Combustion stability	NIMEP_COV ≤ 3%
Fuel type	Regular unleaded gasoline RON 95
Exhaust back pressure	A butterfly valve is used for adjustment, Full opening represents the ambient back pressure

A great deal of attention has been paid to quality of the recorded data in order to have results with highest consistency and accuracy as possible. The followings are the activities which took place before testing to ensure the required accuracy and consistency. In addition to the following actions, all the sensors, analysers and other measurement devices were calibrated thoroughly before starting this experimental work. Among these measurement devices special attention was paid to the flow meters, pressure sensors, temperature sensors, shaft encoder and

emission analysers. Calibration of these devices were also rechecked regularly in order to make adjustments when necessary.

3.6.1 Cam Timings Validation

As it was shown in Figure 3-22 pressure curves are also used for checking and validating the cam and valve timing controls as the precise control of cam timings is key for the experiments. Cam profile characteristics is used to calculate the opening and closing timings of the intake and exhaust valves based on MOP timings which are controlled and measured by ECU. In order to validate the controls, the valve timings are then identified on intake, exhaust and cylinder pressure curves. This validation is necessary and is done every time after engine rebuild.

3.6.2 In-Cylinder Pressure and Fuel Flow Measurements Validation

Since the accurate measurement of the fuel flow and indicated pressure is critical for this project, this section describes the actions took place to ensure a high accuracy for these measurements. A Coriolis type mass flow meter with the sensor size of DN01 1/24" was carefully selected for this single cylinder engine. The flow meter covers a maximum flowrate of 20 kg/h and has a very small error of less than 0.1% when the flow is between 1 kg/h to 20 kg/h (Figure 3-27). This error increases slightly as the flow rate goes below 1 kg/h, for example an error of less than 0.5% might occur when the flow rate is as low as 0.2 kg/h. The calibration of the flow meter was done in the factory with the manufacturer and it was checked again in the university’s laboratory before starting the engine tests.

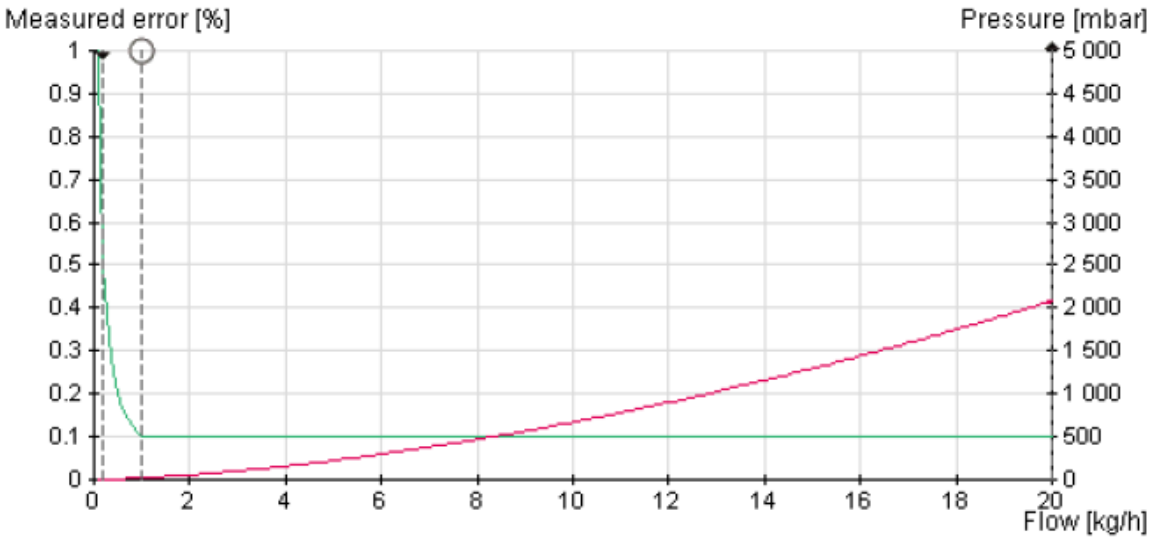

Figure 3-27 Measured error of Endress+Hauser Promass 83A01 flow meter

In order to minimise the error in measuring the indicated pressure, the Kistler transient pressure transducers were checked and calibrated if necessary, on a dead weight tester in the laboratory. In addition, Kistler intake and exhaust absolute pressure transducers and their amplifiers were checked and zero adjusted every time before testing according to the local barometric pressure reading. The exhaust pressure transducer was also cleaned regularly in an ultrasonic bath to avoid carbon deposit accumulation on the sensor for accurate readings. Moreover, a motoring test is designed and performed every time before starting the main experiments at a fixed operating condition (Table 3.10) in order to both check the engine health and measurement system. Peak in-cylinder pressure (Pmax) and the crank angle of Pmax (heat loss angle) can be monitored with this test to check the consistency.

In addition to the above measurements, the accuracy and consistency of all the other measurements were also examined. Emission analysers were also calibrated daily before testing using pure air as zero gas and a specific span gas.

3.6.3 Daily Engine Check Points

Daily motoring and firing tests were performed, and the results were recorded for further analysis every time before the main tests. Firstly, a zero log is recorded after performing daily calibrations in order to check the baseline measurement of all channels. Secondly, a daily motoring test is performed, and the results are logged. The motoring test is performed after the engine warm up to the desired temperature for analyzing the indicated measurements. Finally, a firing test is performed at a fixed operating condition for engine health check and consistency of the overall test system. Operating conditions for daily motoring and firing tests are shown in Table 3.10.

Table 3.10 Motoring and firing daily checks settings

Variables	Daily motoring test	Daily Firing test
Engine speed	1200 rpm	2000 rpm
Engine load	Throttle fully open (barometric intake pressure)	NIMEP = 4.64 bar
Intake and exhaust cam timing (MOP)	Minimum valve overlap	Minimum valve overlap
Exhaust lambda		1
Rail pressure		92 bar
Injection strategy		Single early injection (SOI = 320 CAD BTDCf)
Spark timing		CA50 = 8 CAD ATDCf
Air humidity	Dried air (humidity < 3%)	Dried air (humidity < 3%)

Boost air temperature	40 ± 3°C (pre-throttle)	40 ± 3°C (pre-throttle)
Coolant in temperature	80 ± 3°C	80 ± 3°C
Oil in temperature	85 ± 3°C	85 ± 3°C
LP fuel temperature		20 ± 3°C
Exhaust back pressure		Ambient EBP

An example of daily motoring test results is shown in Figure 3-28. Peak in-cylinder pressure and angle of peak in-cylinder pressure during engine motoring are monitored every time before the main tests.

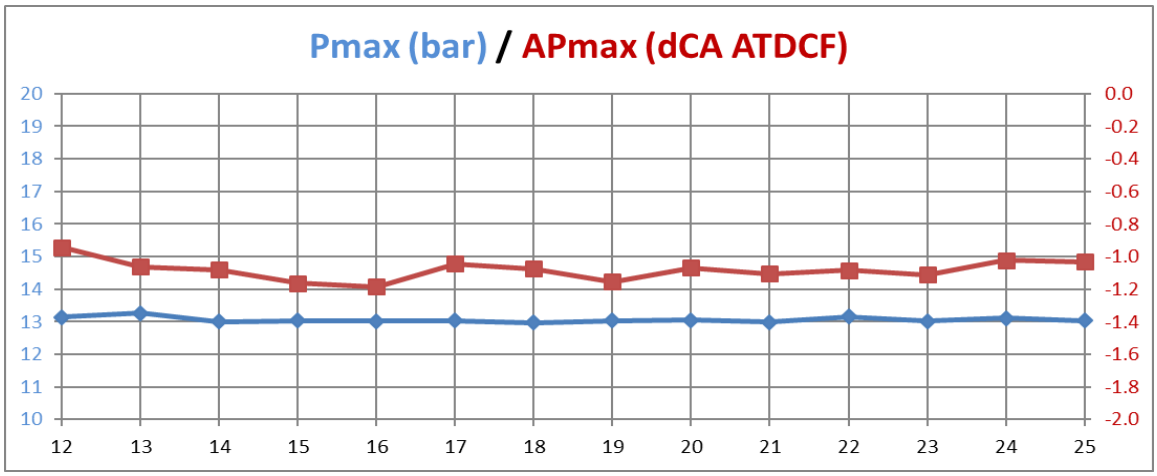

Figure 3-28 Peak cylinder pressure and its angle recorded for daily motoring checks (the x axis shows the test days)

3.7 Summary

The details of the single cylinder engine testbed and all the other facilities used in this experimental work were presented and described in this chapter. The single cylinder downsized gasoline engine equipped with dual injection system (DI and PFI) and intake and exhaust cam phasers, coolant, oil and fuel supply and

conditioning systems, intake and exhaust systems were all presented and explained in detail. In addition, research methodology, operation principles of the main measurement devices and the main equations used for calculations in the combustion analyser software were also presented and discussed. A great deal of effort was put into the accuracy and consistency of the obtained data which was explained in this chapter.

Chapter Four

Effect of PFI / DI Injection Strategies on Combustion, Efficiency and Emissions of Stoichiometric Combustion

Chapter 4 Effect of PFI / DI Injection Strategies on Combustion, Efficiency and Emissions of Stoichiometric Combustion

4.1 Introduction

This chapter describes the effects of dual injection systems on combustion, efficiency and emissions of a downsized single cylinder gasoline direct injection spark ignited (DISI) engine. A set of experiments was conducted with combined port fuel and late direct fuel injection strategy while the overall air / fuel ratio was kept at stoichiometric by means of the closed loop control of exhaust lambda. Several steady state points were selected for this study to represent the typical engine conditions in use. Direct injection timings were varied to find the best injection timing for optimum in-cylinder conditions and therefore optimum efficiency at each speed and load.

4.2 Experimental Setup and Test Conditions

Figure 4-1 shows the schematic diagram of the PFI / DI dual injection system which was used in this experimental study. At each test condition the in-cylinder pressure measurements of 300 cycles were recorded and their average were calculated and used for the heat release and mass fraction burned analysis. For PFI / DI experiments part of the total fuel was injected into the intake port through a PFI. The PFI injection timing was kept constant with the start of injection (SOI) at 90 CAD BTDC. At this time the intake valves were fully closed and therefore there was enough time for the fuel to evaporate in the intake port. The other part of the

fuel was injected directly into the combustion chamber by the DI injector during the compression stroke to create a stratified mixture near the spark plug to facilitate the ignition and the initial flame propagation process. DI injection timings and ratios are swept in a wide range, in order to find the optimum injection timings and ratios for the minimum net indicated specific fuel consumption (NISFC) and highest combustion stability. This is also repeated for split DI at both stoichiometric and lean conditions which is presented in Chapter 5.

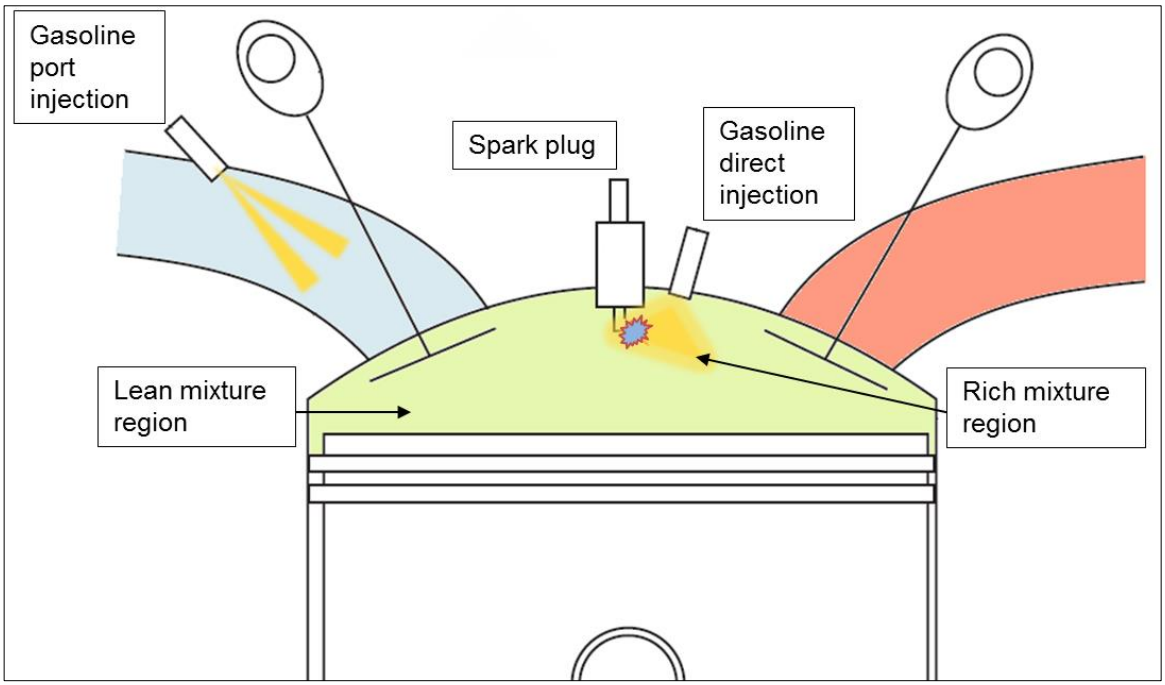

Figure 4-1 Schematic diagram of hybrid PFI / DI combustion system

Furthermore, the tests were conducted at the optimum cam timing achieved with single early DI injection at this speed and load, which were determined in separate experiments. Therefore, the results can be compared with the results achieved by single early direct injection. A combustion stability limit or COV of NIMEP of 3% was applied throughout the experiment.

At lower loads, the spark timing was adjusted to the maximum brake-torque (MBT) timing to produce the minimum net indicated specific fuel consumption (NISFC). However, at the low speed and high load points, the spark advance was restricted by the knocking combustion to the detonation borderline (DBL). All the tests were conducted with the engine fully warmed up to the desired oil and coolant temperature. The target speed was selected by using the dyno controller, and then the throttle opening was adjusted to achieve the target NIMEP. The operating conditions are shown on Table 3.9 in section “3.6 Testing and Data Accuracy”.

Figure 4-2 shows the steady state testing points which were selected for the single cylinder engine experiments. In this study the focus was on area (2) and (3) on the map for the PFI / DI investigations. These two areas represent the most operating conditions of the engine in a typical passenger car during the European driving cycle. Area (2) represents a low load area around 5 bar NIMEP and area (3) shows the mid load region of the map which is around 9 bar NIMEP. Some test points were also selected from area (4) to represent the high load points which are knock limited (16 and 20 bar NIMEP) at various engine speeds (1000 rpm to 3000 rpm) for the water injection experiments.

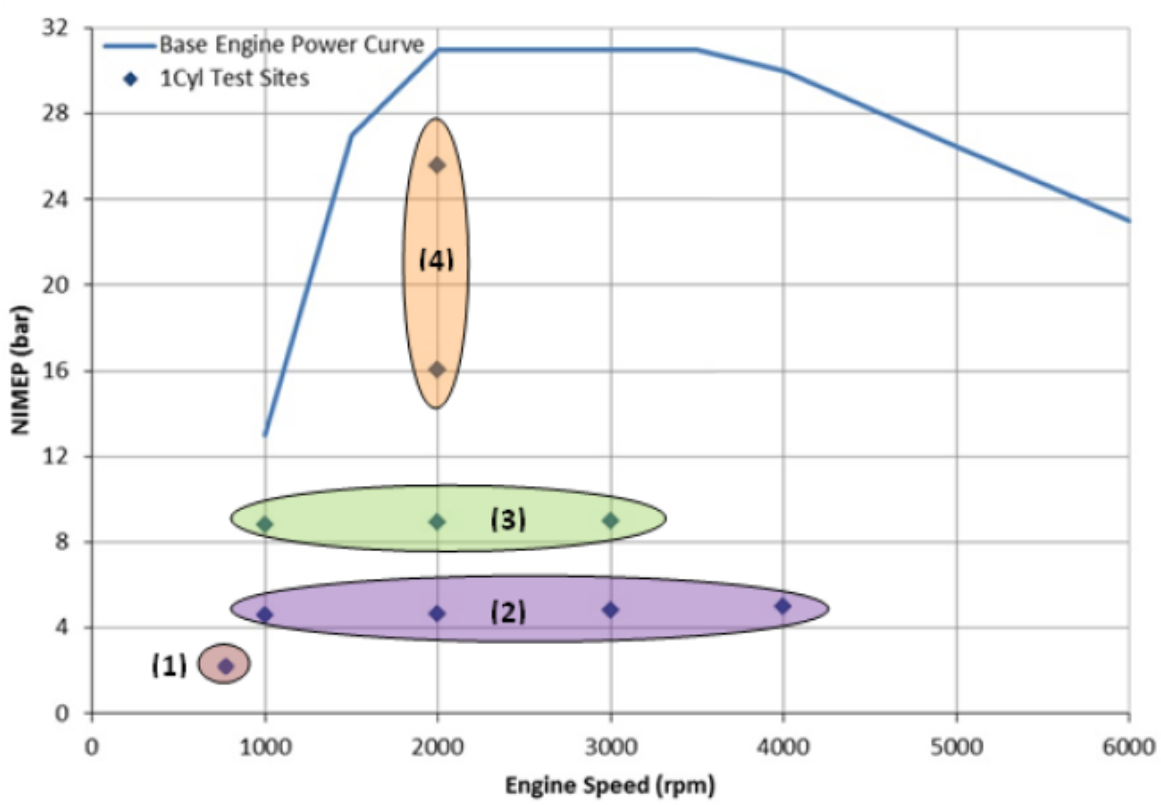

Figure 4-2 Steady state operating points (different colours in this graph represent different operating area on the map and each area is numbered and explained in the above text)

4.3 Results and Discussion

4.3.1 Effects of late DI Injection Timings during the PFI / late DI operation

Figure 4-3 shows the effect of the different late DI stratification timings on NISFC, combustion efficiency and CoV of NIMEP at constant NIMEP during PFI 70% / late DI 30% operation. PFI to late DI ratio of 70% to 30% was selected since this is one of the optimum ratios for the minimum NISFC according to the experimental results (DI ratio investigation is presented in the next chapter). In addition, in order to create as homogeneous as possible mixture the large amount of fuel required to be injected through the PFI which prevents high level of stratification in the cylinder

and helps to reduce the unburned combustion products. In this thesis NISFC is calculated using Equation 4-1:

$$NISFC = \frac{\dot{m}_f}{P_i}$$

Equation 4-1

In this equation, $\dot{m}_f$ is the fuel mass flow and P_i is the net indicated power (calculated from NIMEP).

At all three speeds advancing DI injection timing results in a decrease in NISFC. Furthermore, the combustion stability (NIMEP_CoV) is improved by advancing the late DI injection timing. The minimum NISFC values at 1000 rpm and 2000 rpm are achieved when the end of direct injection timing (EOI) is set at 60 CAD BTDC. However, at 3000 rpm the minimum NISFC is achieve with EOI of 90 CAD BTDC because of the less time available for the fuel to evaporate and mix with air at higher speeds.

Figure 4-3 also shows that the highest combustion efficiency is achieved at the optimum injection timings for the minimum NISFC due to lower CO emissions (Figure 4-5) at these points. The combustion efficiency was calculated using Equation 3-21.

The improvement in NISFC, combustion efficiency and stability can be explained by the slightly shorter combustion duration (Figure 4-4) and higher maximum in-cylinder pressure (Figure 4-7) as the injection timing was advanced.

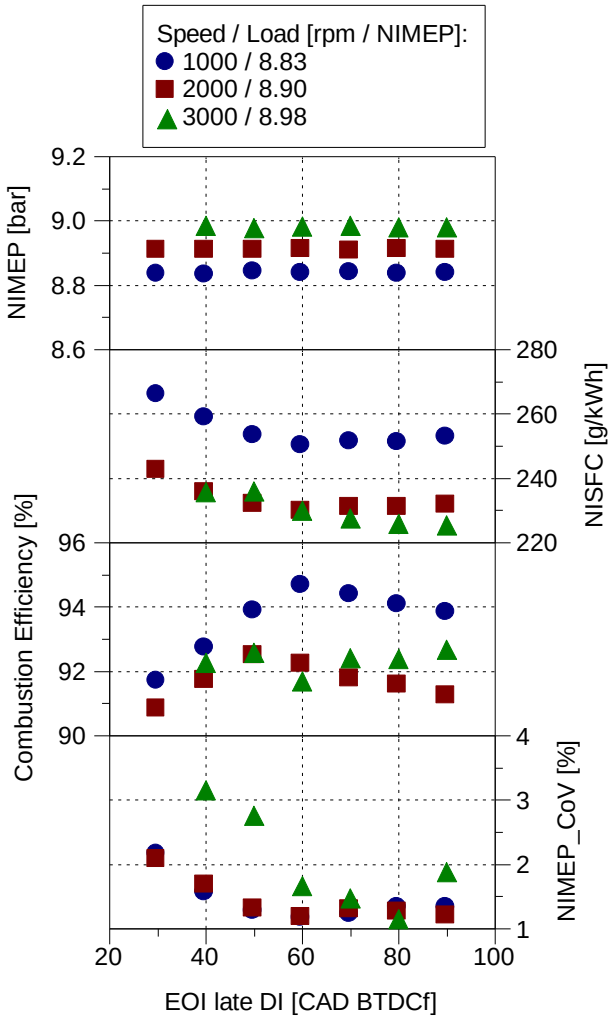

Figure 4-3 NIMEP, NISFC, combustion efficiency and Combustion stability (NIMEP_CoV) at different speeds against late DI timings during the PFI 70% / late DI 30% operation

At 1000 rpm, the flame development angle (spark-CA10 in Figure 4-4) is hardly affected by the injection timing. However, at 2000 and especially 3000 rpm, the flame development angle decreases slightly with the advanced injection timing up to 60 CAD BTDC and then increase slightly again as the injection was advanced further.

At 1000 rpm and 2000 rpm, CA50 was almost constant with only small adjustment. At 3000 rpm, CA50 was slightly more advanced as the EOI was advanced. At 1000

rpm, CA50 is significantly delayed because of the retarded spark timings used to avoid knocking combustion, which was more likely to occur at a lower engine speed.

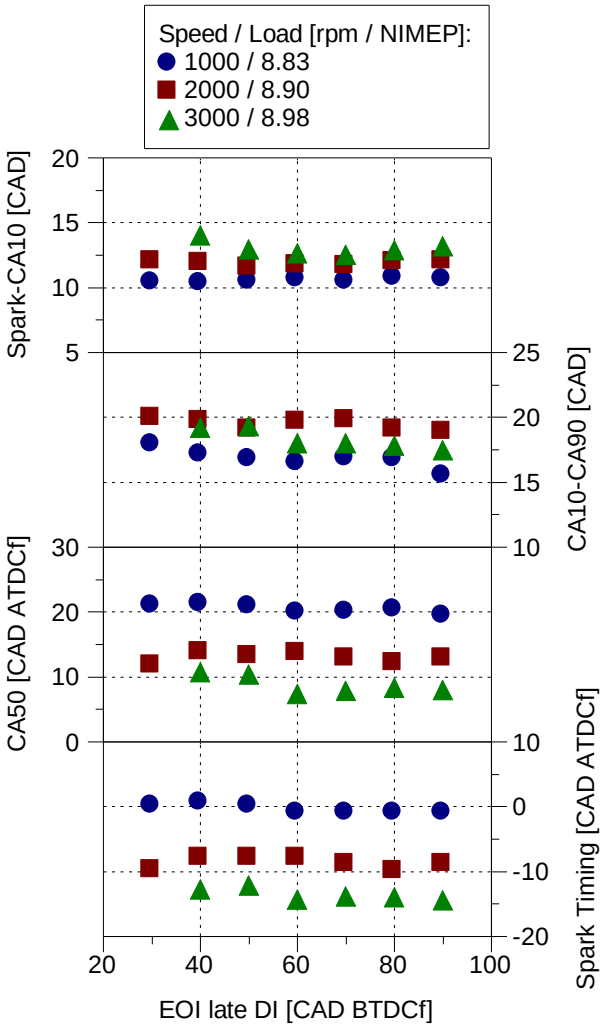

Figure 4-4 Flame development angle (spark to CA10), Combustion duration (CA10 to CA90), CA50 and spark timing at different speeds against late DI timings during the PFI 70% / late DI 30% operation

Measured CO, HC, NO_x and smoke emissions for various late DI injection timings at the three different speeds are shown in Figure 4-5. CO emissions increased as the injection timing was retarded especially at 1000 rpm and 2000 rpm, indicating the presence of inhomogeneous and locally-rich mixture from late fuel injections.

Similarly, the soot concentration went up as the injection was retarded towards the TDC at 2000 rpm and 3000 rpm, which suggested that fuel-rich combustion had taken place. At 1000 rpm the soot emission was less affected and stayed almost constant around 0.05.

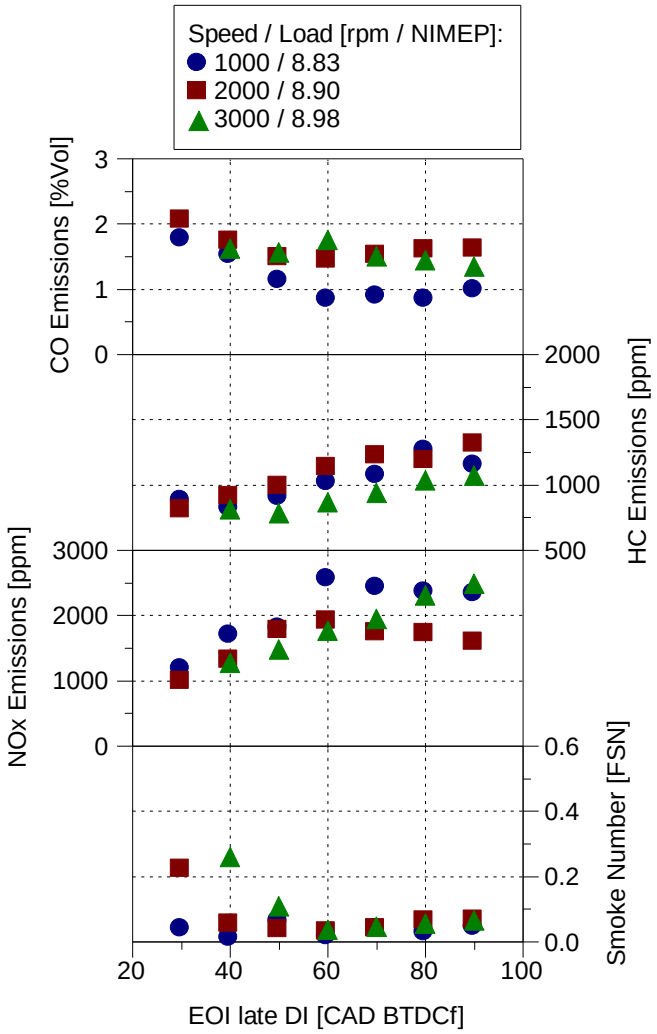

Figure 4-5 CO, HC, NO_x and smoke emissions at different speeds against late DI timings during the PFI 70% / late DI 30% operation

The significantly higher soot emissions at the higher engine speeds could be related to the much shorter dwell angle between the EOI and the spark ignition (SI). When the EOI was 40 CA BTDC, this dwell angle was 40 CAs at 1000 rpm

and reduced to 32 CAs at 2000 rpm and then 27 CAs at 3000 rpm (Figure 4-6). In the absolute time, the time interval between the EOI and SI was reduced from 6.6 ms at 1000 rpm to 2.6 ms at 2000 rpm and 1.5 ms at 3000 rpm, which drastically reduced the time for fuel evaporation and mixing to take place prior to the spark ignition.

In comparison, the HC emission decreased as the in-cylinder injection was retarded. It is known that the unburned hydrocarbons (UHC) in a DI gasoline engine could be produced from fuel rich region due to under-mixing or too lean mixture by over-mixing, the fuel trapped in the crevices and liquid fuel impingement in cylinder wall. The exhaust UHC emission is also affected by the post-flame oxidation. The lower HC emission from the very late injection could be due to less UHC trapped in crevices as the injected fuel was more concentrated in the central region of the cylinder at very late injection. It was also very likely much of UHC in the fuel rich regions was partially oxidized to CO as indicated by the higher CO emission from late injections.

NO_x emissions peak at the optimum injection timings (for the minimum NISFC) for all three speeds. Higher level of NO_x emissions at the more advanced injection timings can be explained by slightly higher peak cylinder pressure (Figure 4-7) and heat release rate (Figure 4-8). Slightly higher peak cylinder pressure and heat release could increase the in-cylinder temperature and lead to higher NO_x emissions. In addition, at 1000 and 2000 rpm NO_x emissions decreased slightly by advancing the injection timing more than 60 CAD BTDC. This also can be explained by slightly lower heat release at these injection timings (such as 70 CAD

BTDC) which led to slightly lower in-cylinder temperature and hence slightly lower NO_x emissions.

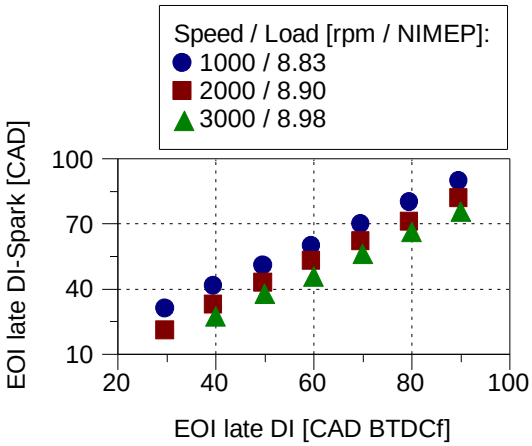

Figure 4-6 Dwell angle between the EOI and the spark timing at different speeds against late DI timings during the PFI 70% / late DI 30% operation

Furthermore, Figure 4-7 also shows that a higher intake pressure was required with the more retarded injection timings to maintain the same NIMEP. As it was mentioned earlier, retarded injection timings led to a poor mixture preparation. Therefore, CO and smoke emissions increase and deteriorate the combustion efficiency. As a result, higher intake pressure and therefore more fuel was required to maintain the load.

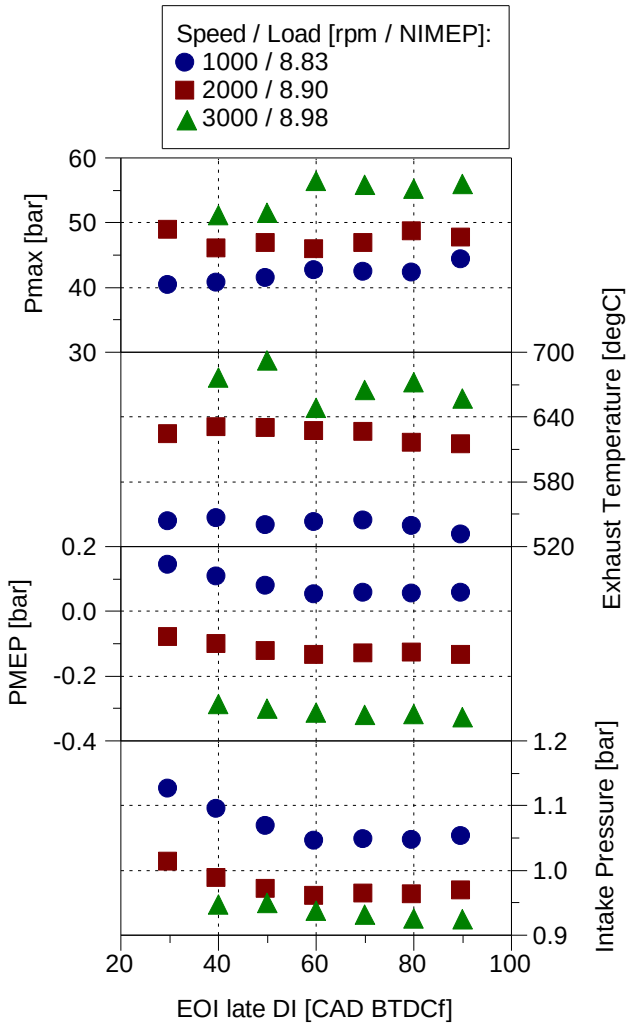

Figure 4-7 Maximum cylinder pressure, exhaust temperature, PMEP and intake pressure at different speeds against late DI timings during the PFI 70% / late DI 30% operation

As a summary of this section, it can be concluded that there is an optimum DI injection timing for best combustion efficiency and lowest NISFC at low engine speeds (1000 and 2000 rpm). As the engine speed went up to 3000 rpm, the advanced DI injection timing improved NISFC due to better mixture preparation. The earlier DI injection timings led to slightly shorter combustion duration, lower CO and smoke emissions but increased UHC emissions. The smoke emission was less sensitive to the DI injection timing at the low engine speed of 1000 rpm.

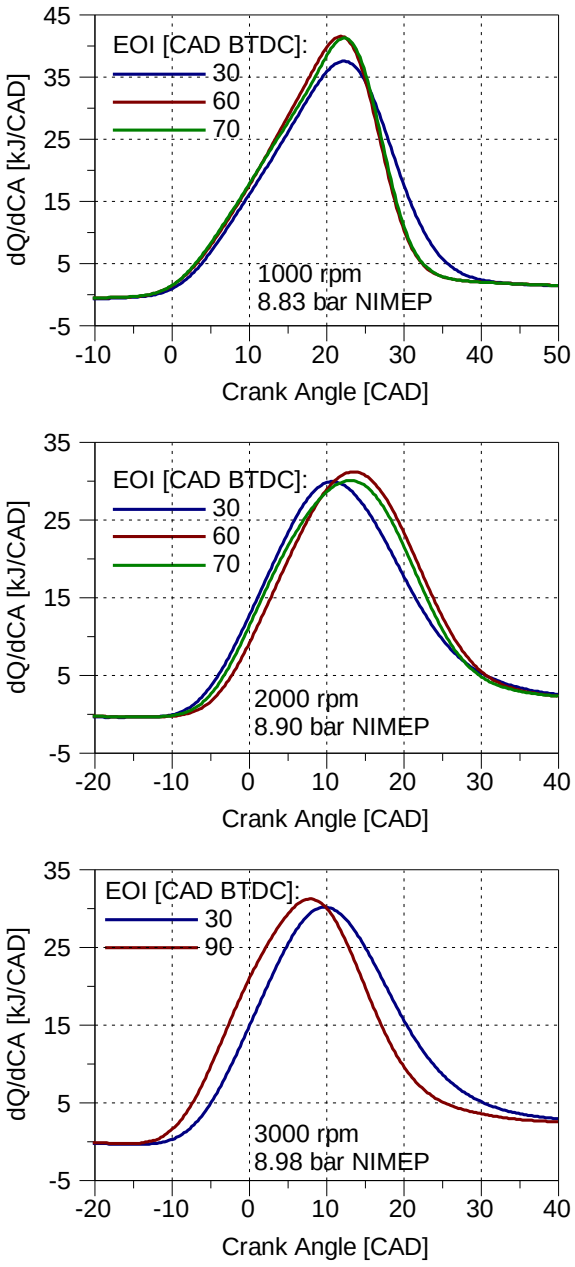

Figure 4-8 Heat release rate vs crank angle during the PFI 70% / late DI 30% operation at different speeds and late DI timings

4.3.2 Comparison between PFI / late DI and single early DI injection strategies

After performing injection sweep test under PFI / late DI operation mode, the late DI timings which produce the minimum NISFC were selected as the optimum

injection timings. In this part the efficiency, combustion characteristics and the emissions of those optimum points are compared to the points with single early DI operation, which has a SOI (start of injection) at 320 CAD BTDC during the intake stroke and is representative of the typical GDI operation mode.

As shown in Figure 4-9, a significant decrease in NISFC (around 9%) under PFI / late DI operation was achieved at 1000 rpm. This significant decrease in NISFC can be explained by combustion phasing and duration as the main parameters for the improved efficiency. As it was mentioned earlier the engine operation at all three speeds and loads was knock-limited therefore the CA50 positions (Figure 4-10) were much delayed. It is noted that both flame development angle and combustion duration (Figure 4-10) were shorter under PFI / late DI operation at 1000 rpm. The shorter flame development angle seems to suggest that combustion was initiated in a stratified charge of near stoichiometric mixture near the spark plug when the ignition took place. The faster combustion reduced the time available for autoignition reactions to take place in the end gas region. In addition, the leaner premixed mixture in the end gas region would slow down the autoignition process. Another factor could be the increased turbulence from the late DI injection, which would have more impact on the lower engine speed when the tumble motion was low at lower engine speeds.

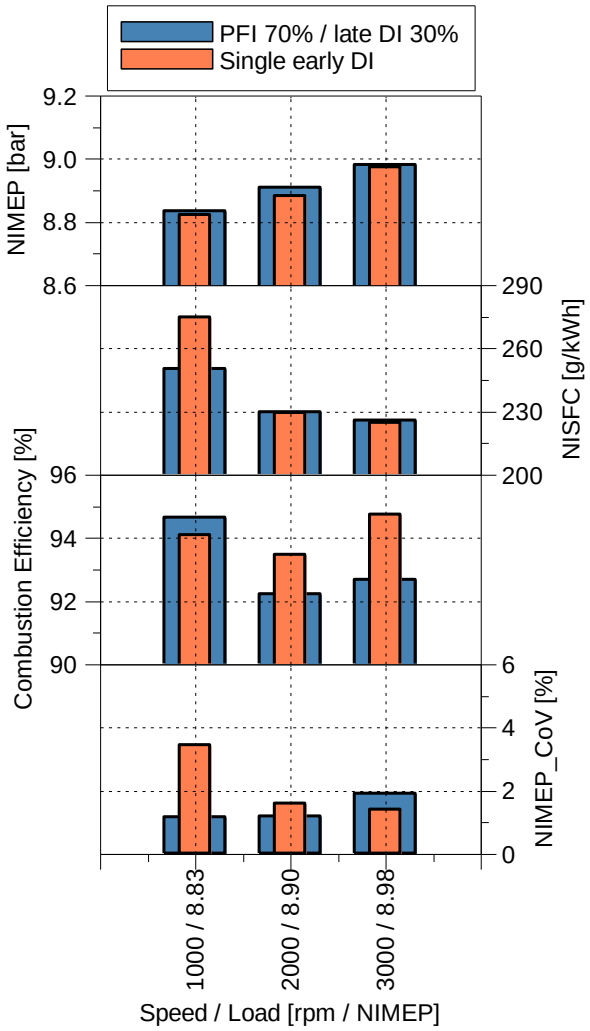

Figure 4-9 NIMEP, NISFC, combustion efficiency and combustion stability (NIMEP_CoV) comparison for single early DI and PFI / late DI injection strategies at different speeds

At 2000 rpm the NISFC (Figure 4-9) is almost the same for both injection strategies. At this speed the engine operation was still knock-limited as can be seen in the CA50 graph (Figure 4-10). Late DI allowed the used of around 2 degree more spark advance under PFI / late DI operation compared to the single early DI operation. This advanced the CA50 around 3 degree. At this speed flame development angle and combustion duration (Figure 4-10) under PFI / late DI operation was very similar to those under single early DI operation. Hence, the

efficiency stayed almost at the same level for both injection strategies. Late DI stratification at this speed led to formation of an inhomogeneous and locally-rich mixture which deteriorates the combustion efficiency (Figure 4-9) compared to the single early DI operation.

At 3000 rpm the NISFC under PFI / late DI operation was also very similar to those of single early DI operation (Figure 4-9). At this speed, late DI injection allowed the use of a more advanced spark timing (around 4 CAD) compared to the early single DI operation, therefore CA50 of around 8 CAD ATDC was achieved (Figure 4-10). Despite the advanced combustion timings and closer spark timing to the MBT, combustion duration (Figure 4-10) was remained almost the same as the DI only operation. Therefore, there wasn't any gain in efficiency under PFI / late DI operation at this speed. In addition, marginally higher intake pressure (Figure 4-12) under PFI / late DI was required to maintain the load due to significantly higher CO emissions (Figure 4-11) and therefore lower combustion efficiency compared to the single early DI operation.

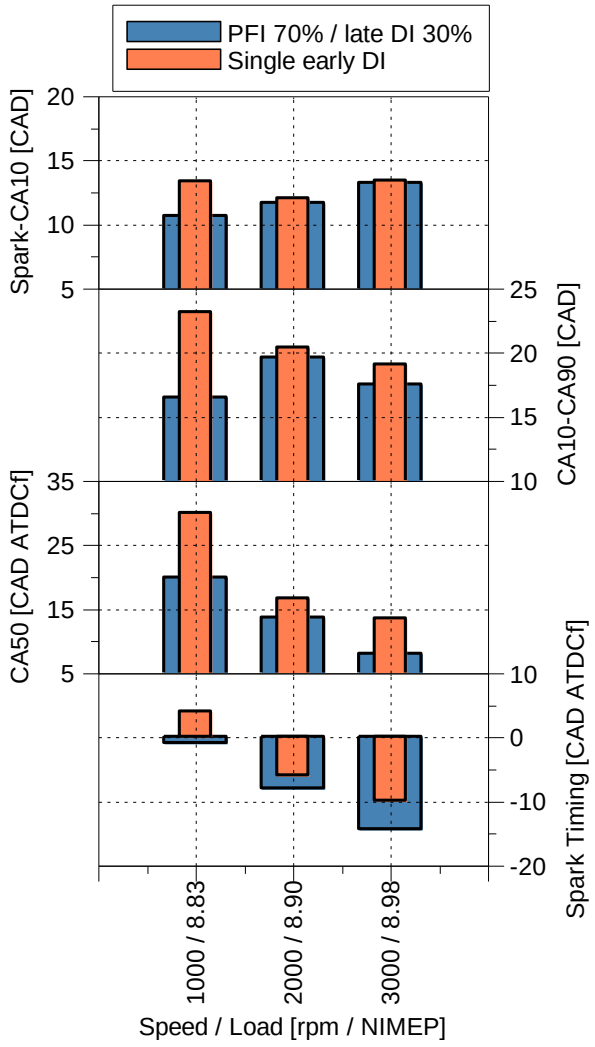

Figure 4-10 Flame development angle (spark-CA10), combustion duration (CA10-CA90), CA50 and spark timing comparison for single early DI and PFI / late DI injection strategies at different speeds

In terms of combustion efficiency, at 1000 rpm highly retarded combustion phasing and long combustion duration (Figure 4-10) under single early DI operation led to a need for higher intake pressure to maintain the load (Figure 4-12). Therefore, significantly higher HC emissions (Figure 4-11) were produced during the single early DI operation. As a result, lower combustion efficiency (Figure 4-9) was achieved under single early DI injection. On the other hand, higher CO emission (Figure 4-11) under PFI / late DI operation was detected due to the

inhomogeneous mixture produced by the late DI injection. However, at 2000 and 3000 rpm, PFI / late DI operation led to lower combustion efficiency than the single early DI operation.

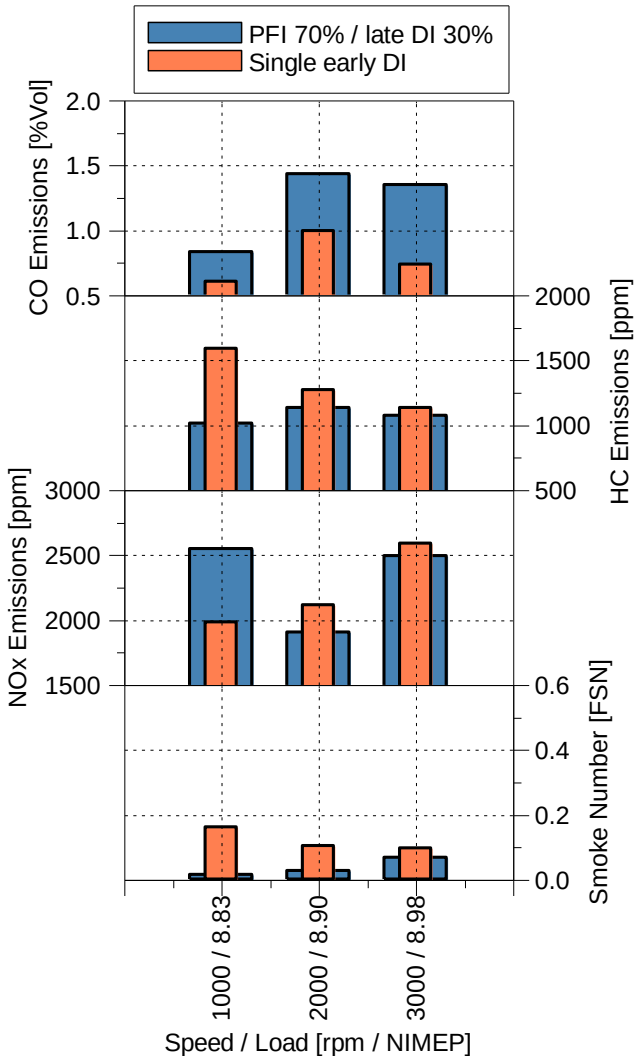

Figure 4-11 CO, HC, NO_x and smoke number comparison for single early DI and PFI / late DI injection strategies at different speeds

In terms of combustion stability, significantly lower CoV of NIMEP was achieved under PFI / late DI operation at 1000 rpm, because of the faster combustion process. As the engine speed increased, PFI / late DI operation maintained its lower CoV at 2000 rpm but exhibited slightly higher CoV at 3000 rpm than the

single early DI injection. This could be a result of larger cycle-to-cycle variation in the mixture formation process associated with the late DI injection.

In general, the PFI / late DI operations produced less UHC emissions than the single early DI injection. This could be attributed mainly to the reduced amount of premixed fuel trapped in the crevices as 30% fuel was not injected until the end of the compression stroke.

As can be seen in Figure 4-11, NO_x emissions under PFI / late DI injection strategy at 1000 rpm are considerably higher than those for single early DI strategy, because of the earlier and faster combustion, higher heat release (Figure 4-13) and hence higher peak in-cylinder pressure and temperature.

As the engine speed was increased to 2000 and 3000 rpm, NO_x emissions under PFI / late DI operation became very similar to those under single early DI strategy despite the higher maximum cylinder pressure with PFI / late DI operation. This can be explained by the heat release diagrams. At 2000 and 3000 rpm the heat release under PFI / late DI and single early DI strategies was the same (Figure 4-13) and combustion timings are also very similar for both strategies.

The PFI / late DI strategy significantly reduced the smoke emissions as 70% fuel was supplied as the premixed and homogeneous air / fuel mixture. The effect was most pronounced at lower engine speed. As the engine speed increased, the mixture quality slightly deteriorated under PFI / late DI operation and led to an increase in incomplete combustion products such as CO and smoke emissions.

Figure 4-12 also shows that the exhaust temperature under PFI / late DI operation is slightly lower than those under single early DI operation at all the three speeds.

This can be explained by a more advanced combustion timing and heat release under PFI / late DI operation. Combustion starts earlier in the cycle under PFI / late DI operation due to more advanced spark timings. As results, heat release (Figure 4-13) begins earlier in the cycle and finishes earlier. Therefore, gas temperature decreases earlier, and the exhaust temperature is lower under PFI / late DI operation.

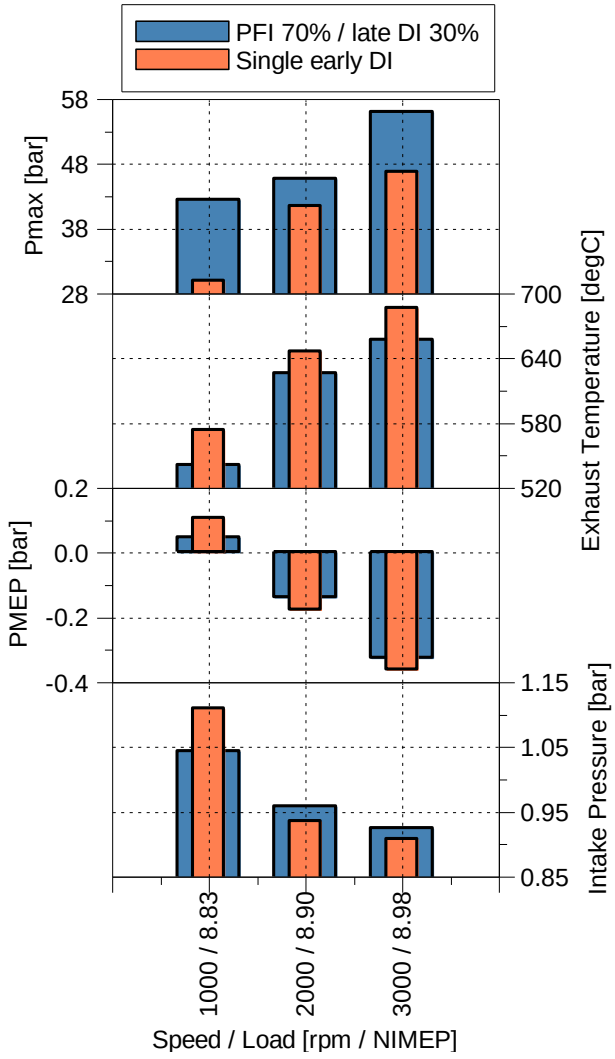

Figure 4-12 Maximum cylinder pressure (Pmax), exhaust temperature, PMEP and intake pressure comparison for single early DI and PFI / late DI injection strategies at different speeds

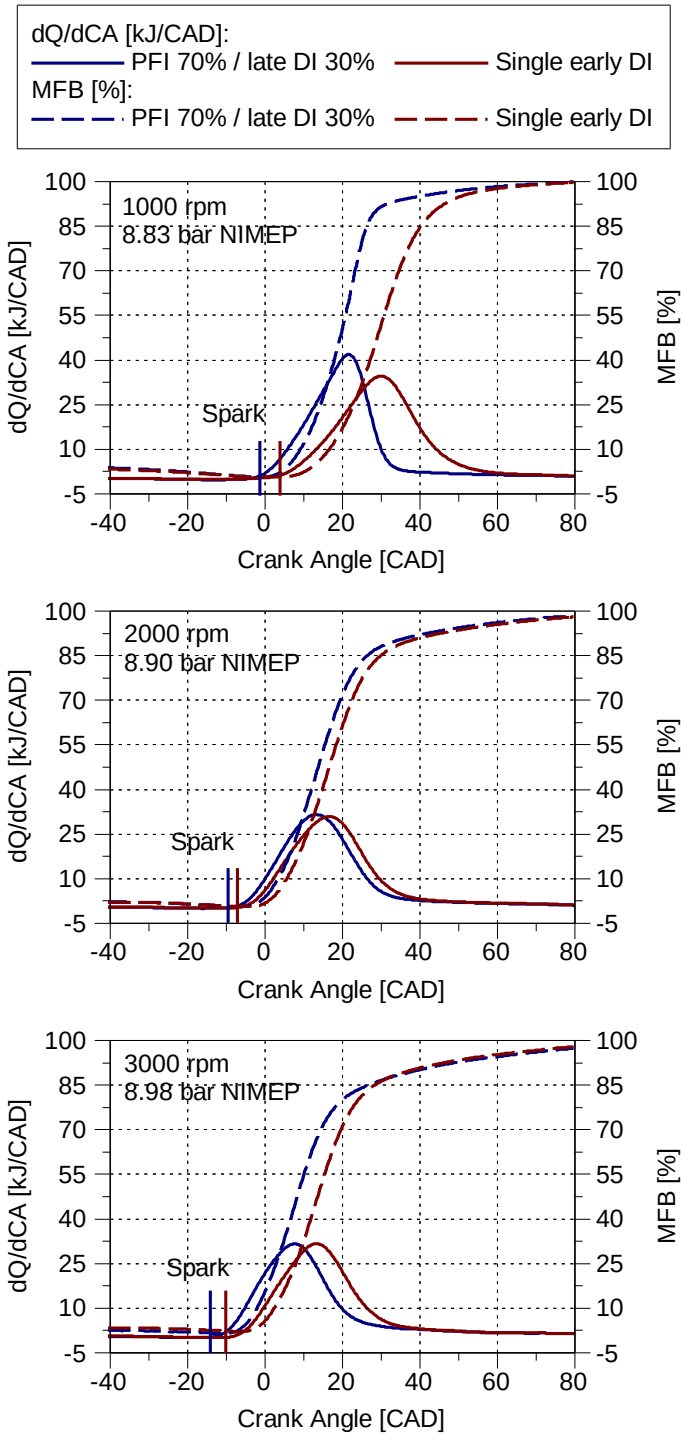

Figure 4-13 Heat release rate and mass fraction burned vs crank angle under PFI / late DI and single early DI strategies at different speeds

4.3.3 Summary

In this chapter, a detailed analysis of the combustion, fuel economy and emissions under single early DI and PFI / late DI injection strategies were carried out on a boosted DISI gasoline engine. The experiments were conducted at three different speeds and mid-high load points. The air-fuel ratio was kept at stoichiometric for all the tests. In the first injection strategy, a single early DI injection was used to create a homogeneous mixture representing the typical DISI gasoline operation. In the second strategy, a port fuel injector was used to inject 70% of the fuel in the intake manifold when the intake valves were closed. The remaining 30% of the fuel was injected late during the second half of the compression stroke directly in the cylinder through an outwardly opening piezo injector with a hollow-cone spray. Injection timing sweep tests were performed for the late DI injection from 30 to 90 CAD BTDC. Then the optimum injection timings were selected for the comparison with the single early DI strategy. The main findings can be summarized as follows:

- During the PFI / late DI operations, the late DI injection timing directly affected the fuel economy, combustion and emissions. Minimum ISFC and highest combustion efficiency were achieved when the EOI of the late DI injection was 60 CAD BTDC at 1000 rpm and 2000 rpm and 90 CAD BTDC at 3000 rpm.
- When the optimum later DI injection was used, it led to faster flame propagation and reduced tendency to knocking combustion so that the combustion process could take place near the TDC for maximum efficiency.

- The CO and soot emissions increased as the late DI injection was retarded towards TDC because of the presence of fuel rich mixtures. Similarly, the UHC tended to be higher as the late DI injection was advanced.
- When comparing single early DI and PFI / late DI operations, significantly lower NISFC (around 9%) at 1000 rpm / 8.83 bar NIMEP was achieved under PFI / late DI operation because the knock limited spark timing was more advanced.
- At 2000 rpm and 3000 rpm, PFI / late DI operations had slightly higher NISFC than the single early DI operation due to lower combustion efficiency.
- PFI / late DI operations produced significantly lower smoke emissions, higher CO but lower UHC emissions than those with the single early DI injections.

Chapter Five

Effect of PFI / DI Injection Strategies on Combustion, Efficiency and Emissions of Lean Combustion

Chapter 5 Effect of PFI / DI Injection Strategies on Combustion, Efficiency and Emissions of Lean-burn Combustion

5.1 Introduction

This chapter describes the effects of dual injection systems and split injection strategies on combustion, efficiency and emissions of a downsized single cylinder gasoline direct injection spark ignited (DISI) engine operated with variable air / fuel ratios. These strategies were explored to create a partially stratified combustion (homogeneous / stratified combustion). In addition to direct injection timings, direct injection ratios were also varied in order to study the effect of these variables on engine parameters and achieve the optimum in cylinder conditions and therefore optimum efficiency at a specific steady state point. The effect of each injection strategy on knock suppression and the lean combustion stability limit was also determined.

5.2 Experimental Setup and Test Conditions

The experimental setup used to obtain the results in this chapter was same as the previous chapter (Chapter 4) with no changes (Figure 4-1 and Figure 4-2). The only difference between the two setups was the compression ratio of the engine which was altered from 12.78 (in Chapter 4) to 11.43 (in this Chapter) in order to be able to operate at higher loads without being significantly knock limited by a very high geometric compression ratio.

5.3 Results and Discussion

5.3.1 Effects of late DI injection timings during the PFI / late DI and early DI / late DI operation at mid load

This section describes the effect of late DI injection timings during PFI / late DI and early DI / late DI injection strategies at 1000 rpm / 8.83 bar NIMEP. This section shows the results for stoichiometric air/fuel ratio in order to find out the optimum late DI timings for the minimum NISFC, then the effect of various PFI / DI injection strategies at lean air/fuel ratios is investigated with the optimum late DI timings and ratios and presented in section 5.3.3 and 5.3.6 of this chapter. As it was mentioned in the previous chapter, PFI to late DI ratio of 70% to 30% was selected since this is one of the optimum ratios for the minimum NISFC according to the experimental results (DI ratio investigation is presented in section 5.3.2 and 5.3.5 of this chapter). In addition, in order to create as homogeneous as possible mixture the large amount of fuel required to be injected through the PFI which prevents high level of stratification in the cylinder and helps to reduce the unburned combustion products. Start of the injection for PFI was set at 90 CAD BTDCf and the PFI rail pressure kept constant at 5 bar gauge. For early DI injection, start of injection was set at optimum which is 276 CAD BTDCf at this test point. DI rail pressure was set at 133 bar. Late DI timings were varied in a wide range of 30 to 180 CAD BTDCf. Cam timings were set at the optimum timings which were achieved with single DI injection at this point (intake MOP=120 CAD ATDC and exhaust MOP=110 BTDC).

Figure 5-1 shows the effect of late DI injection timings (EOI2 (end of the second injection)) on NISFC, combustion efficiency and combustion stability for the two

cases of PFI 70% / late DI 30% and early DI 70% / late DI 30% at 1000 rpm and constant NIMEP of 8.83 bar and stoichiometric air / fuel ratio. In these tests, 70% of the total fuel is introduced through the PFI or early DI injection and the rest of the fuel is injected through the late DI injection during compression stroke. As the EOI2 advances from 30 CAD BTDCf, NISFC decreases and reach its minimum at around 60 CAD BTDCf for both cases. The main reason for this trend is the mixture preparation at different late DI timings. Very late DI timings such as 30 CAD BTDCf produce a rich mixture near the spark plug which can't be fully evaporated and mixed with the air by the time of ignition. These locally rich areas then increase the unburned combustion products such as CO and particulate emissions (Figure 5-10) which consequently reduce the combustion efficiency and increase the fuel consumption. Therefore, higher intake pressure (Figure 5-7) was required to maintain the same load.

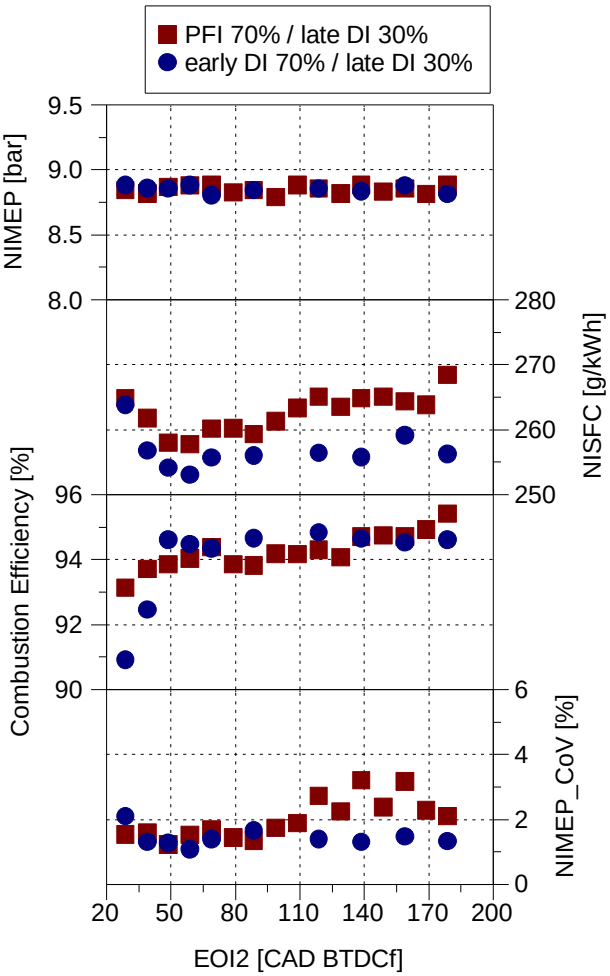

Figure 5-1 NIMEP, NISFC, combustion efficiecny and combustion stability of PFI / late DI and early DI / late DI case for different late DI timings

The amount of time available between the end of the late injection and the spark timing is shown in Figure 5-2 for different late DI injection timings. When the EOI2 is at 30 CAD BTDCf, only 30 CAD is available for the late injected fuel to evaporate and mix with air (at 1000 rpm this is only 5 ms). This time increases in 10 CAD intervals as the EOI2 is advanced, therefore more time is available for mixture formation as the EOI2 is advanced. This is also clear from the lower combustion stability (Figure 5-1) at highly retard and highly advanced injection timings which produce some late burning cycles and increase the cycle-by-cycle variation.

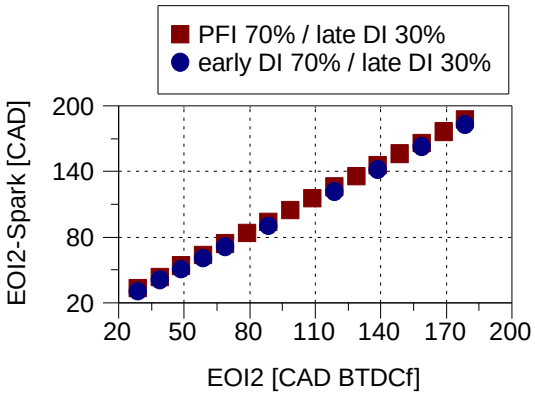

Figure 5-2 End of late injection timing to spark at different late injection timings

Figure 5-3 and Figure 5-4 compares the P-V diagram, cylinder pressure, heat release and mass fraction burned of the early DI / late DI case for the late DI timings of 30, 60 and 160 CAD BTDCf. P-V diagram shows that the higher cylinder pressure during intake stroke leads to higher compression pressure and work while the expansion pressure is almost the same when comparing EOI2 of 30 CAD BTDCf with 60 CAD BTDCf. This decreases the area of the power loop and results in a lower efficiency. This pressure difference can also be seen clearly in the cylinder pressure diagram (Figure 5-4). In addition, the locally rich areas near the spark plug created by very late injection (EOI2 of 30 CAD BTDCf) produces slightly faster heat release initially but when the flame reaches the leaner areas of the chamber near the wall heat release drops faster and the peak is slightly lower for EOI2 of 30 CAD BTDCf (Figure 5-4). Mass fraction burned diagram shows the slower combustion after 80% MFB for EOI2 of 30 CAD BTDCf which confirms the slower combustion compare to EOI2 of 60 CAD BTDCf (Figure 5-4).

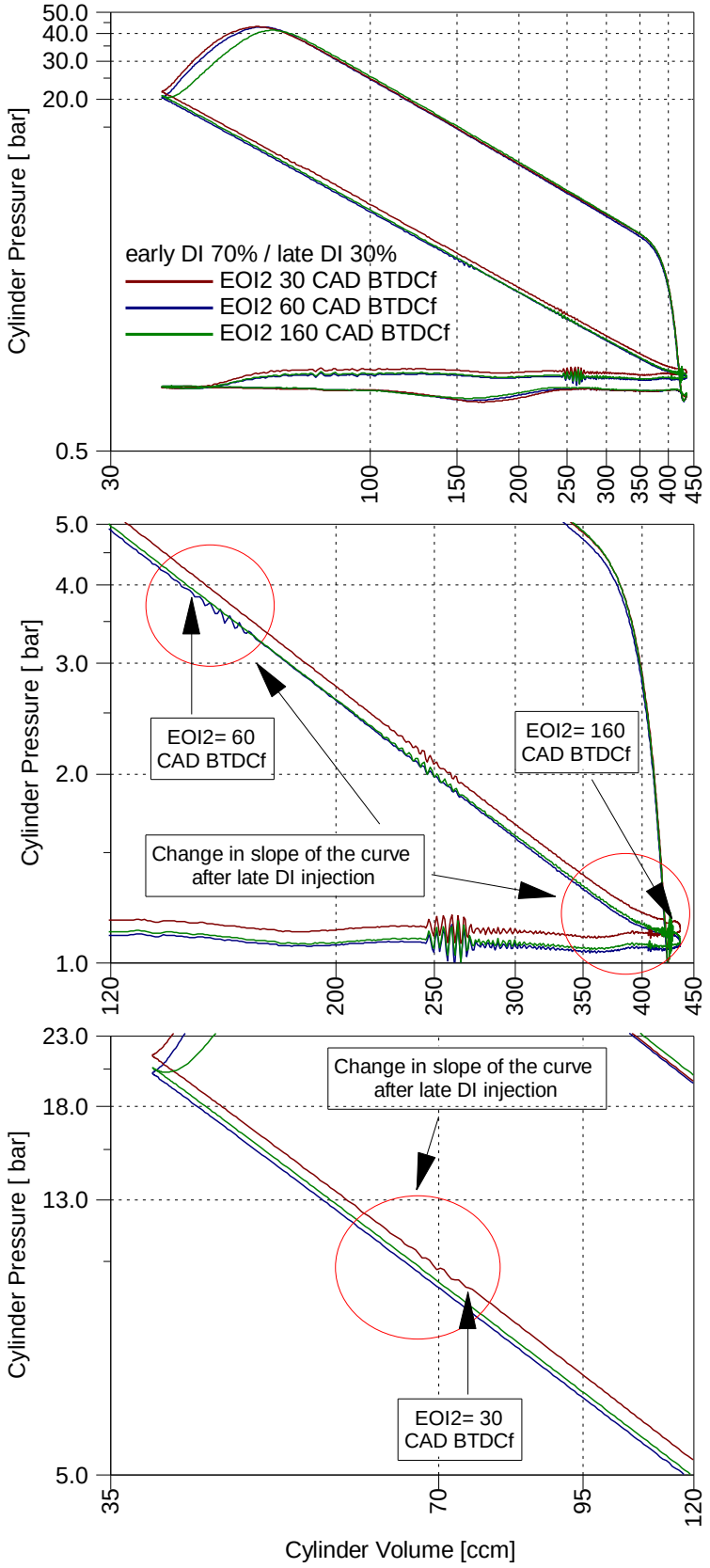

Figure 5-3 LogP - logV diagram of early DI / late DI case for different late DI timings

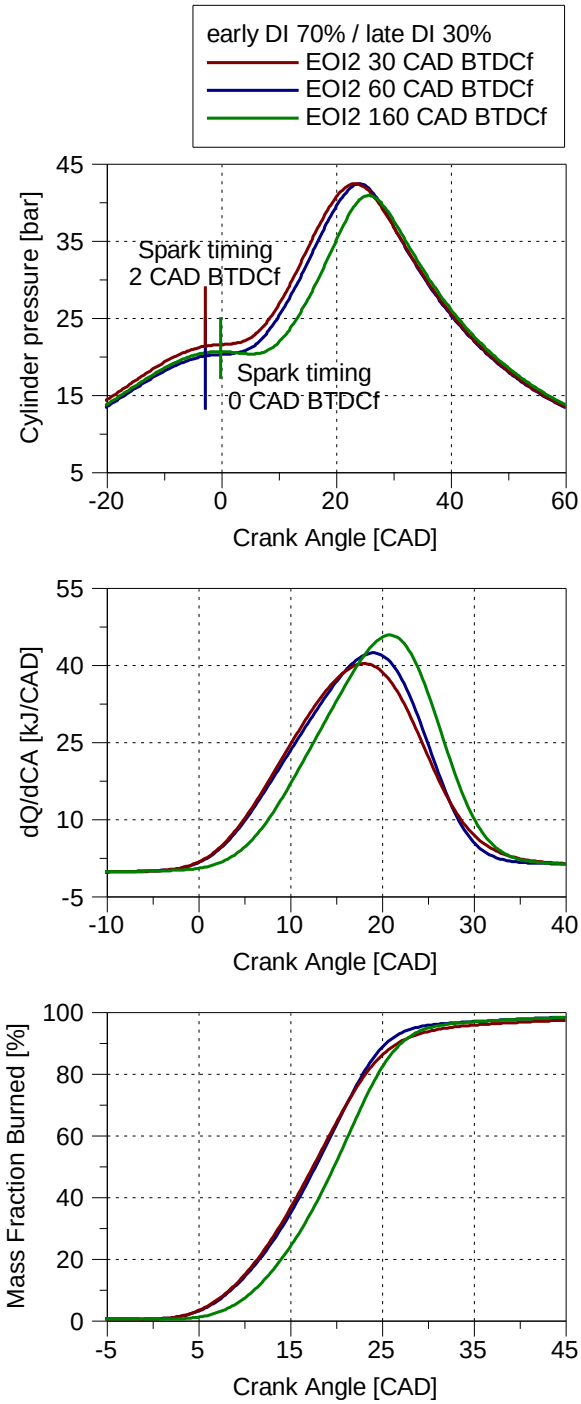

Figure 5-4 Cylinder pressure, heat release, mass fraction burned of early DI / late DI case for different late DI timings

On the other hand, advancing the EOI2 beyond 60 CAD BTDCf also increases the fuel consumption. One reason for this can be the in-cylinder flow characteristic during the early compression stroke which affects the mixture preparation and is

not as favorable as it is at 60 CAD BTDCf to form the ignitable mixture in the area that can be easily ignited. Another reason is that the spark timing (Figure 5-9) was retarded slightly when the injection timings were advanced more than 90 CAD BTDCf. The spark timings were retarded to avoid knocking combustion which was more likely to happen as the second injection was advanced towards BDC. More advanced injection timings during the first half of compression cool down the charge earlier in the compression stroke but as the piston travels towards the TDC the charge temperature stars to increase again and therefore the temperature of the charge at the time of ignition is higher with the more advanced injection timings compare to the more retard ones. This is also clear from the P-V diagram and the in-cylinder pressure curve (Figure 5-3 and Figure 5-4). When the EOI2 is 160 CAD BTDCf the cylinder pressure is higher during the second half the compression stroke compared to the EOI2 of 60 CAD BTDCf. Therefore, the cylinder temperature could be higher at the time of ignition and consequently spark retard is required to avoid knocking combustion. In addition, this shows that the compression work is higher when the EOI2 is at 160 CAD BTDCf which explains the reason for lower efficiency at these points compared to 60 CAD BTDCf.

Basically, when the EOI2 is at 30 CAD BTDCf, spark timing was advanced as much as possible but poor mixture preparation and therefore lower combustion efficiency leads to higher fuel consumption and therefore higher intake pressure (Figure 5-7) is required to maintain the load. On the other hand, when the EOI2 is at 160 CAD BTDCf, the mixture preparation is better due to more time available for fuel evaporation as the higher combustion efficiency and slightly shorter combustion duration (Figure 5-8) suggest but due to higher mixture temperature at the time of ignition, the spark timing was retarded to avoid knocking which shifts

the combustion phasing (Figure 5-9) away from the optimum point, decreases the maximum cylinder pressure and therefore increases fuel consumption.

The same analysis can be used for the PFI / late DI case. Higher compression work during the compression stroke for 30 and 160 cases (Figure 5-5) shows the reason for lower efficiency at these points compared to the EOI2 of 60 CAD BTDCf case which is also highlighted in the pressure curve diagram (Figure 5-6). Heat release diagram shows the same peak heat release for the 30 and 60 case but the heat release at 30 CAD BTDCf increase slightly faster and then drops faster than the 60 case but with the same phasing. However, the 160 case shows a slightly higher peak heat release but with a shift to the right which decreases the efficiency. In terms of mass fraction burned, the 30 case shows slightly faster burn rate and combustion duration than the 60 CAD BTDCf case, but the last part of the combustion is slower than the 60 CAD BTDCf case when the flame reaches the lean part of the chamber.

Figure 5-7, shows the maximum cylinder pressure which decreases as the EOI2 advances from 30 to 80 CAD BTDCf for both PFI / late DI and early DI/late DI cases. There is an increase in maximum pressure at 90 CAD BTDCf which is due to the higher in-cylinder temperature at this point for both cases. After 90 CAD advancing the EOI2 decreases the Pmax due to retarded spark timings. The angle of Pmax also has an increasing trend as the EOI2 advances which is also due to more retarded spark timings.

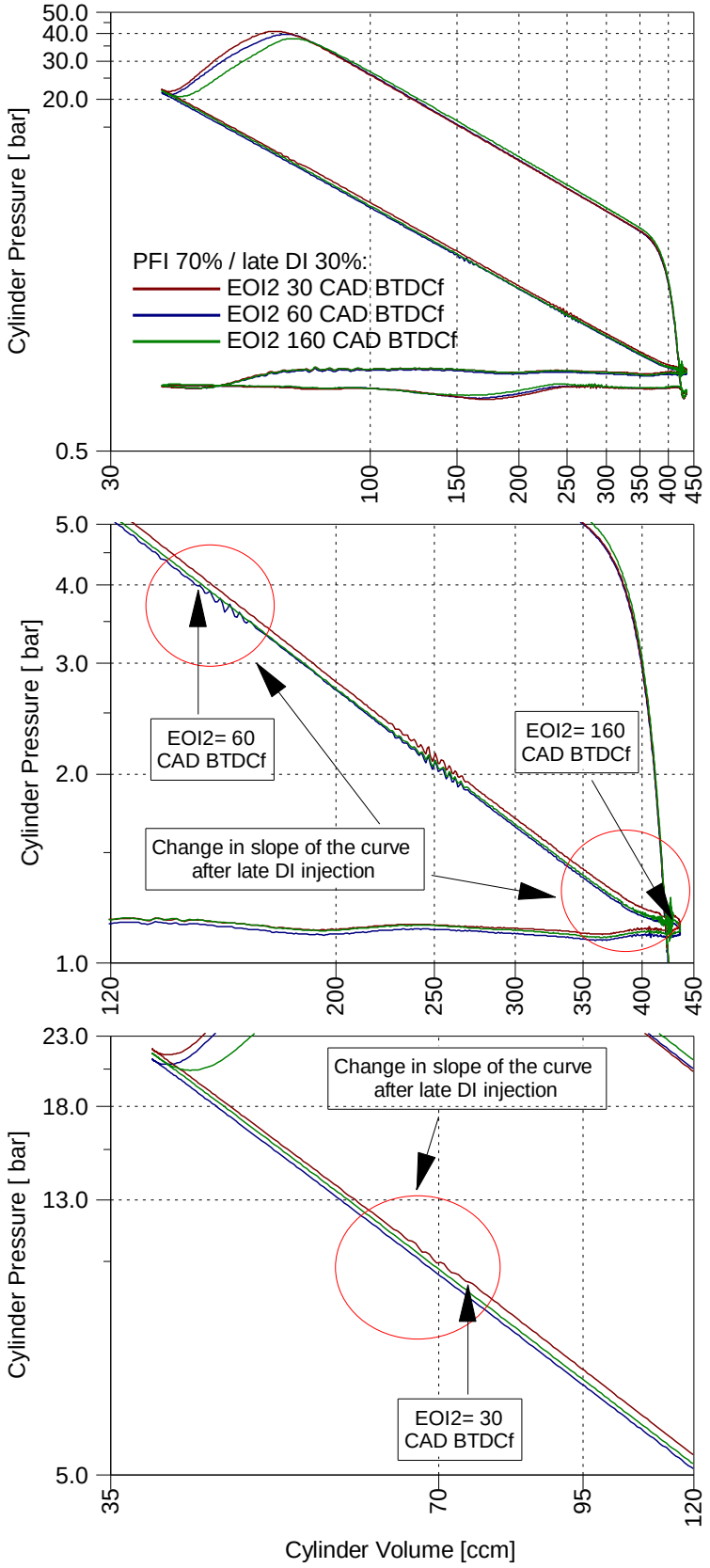

Figure 5-5 LogP - logV diagram of PFI / late DI case for different late DI timings

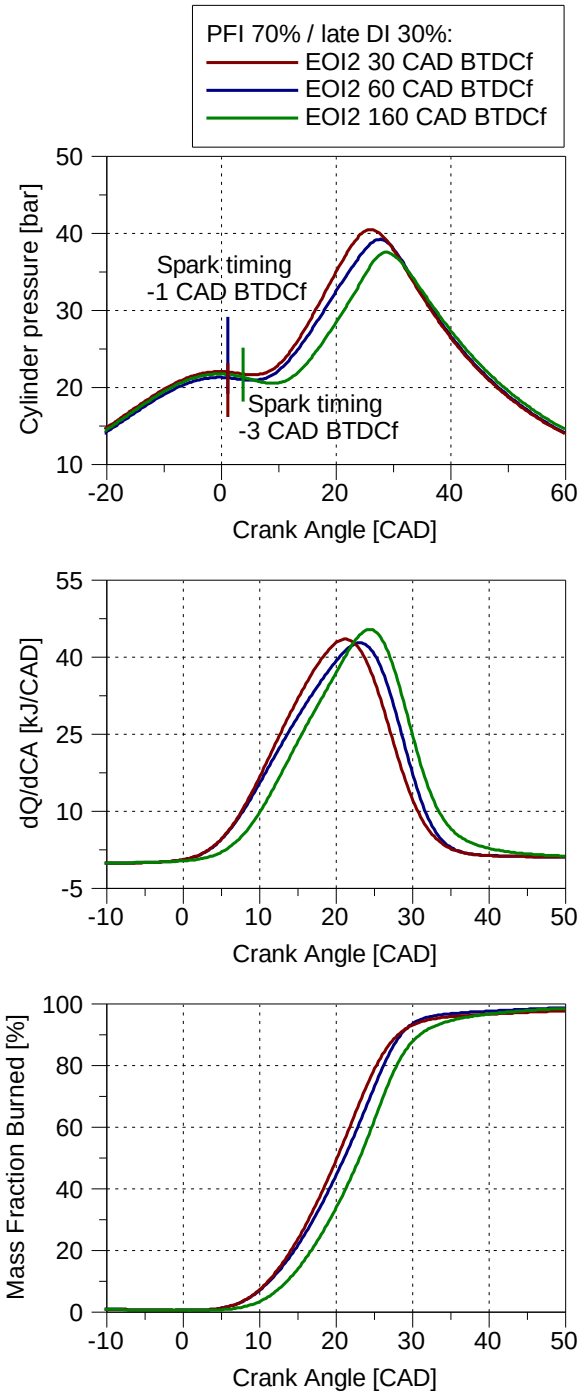

Figure 5-6 Cylinder pressure, heat release, mass fraction burned of PFI / late DI case for different late DI timings

Lower intake pressure was required to maintain the same load as the EOI2 was advanced and therefore positive pumping is lower with the advanced injection timings for both cases.

Figure 5-8, shows the flame development angle. For both cases flame development angle decreases by only 1 CAD when advancing the EOI2 from 30 to 90 CAD BTDCf. Advancing the EOI2 further increases the flame development angle again by around only 1 CAD. Combustion duration decreases slightly by around 2 CAD for early DI/late DI case as the EOI2 advances from 30 to 180 CAD BTDCf despite retarding the spark timing. For the PFI / late DI case combustion duration fluctuates between 15 and 16 CAD but the shortest combustion duration happens at 30 and 90 CAD BTDCf.

Spark timings (Figure 5-9) were kept constant at DBL (detonation border line) for both PFI and DI cases for EOI2 of 30 to 90 CAD BTDCf since there was no need to retard the spark timing. However, advancing the EOI2 further than 90 CAD BTDCf required a slight spark retard by 1 or 2 CAD in order to avoid knocking combustion due to the higher in-cylinder temperature. Therefore, CA10, CA50 and CA90 also follow the same trend and increases as the EOI2 is advanced for both cases.

In terms of emissions (Figure 5-10), CO emissions tend to decrease by advancing the EOI2 for both cases. This is due to more time available for the fuel to be mixed with air as the EOI2 is advanced. Another reason is that as the EOI2 advances, in-cylinder pressure during the compression stroke is lower which increases the spray penetration and helps to decreases the rich local areas concentration near the spark plug, therefore lower CO emissions are achieved at more advanced injection timings.

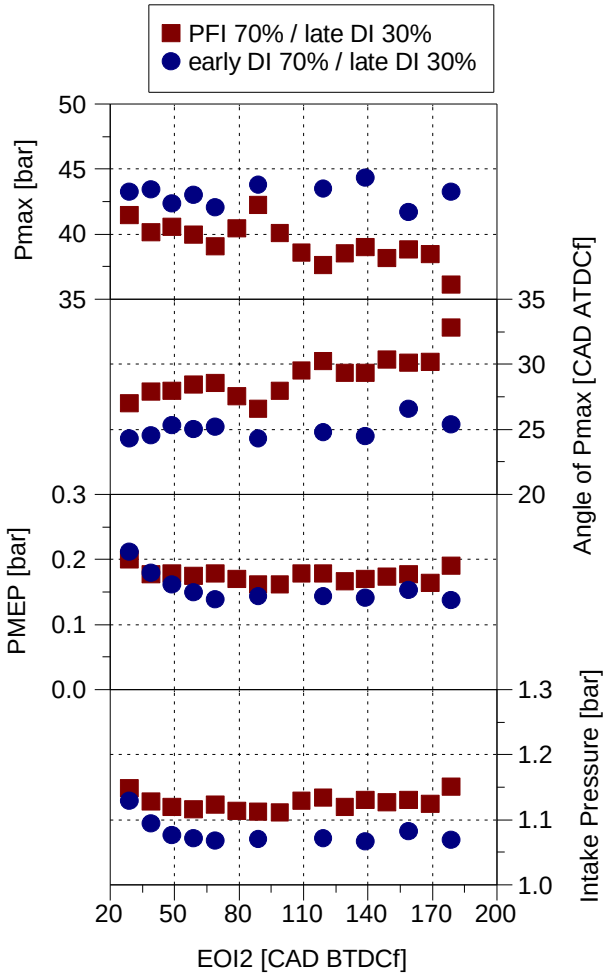

Figure 5-7 Maximum cylinder pressure and its angle, Pumping losses and intake pressure of PFI / late DI and early DI / late DI cases for different late DI timings

When comparing the CO emissions of the two cases, PFI / late DI case shows slightly higher CO emissions. This can be due to higher cylinder pressure for the PFI case during the compression stroke which decreases the pray penetration and therefore the late injection is more concentrated around the spark plug which can create very rich fuel pockets in that area of the combustion chamber and increase the local lambda. Another reason is that with the early DI / late DI case the early DI injection induces a very strong turbulence in the combustion chamber during

the intake stroke which is not exist with the PFI case and this can totally change the flow characteristic and air/fuel mixture of the early DI / late DI case.

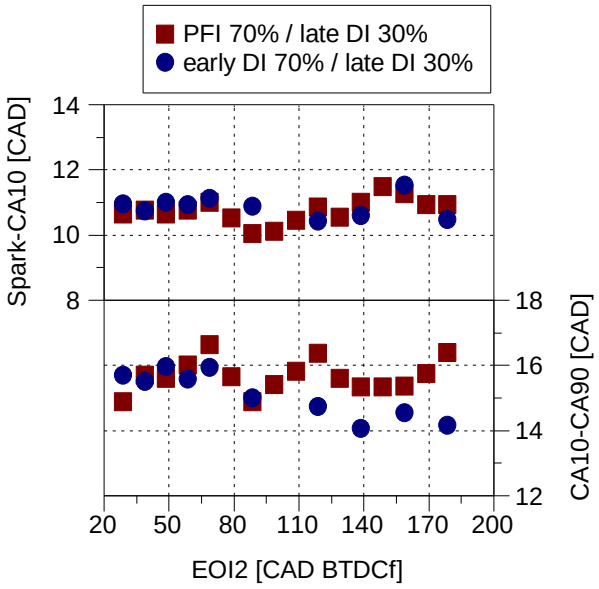

Figure 5-8 Flame development angle and combustion duration of PFI / late DI and early DI / late DI cases for different late DI timings

HC emissions are very similar for both cases and show an increasing trend by advancing the EOI2. It is known that the unburned hydrocarbons (UHC) in a DI gasoline engine could be produced from fuel rich region due to under-mixing or too lean mixture by over-mixing, the fuel trapped in the crevices and liquid fuel impingement in cylinder wall. The exhaust UHC emission is also affected by the post-flame oxidation. The lower HC emission from the very late injection could be due to less UHC trapped in crevices as the injected fuel was more concentrated in the central region of the cylinder at very late injection. It was also very likely much of UHC in the fuel rich regions was partially oxidized to CO as indicated by the higher CO emission from late injections.

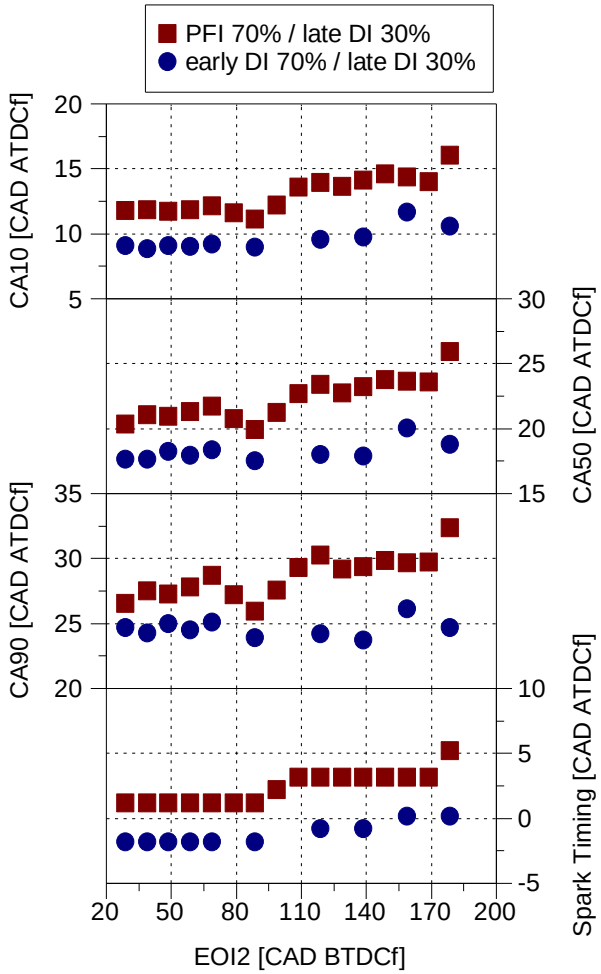

Figure 5-9 CA10. CA50, CA90 and spark timing of PFI / late DI and early DI / late DI cases for different late DI timings

In terms of NO_x emissions, there is an increasing trend for both cases as the EOI2 is advanced. This is mainly due to the higher cylinder temperature with advanced injection timings as it was explained earlier. In addition, as the EOI2 is advanced, the peak heat release increases (Figure 5-4 and Figure 5-6) as well which can be another reason for higher NO_x emissions at these points. When the EOI2 is between 30 and 50 CAD BTDCf both cases produce low levels of NO_x emissions which are almost identical. This is due to the cooling effect of very late injection timings. However, advancing the EOI2 further increases the temperature and therefore NO_x emissions. Also, advancing the injection timings beyond 50 CAD

BTDCf increases the NO_x emissions of early DI / late DI case more than the PFI / late DI case. This is due to more advanced spark timings used with early DI/late DI case (due to the cooling effect of direct injection more advanced spark timings could be used), therefore maximum cylinder pressure of the DI case is higher than the PFI case which ultimately results in higher NO_x emissions of the DI case.

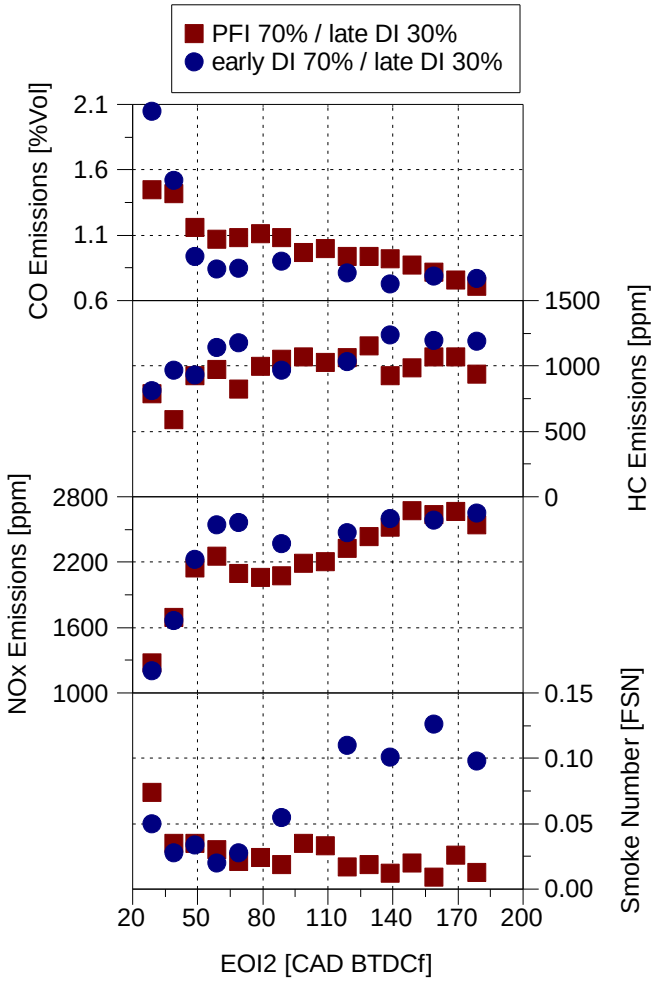

Figure 5-10 CO, HC, NO_x and smoke emissions of PFI / late DI and early DI / late DI cases for different late DI timings

Smoke emissions for PFI / late DI case are generally lower than the early DI / late DI case. This can be due to lower amount of fuel injected directly in the cylinder and therefore lower fuel impingement on the cylinder wall and piston top. Lowest

smoke emissions for early DI / late DI case is achieved with the late DI injection timing set at 60 CAD BTDCf, advancing and retarding the injection timing from this point increases the smoke emissions. High smoke emissions at very advanced injection timings is due to higher spray penetration and impingement on the cylinder wall and piston top in lower cylinder pressure during the early compression stroke.

Exhaust temperature (Figure 5-11) shows a slight increase as the EOI2 is advanced for both cases. At more advanced injection timings, heat release starts later in the cycle and also finishes later due to retard spark timings. On the other hand, at more retard injection timings, heat release starts earlier and finishes earlier in the cycle due to more advanced spark timings.

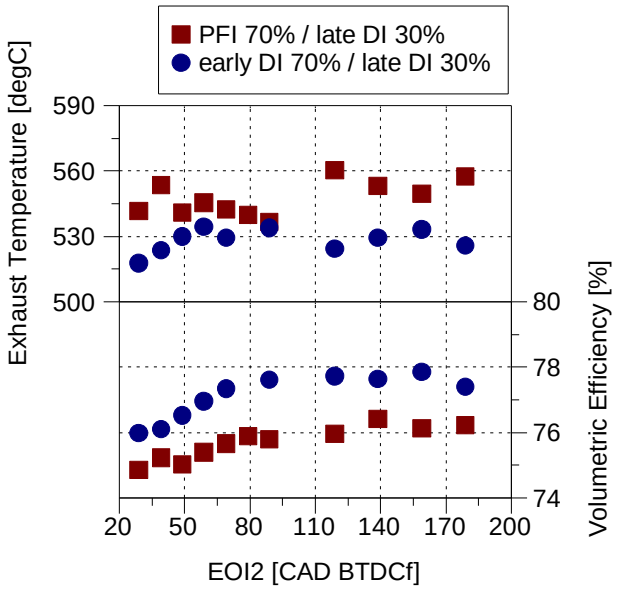

Figure 5-11 Exhaust temperature and volumetric efficiency of PFI / late DI and early DI / late DI cases for different late DI timings

Figure 5-11 also shows the volumetric efficiency of both cases. Volumetric efficiency of early DI / late DI case is around 2% higher than the PFI / late DI case due to the higher cooling effect of early DI which increases the charge density.

Both cases show an increasing trend by advancing the EOI2 timings. Maximum volumetric efficiency also achieved when the injection timing is advanced beyond 120 CAD BTDCf. This is due to the intake valve closure which happens at 120 CAD BTDCf. Before this time the intake valves are about to close but still slightly open, so advancing the injection timing further can increase the volumetric efficiency slightly more. Therefore, advanced injection timings have slightly higher volumetric efficiency compared to the retard ones.

5.3.2 Effects of late DI injection ratios during the PFI / late DI and early DI / late DI operation at mid load

Figure 5-12, shows the effect of the late DI ratio on NISFC, combustion efficiency and combustion stability for both PFI / late DI and early DI / late DI operating conditions at stoichiometric air / fuel ratio. The end of late DI injection timing was kept constant at 60 CAD BTDCf for both cases. As can be seen in the NISFC diagram, second late DI injection can decrease the fuel consumption significantly in both cases compared to the baseline PFI and DI operation. The minimum NISFC is achieved when the late DI ratio is around 40 to 60% and after that adding more fuel increases the fuel consumption again. The main reason for this trend is the cooling effect of the late DI injection which reduces the charge temperature at this knock limited point and allows the use more advanced spark timings, therefore shifts the burn angles (CA10, CA50 and CA90) to a point closer to optimum. On the other hand, increasing the late DI ratio to 70% or more deteriorates the combustion efficiency due to under-mixing effect of stratification (formation of fuel rich areas near the spark plug) and therefore an increase in incomplete combustion products such as CO, HC and smoke emission. Although spark timing

was advanced as the late DI ratio was increased, the effect of better combustion phasing is decreased by the worse combustion efficiency.

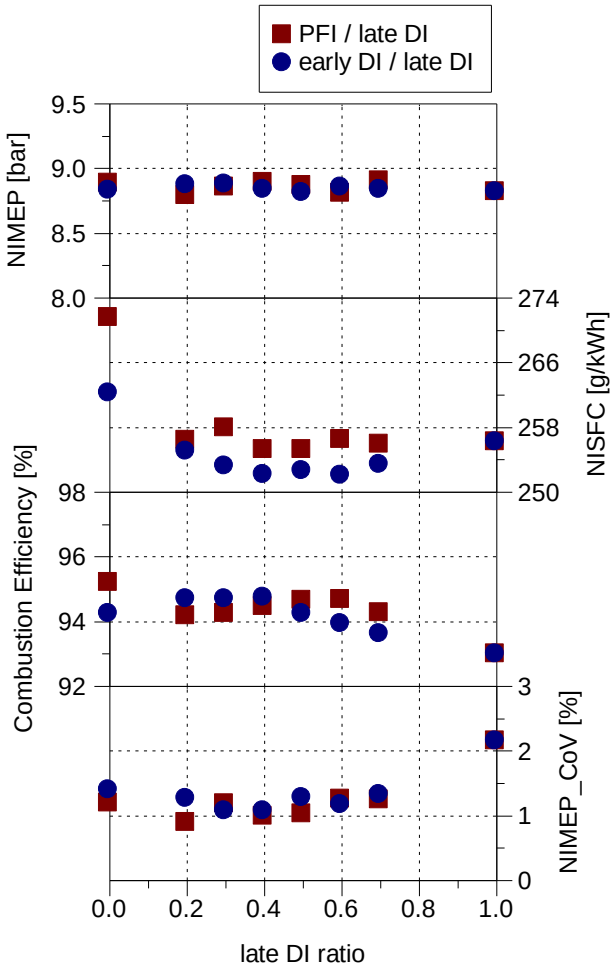

Figure 5-12 NIMEP, NISFC, combustion efficiecny and combustion stability of PFI / late DI and early DI / late DI case for different late DI ratios

In addition, combustion efficiency decreases slightly as the late DI ratio increases up to around 40% and then starts to increase again for both cases. This trend can be explained by a more advanced combustion phasing which is closer to optimum and also shorter flame development angle which both are effective in decreasing the cycle-by-cycle variations. However, as the late DI injection increase beyond

40%, it is harder to initiate the combustion which could ultimately increase the cycle-by-cycle variations and decrease the combustion stability.

Figure 5-13 shows an increase in maximum cylinder pressure as the late DI ratio was increased for both cases. Also, angle of maximum cylinder pressure was advanced with higher late DI ratios. This can be explained by the use more advanced spark timings which was possible due to higher amount of fuel in the late injection and therefore higher charge cooling effect.

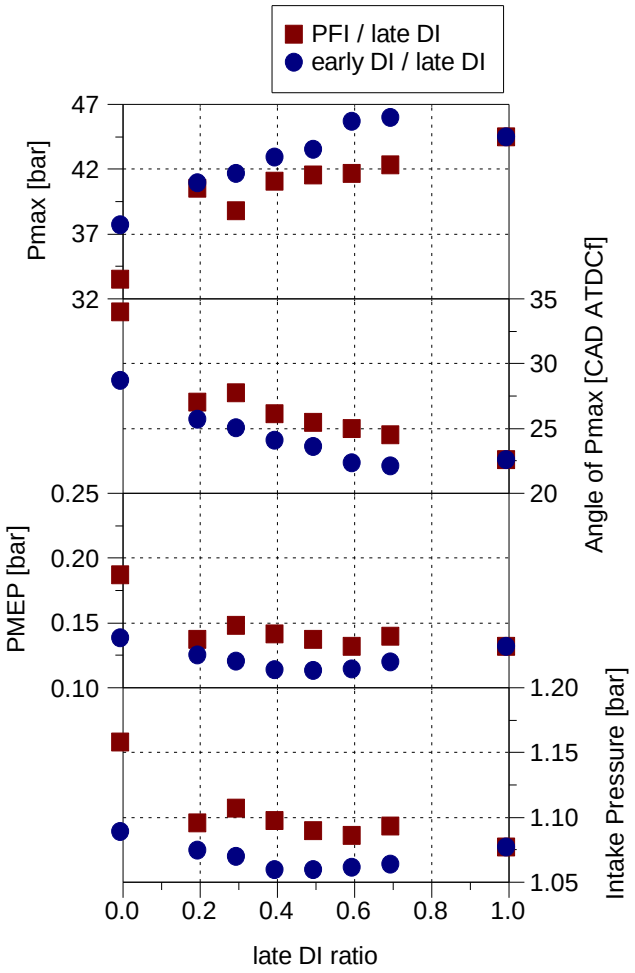

Figure 5-13 Maximum cylinder pressure and its angle, Pumping losses and intake pressure of PFI / late DI and early DI / late DI cases for different late DI ratios

This cooling effect was obviously less for PFI / late DI case since part of the fuel was injected in the intake port, therefore decreased the intake port and valves temperature rather than the cylinder temperature. As a result, the spark timings for the PFI / late DI case are less advanced compared to the early DI / late DI case and lower maximum cylinder pressures are achieved.

Lower intake pressure was required as the late DI ratio was increased for both cases. This is also due to a more efficient combustion phasing which lowers the fuel consumption, therefore lower intake pressure is required to maintain the same load. As a result, positive pumping is also lower. Higher intake pressure of the PFI / late DI case compared to the early DI / late DI case is firstly due to a delayed combustion phasing of the PFI / late DI case and secondly due to displacement of some fuel with air in the intake manifold which increases the intake pressure for the PFI / late DI case.

Figure 5-14 shows the flame development angle and the combustion duration for both cases. As can be seen in the graphs, immediately after using late DI injection, flame development angle deceases and then start to increase gradually again. This immediate drop in the flame development angle can be due to the late DI injection which creates a relatively rich mixture around the spark plug and also the late injection induces a turbulence in that area which helps speeds up the initial party of the combustion. However, injecting too much fuel late also results in a longer flame development angle. Slightly shorter flame development angle of PFI / late DI compared to the early DI / late DI can be explained by higher intake pressures used in the PFI case and also higher mixture homogeneity by PFI. The changes in combustion duration are very small by around only 1 CAD when increasing the late DI injection ratio.

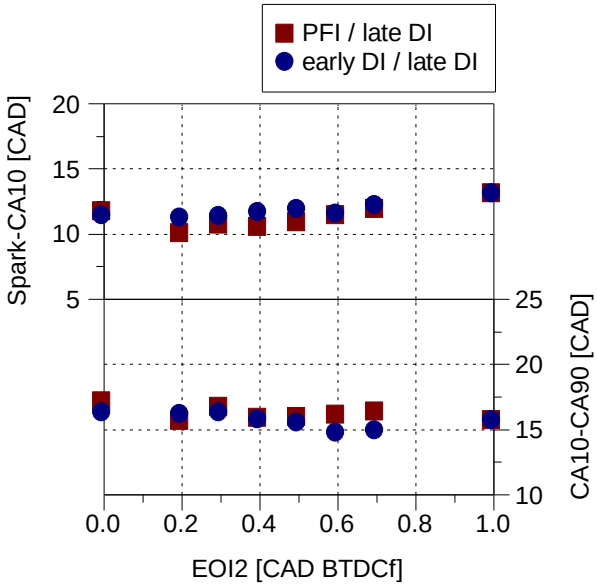

Figure 5-14 Flame development angle and combustion duration of PFI / late DI and early DI / late DI cases for different late DI ratios

Figure 5-15 shows the effect of different late DI ratios on spark timing and combustion phasing. As it was mentioned earlier, increasing the level of late DI injection can reduce the charge temperature more and therefore allows the use of more advanced spark timings which shifts the burn angles to a more efficient point. Figure 5-16, shows the increasing trend for CO emissions as the late DI injection increased. When considering PFI / late DI case, there is a sharp increase in CO emissions immediately after switching to PFI / late DI from the baseline PFI. This increase in CO emissions can be due to the change from a homogeneous charge (100% PFI) to a less homogeneous charge produced by the late DI injection. However, after this peak the CO emissions start to decrease slightly by increasing the late DI injection up to 40% and then increased again. This trend can be explained by the more turbulence created by increasing the late DI injection, but this effect is compensated by higher levels of mixture inhomogeneity when the late DI ratio is too high. Slightly higher levels of CO under PFI / late DI case compared

to the early DI / late DI case can be due to higher cylinder pressures during PFI / late DI which decreases the spray penetration and therefore the late injected fuel was more concentrated in the central region of the cylinder which increased the local lambda at that area and ultimately increased the CO emissions. Lower smoke emissions of the PFI / late DI case also confirm the lower spray penetration compared to the early DI / late DI operation. In addition, there is a higher chance of fuel impingement on the wall and the piston in the case of early DI / late DI operation.

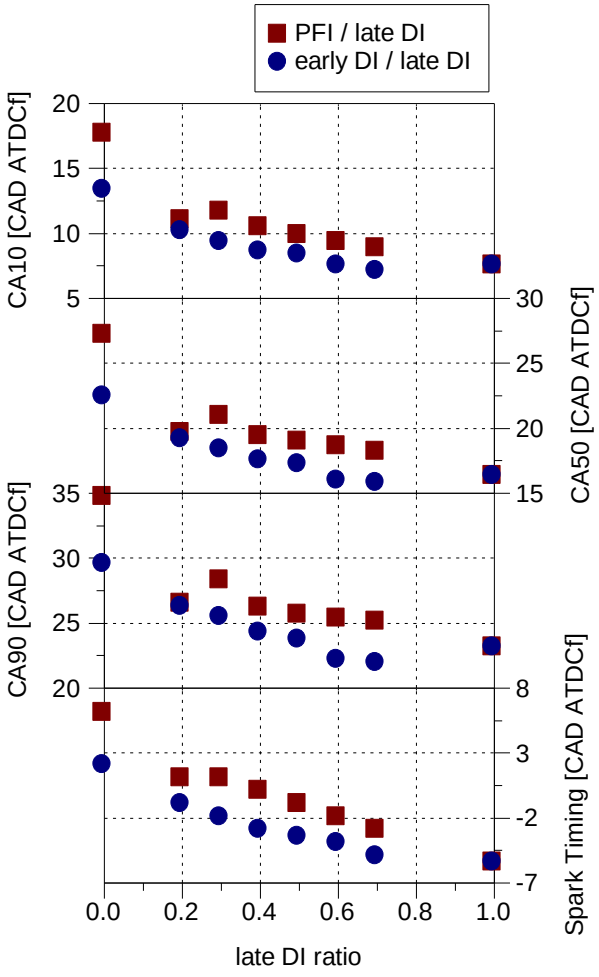

Figure 5-15 CA10. CA50, CA90 and spark timing of PFI / late DI and early DI / late DI cases for different late DI ratios

HC emissions decrease immediately after adding the late DI injection in both cases. Lower HC emissions with the late DI injection could be due to less HC trapped in crevices as the injected fuel was more concentrated in the central region of the cylinder at very late injection. However, after that immediate drop, HC emissions start to increase gradually as the late DI ratio was increased. This can be due to the presence of more liquid fuel at the end of compression stroke as well as lower post flame oxidation. Lower post flame oxidation could happen with very high late DI ratios since most of the fuel is injected very late, a relatively rich mixture is formed near the spark plug but there is a very lean mixture in the rest of the chamber which can decrease the cylinder temperature during the late expansion and exhaust stroke as the lower exhaust temperature suggest.

PFI / late DI case generally produces lower HC emissions compared to early DI / late DI case. This could be firstly due to the presence of more liquid fuel during early DI / late DI operation (impingement during the early DI injection) and secondly due to the more spray penetration with early DI / late DI as the in-cylinder pressure during the intake and compression strokes were lower than the PFI / late DI case.

NO_x emissions have an increasing trend as the late DI ratio was increased due to the use of more advanced spark timings and therefore, higher maximum cylinder pressures for both cases. In addition, NO_x emissions of the early DI / late DI case are higher than the PFI / late DI case which also can be explained by the use of more advanced spark timings and maximum cylinder pressure.

Exhaust temperature (Figure 5-17) decreases as the late DI ratio is increased. This is also due to a more advanced combustion phasing, combustion starts earlier in the cycle and finishes earlier as well so the exhaust temperature decreases.

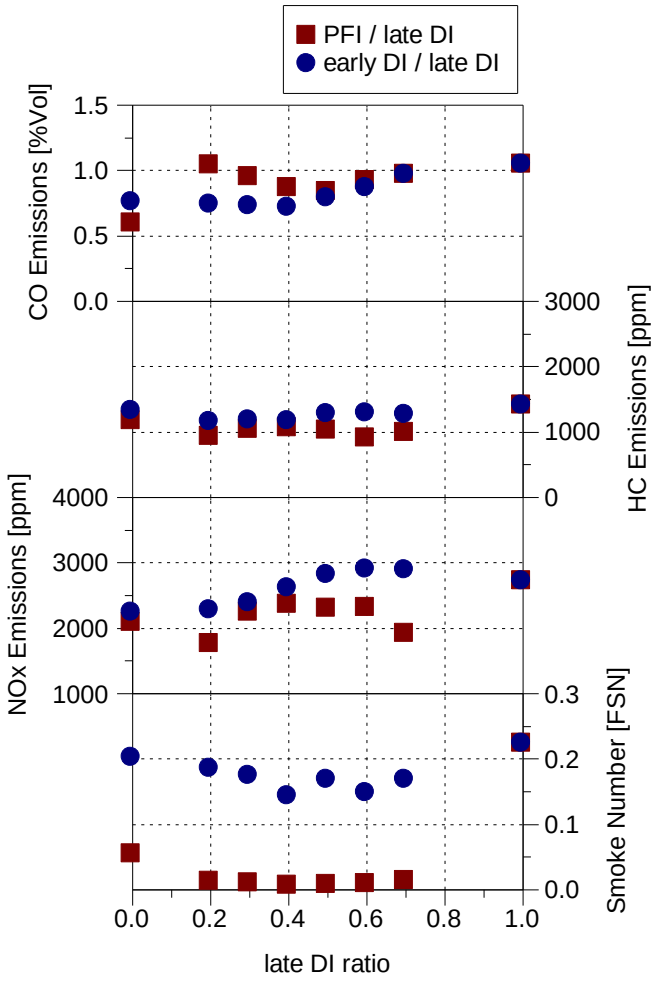

Figure 5-16 CO, HC, NO_x and smoke emissions of PFI / late DI and early DI / late DI cases for different late DI ratios

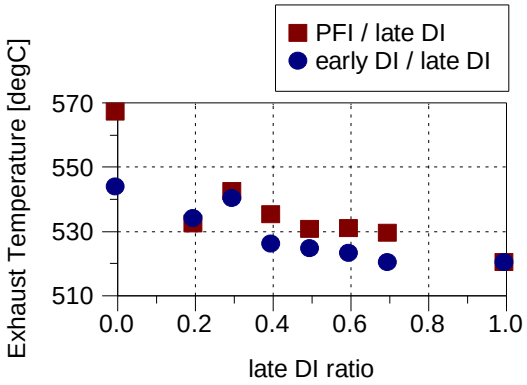

Figure 5-17 Exhaust temperature of PFI / late DI and early DI / late DI cases for different late DI ratios

5.3.3 Comparison of PFI / late DI and early DI / late DI strategies with PFI and DI at stoichiometric and lean air / fuel ratios (mid load)

The impact of this hybrid injection strategy on fuel economy, combustion characteristic and emissions are also studied at lean air fuel ratios. Followings are the results for PFI / late DI and early DI / late DI during lean combustion when only 30% of the fuel was injected late and the end of the late DI injection was 60 CAD BTDCf for both cases. In addition, this lean operation was also conducted for PFI (all the fuel is injected through the port fuel injector when the intake valves were closed) and DI (all the fuel was injected through the DI injector with the injection timing of 276 CAD BTDCf) for comparison.

Figure 5-18 shows the NISFC, combustion efficiency and combustion stability at constant NIMEP of 8.83 bar. NISFC shows a decreasing trend with increasing lambda. All cases show a similar trend except PFI which shows a slight increase in NISFC at lambda 1.1 and then start to decrease again. This is due to an increase in cylinder temperature at lambda 1.1 which limits the use of more advanced spark timing at this knock limited point.

When comparing the fuel consumption of the four cases, early DI / late DI has the lowest NISFC at lambda 1. However, as lambda increases, PFI / late DI case shows a very similar fuel consumption to early DI / late DI and even slightly lower fuel consumption at higher lambda of 1.5 to 1.7. Moreover, NISFC graph shows that the PFI has the highest fuel consumption followed by the DI case. PFI / late DI and early DI / late DI strategies improved the fuel consumption by around 4% and 6.5% respectively compared to the baseline PFI case at lambda 1.

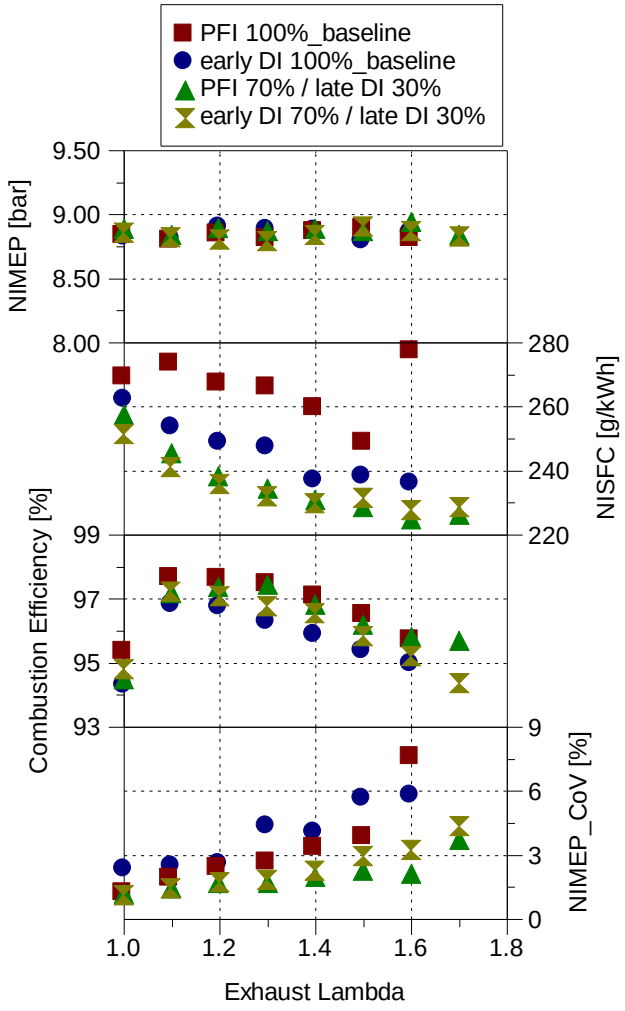

Figure 5-18 NIMEP, NISFC, combustion efficiecny and combustion stability of PFI, DI, PFI / late DI and early DI / late DI strategies

These significant improvements are mainly due to improvements in combustion timings achieved by utilizing more advanced spark timings which was possible by the strong cooling effect of the late DI injection. These differences in efficiency can also be clearly explained by detailed analysis of the P-V diagram of each case at lambda 1 (Figure 5-19).

There are two major differences between PFI and DI fuel injection characteristic. The first one is the different heat sources for fuel evaporation in each system. Fuel heat of vaporization or latent heat can be utilized to reduce the charge temperature and therefore increase the volumetric efficiency and reduce the knocking tendency. However, this phenomenon is totally different in PFI and DI engines. In PFI engines the injected fuel into the intake port covers the surface of the port and valves. Therefore, the main source of fuel evaporation is the heat transfer from the hot surfaces of the port and valves to the fuel film. As a result, evaporation of fuel in this way cannot significantly cool the charge. However, in the case of DI engines, fuel is directly injected into the cylinder and fuel is vaporized by absorbing the heat of the intake air which can cool the charge significantly.

The second main difference is the injection timing which significantly changes the heat transfer rate from the combustion chamber surface to the charge. Early DI injection reduces the charge temperature earlier in the cycle and therefore increases the heat transfer from the combustion chamber surfaces to the charge. Thus, the charge temperature is increased and the cooling effect of the fuel on the final charge temperature is reduced. On the other hand, for the late DI injection the charge temperature is higher before fuel injection and therefore the heat transfer is also lower. After injecting the fuel late, the charge is cooled late in the cycle and therefore the charge temperature at the time of ignition can be lower

which reduces the knocking tendency. In addition, in PFI engines the final gas temperature could be even higher than early DI injection since the fuel is injected even earlier in the cycle (closed valve injection) and there is substantially more time for heat transfer. Therefore, the charge temperature at the time of ignition could be the highest for PFI compared to other cases.

Figure 5-19 shows the log P – log V diagram of all the four cases at lambda 1. It also shows the enlargement of the diagram during the early and late part of the compression stroke. PFI case (red curve) has the highest pressure during the intake and compression strokes. This higher pressure shows that the final charge temperature could be higher which increases the knocking tendency at this point and force the use of less advanced spark timing. In addition, compression work is significantly increased compared to other cases. Higher pressure during the intake is also due to displacement of some air with the injected fuel in this case.

PFI / late DI case (green curve) shows slightly higher pressure during the early part of the compression stroke when comparing with DI case (blue curve) since the majority of fuel is injected in the intake port. Therefore, slightly higher intake pressure was required which also increases the pressure during the early part of the compression stroke before the late DI injection. After starting the late DI injection around 61.5 CAD BTDCf, the pressure decreases and converges with the blue curve. This decrease in the slope of the green curve is due to the strong cooling effect of the late DI injection. During the later stages of compression stroke, PFI / late DI pressure becomes lower than the DI case which indicates that the fuel evaporation and fuel-vapor diffusion may still happen in the late stages of compression long after the end of injection at 60 CAD BTDCf.

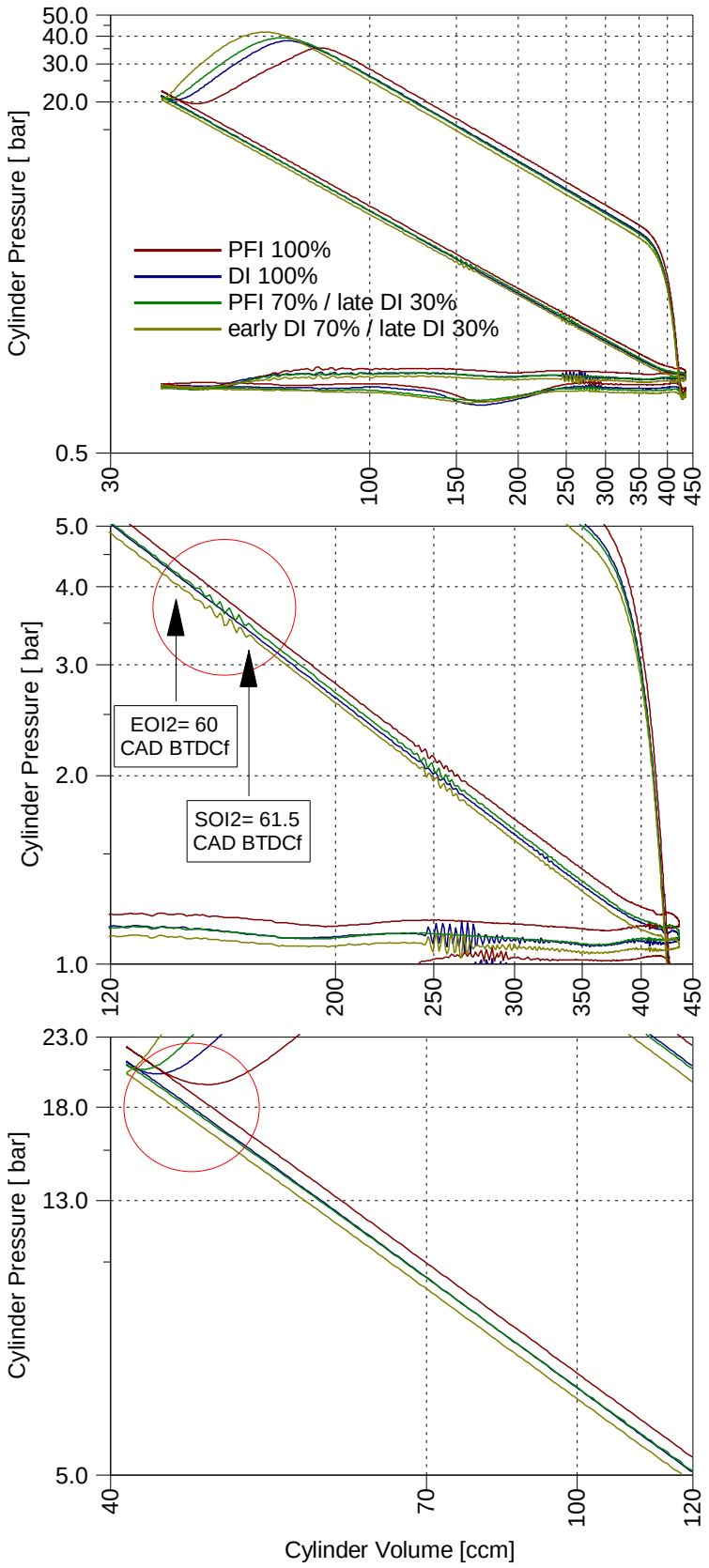

Figure 5-19 P-V diagram and enlargement of the early and late compression pressure for PFI, DI, PFI / late DI and early DI / late DI cases

This decrease in the slope of pressure curve also happens for the late DI / early DI case (yellow curve) after the late DI injection due to a strong cooling effect of the late injection. Late DI / early DI case has the lowest compression pressure and since all the fuel is injected in the cylinder with some of it late during the compression stroke, it could have the lowest charge temperature at the time of ignition. Therefore, more advanced injection timings could be utilized with this strategy which ultimately improved the combustion phasing and fuel consumption.

Figure 5-20 shows how the cylinder pressure, heat release and mass fraction burned change when using these strategies. The two cases with the late DI injections clearly produce higher peak in-cylinder pressure due to more advanced spark timing and combustion phasing. Heat release curve also shows a shift towards the TDC with a lower peak which indicates that less fuel and air was burned to achieve the same load. Mass fraction burned also confirms the improvements in combustion phasing.

Combustion stability of each case is shown in the CoV of NIMEP graph (Figure 5-18). As can be seen in the graph, PFI / late DI and early DI / late DI operation improved the lean combustion stability limit significantly compared to the baseline PFI and DI operation. Considering the limit of 3% CoV, PFI and DI can only reach lambda 1.4 whereas PFI / late DI and early DI / late DI could extend the lean limit to lambda 1.6.

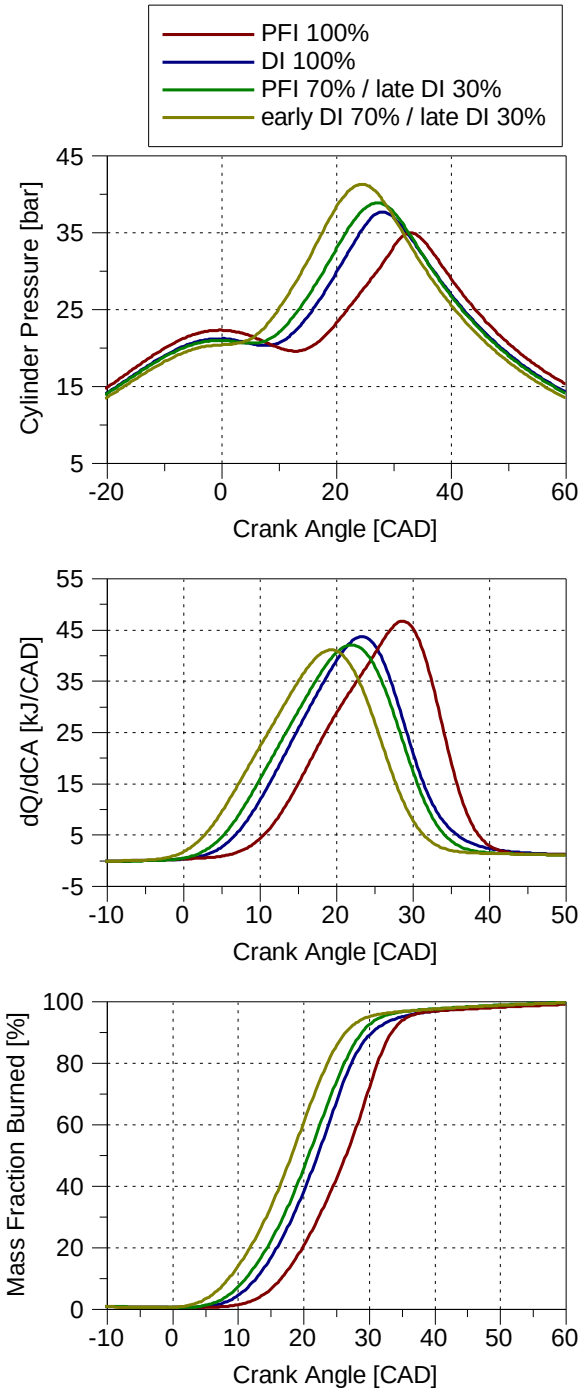

Figure 5-20 Cylinder pressure, heat release, mass fraction burned of PFI, DI, PFI / late DI and early DI / late DI strategies

In addition, CoV for PFI / late DI at lambda 1.7 is around 3.5% which can be still acceptable for stable operation. Higher combustion stability of PFI / late DI case, specifically with very lean mixtures can be due to the formation of a more

homogeneous mixture compared to early DI / late DI case as most of the fuel is injected in the intake port. Therefore, flame development angle and combustion duration were faster for PFI / late DI case specifically at lambda 1.5 to 1.7. This helped to reduce the cycle-by-cycle variations and ultimately increased the combustion stability.

Combustion efficiency graph (Figure 5-18) shows that the PFI case achieves the highest combustion efficiency both at stoichiometric and lean conditions. PFI / late DI and early DI / late DI cases produce slightly lower combustion efficiency than the PFI case and finally DI case has the lowest combustion efficiency among all cases. This can be explained by studying the CO and HC emissions of these cases.

As can be seen on Figure 5-21, CO emissions are high at stoichiometric for all four cases but decrease sharply when increasing the lambda. It is known that CO emissions form during the combustion process when the fuel-air mixture is rich and there is insufficient oxygen to fully burn the carbon in the fuel to CO_2. In addition, CO emissions can still form even in lean mixtures due to dissociation in high-temperature products. Therefore, this trend can be explained using the above CO formation mechanism. PFI case produced lowest amount of CO at stoichiometric which confirms the existence of a more uniform or homogeneous mixture among four cases, therefore there are less fuel-rich areas for CO formation.

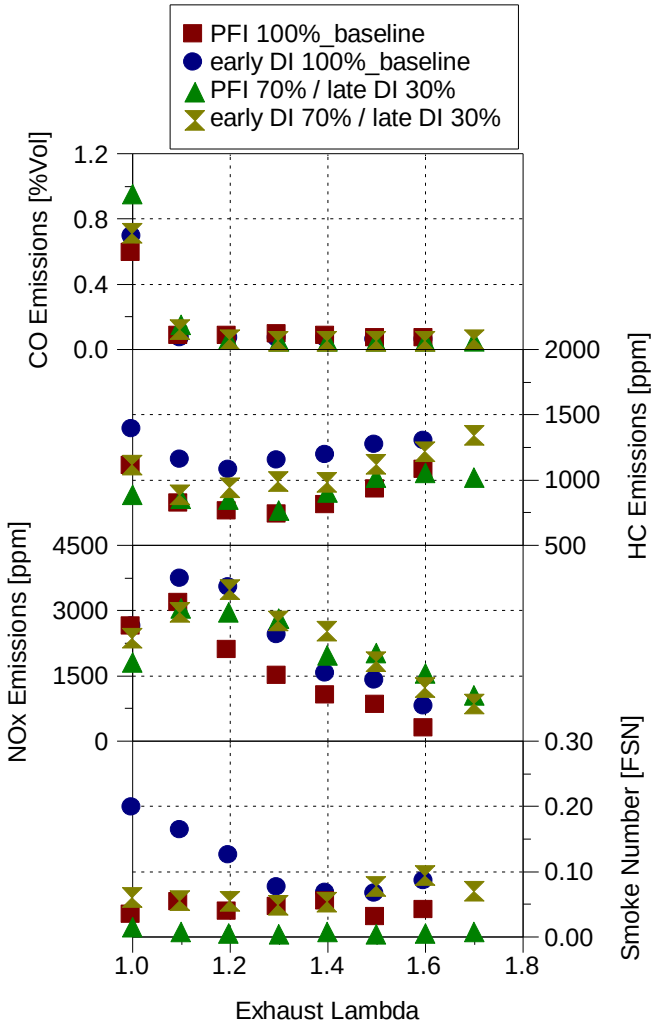

Figure 5-21 CO, HC, NO_x and smoke emissions of PFI, DI, PFI / late DI and early DI / late DI strategies

The two cases with the late DI injection produce the highest amount of CO compared to other cases. The reason for this can be the late DI injection which forms a relatively rich mixture concentrated near the spark plug late in the compression stroke and therefore creates more locally fuel-rich areas and increases CO emissions. The reason for higher CO emissions of PFI / late DI case compare to the early DI / late DI case could be formation of a more concentrated mixture by the late DI since the cylinder pressure (Figure 5-19) is higher for PFI / late DI compared to early DI / late DI during compression at the time of injection.

Therefore, the late DI spray penetration is less for PFI / late DI case which helps to form a locally fuel-rich area and increases CO emissions.

In terms of unburned hydrocarbon (UHC) emissions, DI case has the highest level of UHC both at stoichiometric and lean conditions. In addition, PFI and PFI / late DI case produce lowest amount of UHC compared to other cases at stoichiometric and lean conditions. The formation mechanism of UHC emissions DI gasoline engines could be due to formation of fuel-rich region by under-mixing or too lean mixture by over-mixing, fuel trapped in crevices and liquid fuel impingement on cylinder wall. In addition, post-flame oxidation also can affect the UHC emissions.

The overall trend of the HC graph shows that richer mixtures produce high UHC emissions mainly due to incomplete combustion and increasingly lean mixtures also produce high UHC emissions due to lower combustion temperatures which reduces wall temperatures and lead to less HC burn-up during expansion and exhaust strokes. Additionally, at around lambda 1.2 and 1.3, combustion quality start to decrease slowly and eventually slow and partial burning begins to occur as the combustion stability limit is reached. Therefore, UHC emissions increase further and engine operation becomes erratic. Considering UHC emissions at lambda 1, DI case has the highest emissions due to existence of both fuel impingement and fuel trapped in crevices as the fuel was injected in the cylinder early with high pressure. PFI case has a high possibility for fuel and air mixture trapped in crevices but fuel impingement is much less or unlikely to happen as all of the fuel was injected in the port and was premixed before entering the cylinder. Another reason for lower UHC of PFI compared to DI is the higher post-flame oxidation for PFI as the longer and later combustion and higher exhaust temperature of PFI suggest. Early DI / late DI case has less fuel impingement and

fuel trapped in crevices than the DI case as less fuel was injected early and small portion as injected late at high cylinder pressure so less impingement and less crevices is likely. PFI / late DI has the lowest UHC emissions since most of the fuel was premixed which decreases the chance of impingement and a portion of the fuel was injected late which decreases the chance of fuel trapping in crevices.

The overall trend for NO_x emissions show an increase from lambda 1 to 1.1 then start to decrease gradually as the mixture becomes leaner. NO_x emissions can form throughout the high-temperature burned gases behind the flame front through chemical reaction between nitrogen and oxygen atoms. Therefore, higher burned gas temperatures result in higher NO_x formation. When comparing different cases, despite using less advanced spark timings, PFI and DI produce higher NO_x emissions at lambda 1 and 1.1 compared to PFI / late DI and early DI / late DI case. This can be due to higher combustion temperatures since combustion takes place in slightly higher cylinder pressures for PFI and DI cases. In addition, strong cooling effect of the late DI injection keeps the in-cylinder pressures and temperatures lower for PFI / late DI and early DI / late DI cases. However, PFI / late DI and early DI / late DI cases produce higher NO_x emissions at lean air / fuel ratios. This can be due to the dominant effect of more advance spark and combustion timings which result in higher peak cylinder pressures and therefore higher NO_x emissions. PFI / late DI and early DI / late DI strategies reduced NO_x emissions significantly by around 42 and 54% respectively at lambda 1.6 compared to baseline PFI and DI operation at lambda 1.

At stoichiometric condition, DI and early DI / late DI cases produce highest amount of smoke respectively. This is mainly due to the fact that all of the fuel is injected in the cylinder with these two strategies. Presence of liquid fuel, wall wetting by

the fuel spray and over-rich region created by the late injection (stratification) are the main sources of formation of particulate emissions. It is more likely that some of the fuel impinged on the cylinder wall and piston head during early DI injection. Splitting the DI injection to early and late injections helped to reduce the smoke emissions since less fuel was injected early and therefore result in less impingement and the rest of the fuel was more concentrated in the central region of the combustion chamber due to the less spray penetration with higher compression pressures.

As can be seen in Figure 5-22, early DI / late DI case shows the highest peak cylinder pressure from lambda 1 up to lambda 1.4. This case could provide a strong cooling effect in the cylinder with one injection during the intake and one injection during the compression stroke. Therefore, the cylinder pressure could be lower at the time of ignition and more advanced spark timings were utilized which increased the peak cylinder pressure. However, at very lean air/fuel ratios (lambda 1.4 and above), peak cylinder pressure starts to decrease slightly despite advancing the spark timing.

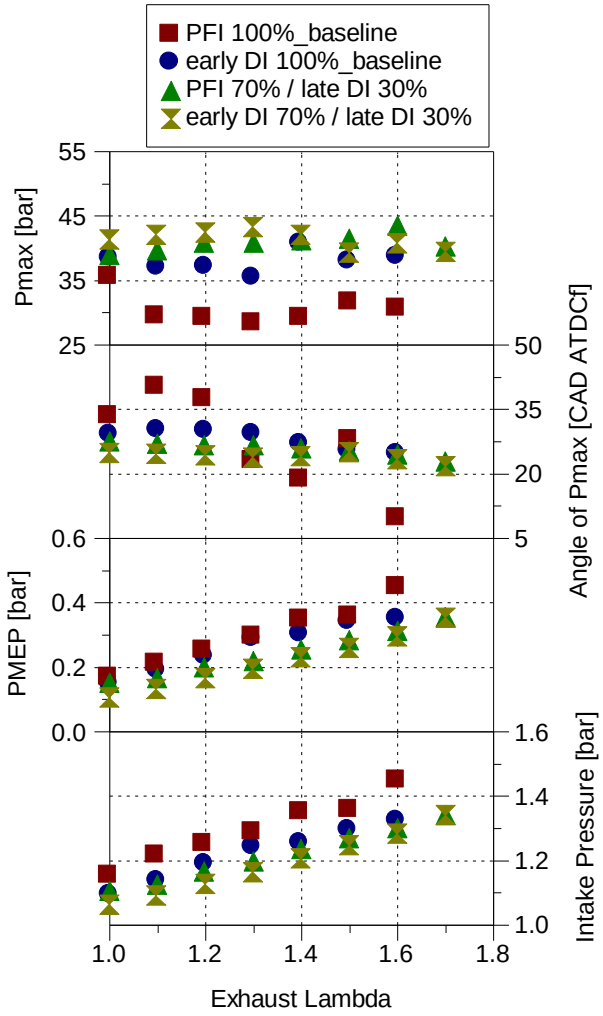

Figure 5-22 Peak cylinder pressure and its angle, pumping losses and intake pressure of PFI, DI, PFI / late DI and early DI / late DI strategies

The reason for this can be the less stable combustion (higher NIMEP_CoV) at high lambda since slow and partial burnings cycles begin to occur as the combustion stability limit is reached. PFI / late DI case also follows a similar trend but in this case cylinder peak cylinder pressure keep increasing up to lambda 1.6. Higher combustion stability of PFI / late DI is the reason for slightly higher peak cylinder pressures at lambda 1.5 to 1.7 when comparing to early DI / late DI case. DI case shows an initial decrease in cylinder pressure which is due to higher in-cylinder temperatures at the time of ignition compared to the two cases with the late DI

injection, therefore this case has lower peak cylinder pressures. In addition, PFI case produced the lowest peak cylinder pressure due to the least advanced spark timings which was used to avoid knocking combustion. Angle of peak cylinder pressure shows a slight decrease at high lambda values due to the advanced and combustion timings.

Intake pressure (Figure 5-22) increased as the dilution level was increased and as a result higher positive pumping was achieved at higher air/fuel ratios. Early DI/late DI and PFI / late DI cases required lower intake pressure mainly due to a better combustion timing which was explained earlier.

Figure 5-23 shows 10, 50 and 90% mass fraction burned angles and spark timing while Figure 5-24 highlights the flame development angle (0-10% burn duration) and combustion duration (10-90% burn duration) across the lambda range for all four cases. It is clear that why early DI / late DI and PFI / late DI can improve the fuel consumption at lambda 1 and tolerate higher levels of dilution in the lean region.

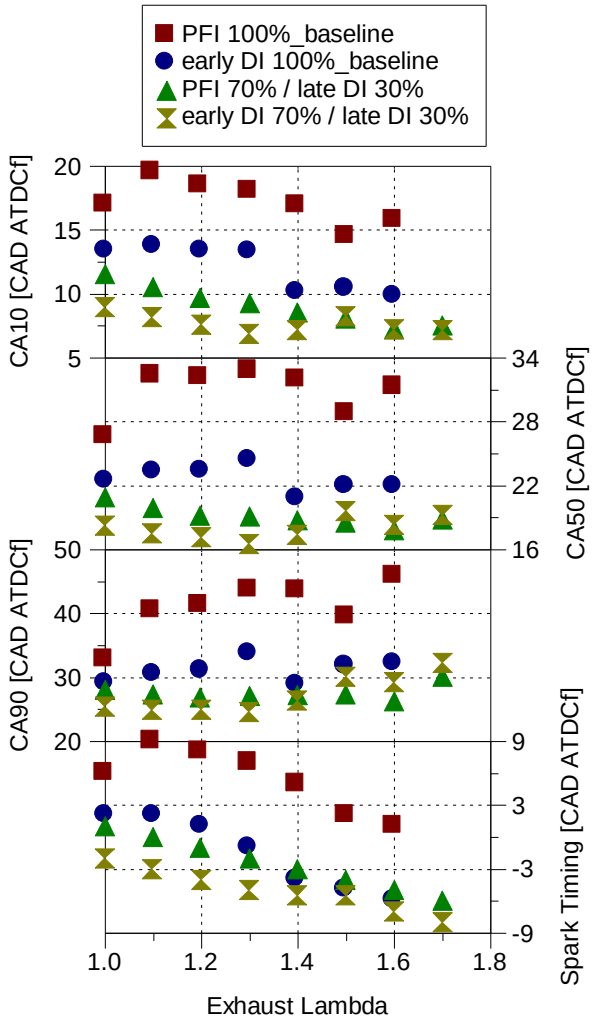

Figure 5-23 Burn angles and spark timing of PFI, DI, PFI / late DI and early DI / late DI strategies

With Early DI / late DI and PFI / late DI cases strong cooling effect of the late DI injection could greatly reduce the in-cylinder temperature during the late part of the compression stroke before spark discharge. Therefore, more advanced spark timings could be utilized which as shown in the CA10, 50 and 90 graphs advance the combustion timings significantly. This shifts the burn angles including CA50 closer to the optimum point. For instance, at lambda1, CA50 is around 27 CAD ATDCf for the baseline PFI case but could improve to around 21 and 18 CAD ATDCf for PFI / late DI and early DI / late DI respectively. This is a significant 6 to

10 CAD improvement in CA50 which results in higher efficiency. In addition, splitting the fuel into two portions helped in forming an overall lean premixed mixture in the periphery of the combustion chamber with early DI or PFI injection and a relatively rich mixture near the spark plug. Therefore, the leaner premixed mixture in the end gas region would slow down the autoignition process and more advanced spark timings could be used.

In addition to improvement in combustion timing, improvement in flame development angle and combustion duration is also apparent in Figure 5-24. When comparing the DI case with early DI / late DI case, it takes less time for early DI / late DI to initiate the flame across the lambda range and this becomes even more evident as the lambda increases. This can be explained by better mixture preparation with early DI / late DI case since the late DI injection increased turbulence at the end of compression stroke, which has a high impact on the in-cylinder flow at this low engine speed when the tumble motion was weak. The shorter flame development angle also seems to suggest that combustion was initiated in a stratified charge of near stoichiometric mixture near the spark plug when the ignition took place.

It is noted that the PFI / late DI case and PFI case both have a shorter flame development angle than the other two cases. One reason for this can be the formation of a more homogeneous mixture with PFI and PFI / late DI case since with PFI case all of the fuel and with PFI / late DI case majority of fuel was premixed before entering the cylinder. Another reason can be the more intense air motion due to the higher intake pressures for PFI cases (Figure 5-22). This is also evident in the P-V diagram (Figure 5-19) as the cylinder pressure of the two PFI cases is higher especially during the intake and early part of the compression stroke. In

addition, as lambda increases beyond 1.3, PFI / late DI shows a faster flame initiation than the PFI case as the late DI injection can improve the flame kernel growth and increase the combustion stability. When considering the overall trend of the 0-10% burn duration, as lambda increases it takes longer to initiate and stabilize the flame kernel after the spark discharge due to the reduced kernel growth associated with the diluted mixture.

Combustion duration or 10-90% mass fraction burned duration shown in Figure 5-24, is an indicative of the mixture's ability to propagate a flame. Combustion duration shows an overall increasing trend with increasing lambda for all cases. Flame propagation slows with increasing dilution due to reduced flame speeds associated with leaner mixtures and lower combustion temperatures. It is noted that the rate at which combustion duration increases across the lambda range is different for each case. For instance, PFI / late DI combustion duration increases with a slower rate as lambda increases (specifically at higher lambdas). The combustion duration graph clearly shows that the slope of the trend line for PFI / late DI case is lower than other cases and it is separated from the other cases as the lean combustion stability limit is reached. The shorter combustion duration of the PFI / late DI case at high air / fuel ratios can be due to combination of better combustion timing and mixture preparation as the PFI injection helped to increases the mixture homogeneity and the small late DI injection helped to reduce the charge temperature during the late compression stroke, increased turbulence and speed up the flame development in initial part of the combustion.

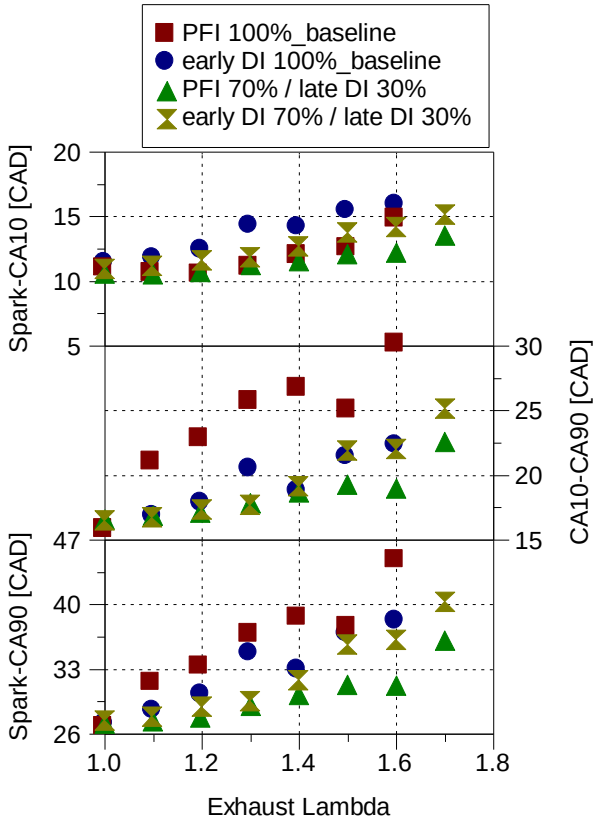

Figure 5-24 Flame development angle and combustion duration of PFI, DI, PFI / late DI and early DI / late DI strategies

Exhaust temperature of the four cases is shown in Figure 5-25. The results highlight the fact that in all cases exhaust temperature decreases as lambda increases due to the lower combustion temperature associated with leaner mixtures. When comparing different cases, the two cases with late DI injection show lower exhaust temperature than the baseline DI and PFI across the lambda range. One reason for this difference in exhaust temperature could be combustion timing which is more advanced for cases with late DI injection. Another reason could be the higher intake pressures with PFI and DI which can increase the in-cylinder temperature at the end of compression stroke and also combustion take place at elevated pressure which also increase the combustion temperature.

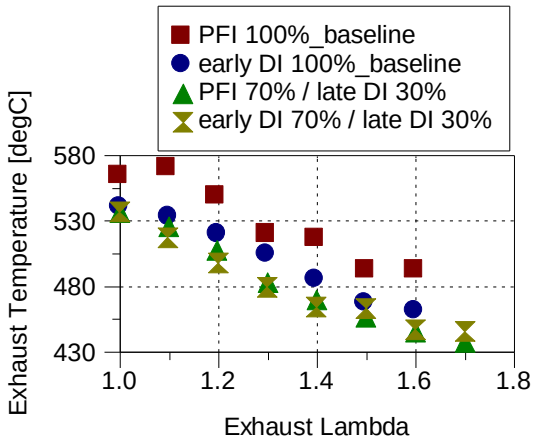

Figure 5-25 Exhaust port temperature of PFI, DI, PFI / late DI and early DI / late DI strategies

5.3.4 Effects of late DI injection timings during the PFI / late DI operation at low load

In this section the effect late DI timings are described at 2000 rpm / 4.64 bar NIMEP. The Start of injection for PFI was kept at 90 CAD BTDCf like the previous test point and the previous chapter. PFI rail pressure was also kept constant at 5 bar gauge. The end of the late DI (EOI2) was varied from 30 CAD BTDCf to 120 CAD BTDCf to find out the maximum indicated efficiency during PFI / late DI operation. DI rail pressure was constant at 92 bar. Cam timings were set at the optimum cam timings at this test point which was obtained with single DI injection (intake MOP=80 CAD ATDC and exhaust MOP=110 CAD BTDC). The experiments were conducted at stoichiometric air/fuel ratio (lambda 1).

As can be seen in Figure 5-26, maximum indicated efficiency and the minimum NISFC is achieved when the end of the late DI injection (EOI2) is between 60 and 70 CAD BTDCf. This can be mainly due to the shorter combustion duration

compared to the more retarded injection timings. In addition, the first part of the combustion or the flame development angle is prolonged when using very advanced injection timings like 120 CAD BTDCf. Therefore, when the EOI2 is between 60 and 70 CAD BTDCf, there is a balance between the flame development angle and combustion duration (Figure 5-26).

It should be noted that CA50 was kept constant around 8 CAD ATDC which is the combustion phasing for optimum efficiency for this engine when the engine is not knock limited at low loads like the current test point. As the late DI timings were advanced, more advance spark timings were required to keep the CA50 around 8 CAD ATDC (Figure 5-26). This was required to catch the stratified flame formed near the spark plug at the right time in order to achieve the highest efficiency.

Figure 5-27 and Figure 5-28 also reveal another reason for the higher indicated efficiency achieved for late DI timings between 60 and 70 CAD BTDCf. Figure 5-27 shows the time available between the end of the late DI and the spark against the late DI timings. As can be seen in this figure, there is only 12 CAD between the end of injection and park timing for the EOI2 = 30 CAD BTDC which gives a very short time for the fuel to evaporate and mix with the air inside the cylinder. This decreases the combustion efficiency significantly (Figure 5-28) for the very late DI timings due to the existence of fuel rich area near the spark plug which increases the unburned combustion products such as CO and smoke emissions (Figure 5-28).

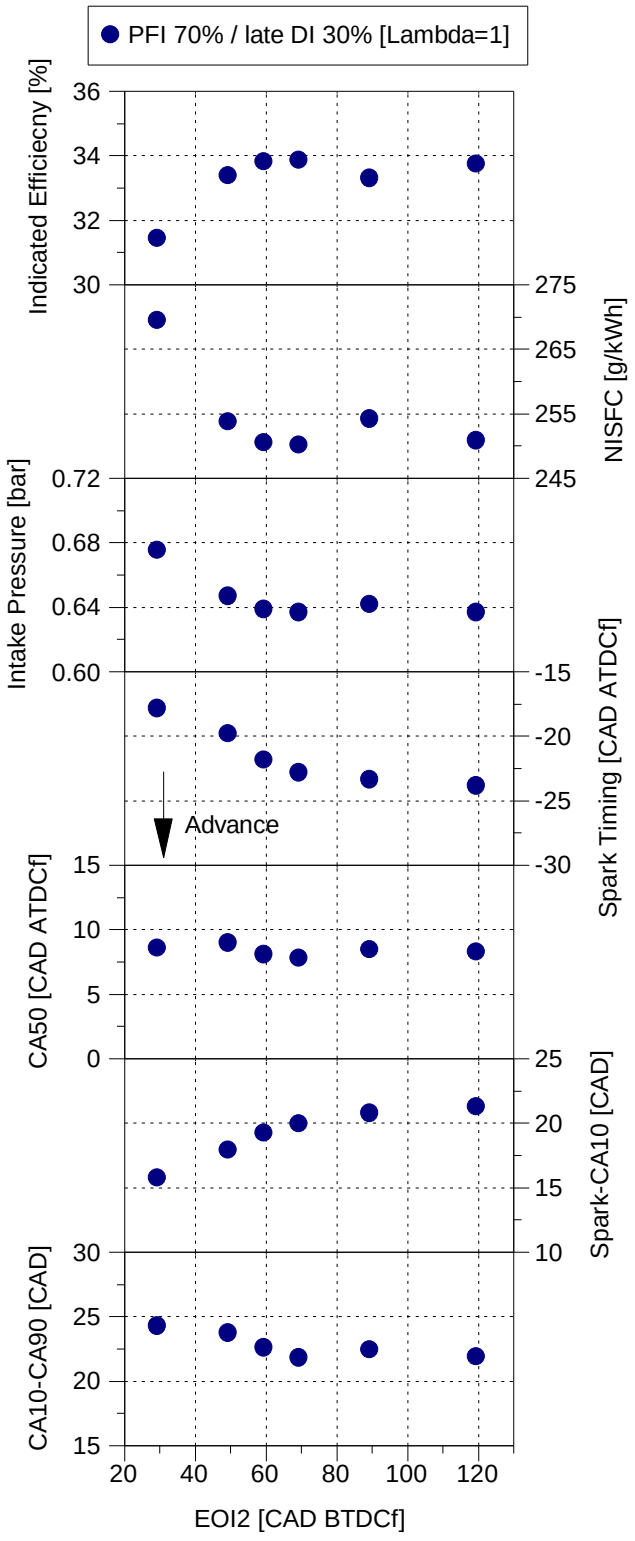

Figure 5-26 Effect of late DI timings on combustion and efficiency at 2000 rpm / 4.64 bar NIMEP

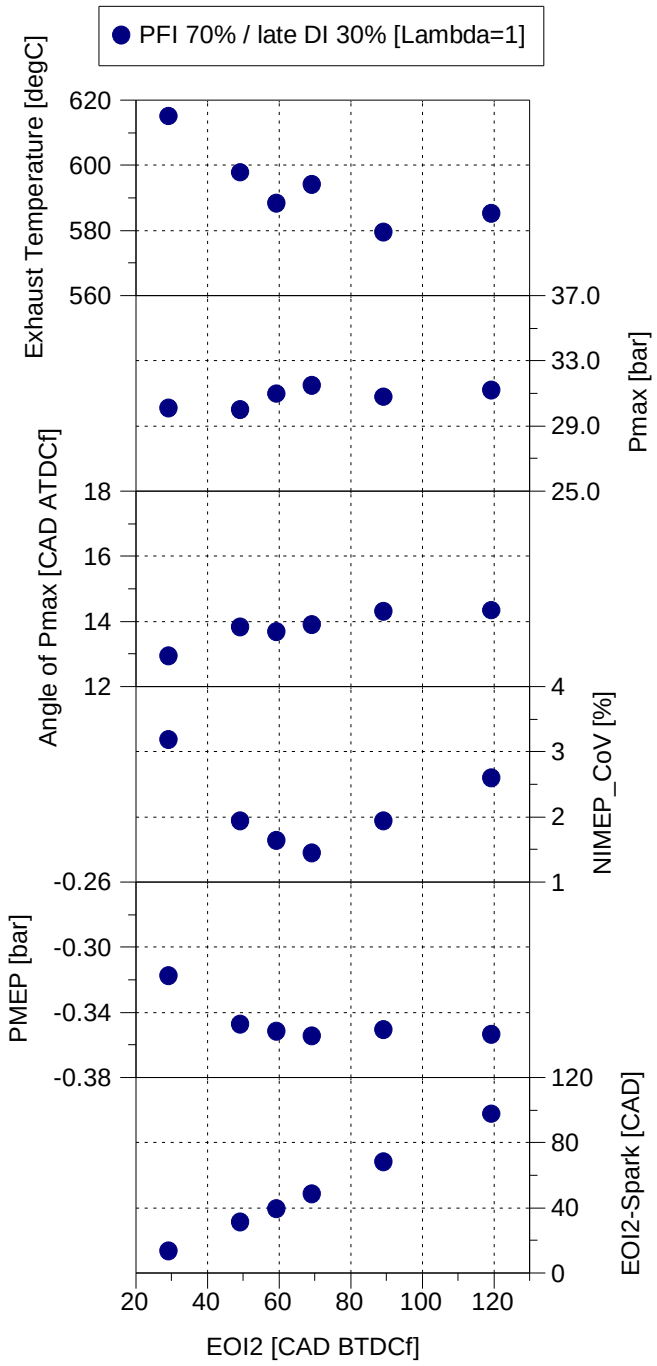

Figure 5-27 Effect of late DI timings on combustion at 2000 rpm / 4.64 bar NIMEP

Exhaust temperature also decreases by advancing the late DI timings due to the shorter combustion duration (Figure 5-27). Highest combustion stability is also achieved at the optimum injection timings (between 60 and 70 CAD BTDCf) due

to the faster overall combustion and therefore less NIMEP variations. Higher peak in-cylinder pressure was also achieved at the optimum late DI timings (Figure 5-27).

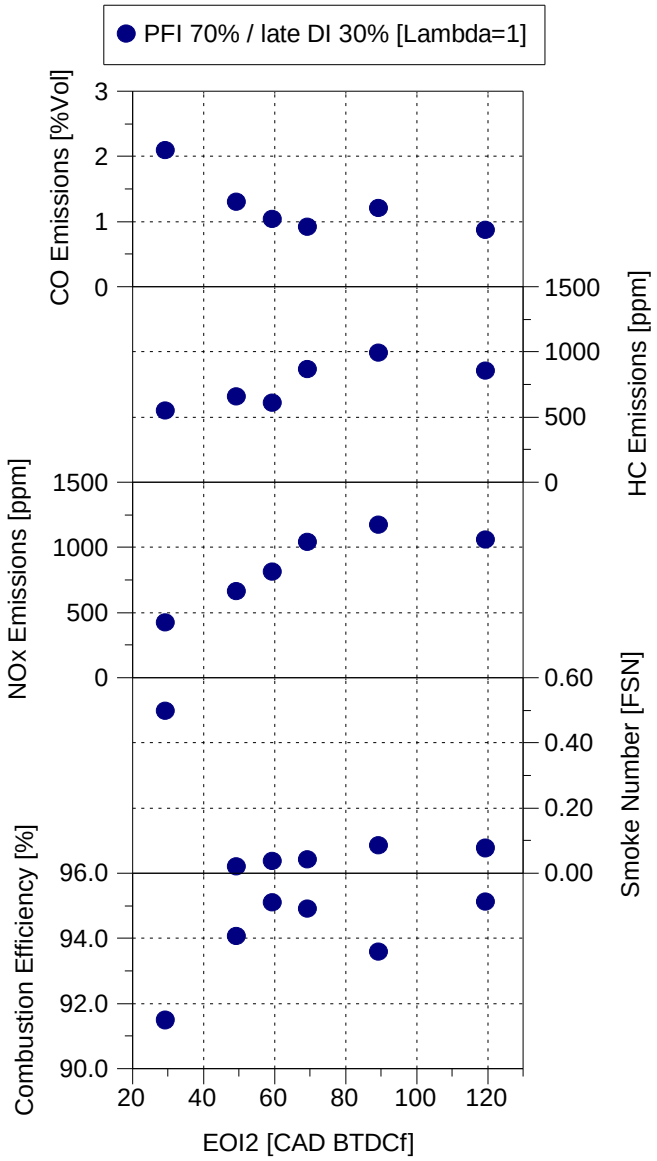

Figure 5-28 Effect of late DI timings on emissions at 2000 rpm / 4.64 bar NIMEP

As it was also explained in the previous chapter HC and NO_x emissions both increased by advancing the late DI timings (Figure 5-28). The lower HC emission from the very late injection could be due to less UHC trapped in crevices as the

injected fuel was more concentrated in the central region of the cylinder at very late injection. And it was also very likely much of UHC in the fuel rich regions was partially oxidized to CO as indicated by the higher CO emission from late injections. Higher NOx emissions can be due to the slightly higher peak in-cylinder pressure and temperature at 60 and 70 CAD BTDCf injection timings as well as slightly higher heat release rate.

5.3.5 Effects of DI injection ratios during the PFI / late DI and PFI / early DI operation at low load

In this section effect of direct injection ratio on combustion, efficiency and emissions of the engine during PFI / late DI and PFI / early DI injection strategies at 2000 rpm / 4.64 bar NIMEP is explained. In these experiments, test parameters such as PFI rail pressure, PFI injection timing, DI rail pressure and cam timings were set at the same values as the previous section with no change. End of the late DI timing was set at 60 CAD BTDCf and the start of the early DI injection was set at 320 CAD BTDCf. The experiments were all conducted at stoichiometric air/fuel ratio or lambda 1.

As can be seen in Figure 5-29, the highest indicated efficiency is achieved when all the fuel is injected through the PFI injector in the intake port. This can be due to the more homogeneous mixture formation by PFI which led to a shorter flame development angle and combustion duration (Figure 5-29). In addition, lower unburned combustion products such as CO and smoke emissions (Figure 5-31) also reveals that PFI creates a more homogeneous mixture in the cylinder and therefore gives the highest combustion efficiency. High CO emissions is an indication of high local lambda and fuel rich area around the spark plug.

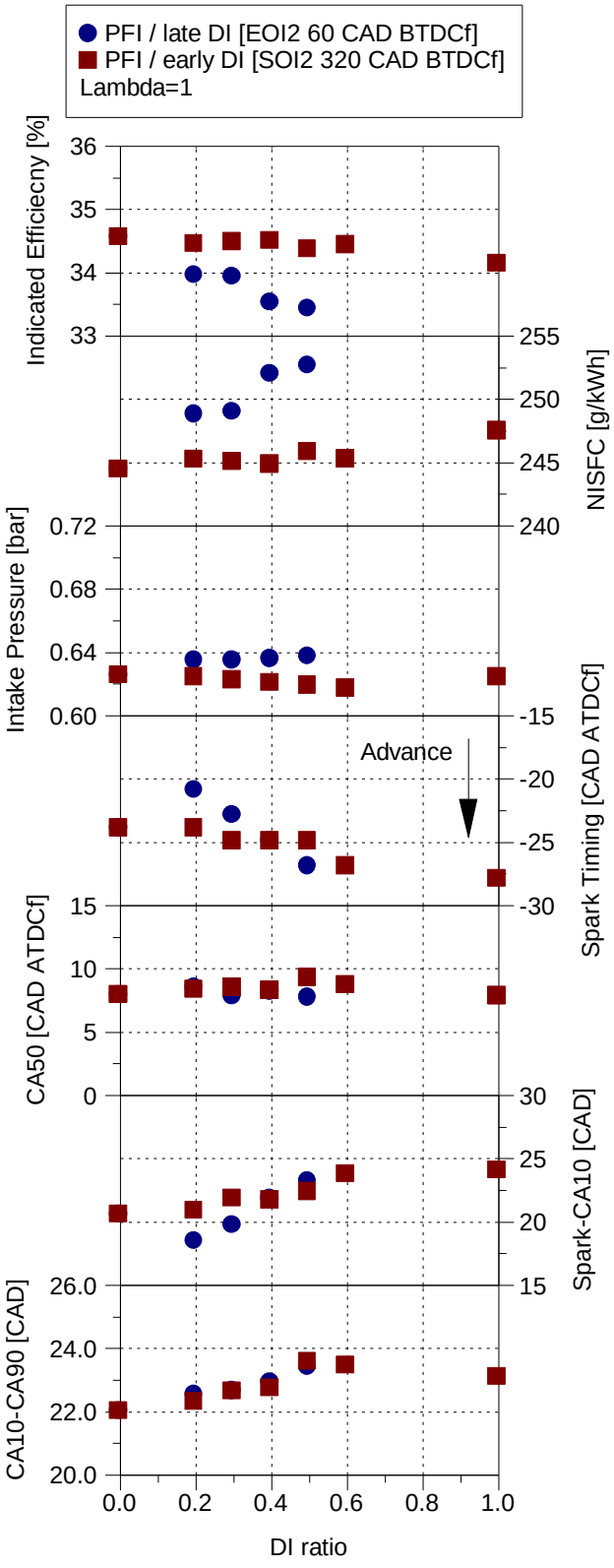

Figure 5-29 Effect of DI ratio sweep on combustion and efficiency during PFI / late DI and PFI / early DI operation at 2000 rpm / 4.64 bar NIMEP

It should be noted that in these experiments spark timing was adjusted to keep the CA50 around 8 CAD ATDC (Figure 5-29) which gives the optimum efficiency. More advanced spark timings were required for both cases to achieve the CA50 of around 8 CAD ATDC.

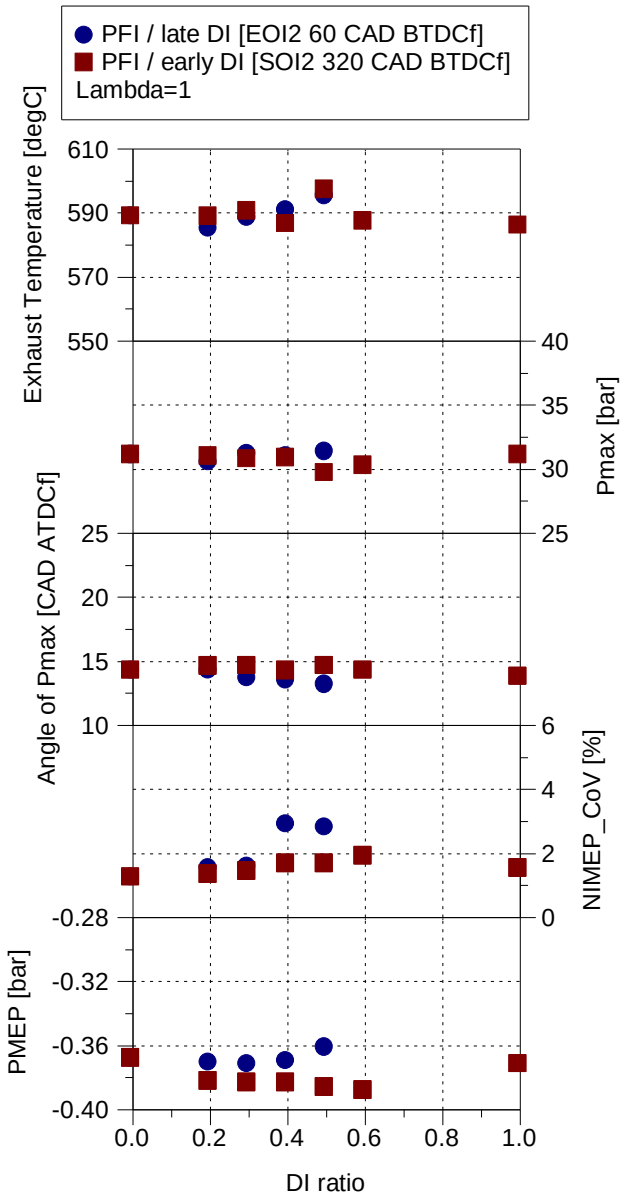

Figure 5-30 Effect of DI ratio sweep on combustion during PFI / late DI and PFI / early DI operation at 2000 rpm / 4.64 bar NIMEP

Increasing the early DI ratio for PFI / early DI case did not change the indicated efficiency and it stayed almost constant throughout the DI ratio range. There was only a small reduction in efficiency when increasing the early DI ratio during the PFI / early DI operation. When injecting all the fuel through the DI injector during PFI / early DI operation there is a slight decrease in efficiency due to the prolonged flame development angle and combustion duration (Figure 5-29). This increase in combustion duration can be due to the less homogeneous mixture formation by DI compared to PFI which is evident by higher CO and smoke emissions and therefore lower combustion efficiency (Figure 5-31).

In case of PFI / late DI operation, as the late DI ratio was increased, the indicated efficiency decreased (Figure 5-29) mainly due to the formation of fuel rich areas around the spark plug which increased the mixture inhomogeneity. This can be explained by prolonged flame development angle and combustion duration as the late DI ratio was increased (Figure 5-29). When switching from 100% PFI to PFI / late DI, initially flame development angle shorten slightly due to the fuel rich area near the spark plug formed by the late DI. However, increasing the late DI ratio more than 40% increased the flame development angle. Increased CO and smoke emissions (Figure 5-31) by increasing the late DI ratio is also another evidence for the formation of inhomogeneous mixture in the cylinder.

Figure 5-30 shows that the exhaust temperature and peak in-cylinder pressure were remained almost unchanged by increasing the DI ratio for both cases. However, combustion stability shows a decrease by increasing the DI ratio for both cases which can be also due to the prolonged flame development angle and combustion duration.

Lower NO_x emission (Figure 5-31) was emitted with PFI / late DI compared to the PFI / early DI which can be due to the cooling effect of the late DI injection which reduces the peak in-cylinder temperature and results in lower NO_x emissions.

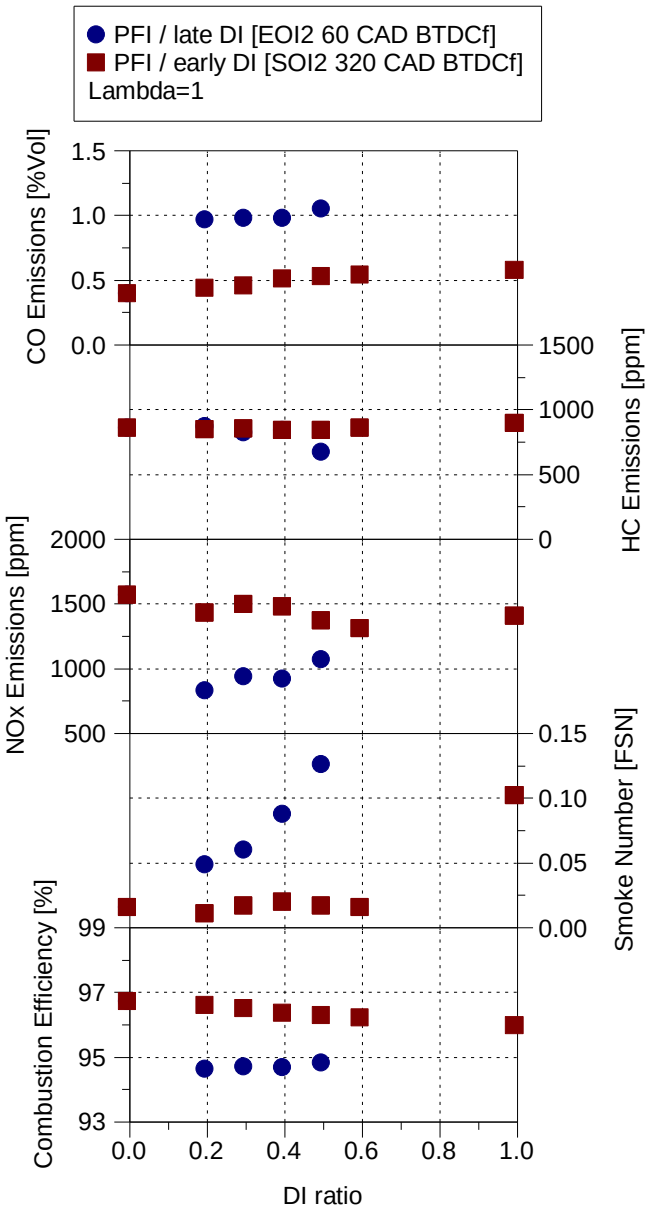

Figure 5-31 Effect of DI ratio sweep on emissions during PFI / late DI and PFI / early DI operation at 2000 rpm / 4.64 bar NIMEP

5.3.6 Comparison of PFI / late DI, PFI / early DI and early DI / late DI strategies with PFI and DI at stoichiometric and lean air / fuel ratios (low load)

In this section various injection strategies such as PFI / late DI, PFI / early DI, early DI / late DI have been investigated under both stoichiometric and lean air/fuel ratios at 2000 rpm / 4.64 bar NIMEP. PFI rail pressure and injection timing, DI rail pressure all remained constant same as the previous section. End of the late DI injection timings was set at 60 CAD BTDCf for all cases with late DI. Start of the early DI injection was set at 320 CAD BTDCf for all cases with early DI injection. Spark timing sweep were performed for CA50 of around 6 and 8 CAD ATDC for all cases. Lambda sweep tests were also performed for all cases for comparison with the baseline PFI and DI (single early injection 320 CAD BTDCf) cases.

As can be seen in Figure 5-32, cases with the late DI injection produce lower indicated efficiency due to the formation of a less homogeneous mixture as it was explained in the previous sections and chapter. Incomplete combustion products such as CO and smoke emissions increase by the formation of fuel rich areas and ultimately deteriorates the combustion efficiency (Figure 5-34).

It should be noted that the spark timing was adjusted for each case throughout the lambda range to keep the CA50 around 6 and 8 CAD ATDC which gives the optimum indicated efficiency (Figure 5-32). PFI 70% / late DI 30% required the minimum spark advanced among all cases to achieve the CA50 of around 8 CAD ATDC. This case also shows the shortest flame development angle and combustion duration for spark timings (Figure 5-32).

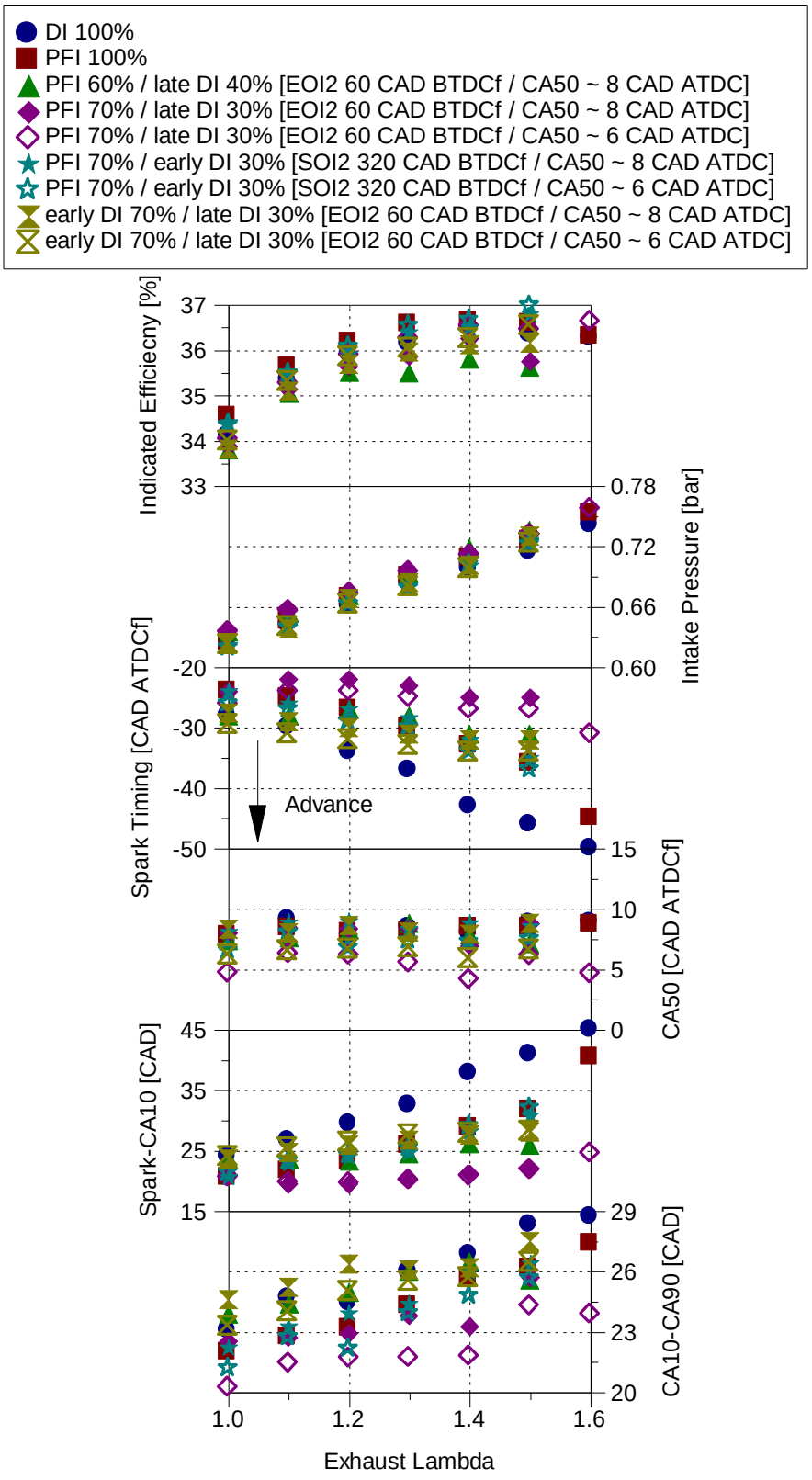

Figure 5-32 Effect of various PFI / DI injection strategies on combustion and efficiency at stoichiometric and lean air/fuel ratios (2000 rpm / 4.64 bar NIMEP)

As the mixture became leaner and lambda increased, flame development angle and combustion duration prolonged for all cases (Figure 5-32). Longer flame development angle is because it takes longer to initiate and stabilize the flame kernel after the spark discharge due to the reduced kernel growth associated with the diluted mixture. Combustion duration prolonged since flame propagation slows with increasing dilution due to reduced flame speeds associated with leaner mixtures and lower combustion temperatures.

Figure 5-32 also shows that indicated efficiency increase by increasing the lambda or dilution. This is due to the combination of factors such as lower pumping losses due to the use of higher intake pressure and excess air during lean operation (Figure 5-33), lower heat loss to the exhaust system (lower exhaust port temperature) (Figure 5-33), higher combustion efficiency due to lower unburned combustion products (Figure 5-34) and lower combustion temperature with lean mixtures which reduces dissociation.

Figure 5-33 also shows that the PFI 70% / late DI 30% has the lowest exhaust temperature among all cases across the lambda range which can be due to the faster combustion. This strategy also exhibited the highest peak in-cylinder pressure with the advance spark timing (CA50 around 6 CAD ATDC).

Combustion stability also decreased for all cases as the lambda was increased mainly due to the slower combustion which increases the variations of NIMEP. In addition, partial burning cycles and misfires start to occur when increasing the lambda more than 1.4 at this speed and load combination which significantly increases the COV of NIMEP. PFI, DI, PFI 70% / late DI 30% and PFI 70% / early DI 30% cases show the highest combustion stability.

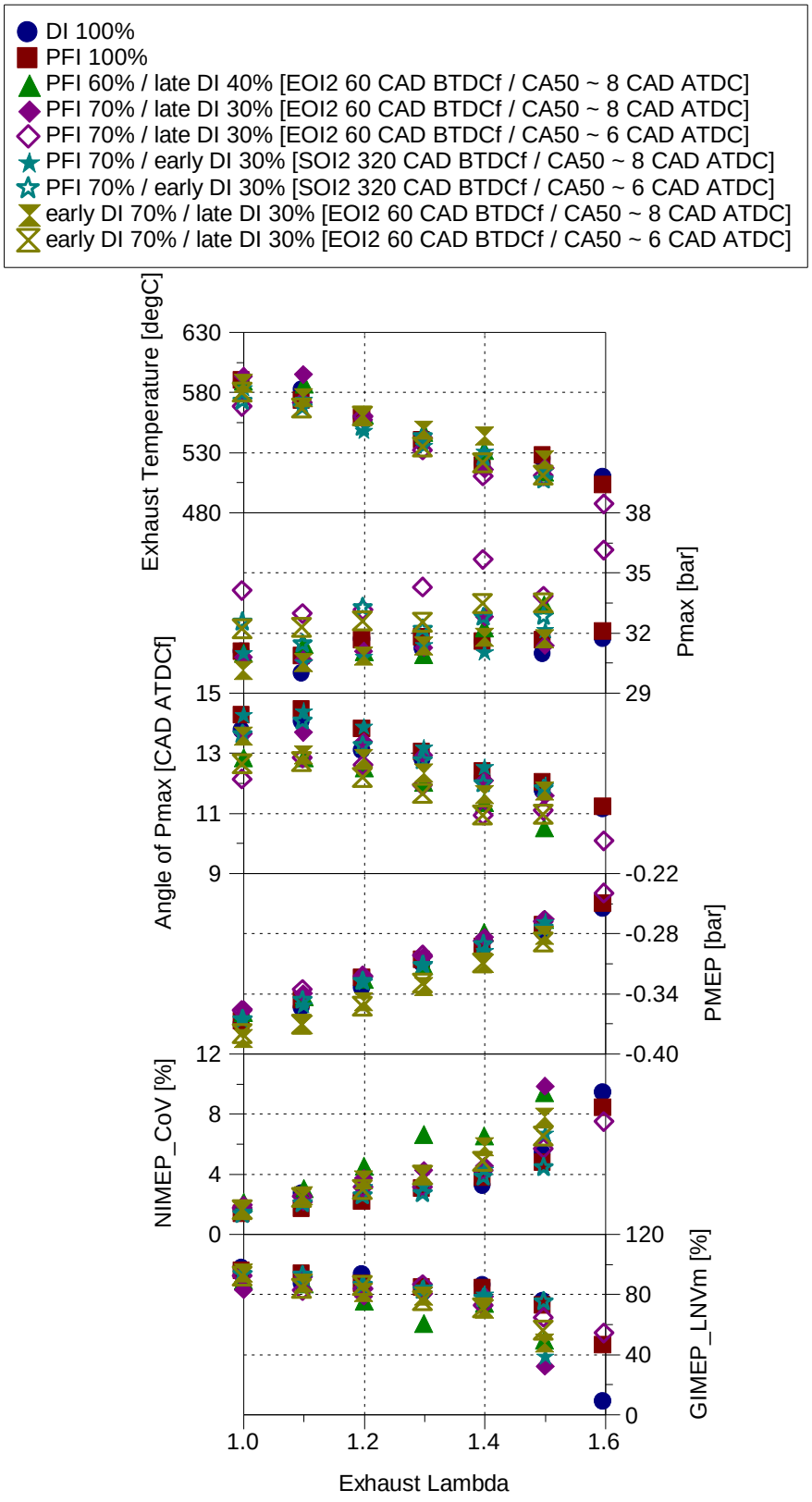

Figure 5-33 Effect of various PFI / DI injection strategies on combustion at stoichiometric and lean air/fuel ratios (2000 rpm / 4.64 bar NIMEP)

Lowest normalised value of gross IMEP (GIMEP_LNV) is also shown in Figure 5-33. Lowest Normalized Value (LNV) of Gross IMEP of 300 cycles equals to minimum GIMEP divided by the average GIMEP (GIMEPmin / GIMEPav*100 (%)). Low LNV at high lambda values show the existence of cycles with very low GIMEP compare to the average GIMEP (some partial burned cycles).

Figure 5-34 shows that CO emissions drop immediately after increasing the lambda from 1 to 1.1 and stayed almost constant by increasing the lambda further for all cases. This is due to the reduced fuel rich areas in the combustion chamber. At lambda 1 or stoichiometric air/fuel ratio PFI shows the lowest level of CO emissions among all cases which shows the formation of a more homogeneous mixture when purely using intake port injection.

HC emissions (Figure 5-34) show a decrease initially after increasing the lambda from 1 to around 1.3 and then start to increase again for all cases. This is mainly due to a lower fuel rich area as the lambda is increased. However, increasing the lambda more than 1.3 increases the partial burning cycles and the COV of NIMEP which lead to an increase in HC emissions.

As can be seen in Figure 5-34, NO_x emissions peak at around lambda 1.1 due to the higher in-cylinder temperature at that lambda for all cases. Early DI 70% / late DI 30% exhibited the highest level of smoke emission among all cases since all the fuel was injected directly in the cylinder as well as the late DI injection which promotes the fuel rich area and increases the smoke emissions. Combustion efficiency peaks at lambda 1.1 for all cases due lower HC and CO emissions at this air/fuel ratio.

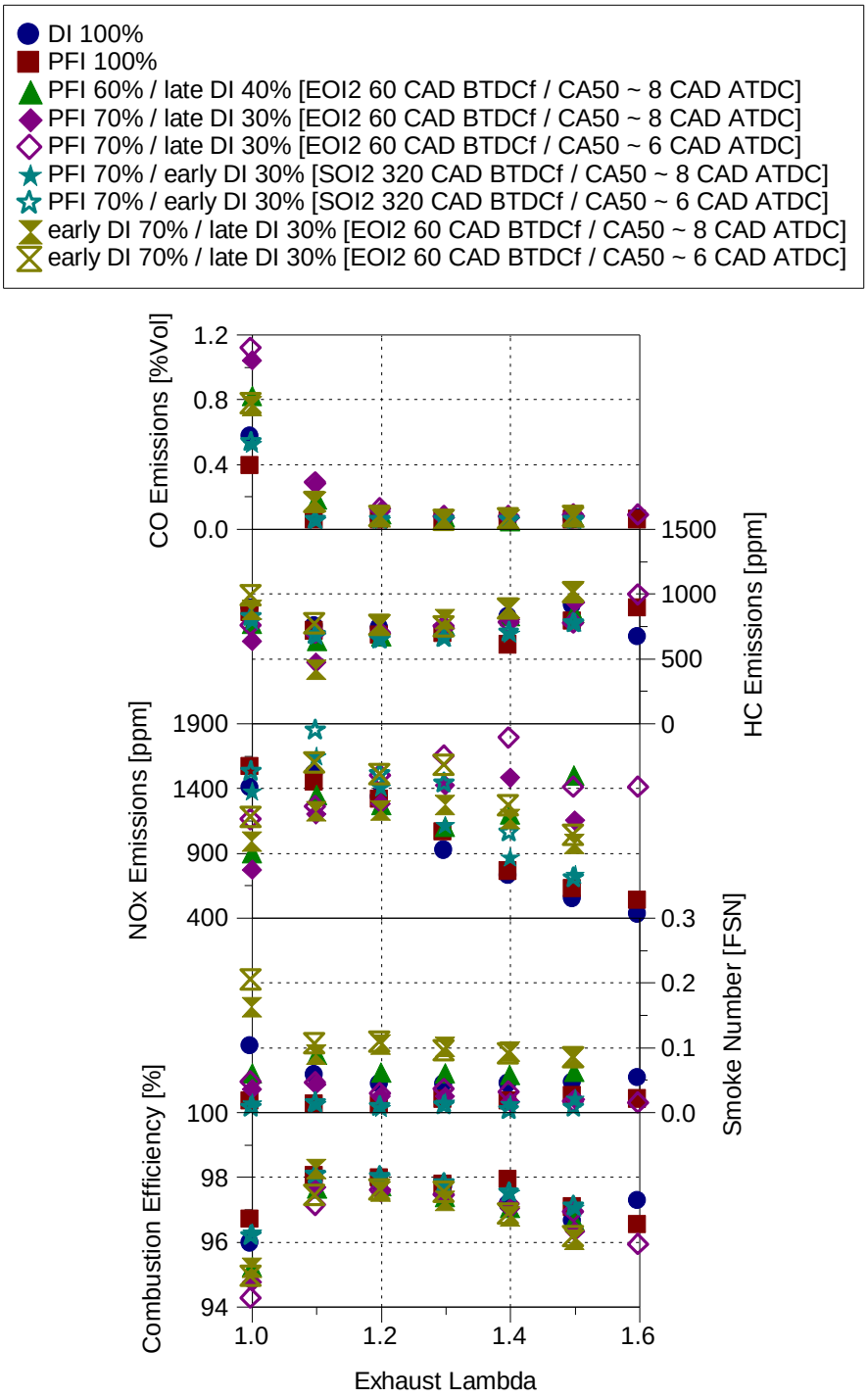

Figure 5-34 Effect of various PFI / DI injection strategies on emissions at stoichiometric and lean air/fuel ratios (2000 rpm / 4.64 bar NIMEP)

5.4 Summary

In order to improve the in-cylinder mixture preparation (in terms of both homogeneity and temperature) and enhance the combustion, dual (PFI / late DI) and split (early DI / late DI) injection strategies were proposed and studied in a single cylinder DISI engine with a centrally mounted outwardly opening piezo injector. These injection strategies can create a homogeneous/stratified (hybrid) combustion which can greatly affect the fuel economy and emissions. The mains findings can be summarized as follows:

- The late DI injection timings greatly affect the fuel consumption and emissions. Minimum NISFC is achieved when the end of the late DI injection is at 60 CAD BTDCf for both PFI / late DI and early DI / late DI strategies at lambda 1. Retarding the late DI injection timing from this point increases the under-mixing effect and unburned combustion products such as CO and smoke emissions. Therefore, combustion efficiency is lower with the very late DI timings. Advancing the late DI timings increases the charge temperature and knocking tendency, therefore forces the use of less advanced spark timings which has a negative effect on combustion timing and efficiency.
- Effect of late DI timings on heat transfer and the charge temperature at the time of ignition is shown by the changes in the slope of the log P – log V diagram during compression stroke right after the late DI injection
- Late DI injection ratio greatly affects the mixture temperature and homogeneity. Minimum NISFC was achieved when the late DI ratio was between 30% and 40% for both PFI / late DI and early DI / late DI cases at

the testing condition. Very low late DI ratios were not able to provide enough cooling effect to decrease the charge temperature. Therefore, combustion timings were retarded, and efficiency was lower. Very high late DI ratios increased the unburned combustion products such as CO, HC and smoke emissions and result in low combustion efficiency. High late DI ratios reduced the charge temperature more and result in more advance combustion timings and reduced exhaust temperature.

- PFI / late DI and early DI / late DI cases can reduce the fuel consumption significantly at mid-high load compared to baseline PFI and DI cases across the lambda range. Strong cooling effect of the late DI injection which affects the heat transfer rate and charge temperature during the late compression stroke is the main reason for higher efficiency at this knock limited point. Lean combustion stability limit was also extended from lambda 1.4 to lambda 1.7 with PFI / late DI strategy. Reduced HC and smoke emissions and lower exhaust temperature across the lambda range are the other advantages of this dual injection system.
- Optimum DI injection timing for best combustion efficiency and lowest NISFC at 2000 rpm / 4.64 bar NIMEP is between 60 and 70 CAD BTDCf. The earlier DI injection timings led to slightly shorter combustion duration, lower CO and smoke emissions but increased UHC emissions
- At 2000 rpm / 4.64 bar NIMEP increasing the DI ratio under PFI / late DI operation increases the mixture inhomogeneity, therefore decrease the combustion efficiency and fuel economy
- In terms of emissions at 2000 rpm / 4.64 bar NIMEP, cases with late DI injection produced the highest levels of CO and soot emissions and lowest

UHC emissions due to a more concentrated fuel in the central region of the combustion chamber therefore, less trapped fuel in the crevices. PFI 100% case produced significantly low smoke emissions but the highest level of NO_x emissions at lambda 1.

Chapter Six

Effect of Intake Port Injection of Water on Combustion, Efficiency and Emissions

Chapter 6 Effect of Intake Port Injection of Water on Combustion, Efficiency and Emissions

6.1 Introduction

As it was described in chapter two of this thesis, water injection can be used as a promising method to mitigate knock and significantly reduce the CO_2 emissions. This is particularly important in highly downsized boosted engines which run under much higher intake pressures and are more prone to knocking combustion. In addition to anti-knock behaviour, water injection is also an effective method for reducing NO_x emissions and exhaust gas temperature at high loads which can protect the turbine and other components in the exhaust system in turbocharged engines instead of enrichment at high speeds and high loads.

This chapter shows the influence of intake port injection of water on efficiency and emissions of a boosted downsized single cylinder gasoline direct injection (GDI) engine in detail. Six different steady state speed and load combinations were selected to represent the conditions that knocking combustion start to occur. Water ratio sweep tests were performed to find out the optimum water / fuel ratio at each test point and the impact on the combustion and emissions. The tests were performed with gasoline with three different research octane number (RON) of 95, 97 and 100 to determine the effective octane number of water. This chapter shows the results for one octane number fuel (gasoline RON 100) to explain the effect of water injection only and chapter seven shows the effect of water injection with all three fuels and make a comparison to explain the effective octane number of water.

6.2 Experimental Setup and Test Conditions

Effect of intake port water injection on efficiency and emission of the engine were also studied with the set-up shown in Figure 6-1. Six different steady state speed and load combinations were selected to represent the conditions that knocking combustion start to occur. These were selected to study the effectiveness of water in suppressing knock. Table 6.1 shows the details of the testing points for water injection experiments.

Water / fuel ratio was varied in the range of 0 to 3 (the water / fuel ratio in water injection experiments is based on mass) to find out the optimum water mass required at each test point and the impact on the combustion and emissions. Gasoline with three different octane numbers (RON 95, 97 and 100) was used to determine the effective octane number of water.

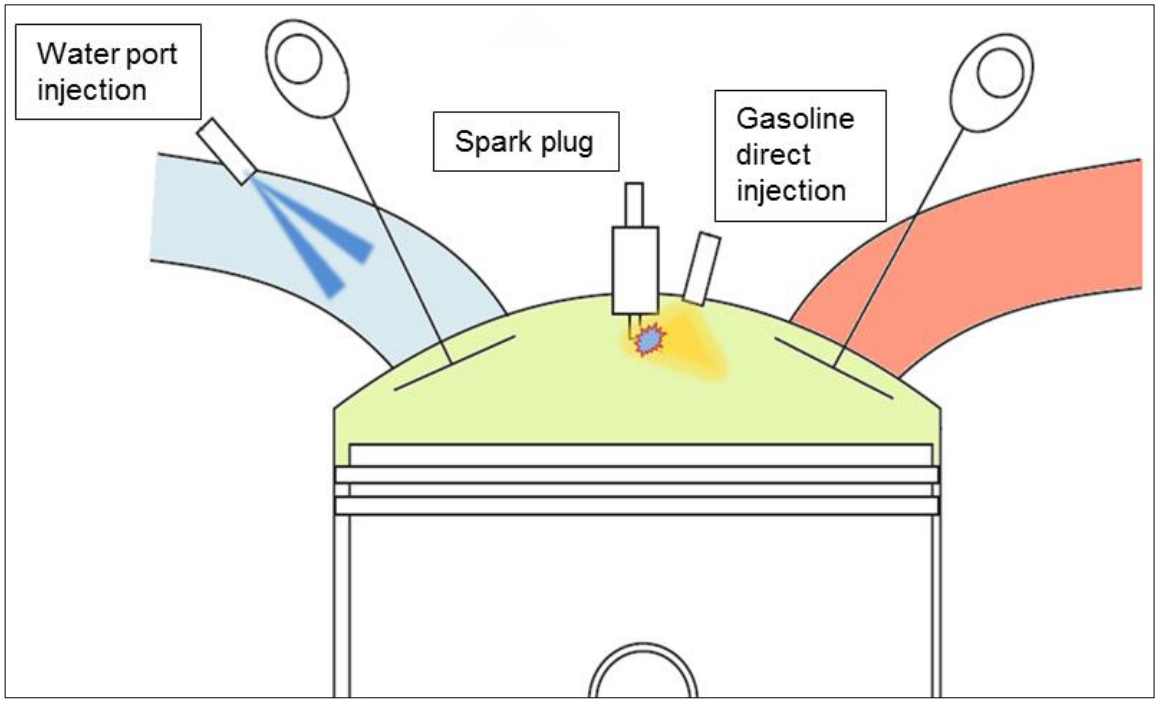

Figure 6-1 Schematic diagram of PFI water / DI gasoline combustion system

In these experiments first, the baseline at each test point was recorded without any water injection (only spark timing sweep was performed for baseline). Then, water injection sweep was performed to find out the optimum water / fuel ratio, started with a very small to large quantities of water until there was no apparent improvement in efficiency. Effect of water injection with and without spark timing advance was then compared to the bassline data. This was repeated for all three fuels for comparison. The PFI injection timing was kept constant with the start of injection (SOI) at 90 CAD BTDCf when the intake valves were fully closed. Experiments were also performed with water injection during intake valve open (IVO) period.

Table 6.1 Steady state operating points for water injection

Speed (rpm) / NIMEP (bar)	1000/ 8.83	2000/ 8.90	2000/ 16.04	2000/ 20	3000/ 16.04	3000/ 20
IMOP (CAD ATDC)	120	120	110	110	110	110
EMOP (CAD BTDC)	110	100	100	100	100	100
Valve overlap at 0.5 mm lift (CAD)	0	10	20	20	20	20
SOI fuel (CAD BTDCf)	276	320	290	290	290	290
Rail pressure fuel (bar)	133	130	170	170	170	170
SOI water IVC (CAD BTDCf)	90	90	90	90	90	90
SOI water IVO (CAD BTDCf)	360	360	370	370	370	370
Rail pressure water (bar)	5	5	5	5	5	5
Spark timing	DBL	DBL	DBL	DBL	DBL	DBL
Lambda	1	1	1	1	1	1

6.3 Results and Discussion

6.3.1 Effect of water injection on engine performance at medium load condition when knock starts to occur

Experiments were started at the engine speed of 1000 rpm and load of 8.83 bar NIMEP. This test point was selected since for the current engine hardware setup knock start to occur at this low speed/medium load point and for boosted downsized engines LSPI (low speed pre-ignition) might occur as the load is increased at low speed. Therefore, this is an important test point to demonstrate the potential of water injection in knock suppression.

At each test point experiments first began with a spark timing sweep before adding any water into the mixture. This was done to determine the baseline efficiency and the knock limited spark advance (KLSA) without water injection.

Figure 6-2 shows the results of spark timing sweep at 1000 rpm and 8.83 bar NIMEP which is a knock limited point due to the high compression ratio and the low speed. There was a significant improvement in indicated efficiency as the spark timing was advanced. This improvement mainly was due to a more advanced combustion timing and shorter flame development angle and combustion duration. 50% mass fraction burned angle is advanced by around 6 CAD (crank angle degree) and combustion duration is also shorter by around 2 CAD.

In addition, Figure 6-2 also shows a notable increase in peak cylinder pressure as the knock limited spark timing was advanced. Advancing the spark timing also

results in an increase in maximum cylinder pressure rise rate. Thus, lower boost pressure was required to achieve the same load which consequently results in lower fuel consumption.

After performing the spark timing sweep tests, a baseline is now established which can be used for comparison with the water injection tests. In the next step the engine was run at the baseline condition and a small quantity of water (water / fuel ratio of 0.3) was injected in the intake port while the spark timing was the same as the baseline to understand the effect of water injection only with no spark advance. Figure 6-3 shows the results in detail. As can be seen in this figure when a small quantity of water was added to the mixture without any spark advance, the combustion timing (mass fraction burned history), peak cylinder pressure, and heat release were all retarded (blue curves in Figure 6-3).

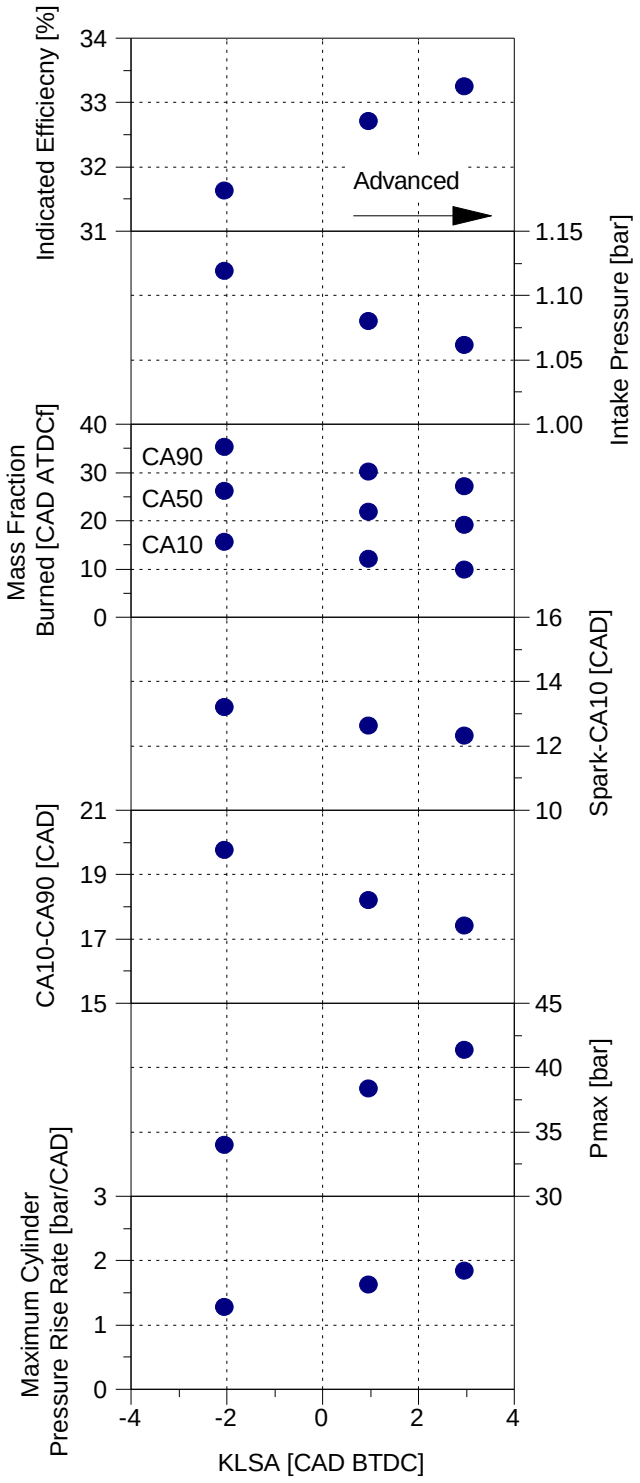

Figure 6-2 Spark timing sweep for baseline without water injection at 1000 rpm / 8.83 bar NIMEP (RON 100)

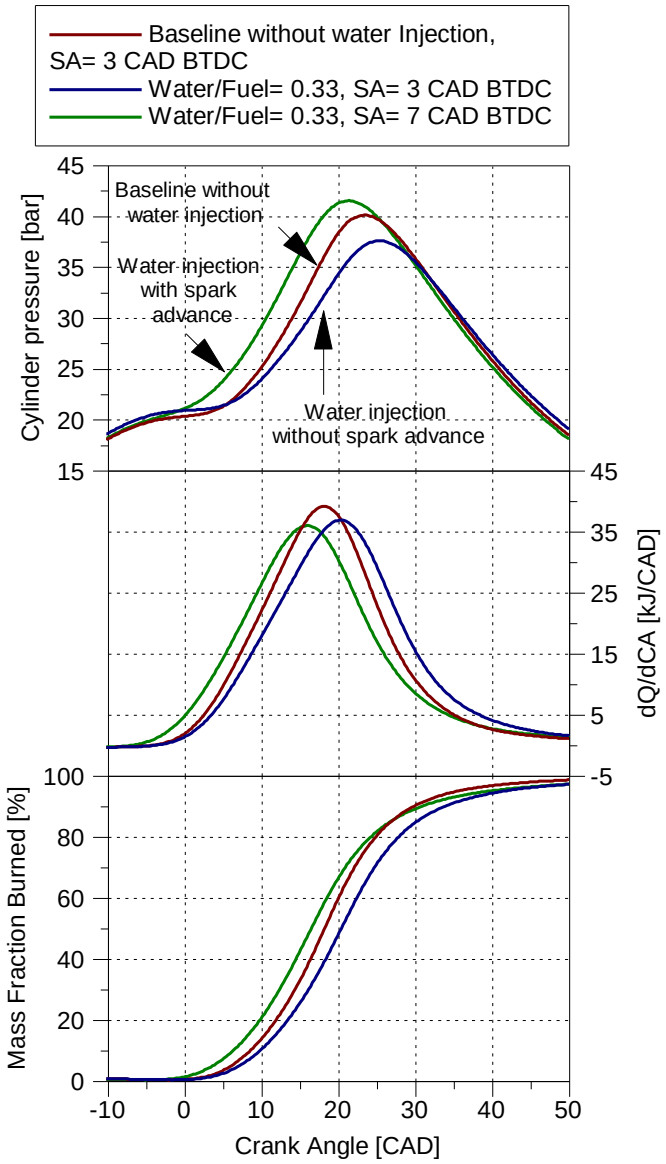

Figure 6-3 Effect of water injection and spark advance on cylinder pressure, heat release and MFB at 1000 rpm / 8.83 bar NIMEP (RON 100)

In addition, peak cylinder pressure and heat release also decreased. The injected water in the intake port absorbed the heat from the intake air, valves and ports and acted as an inert gas after vaporization. Hence, combustion timing was retarded and as a results efficiency was lower when the spark timing remained constant compared to the baseline. However, spark timing could be advanced further due to this inert gas effect. Therefore, combustion timing, heat release and peak

cylinder pressure were all advanced without occurrence of knock by injecting the same amount of water and advancing the spark timing simultaneously (green curves in Figure 6-3).

Peak cylinder pressure was also clearly increased by around 2 bar compared to the baseline. These improvements in spark timing and combustion phasing eventually led to an increase in efficiency. It is worth mentioning that when the injected water mass is small, all the water might have been vaporized before entering the cylinder but when the injected water mass is large, only part of the water evaporates before entering the cylinder and the other part might enter the cylinder in the liquid phase.

Figure 6-4 shows the effect of the injected water quantity on efficiency and combustion characteristics of the engine at 1000 rpm and 8.83 bar NIMEP. Increasing the injected water mass could increase the knock tolerance due to the increased cooling effect of water and therefore the knock limited spark advance (KLSA) could be advanced further by a maximum of around 17 CAD without knock occurrence. Indicated efficiency increased by around 4% mainly due to the use of more advanced spark timings which shifts the combustion phasing towards the optimum point (CA50 of around 8 CAD ATDC). Mass fraction burned angles, CA10, CA50 and CA90 were all advanced by around 10 CAD. As a result, combustion phasing and angle of maximum cylinder pressure moved closer to TDC where the combustion is exposed to high-temperature and pressure environment.

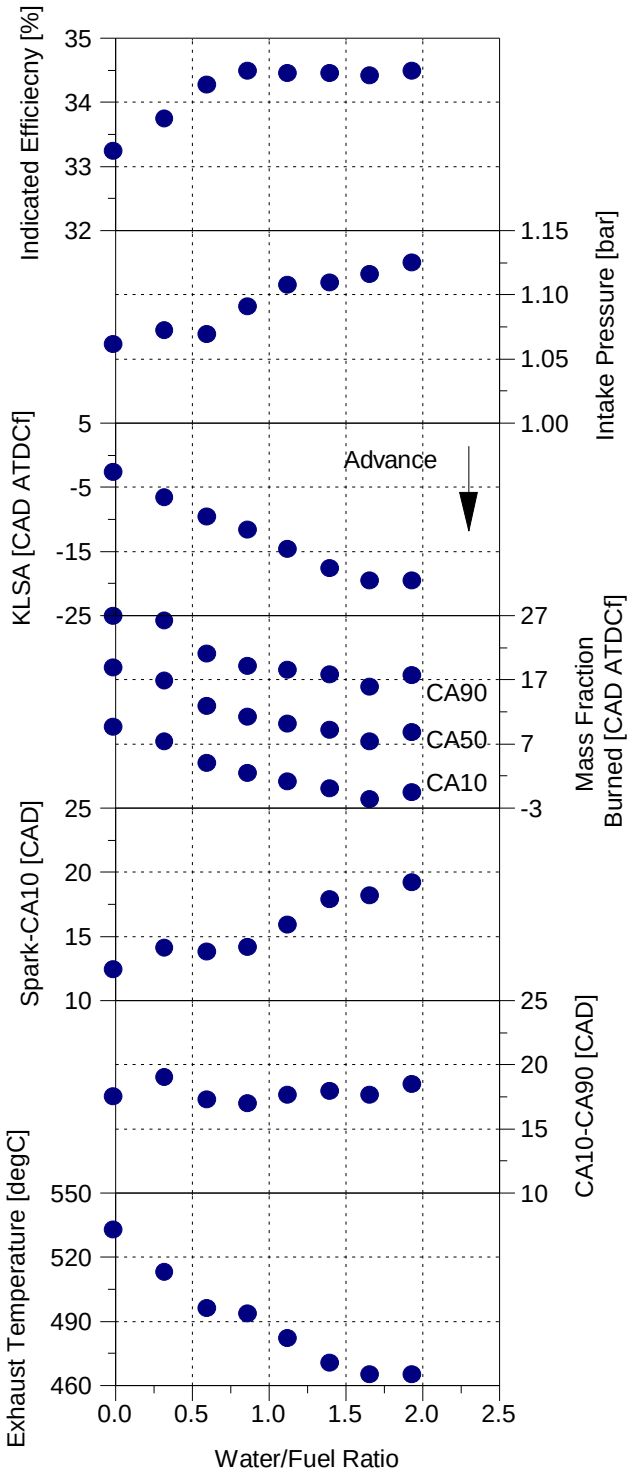

Figure 6-4 Impact of water / fuel ratio sweep on stoichiometric combustion and efficiency at 1000 rpm / 8.83 bar NIMEP (RON 100)

Increased water mass however had a negative effect on initial part of the combustion as flame development angle was prolonged when water/fuel ratio was

increased. Flame development angle was prolonged by around 7 CAD comparing the baseline to the maximum water/fuel ratio which was more pronounced than the slight increase, around 1.5 CAD, in combustion duration. A reason for prolonged flame development angle can be the effect of charge dilution which increased by increasing in this case, the injected water mass. As the charge dilution increases, it takes longer to initiate and stabilize the flame kernel after the spark discharge due to the reduced kernel growth as the prolonged spark-CA10 suggests.

In terms of combustion duration, overall it stayed fairly constant across the water/fuel ratio range. The effect of spark advance improvement is offset by slower flame development speed and the combustion duration (CA10-CA90) remains nearly the same throughout the variations. Initially there was a slight increase of around 1.5 CAD in combustion duration immediately after switching from baseline to water injection. Combustion duration decreased slightly when the water/fuel ratio was between 0.5 and 1. It then started to increase slightly as the water was increased further to its maximum level. The reason for slight increase in combustion duration at very high water/fuel ratios (above 1) could be also the dilution effect of water which could not be compensated by the advanced spark timing and combustion phasing anymore. As the dilution effect of water increases, it slows flame propagation due to reduced flame speeds associated with diluted mixtures and lower combustion temperatures. As a result, improvement in indicated efficiency slowed down as the water/fuel ratio increased beyond 1 since the positive effect of earlier combustion phasing was not as effective as it was at the beginning. Another reason for this slow improvement in efficiency was lower

combustion efficiency at high water/fuel ratios which will be explained later in Figure 6-16 in the emission.

Figure 6-4 also shows the intake pressure which increased despite higher indicated efficiency and lower fuel consumption as the injected water mass increased. The reason for increase in intake pressure is the displacement of some air with water which increased as the water mass increased. Therefore, slightly higher intake pressure was required to compensate for that displacement.

Furthermore, as it is depicted in Figure 6-4, exhaust temperature was around 80°C lower with the maximum water/fuel ratio compared to the baseline mainly due to a more advanced combustion timing and increased heat capacity of charge. Combustion and heat release began earlier in the cycle and finished earlier with water injection compared to the baseline (Figure 6-3) which minimized the heat lost to the exhaust system and kept the exhaust temperature lower. This is advantageous in turbocharged engines specifically at high loads and speeds when fuel enrichment is used to protect the turbine and other components which are exposed to high exhaust gas temperature. Therefore, eliminating the need for fuel enrichment and extending the lambda 1 (λ=1 or stoichiometric air/fuel ratio) operating area of the engine map. However, the performance of the aftertreatment system also need to be considered carefully as excessive temperature reduction might lower the aftertreatment system performance.

Figure 6-5 also shows the effect of water injection on some other combustion parameters such as maximum in-cylinder pressure (Pmax) and its crank angle, maximum cylinder pressure rise rate and its crank angle, combustion stability (NIMEP_CoV) and knocking intensity.

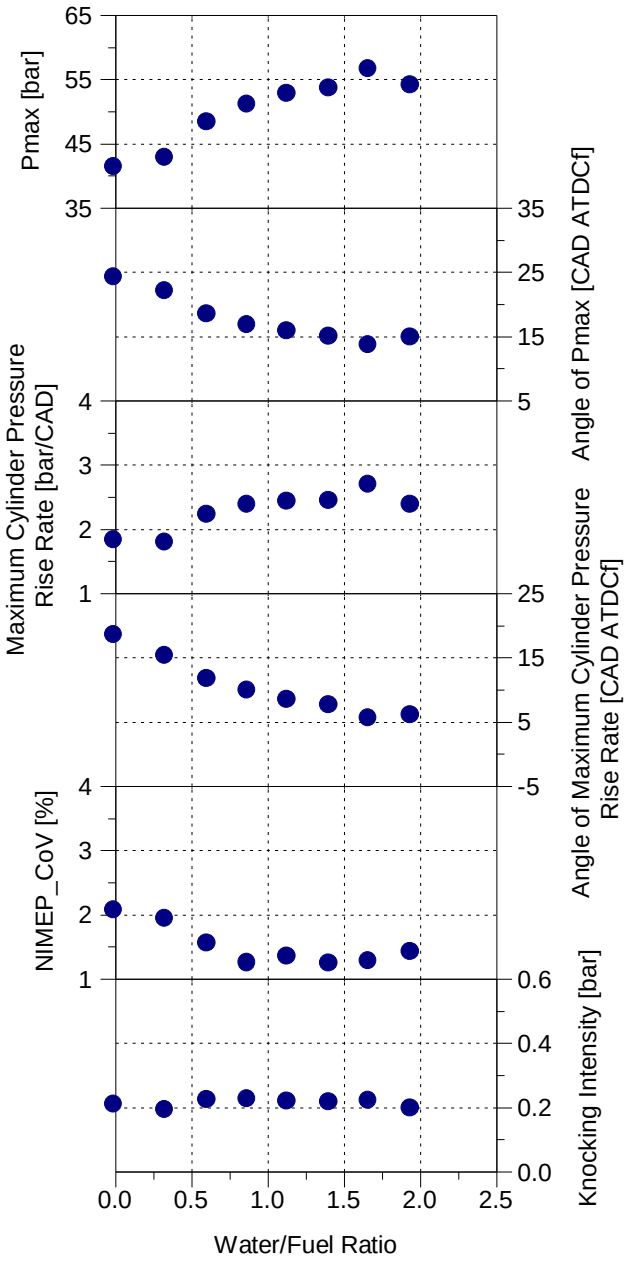

Figure 6-5 Impact of water / fuel ratio sweep on stoichiometric combustion at 1000 rpm / 8.83 bar NIMEP (RON 100)

As can be seen in Figure 6-5, both maximum in-cylinder pressure and maximum cylinder pressure rise rate increased by a maximum of around 15 bar and 1 bar/CAD respectively compared to the baseline. The reason for this increase was the advancement in spark timing and combustion phasing as explained earlier. Angle of Pmax and angle of maximum cylinder pressure rise rate also was

advanced by a maximum of around 10 CAD compared to the baseline without water injection. Combustion stability also improved due to the more advanced combustion phasing and achieving the optimum CA50 of around 8 CAD ATDC. Knocking intensity was remained almost constant.

Figure 6-6 shows the shift of combustion phasing to an optimum position by adding water and advancing the spark timing. The graph compares the minimum and maximum water/fuel ratios with the baseline without water. Adding a small quantity of water exhibited relatively small improvements in peak cylinder pressure, combustion phasing and burn rate. However, when the water / fuel ratio increased to a maximum of 1.95, CA50 of around 8 CAD ATDC could be achieved and all the other benefits such as higher peak in-cylinder pressure and earlier heat release are more pronounced and clearer in the graphs as it was explained above. At this speed and load combination optimum efficiency is achieved with the water / fuel ratio of around 0.8. Efficiency stayed almost constant by increasing the water / fuel ratio beyond 1 as it was depicted in Figure 6-4. When the water / fuel ratio is around 1, CA50 is around 10 CAD ATDC which is very close to optimum and after that adding more water could only slightly advanced the CA50 to around 8 CAD ATDC, therefore efficiency stayed almost the same.

In-cylinder average temperature against crank angle is plotted in Figure 6-7 using the ideal gas law equation. Calculations were performed assuming the mass of residual gas to be equal to mass of cylinder at the time when exhaust valves are just closed (cylinder temperature is assumed to be equal to the exhaust temperature at this time).

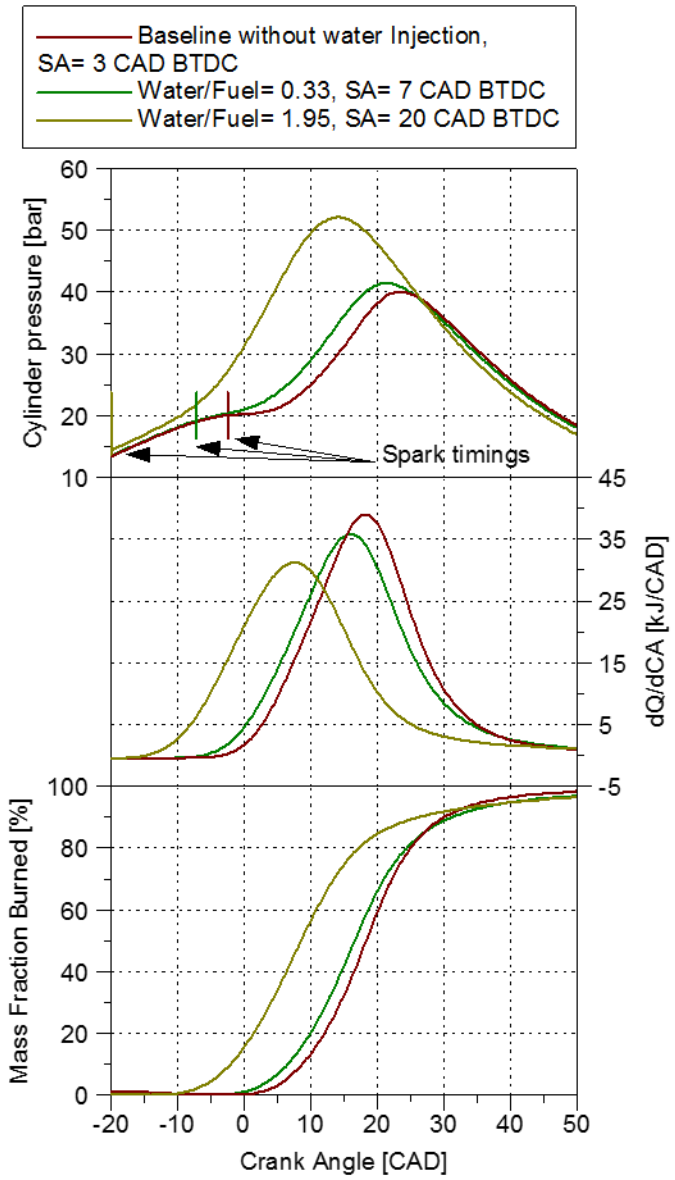

Figure 6-6 Effect of different water / fuel ratios and spark advance on in-cylinder pressure, heat release and MFB at 1000 rpm / 8.83 bar NIMEP (RON 100)

Peak in-cylinder average temperature dropped significantly by around 200 K when injecting a large amount of water (water / fuel ratio of around 2) into the intake port compared to the baseline without water injection. This can be the main reason for lower NO_x emissions which will be discussed later in the emissions section (Figure 6-16). The main effect of adding water into the intake air on the NO formation is

that it reduces the flame temperature by increasing the heat capacity of charge. This is reflected on the peak in-cylinder temperature which is lower with water injection. In addition, with water injection in-cylinder temperature was around 10 K lower during the compression stroke after the intake valves closure which enabled the use of a more advanced spark timing without occurrence of knock.

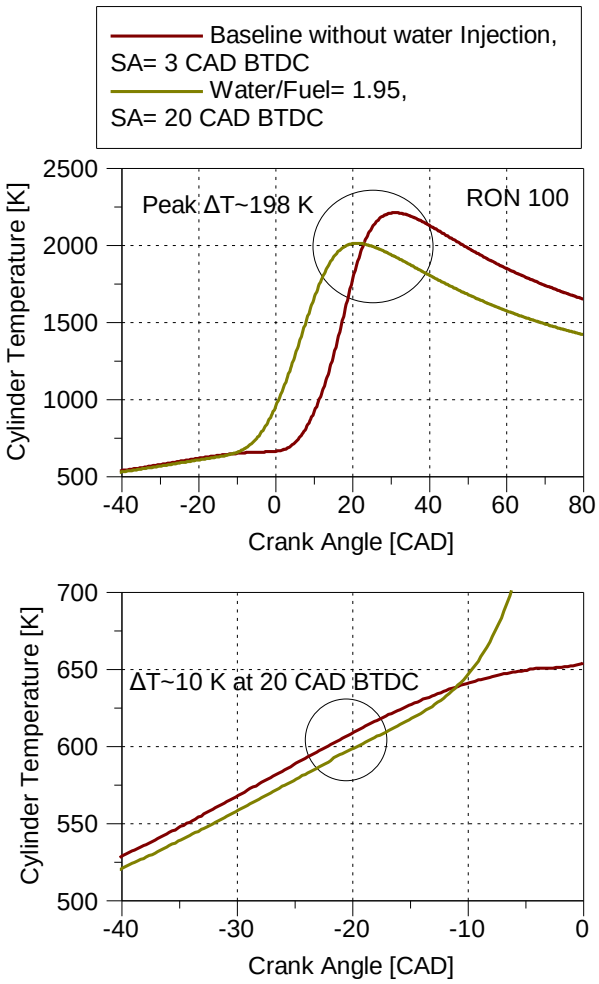

Figure 6-7 Effect of water injection on in-cylinder temperature at 1000 rpm / 8.83 bar NIMEP (RON 100)

Figure 6-8 shows the impact of water injection on combustion at 2000 rpm and 8.90 bar NIMEP. As the speed increased from 1000 rpm to 2000 rpm, the effect of water injection on combustion and efficiency also changed. At this speed and

load knock sensitivity was much less than the lower speed of 1000 rpm and therefore knock tendency was much lower compared to the previous test point. As a result, spark timing could be set to keep the CA50 around 8 CAD ATDC even without water injection. Adding water to the mixture at this test point decreased the indicated efficiency by around 3% when comparing the baseline to maximum water / fuel ratio.

At this point increasing the injected water mass led to a significantly slower combustion as the longer flame development angle and combustion duration show. Spark timing was advanced to maintain the CA50 of 8 CAD ATDC, but the dilution effect of water slowed the combustion significantly. In addition, the final part of the combustion (CA90) is delayed by around 5 CAD. As the water/fuel ratio increases, dilution effect of water increases and slows the flame propagation and flame speed due to the lower combustion temperature. Therefore, slightly higher intake pressure and consequently more fuel was required with the water injection in order to maintain the same load.

Exhaust temperature decreased by around 100°C as the water / fuel ratio increased. The main for this is the increased heat capacity of charge.

As can be seen in Figure 6-9, both maximum in-cylinder pressure (Pmax) and maximum pressure rise rate decreased as the injected water mass increased due to the dilution effect of water injection. Combustion stability also decreased by increasing the water / fuel ratio at this point due to the slower combustion as it was mentioned earlier. Furthermore, knocking intensity decreased as the injected water mass increased due to the slower combustion and reduced maximum in-cylinder pressure rise rate.

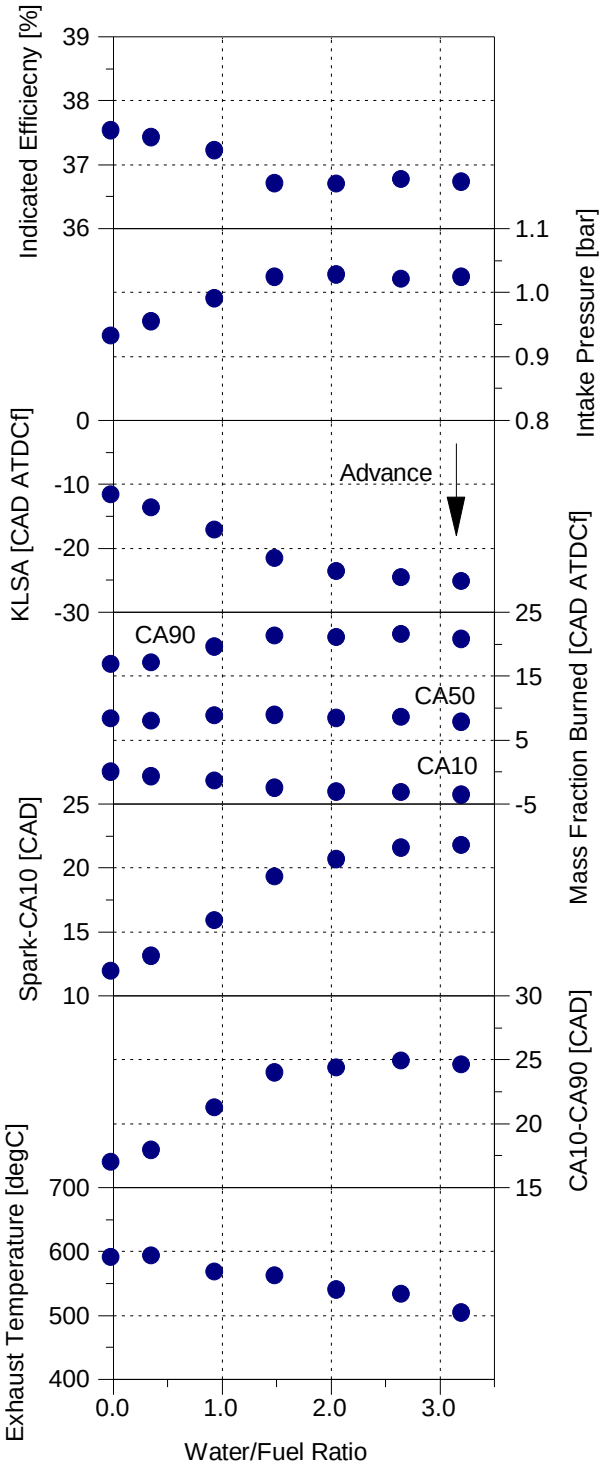

Figure 6-8 Impact of water / fuel ratio sweep on stoichiometric combustion and efficiency at 2000 rpm / 8.90 bar NIMEP (RON 100)

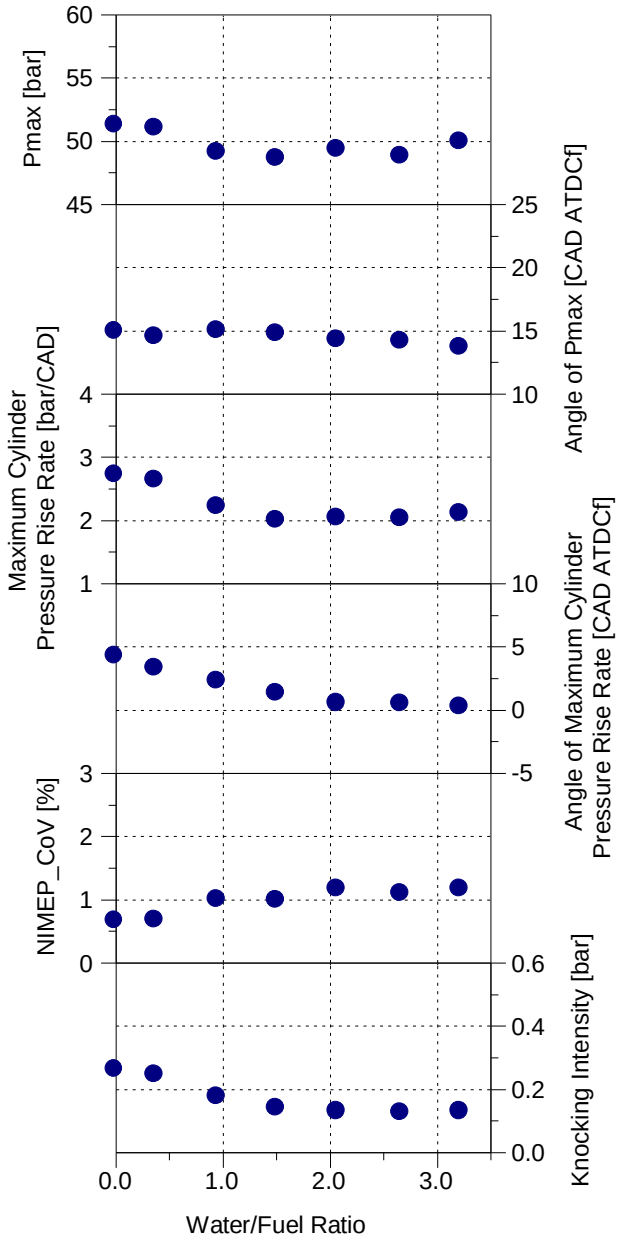

Figure 6-9 Impact of water / fuel ratio sweep on stoichiometric combustion at 2000 rpm / 8.90 bar NIMEP (RON 100)

6.3.2 Effects of water injection on engine performance at high-load condition

As the low speed and mid load results showed the high potential of water injection in knock mitigation, more experiments were conducted to study the effect of water injection on high load and different speeds under stoichiometric air / fuel ratio. The

same steps as the previous section were repeated for the high load conditions. First, a spark timing sweep was performed without water injection at each test point. Then a water / fuel ratio sweep, and simultaneous optimization of spark timing were performed. Water / fuel ratio was increased to a maximum until there was no apparent improvement in efficiency (or NISFC (net indicated specific fuel consumption)) or in some cases efficiency started to decrease. The maximum water / fuel ratio was around 3 at 3000 rpm / 16.04 bar NIMEP.

Figure 6-10 shows the impact of water injection on efficiency and combustion characteristics for four different speed and load combinations. As the injected water mass increased, the knock limited spark timing could be advanced, which led to a significant improvement of NISFC and ultimately indicated efficiency. Indicated efficiency increased to a maximum value as the water mass increased due to mitigation of knock and improvements in combustion phasing. This is highly beneficial specifically for modern highly downsized turbocharged GDI engines which run under increased intake pressures compared to naturally aspirated engines.

At low speed / high load in these engines water injection can suppress LSPI (low speed pre-ignition) or super knock. At high speed / high load conditions water injection can both prevent knock occurrence and eliminate the need for over-fuelling or enrichment which is used to protect the exhaust system from too high exhaust gas temperature (usually exhaust gas temperature is limited to around 950°C-980°C).

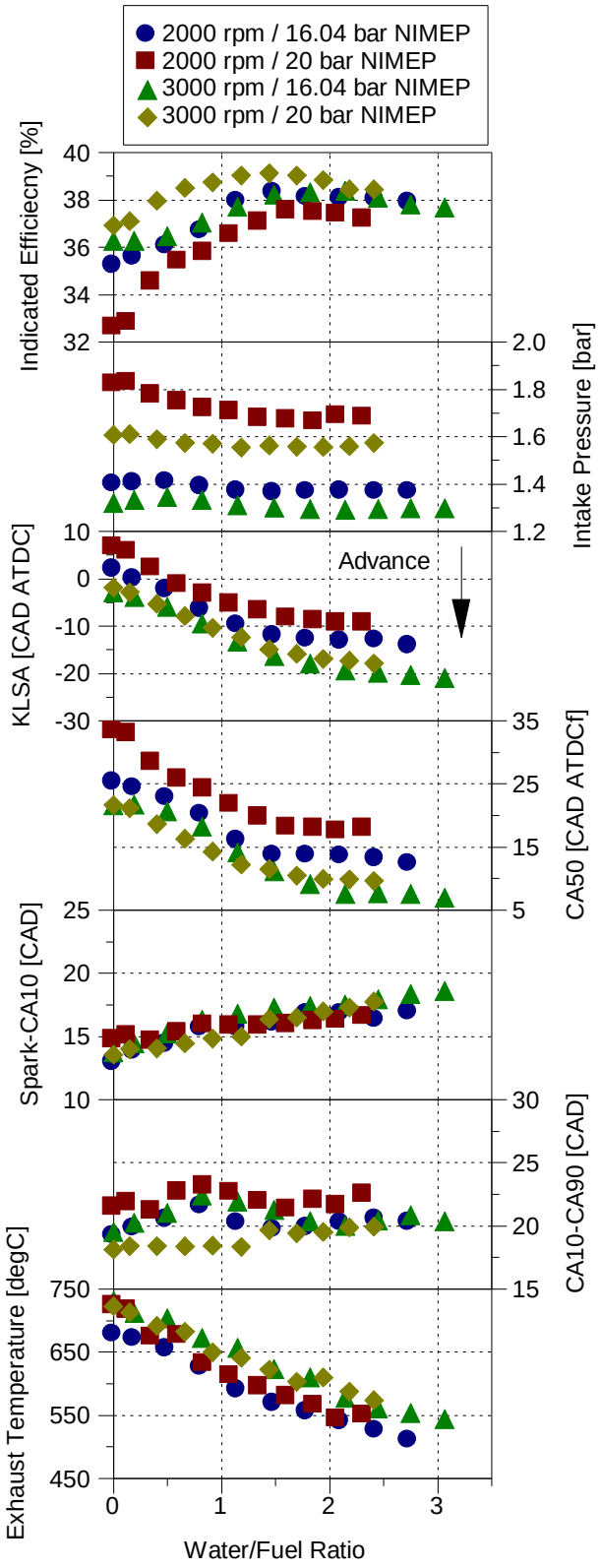

Figure 6-10 Impact of water / fuel ratio sweep on stoichiometric combustion and efficiency at high load (RON 100)

Hence, the stoichiometric operation area of the engine map can be extended, and fuel consumption can be reduced considerably. Addition of water effectively advanced the combustion phasing and reduced the exhaust temperature. Continuous increase in water mass increased the efficiency until a maximum value was reached (optimum efficiency). Increasing the injected water further beyond the optimum value led to a decrease in indicated efficiency. The possible factors that contribute to these results are mainly the changes in combustion phasing and duration (both spark-CA10 and CA10-CA90), combustion efficiency, and net integrated area of the P-V diagram which are all discussed in this section.

In all cases, the initial part of the combustion (spark to CA10) was prolonged by increasing the water / fuel ratio. As it was mentioned in the previous test point, the main reason for this is the dilution effect of water which makes it difficult to initiate and stabilize the flame kernel after spark discharge. Combustion duration also increases slightly by addition of a small mass of water at the beginning, then decreased slightly as the injected water mass was increased to optimum and ultimately started to increase again as the water mass kept increasing beyond the optimum point. For all these tests points spark timing was very close to TDC or mostly after TDC where the piston started to move down and expand. Therefore, the combustion initially occurred in lower ambient temperatures and pressures conditions as well as cylinder volume expansion. In addition, combustion phasing could be advance only slightly at the beginning by adding a small quantity of water. Thus, combustion duration increased slightly initially. However, increasing the water / fuel ratio further towards the optimum ratio to (around 1.5) decreased the combustion duration. This was due to the higher cooling effect as more water was injected and as a result combustion phasing could be advanced more. Hence, the

effect of advance combustion phasing was more pronounced this time as the combustion phasing was closer to TDC and combustion was exposed to a higher temperature and pressure environment near TDC. The highest indicated efficiencies were achieved when the water/fuel ratio was around 1.5.

Moreover, as the injected water was increased further to its maximum level (water / fuel ratio of around 3), combustion duration increased again, and efficiency dropped slightly due to the decreased reactivity of air-fuel mixture with higher dilution effect of water. Excessive amount of water could decrease the local flame temperature too much due to the increased heat capacity of charge and a high charge cooling effect prior to combustion which slows down the combustion. Combustion duration ultimately increased since the negative effect of charge dilution could not be compensated by the positive effect of spark timing and combustion phasing advancement.

Furthermore, exhaust temperature also decreased significantly by around 150 °C which, as it was explained in the previous section, was due to the more advanced combustion phasing and increased heat capacity of charge. Therefore, heat lost to the exhaust system is minimized. This can eliminate the need for fuel enrichment and extend the operation area under stoichiometric condition as well as reducing the unburned combustion products specifically CO which increases significantly under fuel-rich conditions.

Intake pressure also decreased by increasing the level of water due to the improved combustion phasing which led to improved efficiency. Consequently, lower air and fuel mass was required to maintain the load. This reduction in intake pressure is more pronounced at higher load and lower speed. For example, 2000

rpm / 20 bar NIMEP required the highest intake pressure since the combustion is more prone to knock at this high load and the spark timing is the least advanced among these four test points, as a result CA50 is the most retarded (around 33 CAD ATDC) for the baseline without water injection. Increasing the level of water to its optimum ratio significantly improved the CA50 by around 15 CAD compared to the baseline and reduced the need for high intake pressure. At higher engine speeds the reduction in intake pressure is lower due to the less sensitivity to knock at higher engine speeds.

CA50 was advanced between 12 and 16 CAD for these four cases when comparing the baseline without water injection to the optimum water/fuel ratio which gives the highest efficiency. This advancements in CA50 are more pronounced at high load and lower speed. For instance, when comparing the 2000 rpm / 20 bar NIMEP case to the 3000 rpm / 20 bar NIMEP case, CA50 was advanced around 16 CAD for the first case as opposed to 12 CAD for the latter. In addition, at 3000 rpm CA50 of around 10 CAD ATDC (which is very close to optimum of 8 CAD ATDC) is achieved with the same amount of water as 2000 rpm. As it was mentioned earlier this is due to less sensitivity to knock at higher engine speeds. It should be noted that, when the CA50 is too far from the optimum, like the 2000 rpm / 20 bar NIMEP case, the magnitude of improvements in indicated efficiency are higher as the spark is advanced compared to the other cases when the CA50 is closer to optimum. This is clear from the indicated efficiency graph which increases with a steeper gradient for both 2000 cases (especially 2000 rpm / 20bar NIMEP) compared to the 3000 rpm cases.

Figure 6-11 shows the impact of small and optimum quantity of water on in-cylinder pressure, heat release and MFB history at 2000 rpm / 20 bar NIMEP. As the

injected water mass increased to the optimum level, peak cylinder pressure increased considerably and shifted towards TDC due to the advancement of the combustion phasing. This shift towards TDC also can be seen in heat release and MFB curves.

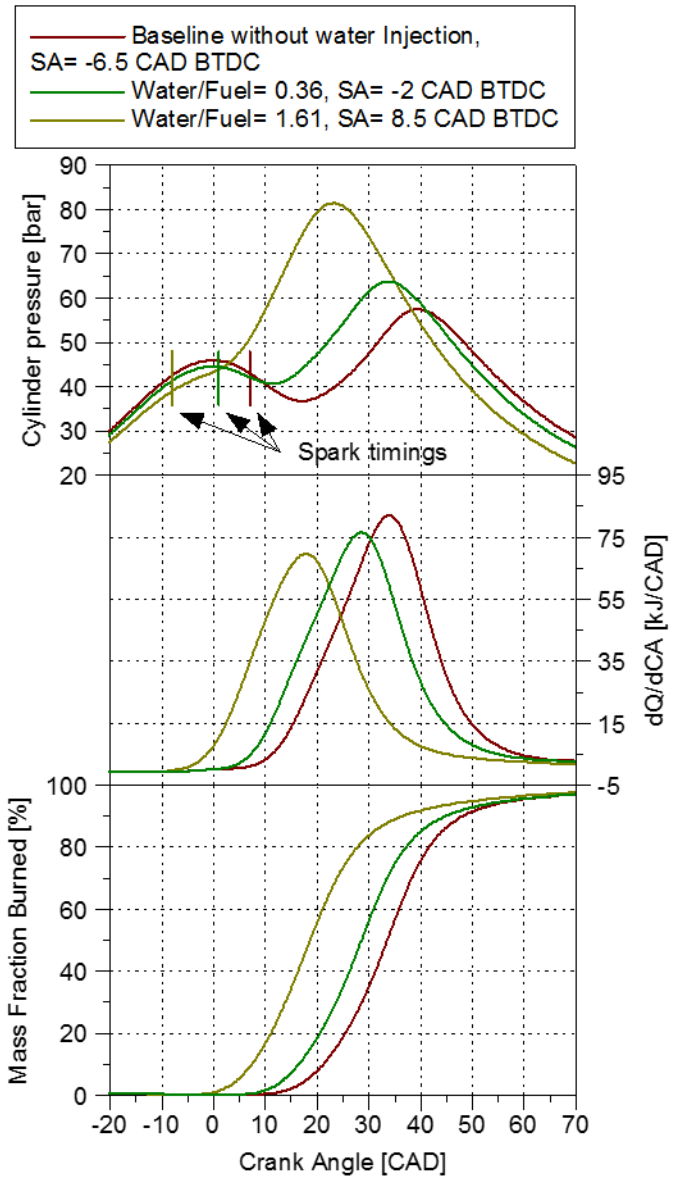

Figure 6-11 Effect of different water / fuel ratios and spark advance on in-cylinder pressure, heat release and MFB at 2000 rpm / 20 bar NIMEP (RON 100)

The difference between the in-cylinder temperature of the baseline and the optimum water injection case during the late compression and the early expansion strokes at 2000 rpm / 20 bar NIMEP is shown in Figure 6-12. In-cylinder temperature was calculated using the same method which was explained in the previous section.

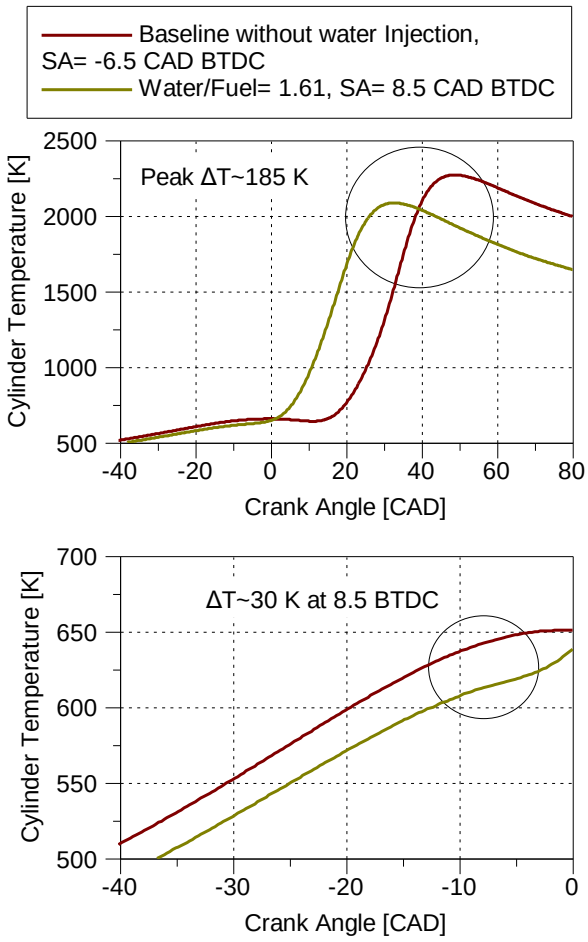

Figure 6-12 Effect of water injection on in-cylinder temperature at 2000 rpm / 20 bar NIMEP (RON 100)

Temperature started to rise earlier in the cycle after the spark discharge for the water injection case due to a more advanced spark timing and combustion phasing. Water injection decreased the charge temperature and pressure and allow the advancement of spark timing. Cylinder pressure was around 3.5 bar

lower and temperature around 30 K lower than the baseline. The injected water increased the heat capacity of the charge and absorbed more heat from the surroundings during compression stroke, therefore in-cylinder temperature was lower. Peak in-cylinder temperature was also significantly lower with water injection, which can be the main reason for lower NO_x emissions (Figure 6-18).

Log P-log V diagrams of the baseline and different water/fuel ratios at different speed and loads are plotted in Figure 6-13. As the injected water mass was increased to the optimum level, in-cylinder pressure during compression stroke decreased which can be seen on the log P-log V diagram and pressure curve in Figure 6-11. Lower cylinder pressure during compression resulted in lower compression work due to the charge cooling effect of water.

In addition, the polytropic coefficient (Figure 6-14), which is calculated from the in-cylinder pressure data between 90 and 30 CAD BTDC, only shows a slight decrease by increasing the injected water mass. Therefore, the slope of the compression line did not change a lot but the whole line just shifted down to a lower pressure.

Furthermore, cylinder pressure also decreased during the expansion stroke by increasing the injected water mass which resulted in lower expansion work and smaller net integrated area of the P-V diagram. Heat capacity of charge increased by increasing water mass which resulted in lower in-cylinder pressure rise rate after combustion.

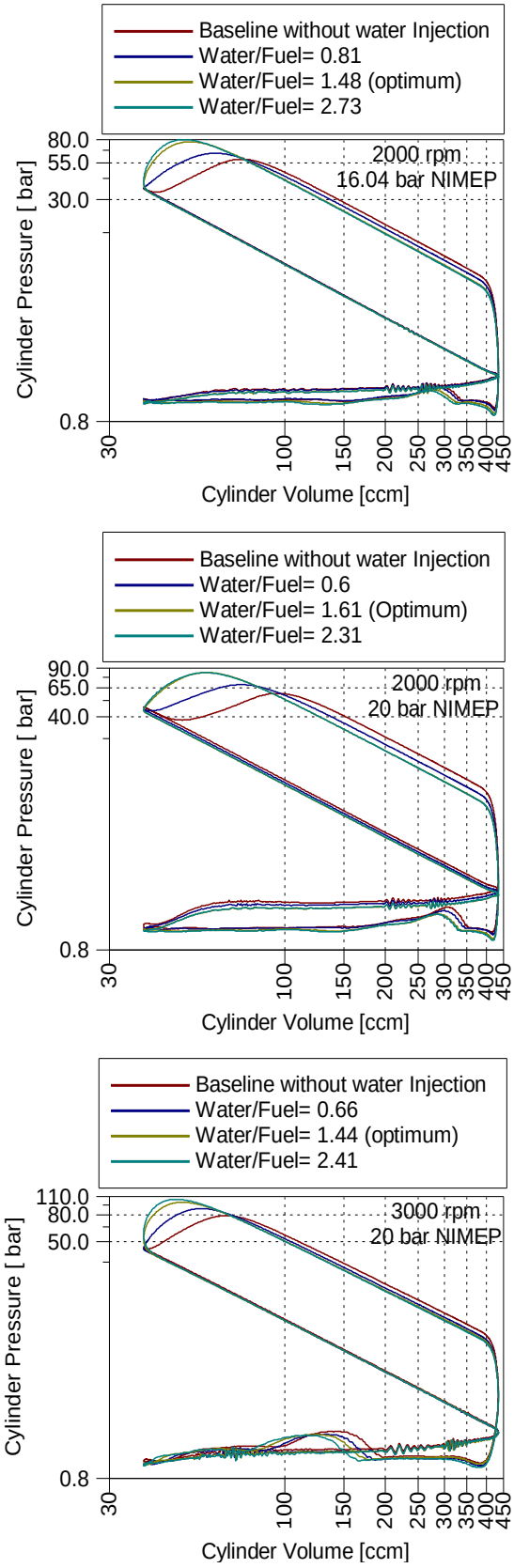

Figure 6-13 Log P - log V diagram of the baseline and different water/fuel ratios at various engine speed and loads (RON 100)

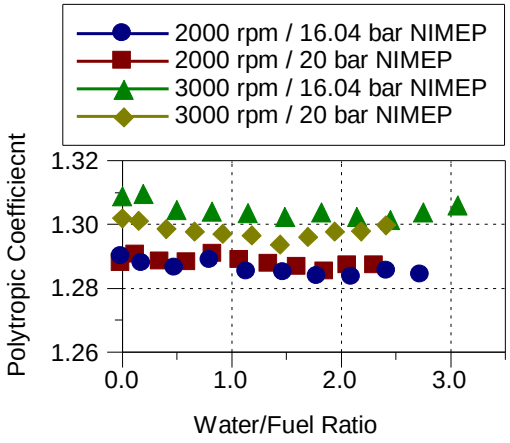

Figure 6-14 Effect of water injection on polytropic coefficient at different operating conditions (RON 100)

Figure 6-15 is extracted from Figure 6-4 and Figure 6-10 and summarizes the optimum water/fuel ratio for maximum efficiency and lowest fuel consumption at 1000 rpm / 8.83 bar NIMEP, 2000 rpm / 20 bar NIMEP and 3000 rpm / 20 bar NIMEP (RON 100). These are compared to the results without water injection and the efficiency improvements are around 4%, 15% and 6% at 1000, 2000 and 3000 respectively. Higher efficiency improvement at 2000 rpm / 20 bar NIMEP is due to a significantly retarded combustion phasing without water injection (CA50 of around 35 CAD ATDC) which was considerably improved by using water injection (CA50 was advanced to around 15 CAD ATDC). This improvement was lower at 1000 rpm / 8.83 bar NIMEP since the engine load was much lower and combustion phasing was closer to the optimum without water injection compared to the other two operating points. In addition, both exhaust gas temperature and NO_x emissions substantially decreased with water injection. Overall, higher improvements were achieved at higher loads where the combustion phasing was most retarded.

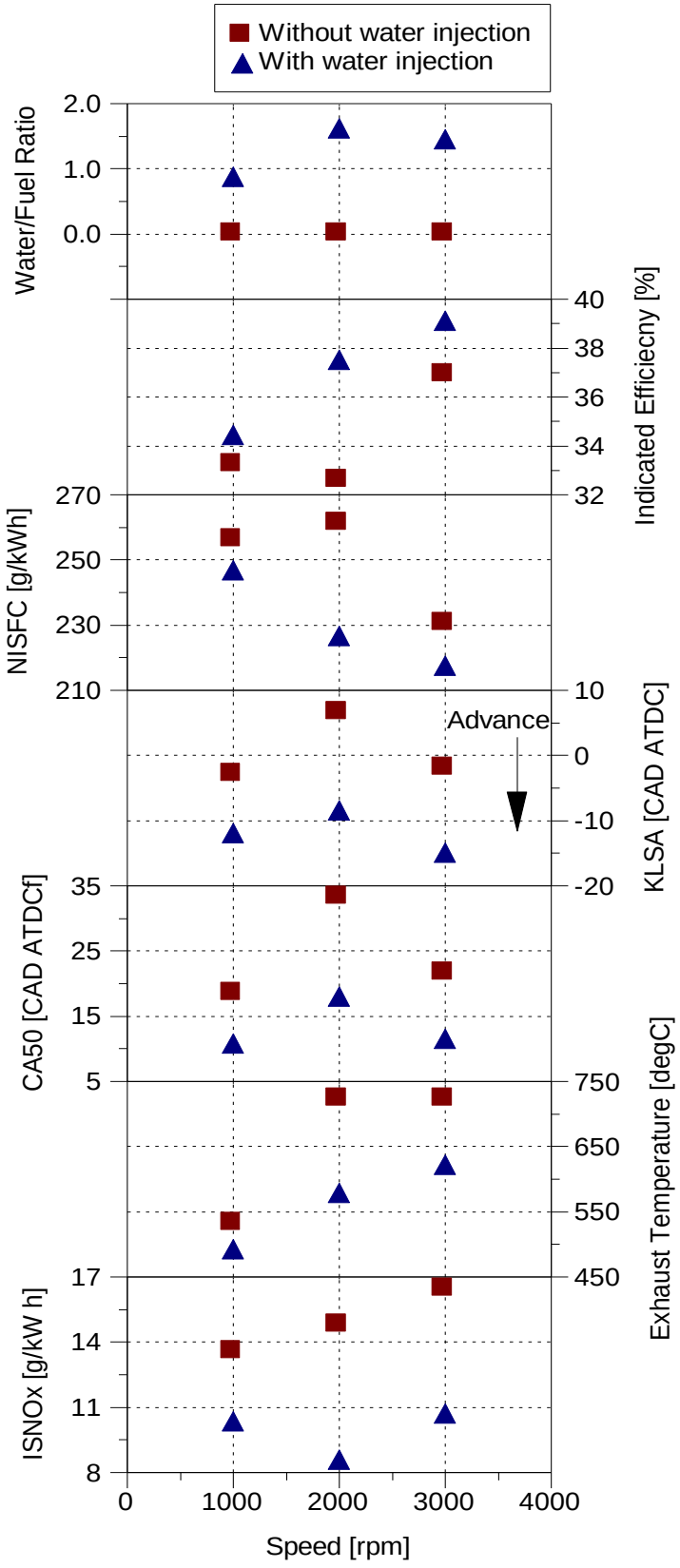

Figure 6-15 Engine performance with and without water injection at 1000 rpm / 8.83 bar NIMEP, 2000 rpm / 20 bar NIMEP and 3000 rpm / 20bar NIMEP

6.3.3 Effects of water injection on engine out gaseous emissions at medium and high-load conditions

Figure 6-16 shows the impact of water injection sweep on exhaust emissions and combustion efficiency at medium load of 8.83 bar NIMEP. As can be seen in this figure, NO_x emission decreased significantly by increasing the injected water mass. NO_x emissions dropped by approximately 50% when comparing the baseline without water injection to the maximum water/fuel ratio of around 2, despite advancing the spark timing and higher peak cylinder pressure. Although combustion phasing was advanced which should normally result in higher peak pressure and therefore higher NO_x emission, the cooling effect of water injection was dominant in this case which led to a lower peak combustion temperature and ultimately lower NO_x emissions especially at high water/fuel ratios. In addition, it could be argued that the injected water act as an inert gas and had a dilution effect on the mixture which increased the heat capacity of charge and reduced the in-cylinder temperature similar to cooled EGR effect which has also proven to be an effective method in NO_x reduction.

The primary effect of diluent in the mixture on the NO formation process is that it reduces the flame temperature by increasing the heat capacity of charge. This was discussed in Figure 6-7 where the average in-cylinder temperature is plotted against crank angle. In addition to high flame temperature, NO_x formation is also affected by O_2 concentration as NO_x emissions peak at relative air/fuel ratio of around 1.1 (slightly lean of stoichiometric). It has been shown by an study by Hyundai Motor that water injection can reduce the O_2 concentration in the mixture significantly from around 21% to as low as 16% due to the dilution effect [137]. However, in this case reduced flame temperature is more likely to be the primary

reason for reduced NO_x emissions. Reduced peak heat release can also be another reason for lower NO_x emissions.

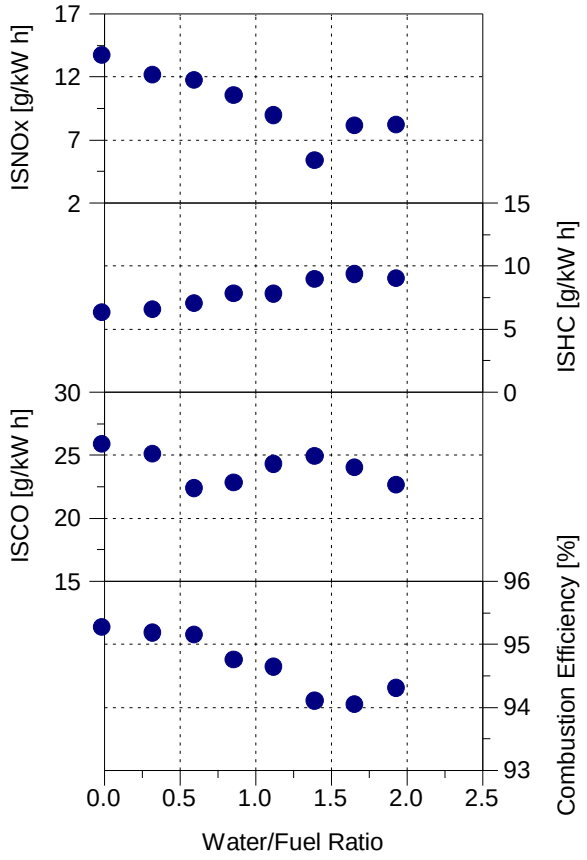

Figure 6-16 Impact of water / fuel ratio sweep on specific exhaust emissions and combustion efficiency at 1000 rpm / 8.83 bar NIMEP (RON 100)

Unburned hydrocarbon (UHC) emissions increased by increasing the water/fuel ratio mainly due to the dilution effect of the water. It is known that the unburned hydrocarbons in DI gasoline engine could be produced from fuel rich region due to under-mixing or too lean mixture by over-mixing (flame quenching), the fuel trapped in the crevices and liquid fuel impingement in cylinder wall. The exhaust UHC emission is also affected by the post-flame oxidation. When a large amount of water is injected in the intake port, only part of it evaporates in the intake port

before entering the cylinder and the other part could be in the liquid phase. This water enters the cylinder in the liquid phase and significantly decreases the local temperature where the evaporation takes place. This can promote flame quenching which is a source of increased HC emissions. Furthermore, the lower in-cylinder temperature associated with the cooling and dilution effect of water lowers the wall temperature and reduces post-flame oxidation effect during the expansion and exhaust strokes more than that of the baseline without water.

CO emissions decreased slightly by addition of water at the beginning then increased slightly again. This also can be due to the dilution effect of water which had a positive effect at the beginning but as the injected water mass increased, the local temperature decreased significantly and deteriorated combustion. Ultimately, combustion efficiency decreased mainly due to increased HC emissions.

At 2000 rpm / 8.90 bar NIMEP gaseous emissions show a similar trend to the 1000 rpm / 8.83 bar NIMEP test point. As can be seen in Figure 6-17, specific NO_x emissions decreased significantly as the water/fuel ratio increased. The main reason for this reduction was the reduced flame temperature and lower peak combustion temperature with water injection compared to the baseline as it was shown in Figure 6-7 and Figure 6-12. HC emissions increased by around 5 g/kWh mainly due to the lower combustion temperature and therefore lower wall temperature which can promote flame quenching and less HC burn-up during expansion and exhaust. In addition, slow combustion and slow burning cycles (Figure 6-8) could increase the HC emissions further as the water /fuel ratio increased at this load and speed. Decrease in CO emissions is also attributable to

the dilution effect of water injection. Increased HC emission ultimately led to a decrease in combustion efficiency as the injected water mass increased.

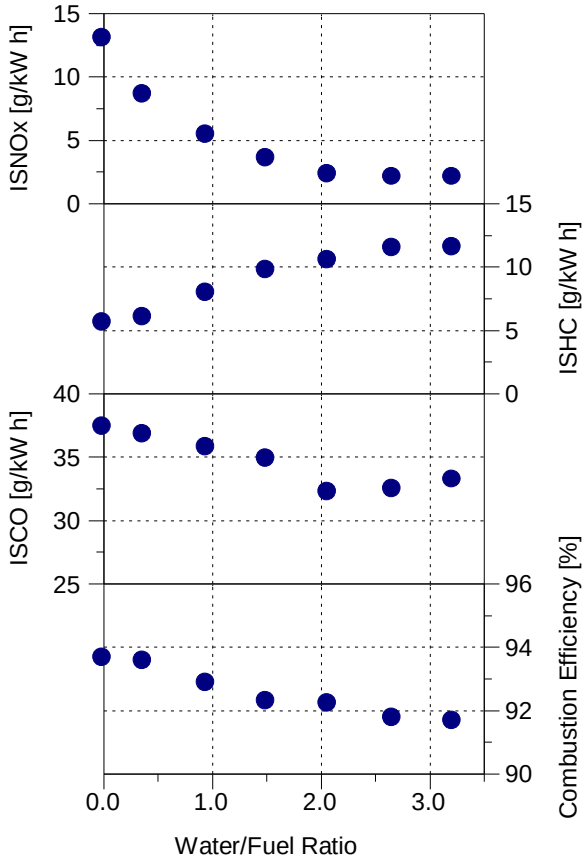

Figure 6-17 Impact of water / fuel ratio sweep on specific exhaust emissions and combustion efficiency at 2000 rpm / 8.90 bar NIMEP (RON 100)

Although with water injection there was a decrease of around 2.5% in indicated efficiency at 2000 rpm / 8.90 bar NIMEP test point, significantly lower NO_x emissions (around 80% lower) were emitted when the water/fuel ratio is around 3 compared to the baseline without water injection.

Figure 6-18 shows the impact of the injected water mass on NO_x, HC and CO emissions as well as the combustion efficiency at high load conditions. As can be

seen, the unburned HC emissions increased as the injected water mass increased, mainly due to the dilution effect of water as it was explained for the medium load condition. Dilution and cooling effect of water reduced the in-cylinder temperature and promoted flame quenching. Reduced in-cylinder temperature also reduced the post-flame oxidation.

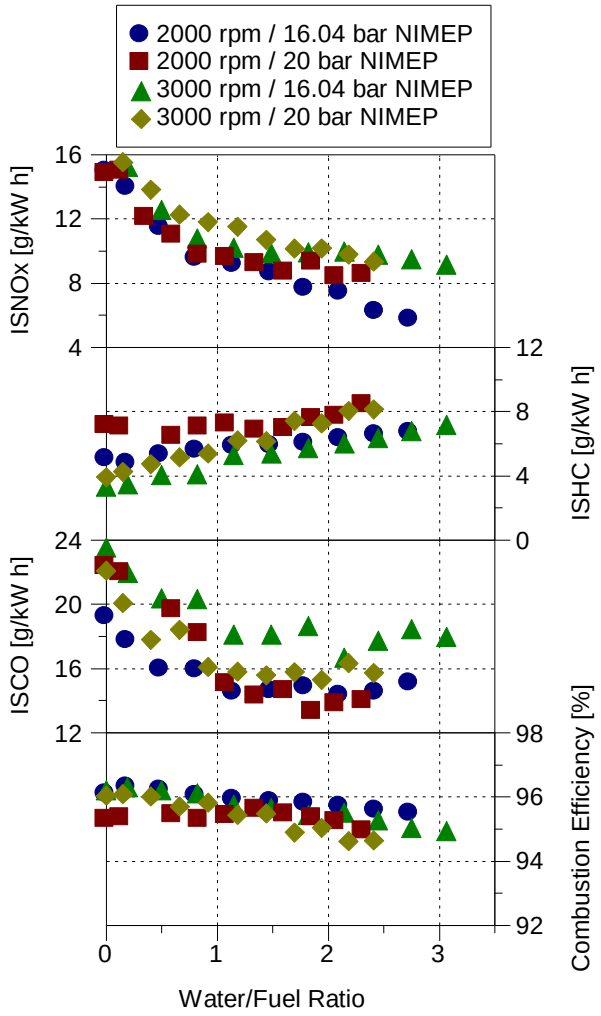

Figure 6-18 Impact of water/fuel ratio sweep on specific exhaust emissions and combustion efficiency at high load (RON 100)

NOx emissions decreased significantly by around 60% mainly due to a lower peak in-cylinder temperature (Figure 6-12) by water injection when comparing the maximum water/fuel ratio with baseline without water. The addition of water to the

mixture reduced the flame temperature by increasing the heat capacity of the charge which ultimately decreased the peak in-cylinder temperature and NO_x emissions.

CO emissions also decreased to a minimum level then stayed almost constant as the injected water quantity increased. This decrease in CO emissions could be due to the dilution effect of water which resolves the relatively fuel-rich areas (such as the area near the injector tip and spark plug which has a lower local lambda) in the cylinder. Water injection can reduce the CO emissions significantly when air/fuel ratio is rich of stoichiometric. Main reason for high CO under rich combustion is the lack of O_2 which prevents complete oxidation of CO to CO_2.

Furthermore, there was a slight increase in combustion efficiency when adding a small quantity of water at the beginning (water/fuel ratio around 0.2) due to lower CO emissions. However, Combustion efficiency decreased again soon after increasing the injected water mass due to increased HC emissions. As it was mentioned earlier, reduction in combustion efficiency at maximum water/fuel ratios is one of the contributors to decreased indicated efficiency compared to the optimum water quantity.

6.3.4 Effects of water injection on engine out particulate emissions at medium and high-load conditions

In this section, the results related to the particulate size spectral density are presented and discussed. The tests were performed with a Cambustion DMS 500 fast response particulate analyzer.

Figure 6-19 shows the particulate number against the particulate size at 1000 rpm / 8.83 bar NIMEP for the baseline without water injection in comparison with water

injection with different water / fuel ratios. As can be seen in this figure, by only advancing the spark timing for the baseline without water injection, number of particles which have a diameter of around 20 nm dropped significantly from around 1.77E+07 to around 9.99 E+06. Addition of water and advancing the spark timing at the same time decreased the number of particles even further across the diameter spectrum. The particle number (PN) continued to drop until the minimum number of particles were emitted when the water / fuel ratio was around 1.14. Increasing the water / fuel ratio further to around 2, caused an increase in particle numbers again.

Figure 6-20, shows the PN at 2000 rpm / 16.04 bar NIMEP. Similar results are achieved at this test point as well. Advancing the spark timing and adding water to the mixture decreased the PN significantly until a minimum value. Increasing the water/fuel ratio further increased the PN again.

It is known that soot is produced under high temperature conditions and in fuel-rich areas in combustion chamber when hydrocarbon fuels are burned. Over-rich regions near the piston top or cylinder walls due to wall wetting by the fuel spray contribute to unburned fuel and soot formation. In addition, the presence of liquid fuel is another source of soot particles and subsequent particulate emissions [2,177]. Furthermore, a large number of chemical processes are involved in the formation of particulates.

One reason for this decrease in PN could be the advancement in spark timing with water injection and therefore lower amount of injected fuel in the cylinder. Moreover, during water injection combustion took place at lower temperature (as it was shown earlier in Figure 6-7 and Figure 6-12) which could be the main reason

for lower particle emissions. The injected water into the intake port (which can be vapor or liquid before combustion) enters the cylinder and there is a possibility that this water decomposes into hydrogen and oxygen at high temperature during combustion. Increased oxygen and OH radicals then helped to oxidize more fuel [177].

Another reason for the reduction in PN could be the dilution effect of water injection which resolved the over-rich regions in the combustion chamber.

Furthermore, there is a hypothesis that higher water / fuel ratios increase the fuel inhomogeneity at the start of combustion which is supported by increased unburned HC emissions which also increases as the water / fuel ratio is increased [196].

Figure 6-21, Figure 6-22 and Figure 6-23 also show the effect of water injection on PN size distribution at other operating points. These figures show a similar trend to Figure 6-19 and Figure 6-20 which demonstrate that PN decreased as water / fuel ratio increased. In order to fully understand the effect of water injection on particulate emissions, further investigation at various operating conditions is required.

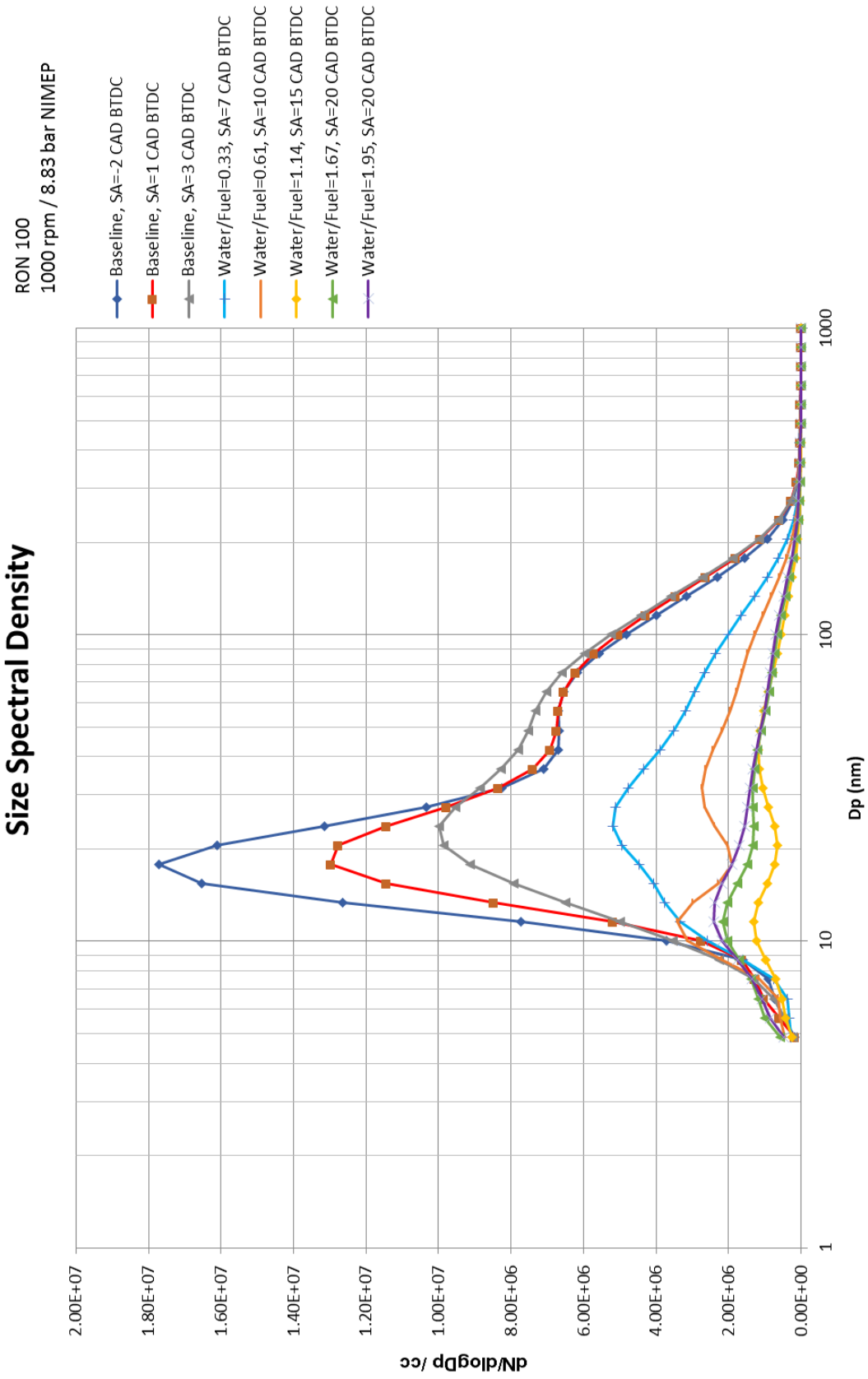

Figure 6-19 Impact of water injection on particles size and number at 1000 rpm / 8.83 bar NIMEP (RON 100)

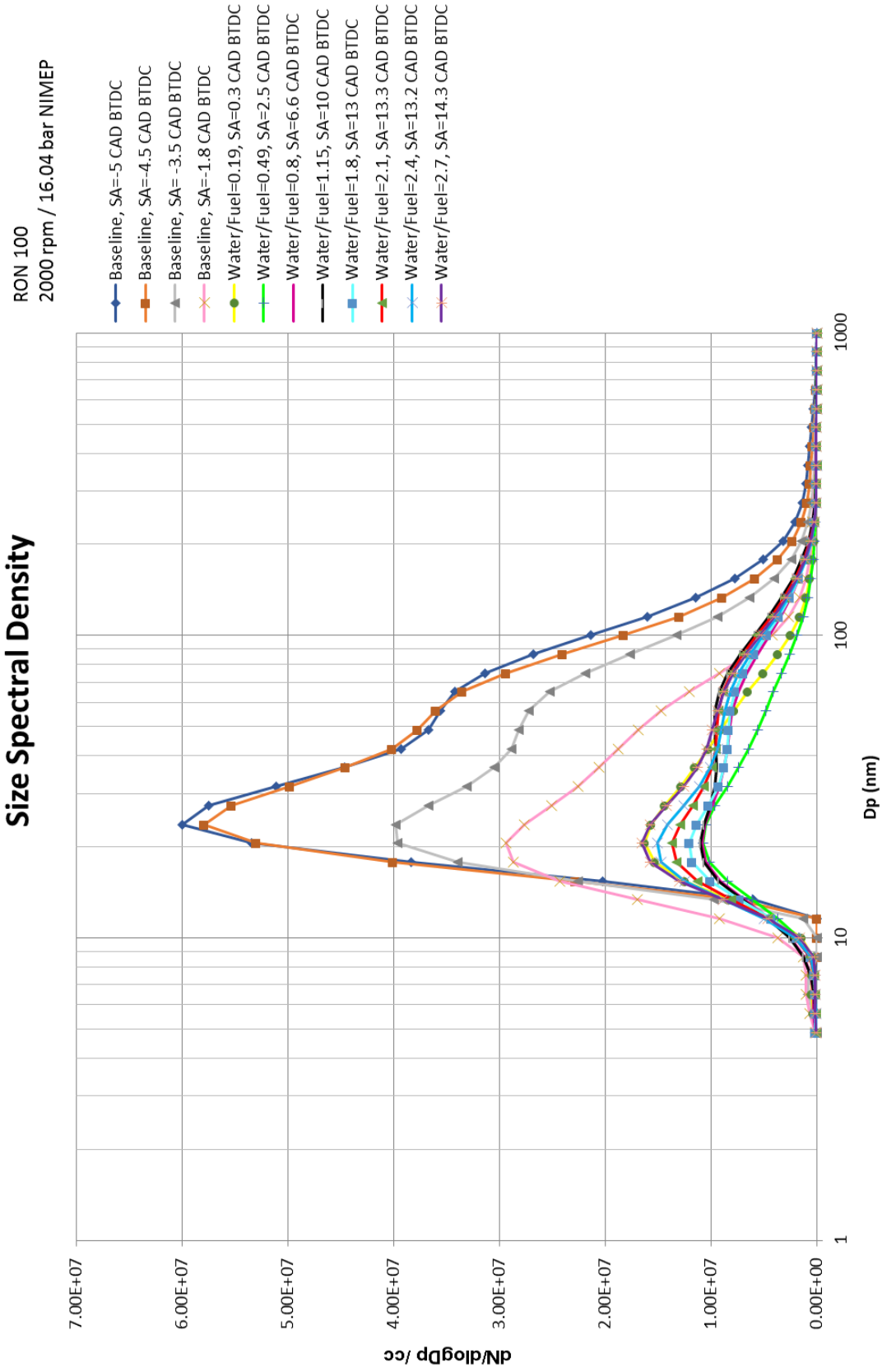

Figure 6-20 Impact of water injection on particles size and number at 2000 rpm / 16.04 bar NIMEP (RON 100)

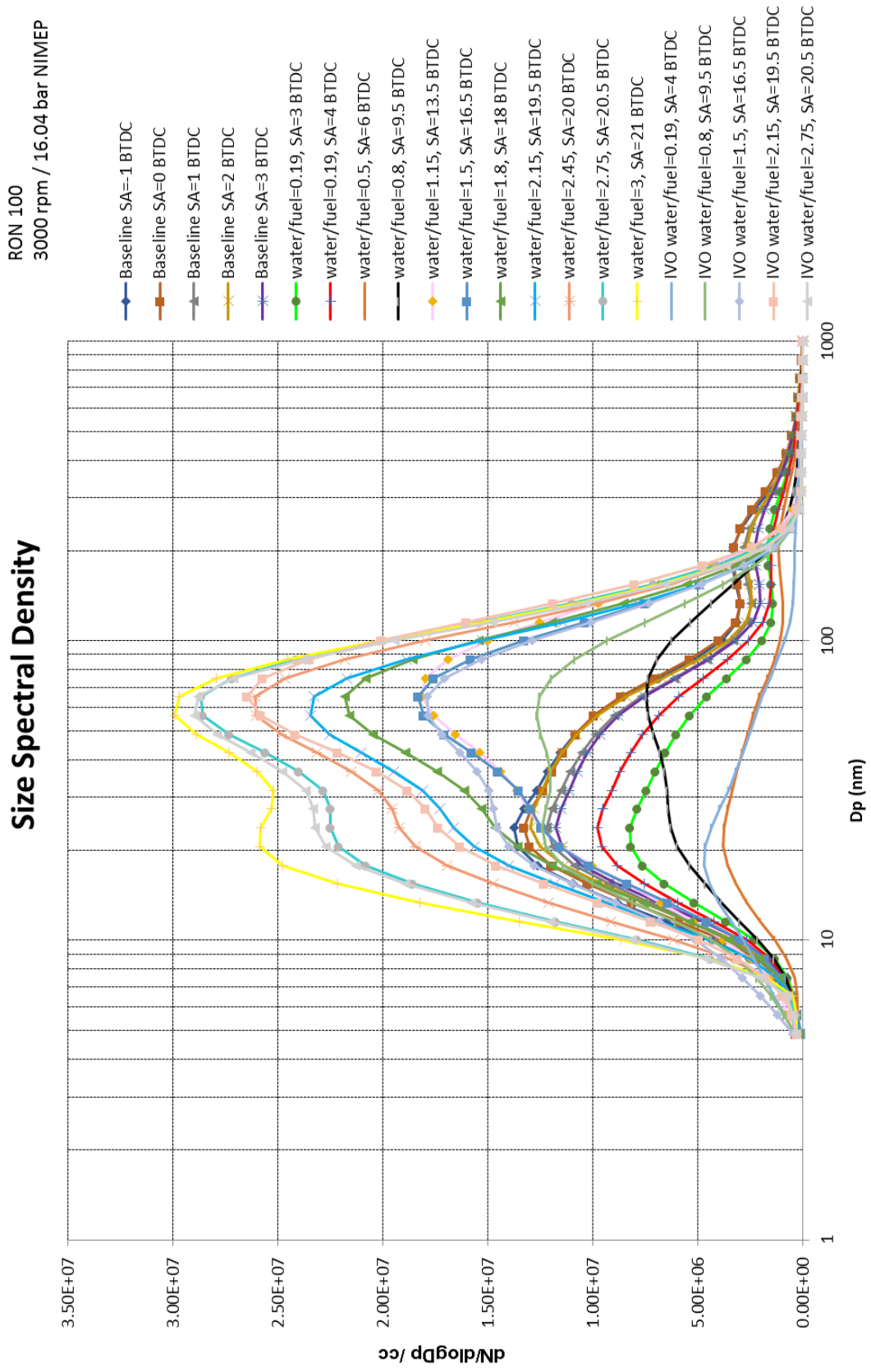

Figure 6-21 Impact of water injection on particles size and number at 3000 rpm / 16.04 bar NIMEP (RON 100)

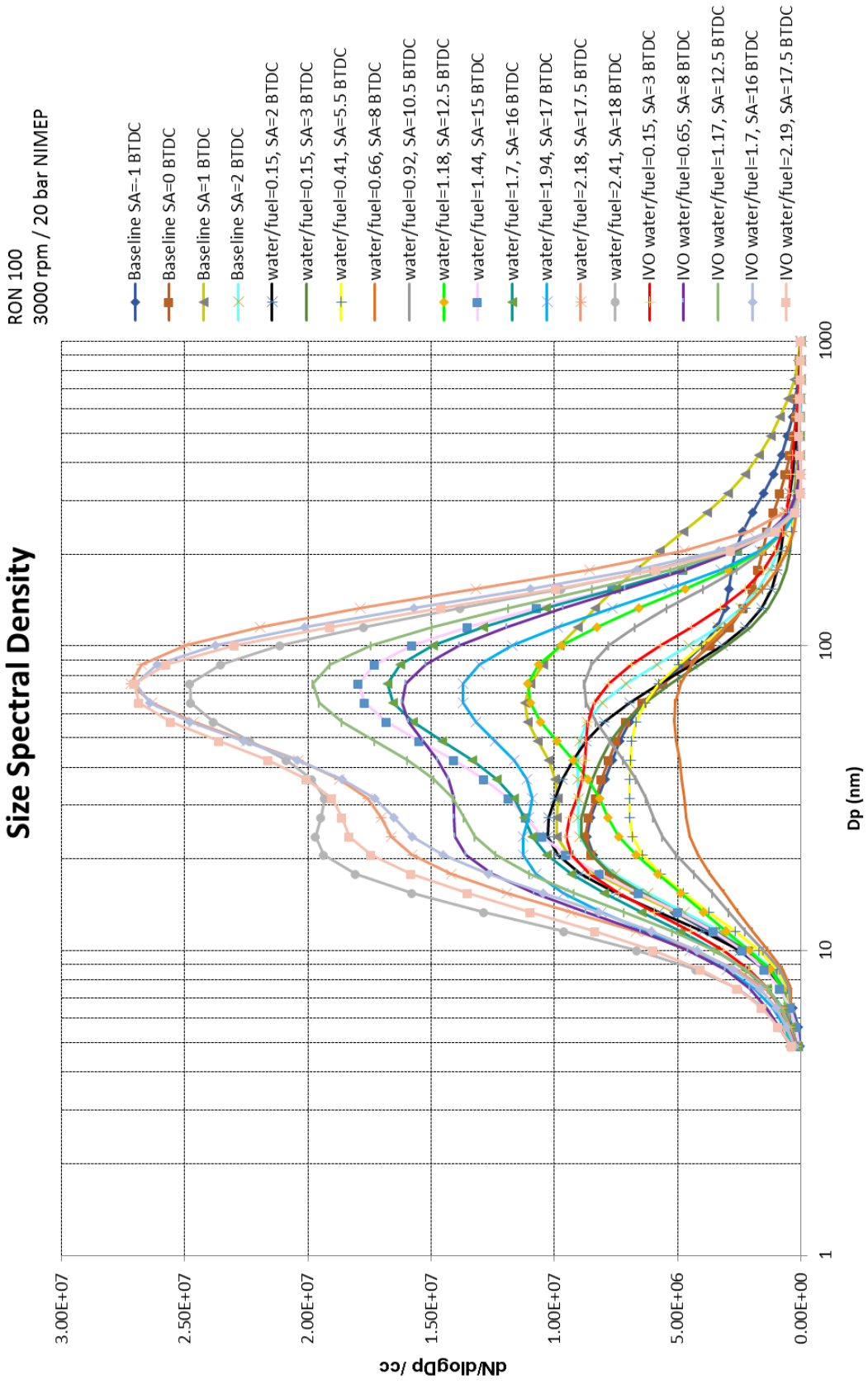

Figure 6-22 Impact of water injection on particles size and number at 3000 rpm / 20 bar NIMEP (RON 100)

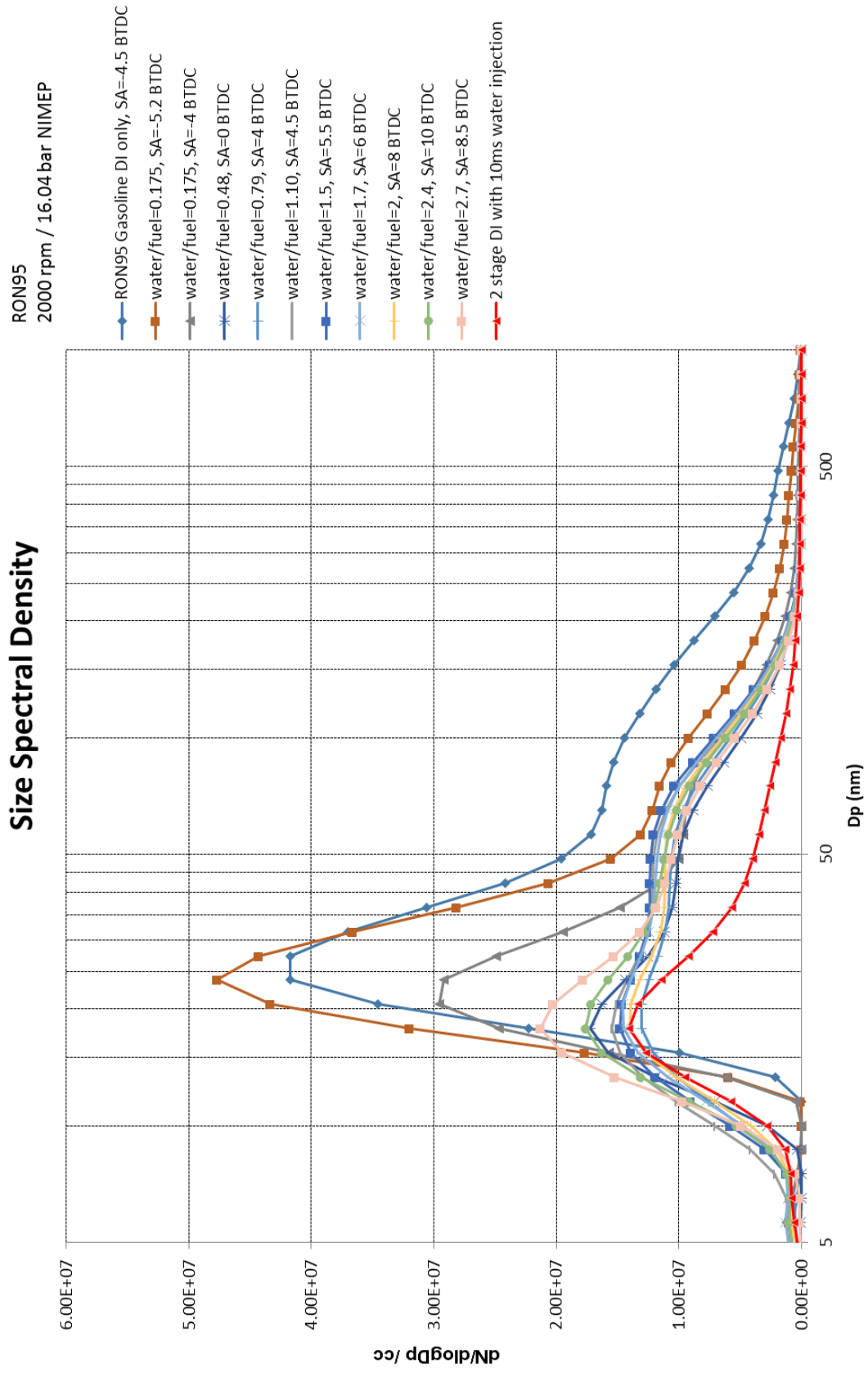

Figure 6-23 Impact of water injection on particles size and number at 2000 rpm / 16.04 bar NIMEP (RON 95)

6.3.5 Effect of water injection into opened intake valves on combustion and efficiency at mid load

This section shows and describes the results for water injection into the intake manifold when the intake valves are opened at medium load.

At 1000 rpm / 8.83 bar NIMEP the water injection timing was set at 360 CAD BTDCf which is exactly at the time which intake valves start to open. Spark timings for the opened intake valves injection were set at the same timings as the closed intake valve injection (Figure 6-24). Generally, the trend from the results show no or little difference between the closed and opened intake valves injection at this medium load.

At the beginning by injecting a small quantity of water, opened intake valve injection exhibited a slightly higher indicated efficiency due to slightly faster combustion and slightly more advanced combustion phasing. However, as the water / fuel ratio was increased to its maximum, indicated efficiency decreased slightly due to slightly slower combustion and slightly delayed combustion phasing. At high water / fuel ratios a large quantity of water in liquid phase enters the cylinder when injecting into opened intake valves. Therefore, there is less time for evaporation and mixing with the intake air compared to closed intake valves injection which could be the reason for delayed and slower combustion, and slightly lower indicated efficiency.

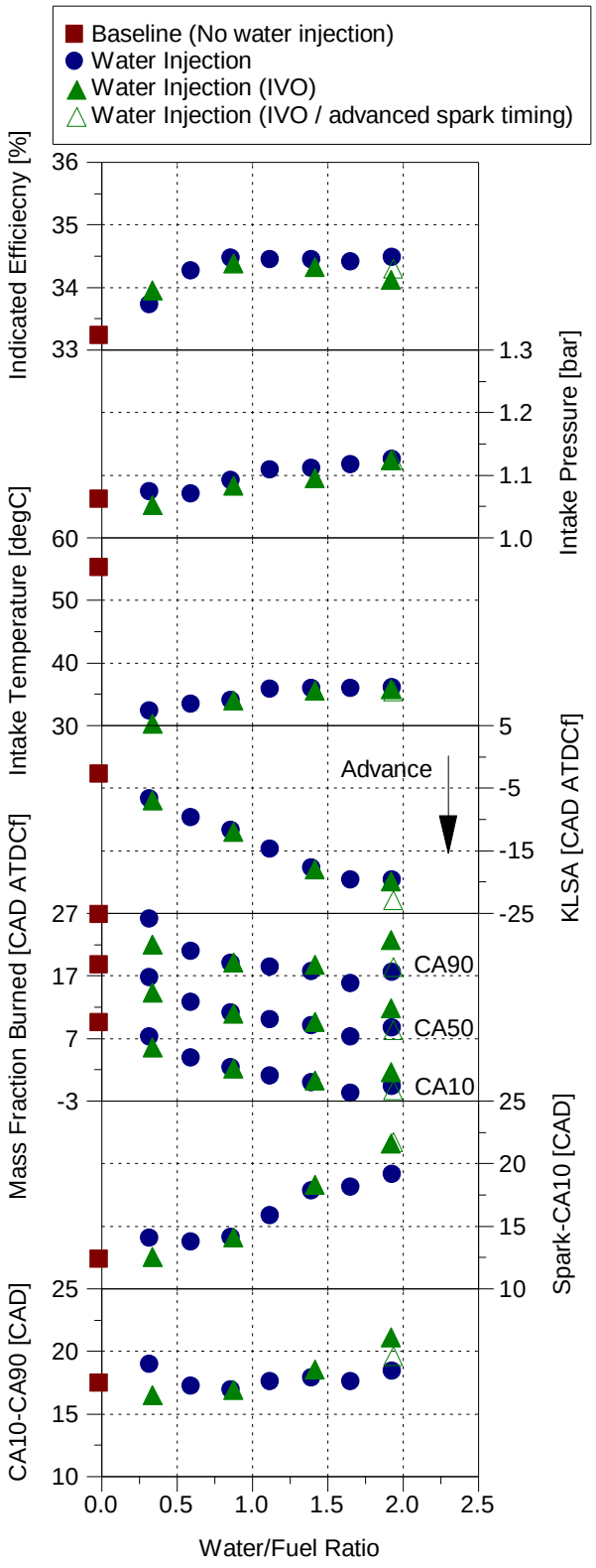

Figure 6-24 Impact of water injection into opened intake valves on stoichiometric combustion and efficiency at 1000 rpm / 8.83 bar NIMEP (RON 100)

Intake temperature drops significantly after switching to water injection partly due to the cooling effect of water injection and partly due to the location of intake port injector relative to the thermocouple located in the intake port for intake temperature measurements. Since the PFI injector is located right behind the thermocouple in an angle that water comes to contact with the thermocouple after water injection, the temperature recorded by the intake thermocouple is significantly lower with water injection compared to the baseline. As can be seen in Figure 6-24, intake temperature is slightly lower with the opened intake valves injection case compared to the close intake valves injection which could be due to the shorter presence time of the injected water in the intake port with the opened intake valves injection case.

Figure 6-25 shows some additional parameters related to the combustion which helps to better understand the difference between closed and opened intake valves injection at 1000 rpm / 8.83 bar NIMEP. As can be seen in this figure, exhaust temperature for the opened intake valves injection case was slightly lower than the closed intake valves case at low water / fuel ratios but increased slightly at the maximum water / fuel ratio. This is also due to the slight differences in combustion phasing between the two cases at it was shown in the previous figure (Figure 6-24).

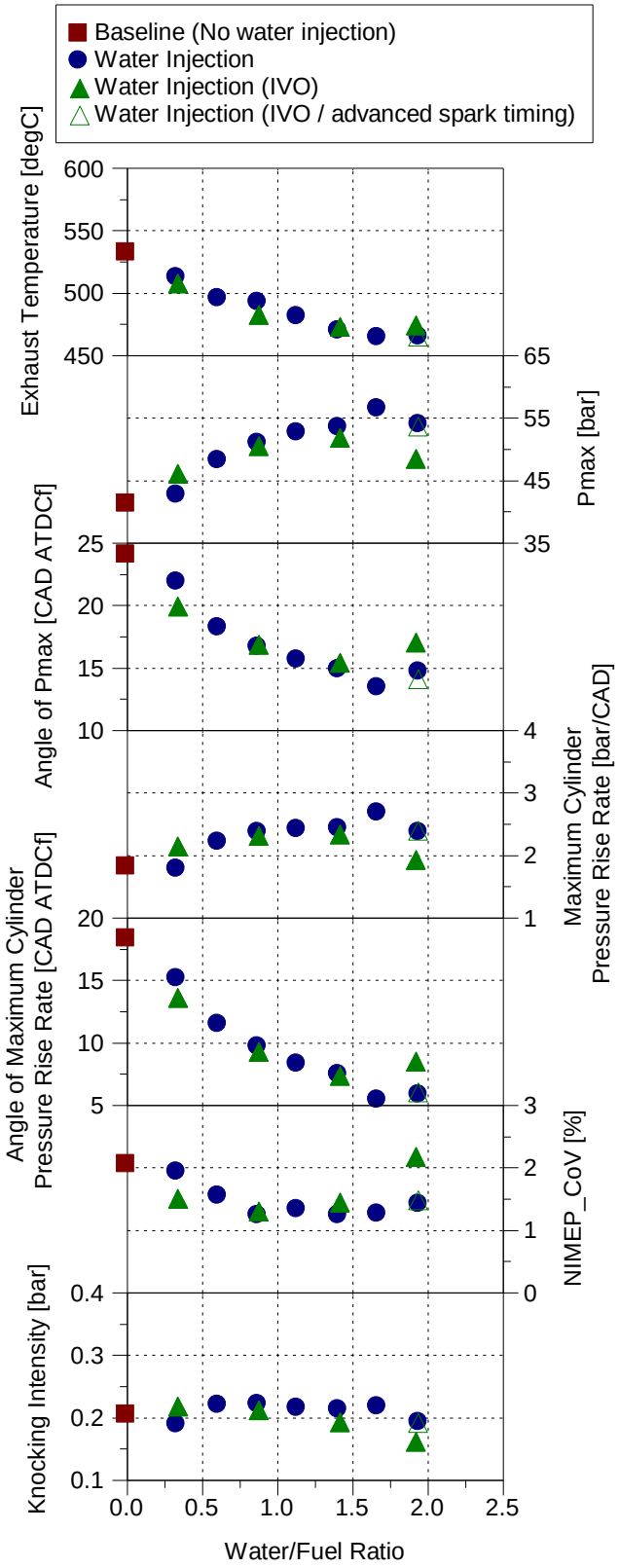

Figure 6-25 Impact of water injection into opened intake valves on stoichiometric combustion at 1000 rpm / 8.83 bar NIMEP (RON 100)

Maximum in-cylinder pressure and maximum cylinder pressure rise rate were both slightly higher for the opened intake valves injection compared to the closed intake valves case at low water/fuel ratios. This trend changed as the injected water mass increased to its maximum and opened intake valves case exhibited slightly lower peak in-cylinder pressure and peak in-cylinder pressure rise rate compared to the other case. This is also attributable to the changes in combustion phasing and duration which was discussed earlier in this section.

Figure 6-25 also shows the combustion stability in terms of CoV of NIMEP which by adding small quantities of water started to improve for both cases until around water/fuel ratio of 1.5. Increasing the injected water mass further caused and slight increase in NIMEP_CoV for both cases. Opened intake valves injection showed slightly higher combustion stability at the beginning by adding small quantity of water compared to the closed intake valves case due to slightly faster combustion and slightly more advanced combustion phasing. On the other hand, closed intake valves injection showed slightly higher combustion stability at the maximum water / fuel ratio also because of the faster and more advanced combustion. At high water / fuel ratios there is more time available for the injected water to evaporate with the closed intake valves injection case. This leads to a better mixing and avoids large quantities of liquid water entering the cylinder and prevents impingement of liquid water on piston crown and cylinder wall which could promote flame quenching and ultimately deteriorating combustion efficiency.

Furthermore, as it is shown in Figure 6-24 and Figure 6-25, when the water / fuel ratio is around 1.9, the spark timing could be advanced more (by 3 CAD) with opened intake valves injection case (transparent triangle in the figures) due to the lower combustion temperature. However, even with the more advanced spark

timing the efficiency was still slightly lower compared to the closed intake valves injection case. In addition, Figure 6-26 compares the gaseous emissions of the closed and opened intake valves injection case. The results show an almost identical trends for both cases with minor difference.

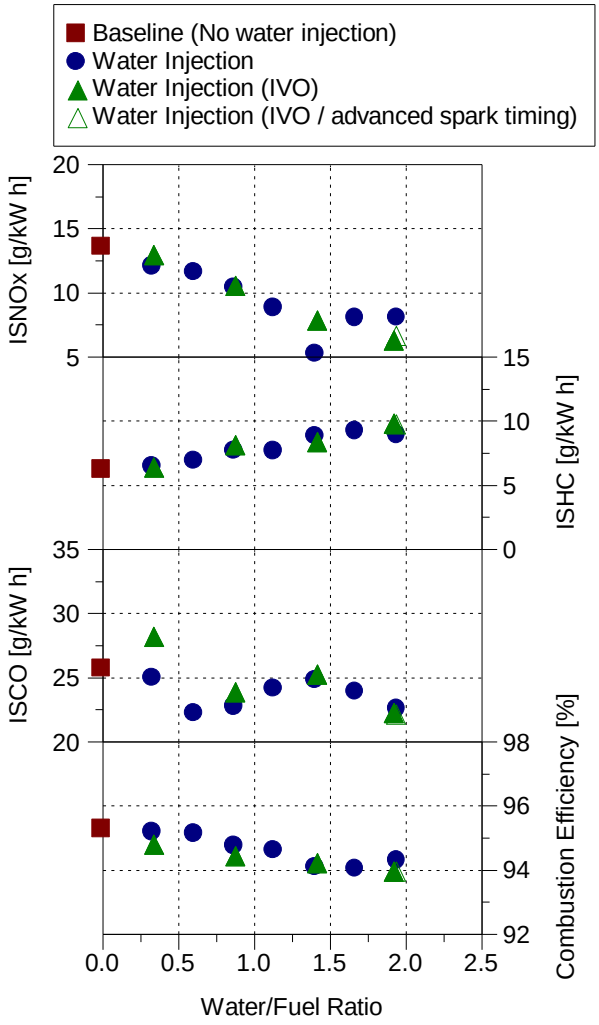

Figure 6-26 Impact of water injection into opened intake valves on specific exhaust emissions and combustion efficiency at 1000 rpm / 8.83 bar NIMEP (RON 100)

Similarly, Figure 6-27, Figure 6-28 and Figure 6-29 show the effect of intake port water injection sweep (water injection into closed and opened intake valves) on combustion characteristics and emissions.

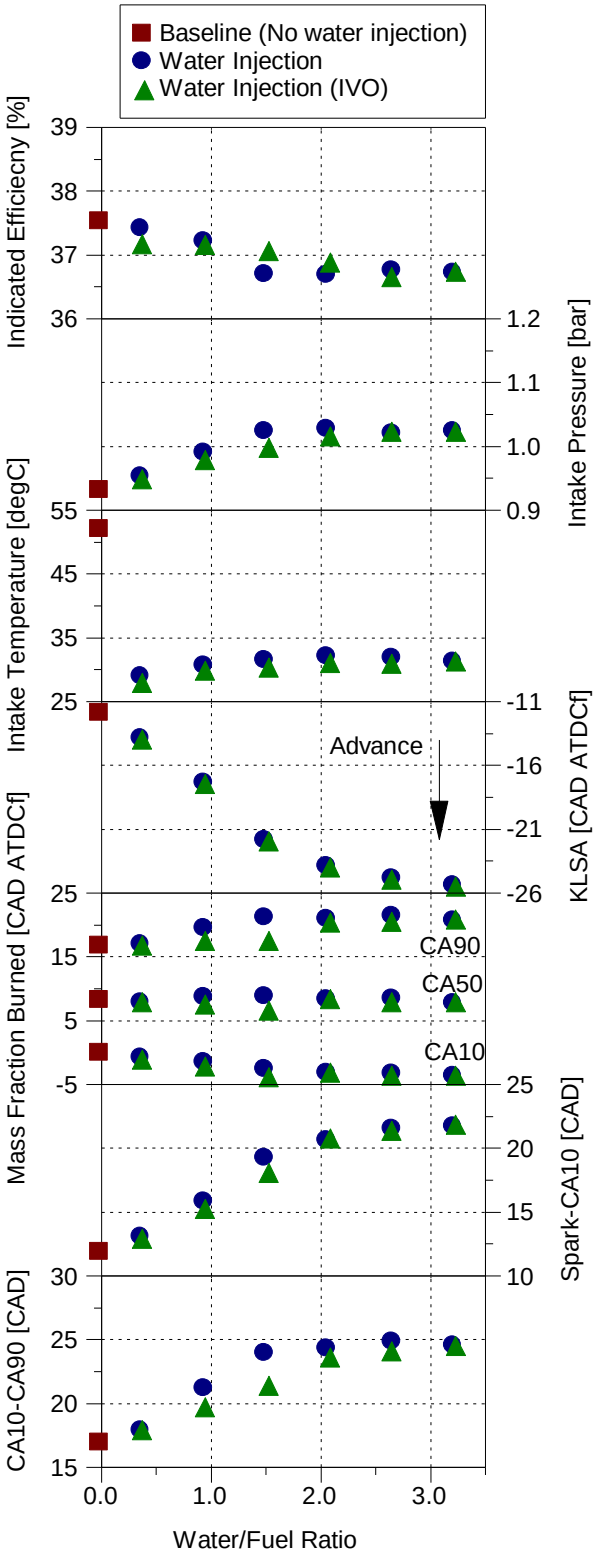

Figure 6-27 Impact of water injection into opened intake valves on stoichiometric combustion and efficiency at 2000 rpm / 8.90 bar NIMEP (RON 100)

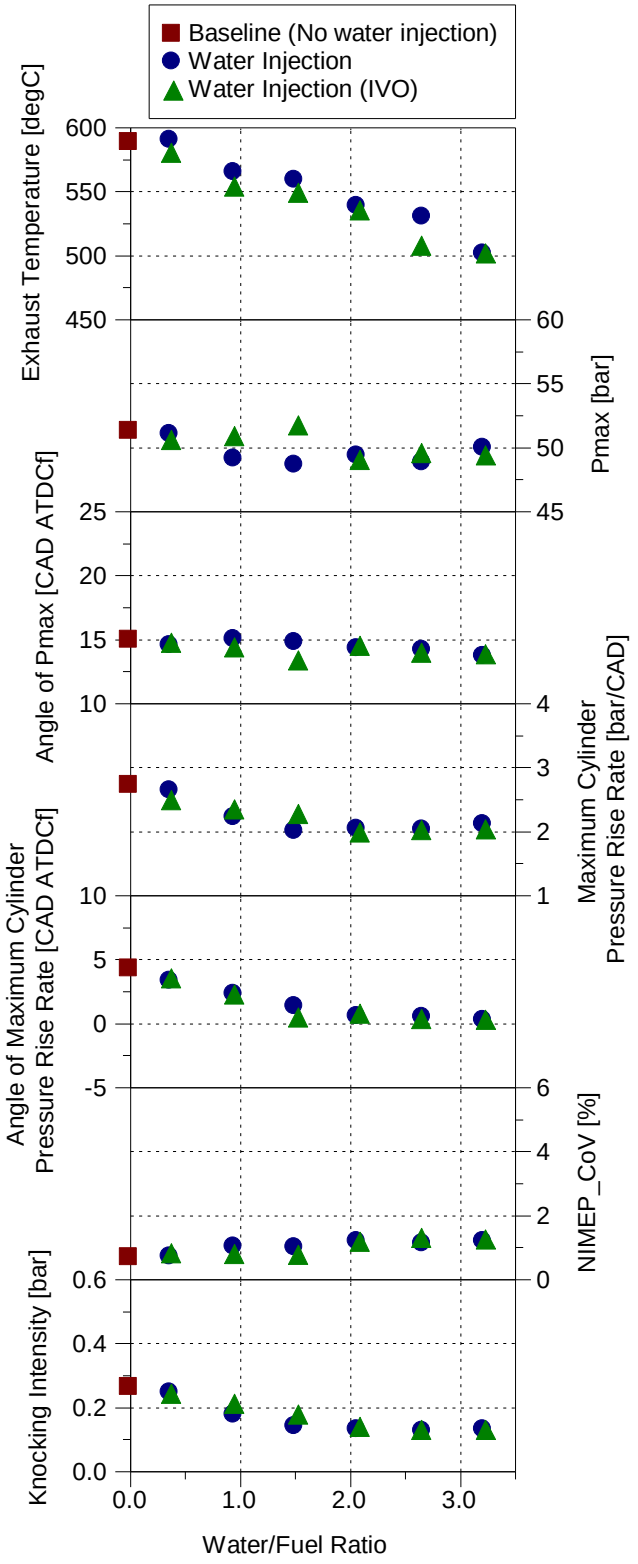

Figure 6-28 Impact of water injection into opened intake valves on stoichiometric combustion at 2000 rpm / 8.90 bar NIMEP (RON 100)

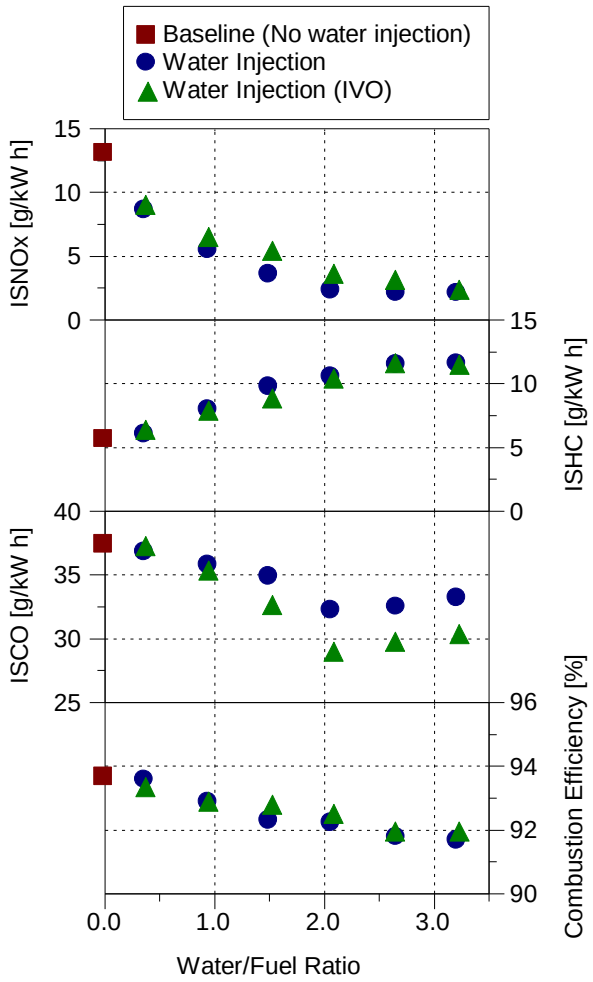

Figure 6-29 Impact of water injection into opened intake valves on specific exhaust emissions and combustion efficiency at 2000 rpm / 8.90 bar NIMEP (RON 100)

6.3.6 Effect of water injection into opened intake valves on combustion and efficiency at high load

This section shows and describes the results for water injection into the intake manifold when the intake valves are opened at high load. At 2000 rpm / 16.04 bar NIMEP the water injection timing was set at 370 CAD BTDCf which is exactly at the time which intake valves start to open. Spark timings for the opened intake valves injection were set at the same timings as the closed intake valve injection

(Figure 6-30, Figure 6-31 and Figure 6-32). Basically, the trend from the results show no or little difference between the closed and opened intake valves injection at this test point.

Indicated efficiency graph (Figure 6-30) shows the same results for both closed and opened intake valves injection cases. Intake temperature was slightly lower with the opened intake valves injection at the beginning when injecting small quantities of water. This could be due to the shorter residence time of the water in the intake port with the opened intake valves injection case and therefore slightly higher cooling effect and lower intake temperature. Combustion timings of both cases are also very similar at this test point.

Figure 6-32 compares the exhaust temperature, gaseous emissions and the combustion efficiency of both cases. The results show no or slight difference in terms of emissions when comparing the two cases. The slightly lower NO_x emissions with the opened intake valves injection could be due to slightly lower peak combustion temperature.

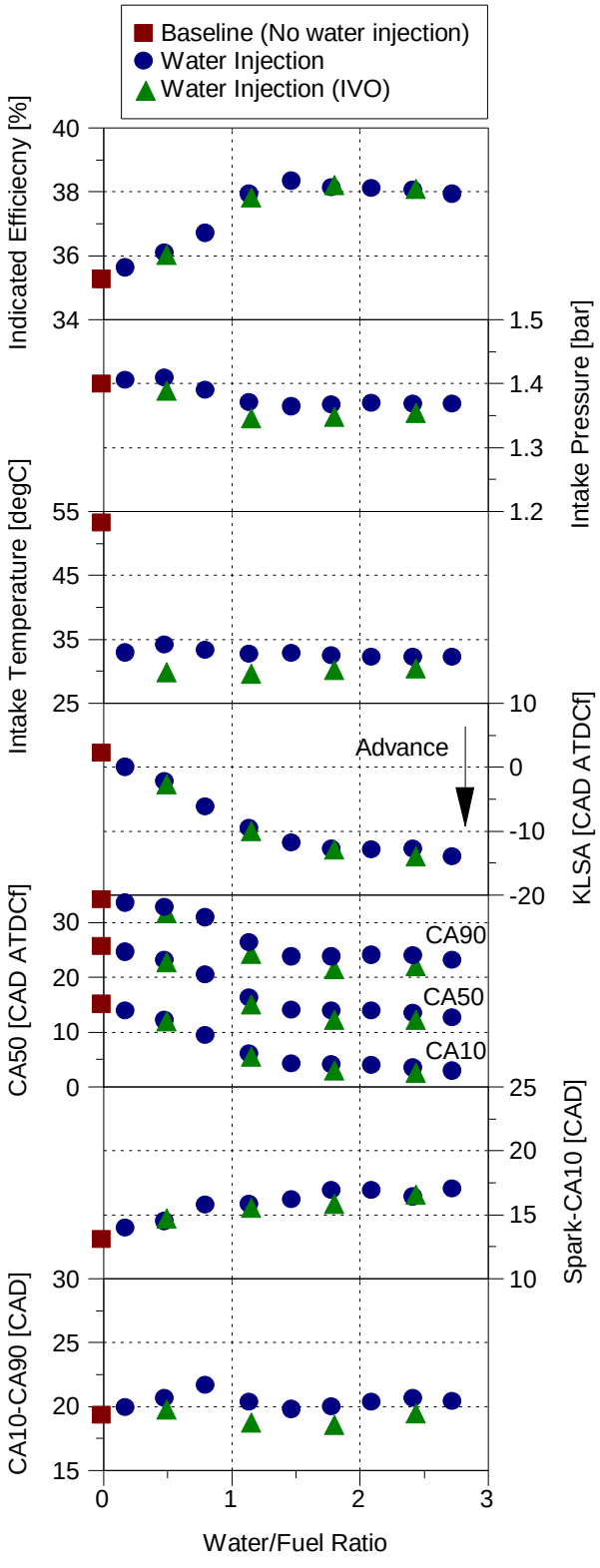

Figure 6-30 Impact of water injection into opened intake valves on stoichiometric combustion and efficiency at 2000 rpm / 16.04 bar NIMEP (RON 100)

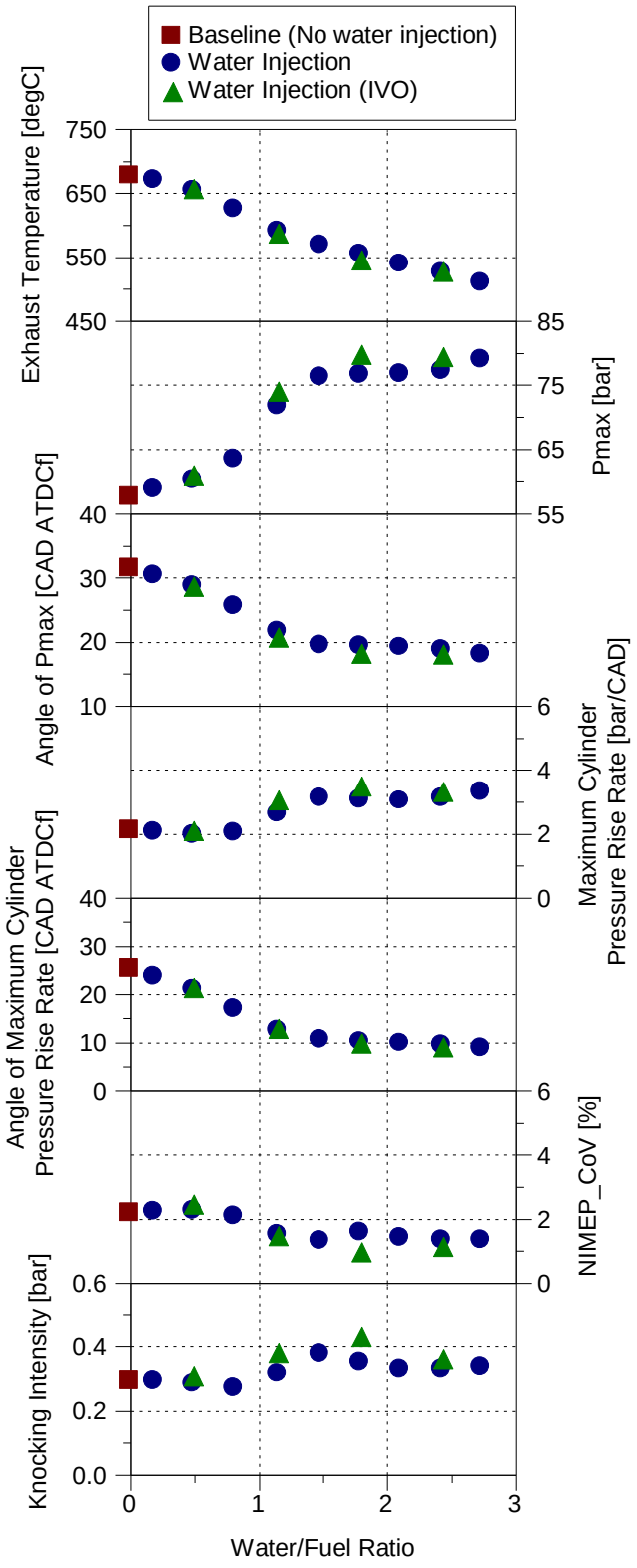

Figure 6-31 Impact of water injection into opened intake valves on stoichiometric combustion at 2000 rpm / 16.04 bar NIMEP (RON 100)

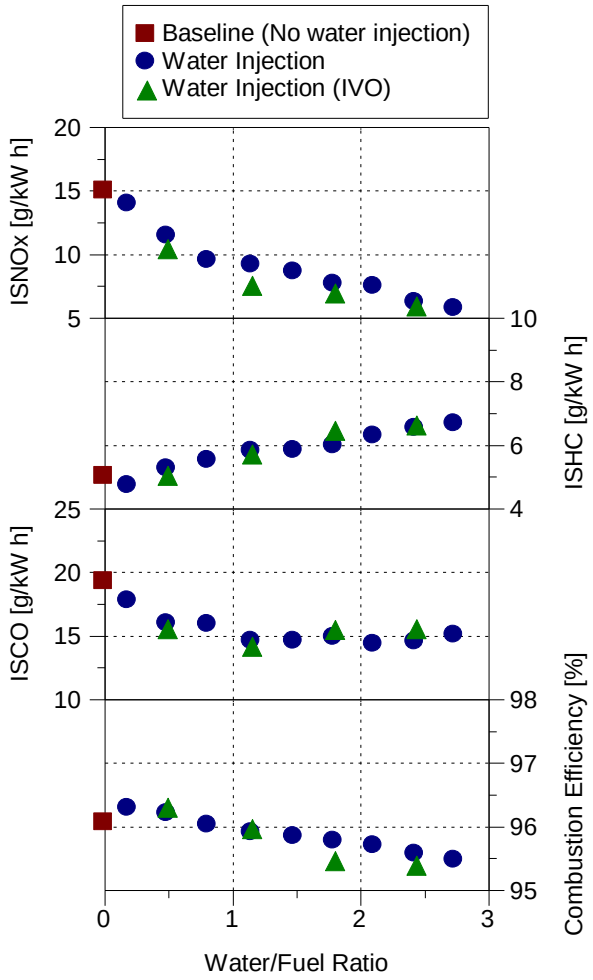

Figure 6-32 Impact of water injection into opened intake valves on specific exhaust emissions and combustion efficiency at 2000 rpm / 16.04 bar NIMEP (RON 100)

At 2000 rpm / 20 bar NIMEP the water injection timing was set at 370 CAD BTDCf which is exactly at the time which intake valves start to open. Spark timings for the opened intake valves injection were set at the same timings as the closed intake valve injection (Figure 6-33, Figure 6-34 and Figure 6-35). The trend from the results shows generally no or little difference between the closed and opened intake valves injection at this test point.

The indicated efficiency graph shows that results for opened intake valves injection case match the results for the closed intake valves injection case. This trend also continues for almost all the other graphs in Figure 6-33. However, there are slight differences between the two cases in intake pressure, intake temperature and combustion duration.

Figure 6-34 also shows no major difference between the two cases except the slightly higher combustion stability achieved with the opened intake valves injection case.

In terms of specific emissions Figure 6-35 shows almost identical results for the both closed and opened intake valves injection.

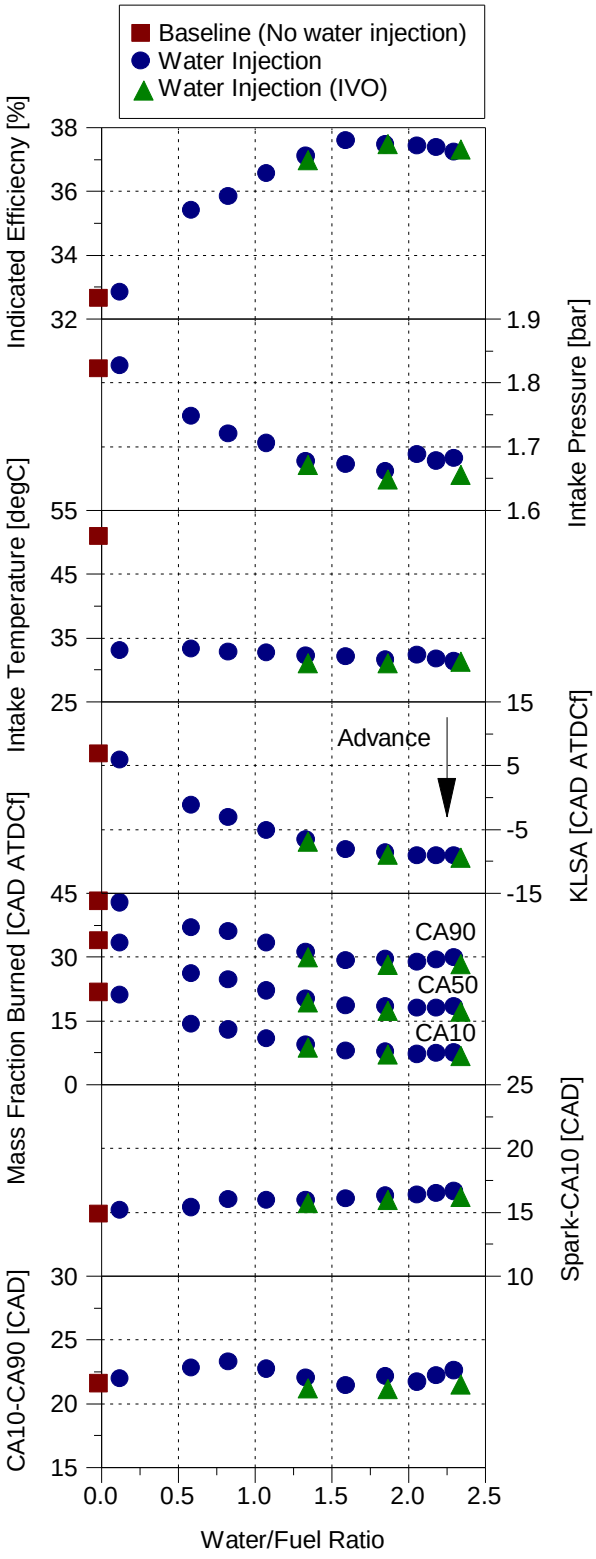

Figure 6-33 Impact of water injection into opened intake valves on stoichiometric combustion and efficiency at 2000 rpm / 20 bar NIMEP (RON 100)

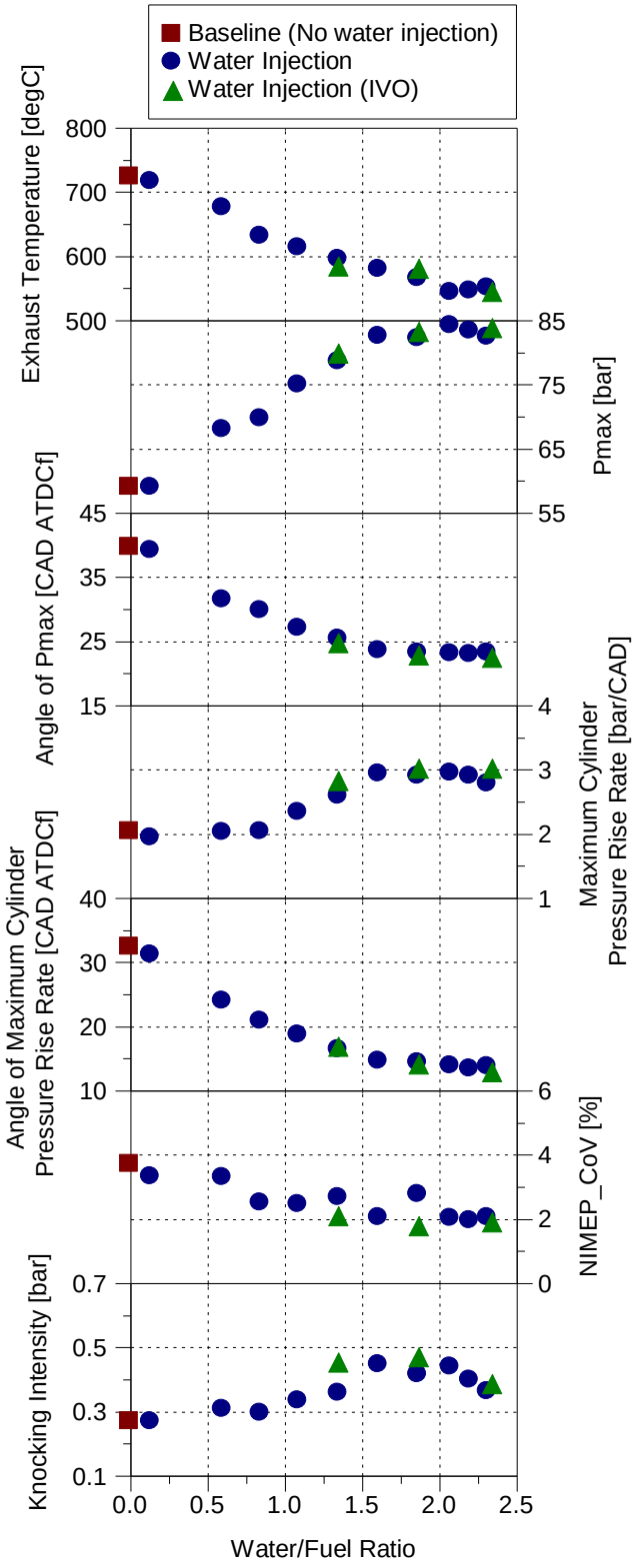

Figure 6-34 Impact of water injection into opened intake valves on stoichiometric combustion at 2000 rpm / 20 bar NIMEP (RON 100)

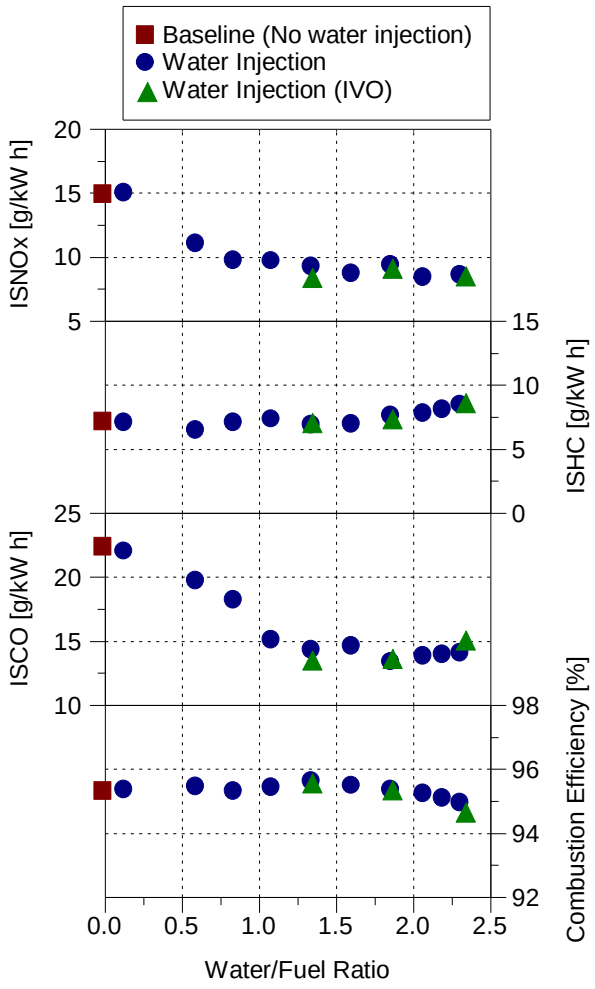

Figure 6-35 Impact of water injection into opened intake valves on specific exhaust emissions and combustion efficiency at 2000 rpm / 20 bar NIMEP (RON 100)

At 3000 rpm / 16.04 bar NIMEP the water injection timing was set at 370 CAD BTDCf which is exactly at the time which intake valves start to open. Spark timings for the opened intake valves injection were set at the same timings as the closed intake valve injection (Figure 6-36, Figure 6-37 and Figure 6-38). Basically, the trend from the results show no or little difference between the closed and opened intake valves injection at this test point.

As can be seen in Figure 6-36 there is no major difference between the closed and opened intake valves injection cases in terms of the main combustion parameters such as combustion phasing and duration. There is only a slight difference in intake pressure and temperature of the two cases just at low water/fuel ratios.

In addition, as Figure 6-37 shows, other combustion parameters such as peak in-cylinder pressure, peak pressure rise rate and combustion stability (NIMEP_CoV) are almost identical for the two cases.

Furthermore, as it is shown in Figure 6-38, both cases produced similar results in terms of gaseous emissions.

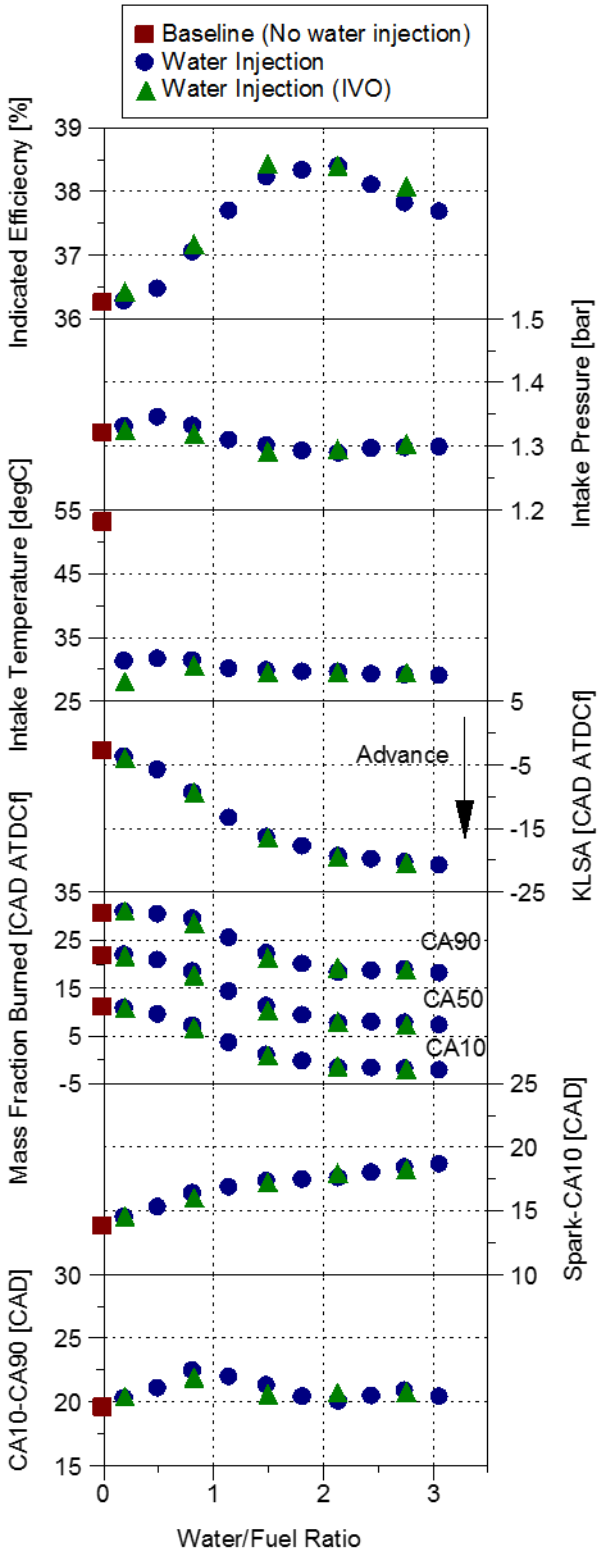

Figure 6-36 Impact of water injection into opened intake valves on stoichiometric combustion and efficiency at 3000 rpm / 16.04 bar NIMEP (RON 100)

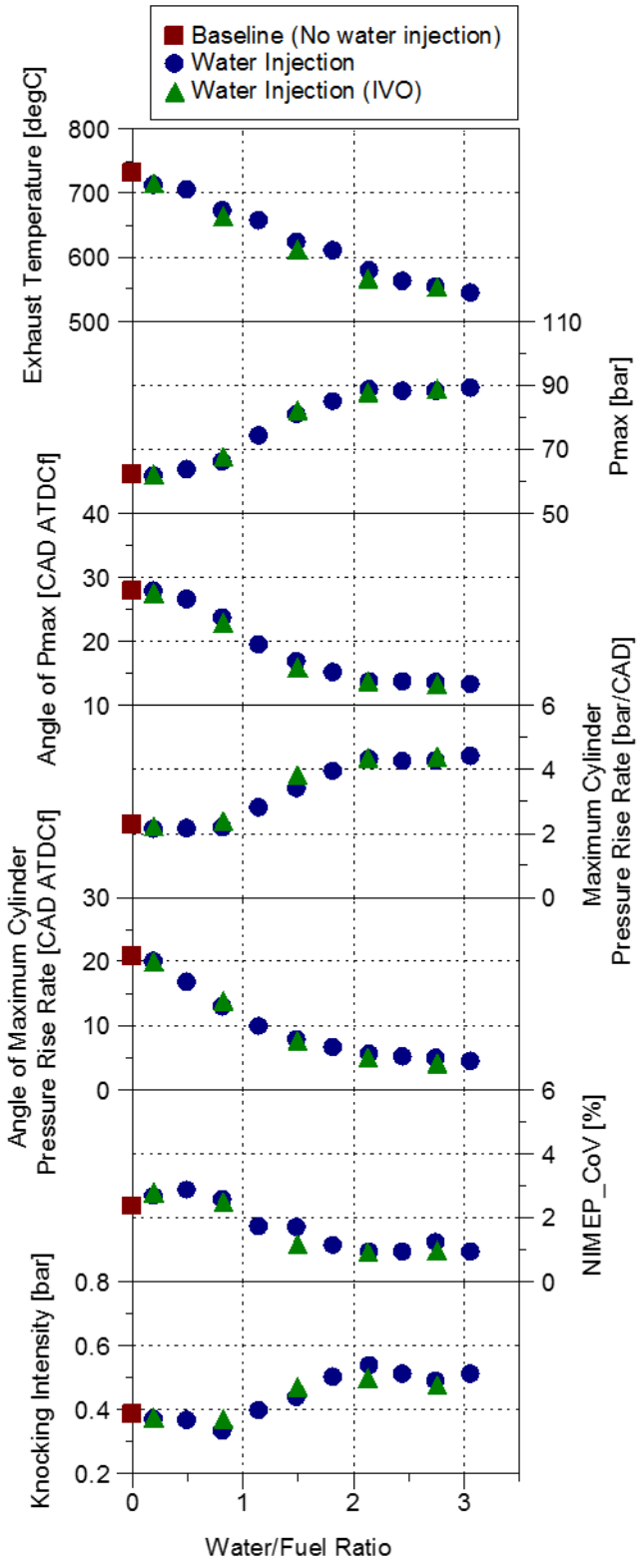

Figure 6-37 Impact of water injection into opened intake valves on stoichiometric combustion at 3000 rpm / 16.04 bar NIMEP (RON 100)

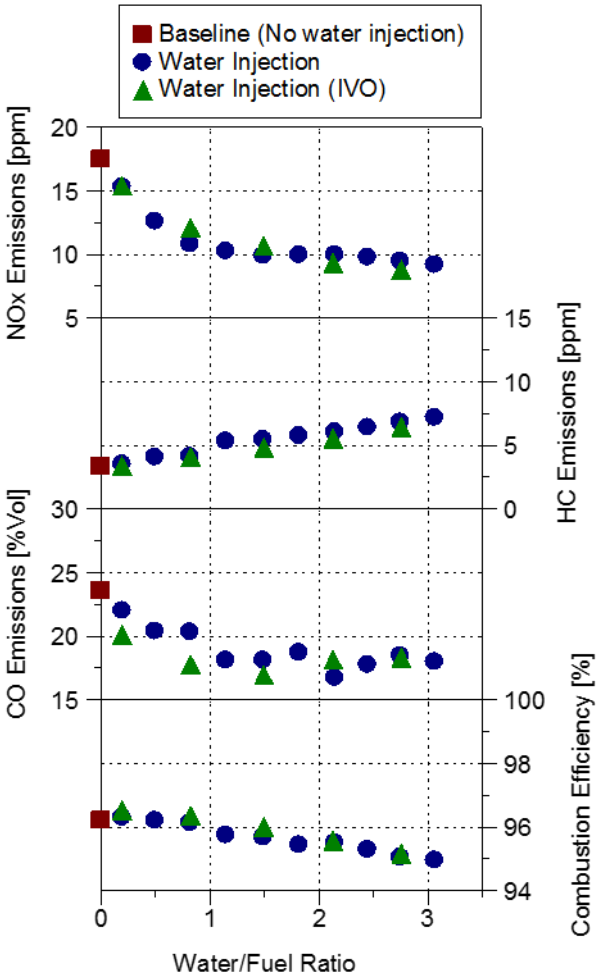

Figure 6-38 Impact of water injection into opened intake valves on specific exhaust emissions and combustion efficiency at 3000 rpm / 16.04 bar NIMEP (RON 100)

At 3000 rpm / 20 bar NIMEP the water injection timing was set at 370 CAD BTDCf which is exactly at the time which intake valves start to open. Spark timings for the opened intake valves injection were set at the same timings as the closed intake valve injection (Figure 6-39, Figure 6-40 and Figure 6-41). Basically, the trend from the results show no or little difference between the closed and opened intake valves injection at this test point.

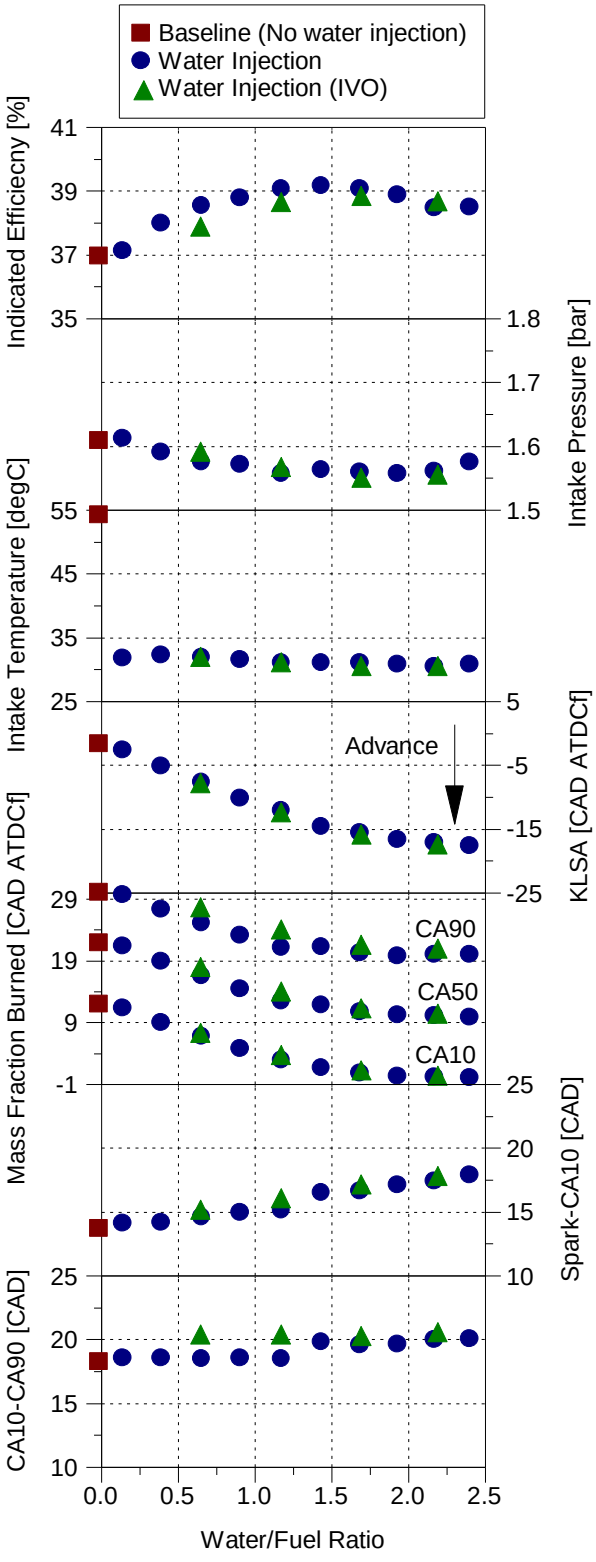

Figure 6-39 Impact of water injection into opened intake valves on stoichiometric combustion and efficiency at 3000 rpm / 20 bar NIMEP (RON 100)

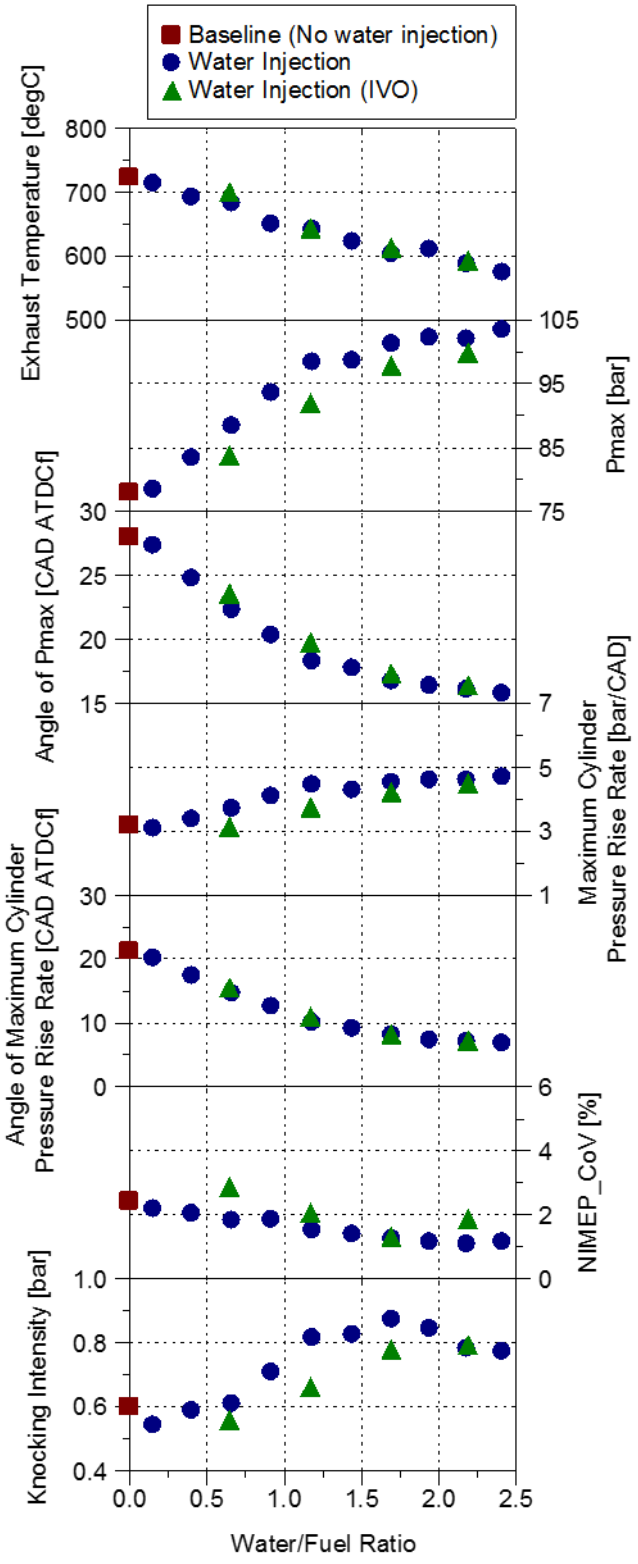

Figure 6-40 Impact of water injection into opened intake valves on stoichiometric combustion at 3000 rpm / 20 bar NIMEP (RON 100)

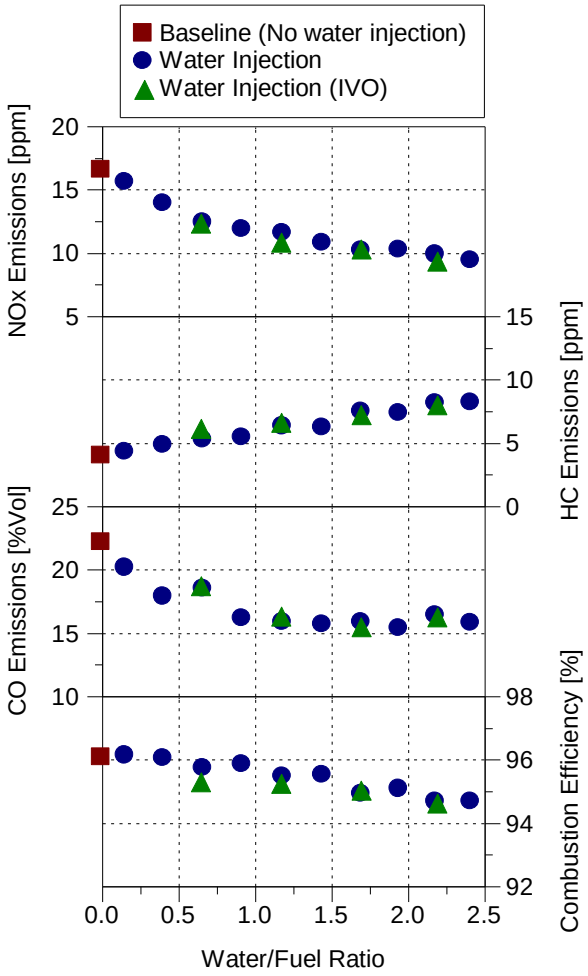

Figure 6-41 Impact of water injection into opened intake valves on specific exhaust emissions and combustion efficiency at 3000 rpm / 20 bar NIMEP (RON 100)

This section demonstrated the differences between the closed and opened intake valves water injection cases. As it was shown in most cases there was no or slight difference between the two cases. However, the slight difference at low and high water/fuel ratios between the two cases could be due to the differences in the amount of water vaporized and the source of vaporization. In the case of closed intake valves injection, longer time (360 CAD during expansion and exhaust strokes) is available for the injected water mass to absorb the heat from the intake ports and valves and evaporate and mix with the intake air (full vaporization of the

injected water might not happen at high water/fuel ratios but still higher amount of water can be vaporized compared to the opened intake valves injection due to the longer time available for the closed intake valves injection). However, with the opened intake valves injection case the injected water mass impinges on the intake ports and valves and the large portion of it enters the cylinder in the liquid phase which might also impinge on cylinder wall and piston top. Therefore, water can absorb the heat from the in-cylinder air, cylinder wall and piston top. This liquid water on cylinder wall and piston top promotes flame quenching at high water/fuel ratios when the water is not fully vaporized before combustion which deteriorates the combustion and increases the emissions. In addition, opened intake valves injection also promotes oil dilution due to the water impingement on cylinder wall which can be problematic for the engine in long term. Figure 6-42 shows the difference between the opened and closed intake valves injection.

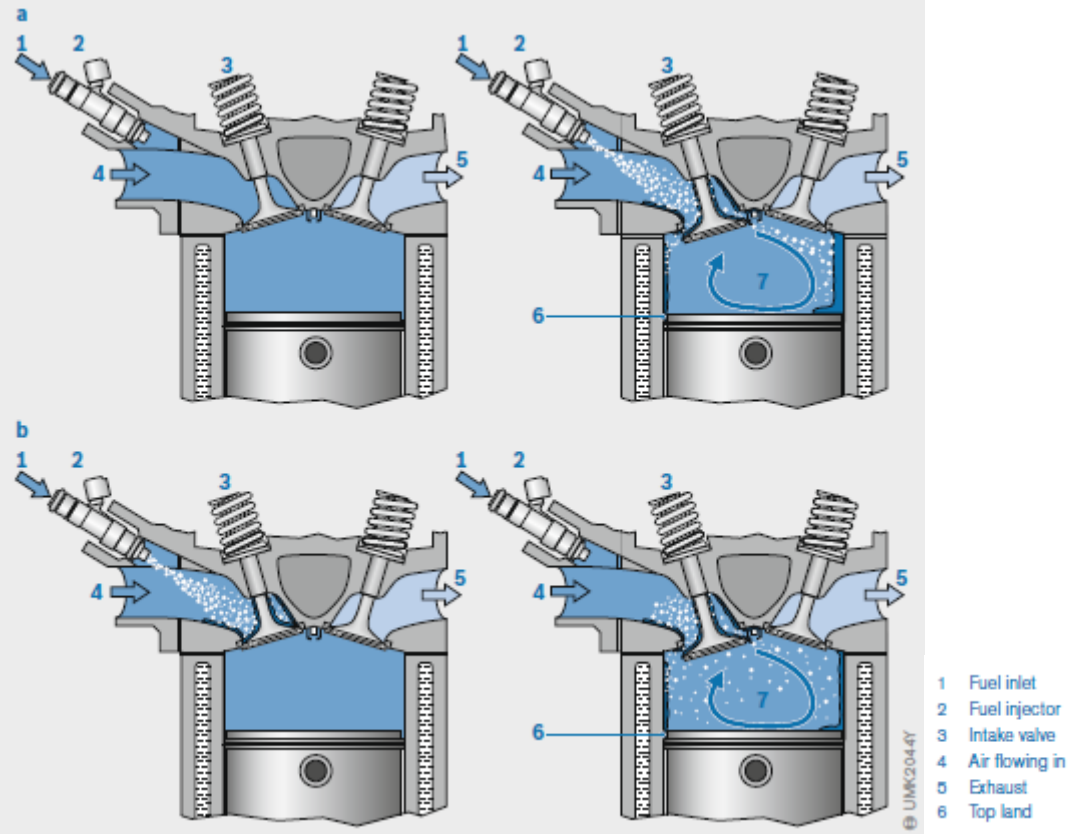

Figure 6-42 Intake-synchronous injection (a) Pre-intake injection (b) [22]

6.4 Summary

The aim of this chapter was to investigate the impact of intake port water injection on performance, fuel consumption and exhaust emission of the boosted downsized single cylinder GDI engine operating at medium and high loads. Gasoline was injected directly into the cylinder, while water was port injected. During these experiments water injection timing and pressure were remained constant at 90 CAD BTDCf and 5 bar respectively. Several steady state points from medium to high load (8.83 to 20 bar NIMEP) and low to mid speed (1000 to 3000 rpm) where the knock start to occur were selected for these experiments. Experiments first began by performing a spark timing sweep without water injection at each test point in order to find the baseline. Then the water/fuel ratio

sweep was performed by adding water and increasing the injected water mass until there was no apparent improvement in efficiency. Finally, the data for all the test points were analysed and compared to the baseline without water injection. The main findings of this study are summarized below:

- Water injection mitigated the possibility of knock occurrence at 1000 rpm / 8.83 bar NIMEP. Hence, spark timing could be advanced further which shifted the combustion phasing to the optimum point and increased the indicated efficiency.
- The injected water mass was increased to a maximum level until there was no improvement in efficiency. The highest level of water injected was between 200 and 300% of the mass of fuel at various speed and loads. There was a significant improvement in efficiency as the water/fuel ratio increased to its optimum value especially at low speed and high loads such as 2000 rpm / 8.83 bar NIMEP which were more prone to knock.
- There is an optimum water/fuel ratio at each test point. Increasing the injected water mass further decreased the efficiency and increased the unburned combustion products such as HC emissions. This was mainly due to the prolonged flame development angle and combustion duration, and decreased combustion efficiency with higher HC emissions due to the dilution effect of water. In addition, too much water decreased the in-cylinder pressure after combustion during expansion stroke due to increased heat capacity of charge, thus the net integrated work area of the P-V diagram was reduced.
- Improvements in efficiency with water injection were lower at higher engine speed (for example 2000 rpm compared to 3000 rpm). The main reason for

this could be the increase in intrinsic knocking tolerance by increasing engine speed as knocking combustion is more likely to happen at low engine speeds.

- Number of particles emitted dropped significantly by intake port water injection and advancing the knock limited spark advance until a minimum value was reached. Increasing the water/fuel ratio further increased the number of particles again.
- This study also demonstrated the differences between the closed and opened intake valves water injection cases at both medium and high load operating conditions. As it was shown in most cases there was no or slight difference between the two cases. However, the slight difference at low and high water/fuel ratios between the two cases could be due to the differences in the amount of water vaporized before combustion takes place and the source of vaporization.

In addition, gasoline with different octane number has been tested to investigate the effective RON of water which will be presented in the next chapter. Further experiments are required to explore the potential of DI water and PFI gasoline configuration which takes full advantage of the high heat of vaporization of water for maximum charge cooling effect.

Chapter Seven

Effect of Intake Port Injection of Water on Gasoline Octane Number

Chapter 7 Effect of Intake Port Injection of Water on Gasoline Octane Number

7.1 Introduction

As it was explained and shown in chapter two and six, water injection can be used as a promising method to mitigate knock and significantly reduce the CO_2 emissions. This is particularly important in highly downsized boosted engines which run under much higher intake pressures therefore more prone to knocking combustion. In addition to knock, water injection is an effective method to reduce NO_x emissions and decrease exhaust gas temperature at high loads which can protect the turbine in turbocharged engines and eliminate the need for fuel enrichment.

This chapter shows the influence of intake port injection of water on efficiency and emissions of a boosted downsized single cylinder gasoline direct injection (GDI) engine in detail. Six different steady state speed and load combinations were selected to represent the conditions that knocking combustion start to occur. Water / fuel ratio was varied in the range of 0 to 3 to find out the optimum water mass required at each test point and the impact on the combustion and emissions. Gasoline with three different octane numbers (RON 95, 97 and 100) was used to determine the effective octane number of water. The efficacy of water as an anti-knock agent is also considered at the selected steady state test points. In addition to the gaseous emissions, particulate emissions were also measured for the three fuels.

7.2 Experimental Setup and Test Conditions

The experimental setup used to obtain the results in this chapter and the test conditions were same as the setup and conditions used in Chapter 6. Figure 6-1 and Table 6.1 show the experimental setup and the test conditions. All the tests in this chapter were performed with water injection into closed intake valves. As it was mentioned earlier, in addition to the effect of water injection on combustion, this chapter also investigates the effect of water injection on gasoline octane number. Therefore, gasoline with research octane number (RON) of 95, 97 and 100 were used to perform the experiments at each test point which then were used for comparison.

7.3 Results and Discussion

7.3.1 Effect of spark timing sweep without water injection on combustion, efficiency and emissions using gasoline with different RONs

Spark timing sweep test was performed at each test point first before adding any water into the mixture. This was done to find out the baseline efficiency and the knock limited spark advance (KLSA) without water injection. Gasoline with three different octane numbers (Table 3.8) were used so the results can be compared, and effective RON of water can be assessed.

Figure 7-1 and Figure 7-2 show the results of spark timing sweep at 2000 rpm and 16.04 bar NIMEP. There were clear improvements in indicated efficiency as the spark timing was advanced for all three fuels. These improvements were mainly due to a more advanced combustion phasing and shorter flame development angle and combustion duration.

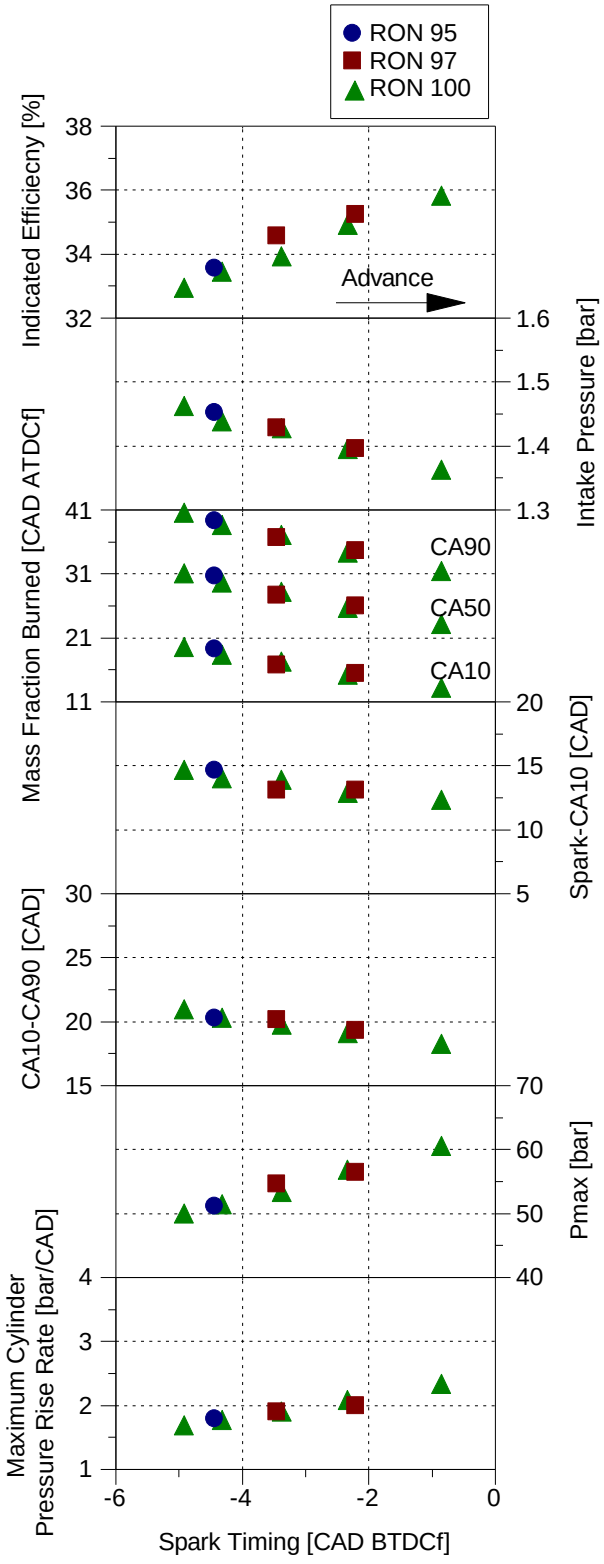

Figure 7-1 Spark timing sweep for baseline test without water injection at 2000 rpm / 16.04 bar NIMEP for three fuels

In terms of combustion phasing, 50% mass fraction burned angle was advanced by around 8 CAD for RON 100 when advancing the spark timing by 4 CAD (from -5 CAD BTDCf to -1 CAD BTDCf). Combustion duration was also shortened by around 3 CAD for RON 100. This confirms that the advancement in spark timing has a more pronounced influence on the combustion phasing than combustion duration. Flame development angle was also shortened by around 3 CAD.

In addition, Figure 7-1 also shows a notable increase maximum in-cylinder pressure as the knock limited spark timing was advanced. Peak in-cylinder pressure occurred earlier and closer to TDC where combustion was exposed to a higher temperature and pressure environment. Advancing the spark timing also results in an increase in maximum cylinder pressure rise rate due to the advancement of combustion phasing. Thus, lower boost pressure was required to achieve the same load which consequently results in lower fuel consumption.

Figure 7-2 shows that exhaust temperature was also reduced by around 50°C for RON 100 when advancing the spark timing due to the shift of combustion phasing to a more efficient point. Clear improvement in combustion stability also can be seen in this figure due to the improved combustion phasing and duration. earlier and faster combustion led to less variation of NIMEP. Knocking intensity also increases as expected when the spark timing is advanced due to a higher peak pressure rise rate and higher in-cylinder pressure and temperature at the same crank angle.

Advancing the spark timing for RON 97 also followed the same trend and led to advancement in combustion phasing, faster combustion, higher peak in-cylinder pressure, higher combustion stability (NIMEP_CoV), lower exhaust temperature

and ultimately higher indicated efficiency. In addition, when the spark timing is remained constant for the all three fuels, the combustion timing and efficiency also remains the same for the different fuels. These results were expected and particularly important as the baseline is determined by these results and allow a fine comparison of three fuels with water injection as well which will be presented in the next section.

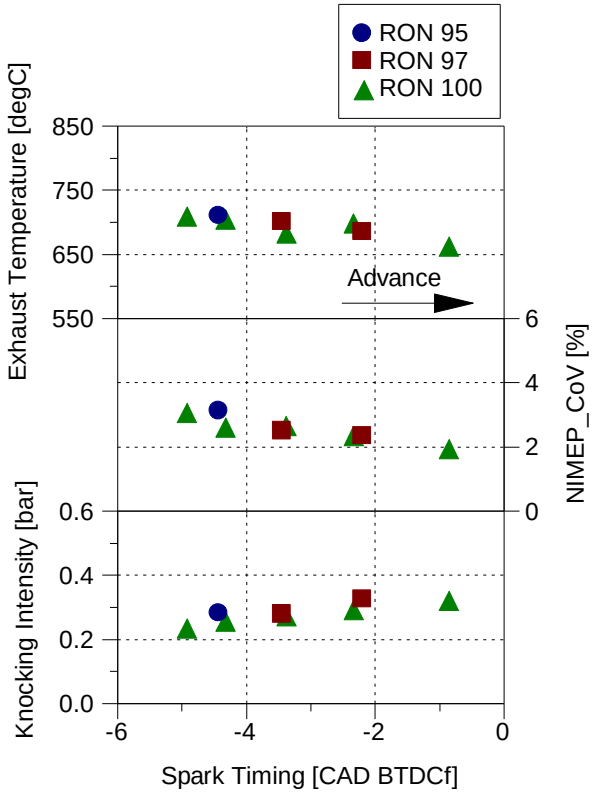

Figure 7-2 Spark timing sweep for baseline test without water injection at 2000 rpm / 16.04 bar NIMEP for three fuels

Figure 7-3 show the effect of spark timing sweep without water injection on combustion of gasoline with three different RONs at 2000 rpm / 8.90 bar NIMEP. As it was explained for the previous load and speed, advancing the spark timing increased the indicated efficiency by advancing the combustion phasing, reducing combustion duration and increasing the maximum in-cylinder pressure.

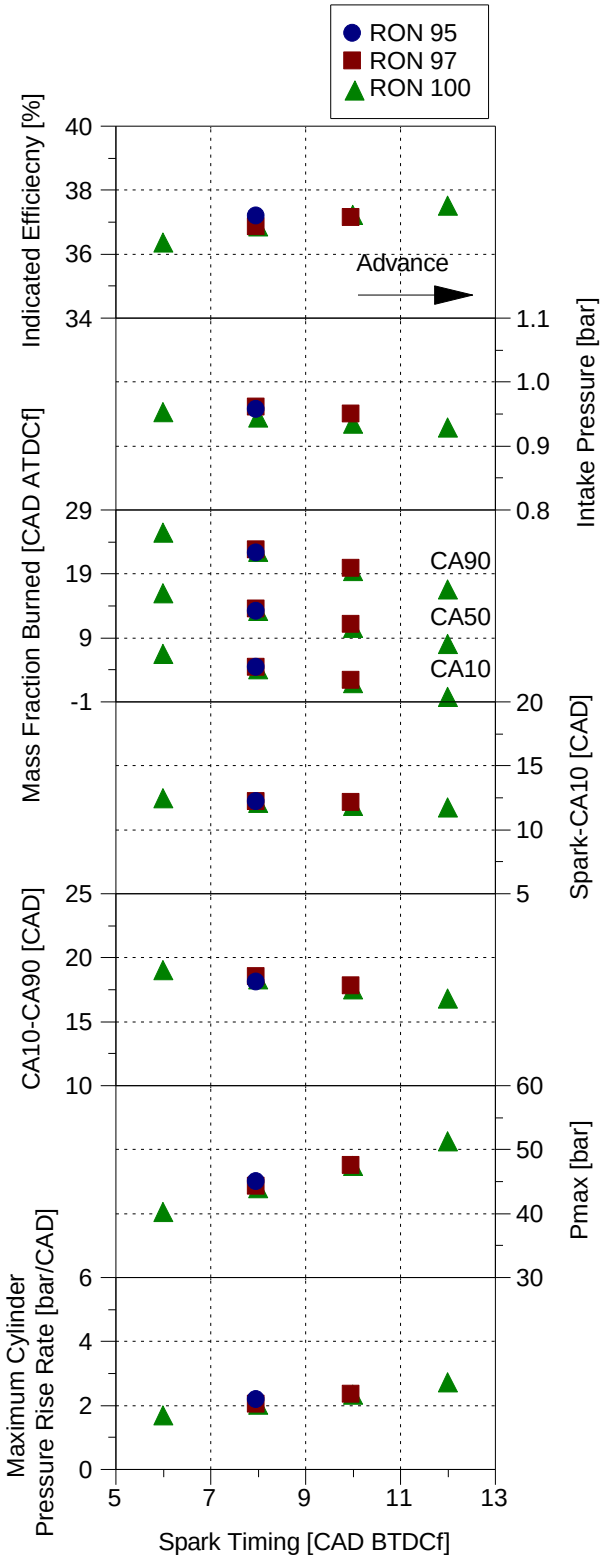

Figure 7-3 Spark timing sweep for baseline test without water injection at 2000 rpm / 8.90 bar NIMEP for three fuels

Considering RON 100, indicated efficiency increased by around 3% when advancing the spark timing by 6 CAD (from 6 CAD BTDCf to 12 CAD BTDCf). In term of combustion phasing, advancing the spark timing led to the advancement of CA50 by 8 CAD for RON 100. Flame development angle decreased slightly, however combustion duration decreased by around 2 CAD. Peak in-cylinder pressure and peak in-cylinder pressure rise rate also increased by around 10 bar and 1 bar/CAD respectively. These improvements were less for RON 97 since the spark timing could be advanced less by only 2 CAD.

Earlier and faster combustion with more advanced spark timings also helped in reducing the exhaust gas temperature and increased the combustion stability (Figure 7-4).

The emission results in Figure 7-4 shows an increase in specific NO_x emissions for all cases which is due to higher peak in-cylinder pressure and temperature as the spark timing was advanced. However, CO and HC emissions remained almost unchanged across the spark timing range.

In addition, these results show that when the spark timing is remained the same for the three fuels, the combustion phasing and indicated efficiency also remained the same for the different fuels.

Figure 7-5 shows the spark timing sweep at 3000 rpm / 20 bar NIMEP for RON 97 and 100 which demonstrates an increase in indicated efficiency and improvements in other combustion parameters by advancing the spark timing. At this operating point the data for RON 95 was not recorded due to a very high knock sensitivity with RON 95 under this high load condition which did not allow logging the data without knock or misfire occurrence.

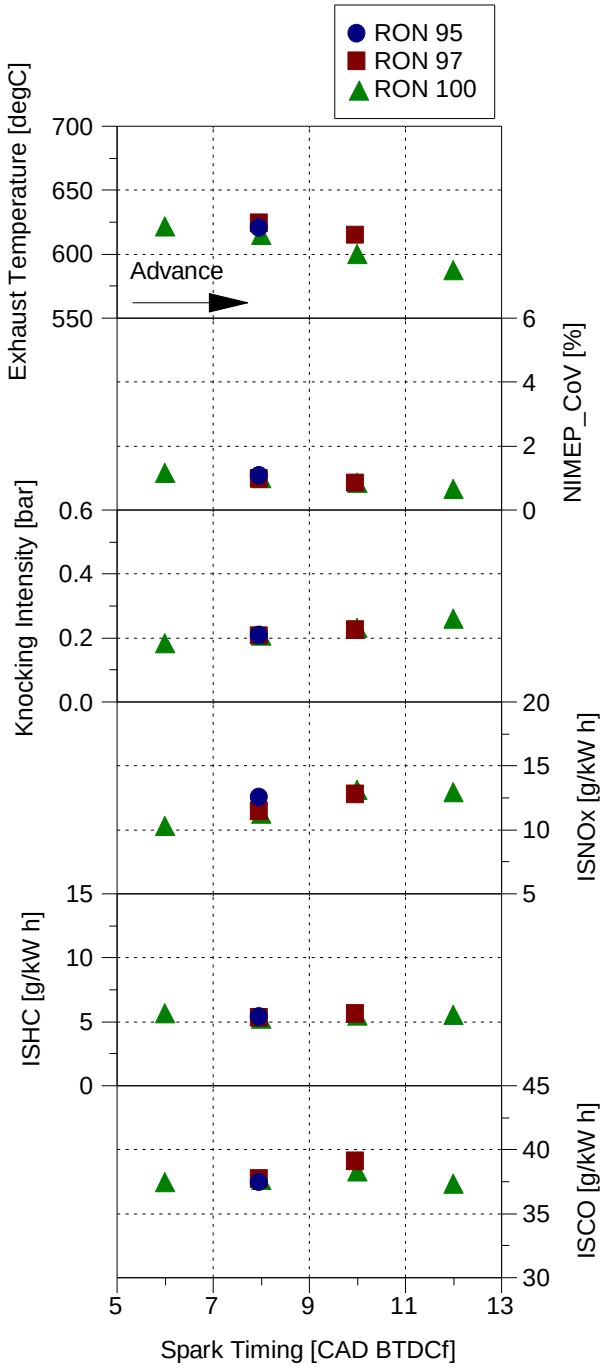

Figure 7-4 Spark timing sweep for baseline test without water injection at 2000 rpm / 8.90 bar NIMEP for three fuels

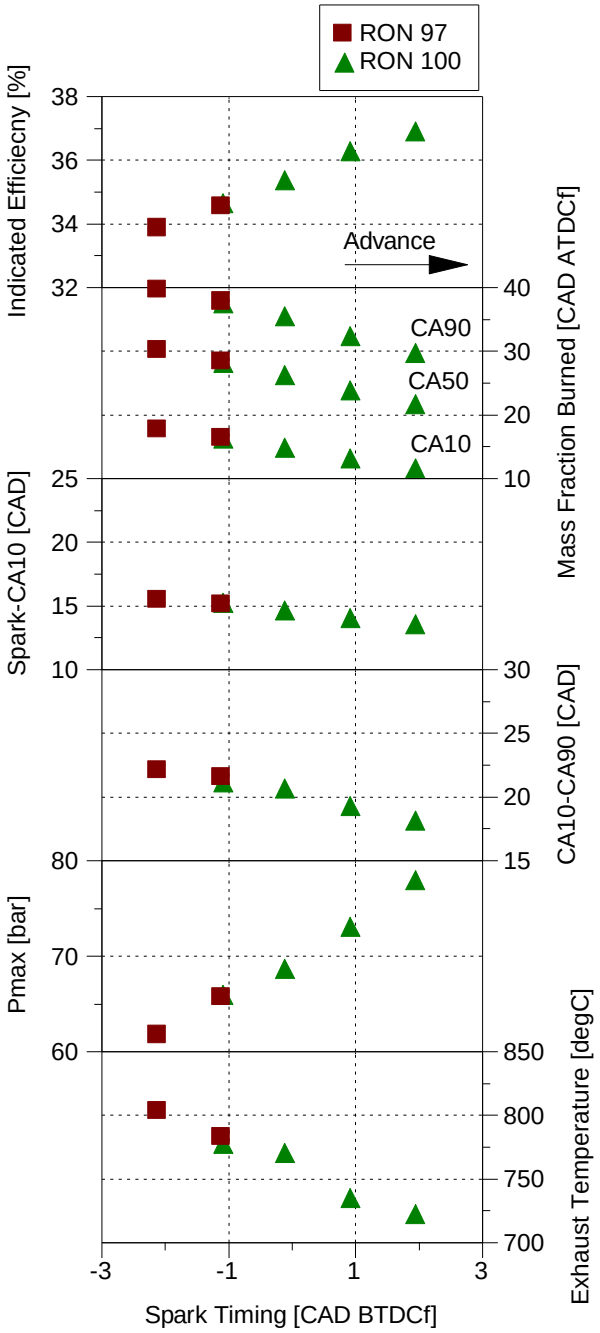

Figure 7-5 Spark timing sweep for baseline test without water injection at 3000 rpm and 20 bar NIMEP for three fuels

The spark timing sweep tests were conducted at all the test points and in all cases advancing the spark timing showed an increase in indicated efficiency when the spark advanced is knock limited.

7.3.2 Effects of water injection on gasoline octane number, engine performance and emissions at mid-load condition

This section shows and discusses the results of water injection at engine speeds and loads of 1000 rpm / 8.83 bar NIMEP and 2000 rpm / 8.90 bar NIMEP for the three fuels. These test points were selected since for the engine with current hardware setup knock starts to occur at these speeds and loads, and also for boosted downsized engines LSPI (low speed pre-ignition) might occur as the load is increased at low speed. Therefore, this is an important test point to demonstrate the potential of water injection in knock suppression.

After performing the spark timing sweep tests, a baseline is now established which can be used for comparison with the water injection tests. In the next step the engine was run at the baseline condition and a small quantity of water was injected in the intake port while the spark timing was same as the baseline to understand the effect of water injection only with no spark advance. These tests were performed for all three fuels at 1000 rpm / 8.83 bar NIMEP and 2000 rpm / 8.90 bar NIMEP, and the results show that the addition of water alone deteriorates the combustion and reduces indicated efficiency for all three fuels as it is shown in Figure 7-6.

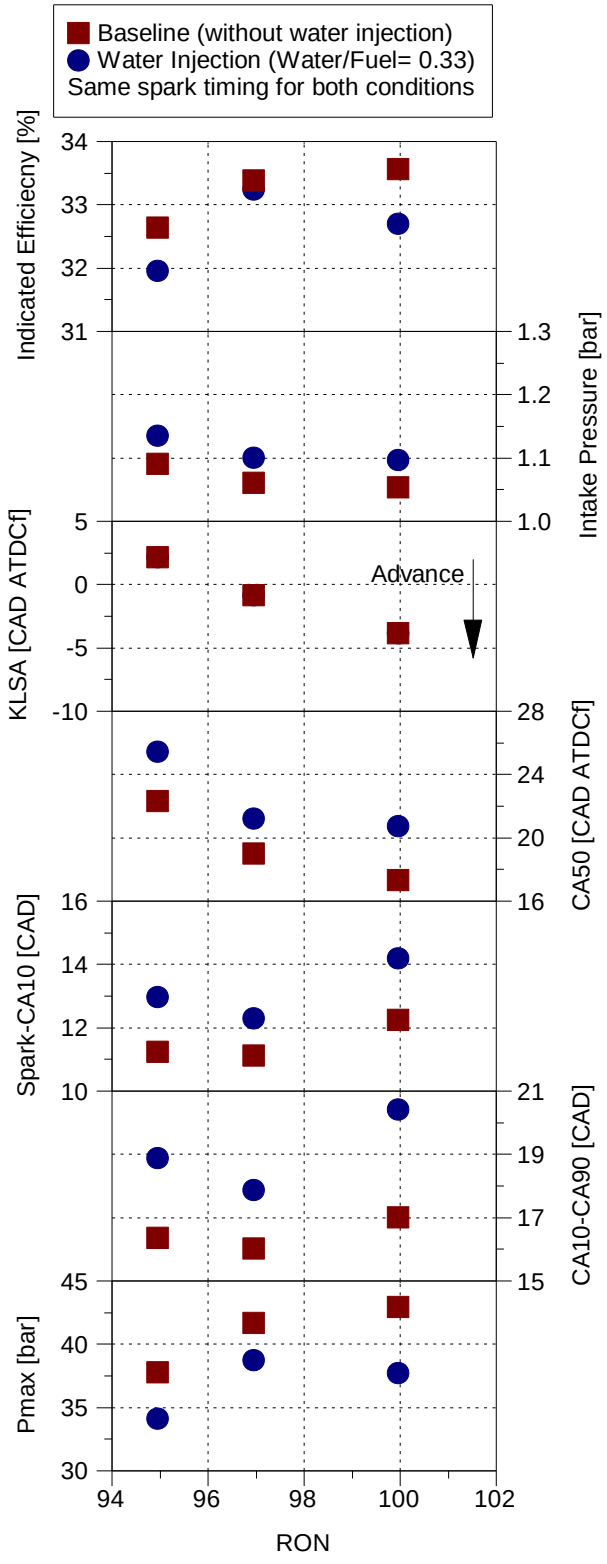

Figure 7-6 Effect of water injection alone without spark advance on efficiency, combustion phasing and duration for three fuels at 1000 rpm / 8.83 bar NIMEP

Addition of water without spark advance delayed the 50% mass fraction burned, prolonged the flame development angle and combustion duration, and reduced the peak in-cylinder pressure for all three fuels due to the dilution effect of water. The water absorbed the heat from the intake air, ports and valves, and acted as an inert gas after vaporization and entering the cylinder. Hence, combustion phasing was retarded. This followed by an increase in ISFC (indicated specific fuel consumption) and therefore a reduction in indicated efficiency when the spark timing remained constant. As a result, slightly higher intake pressure was required to maintain the same load with water injection for all three fuels (Figure 7-6).

Figure 7-7 shows additional combustion parameters such as combustion stability, exhaust gas temperature and knocking intensity as well as the emissions at 1000 rpm / 8.83 bar NIMEP. Exhaust gas temperature stayed almost the same for both baseline and water injection cases at this test point. Although water injection increased the heat capacity of charge, combustion phasing was retarded due to the dilution effect of water. Therefore, the increased heat capacity of charge was compensated by the retarded combustion phasing and exhaust gas temperature remained constant for all three fuels when comparing the baseline to water injection case without spark advance.

Intake temperature (Figure 7-7) dropped by around 20 °C when switching from the baseline to water injection operation due to the cooling effect of water in the intake port. As it was mentioned in the previous chapter, intake temperature was measured by a thermocouple which was fitted right in front of the PFI injector in the intake port. Therefore, the thermocouple could have been wet by the water spray from the PFI injector when running with water injection.

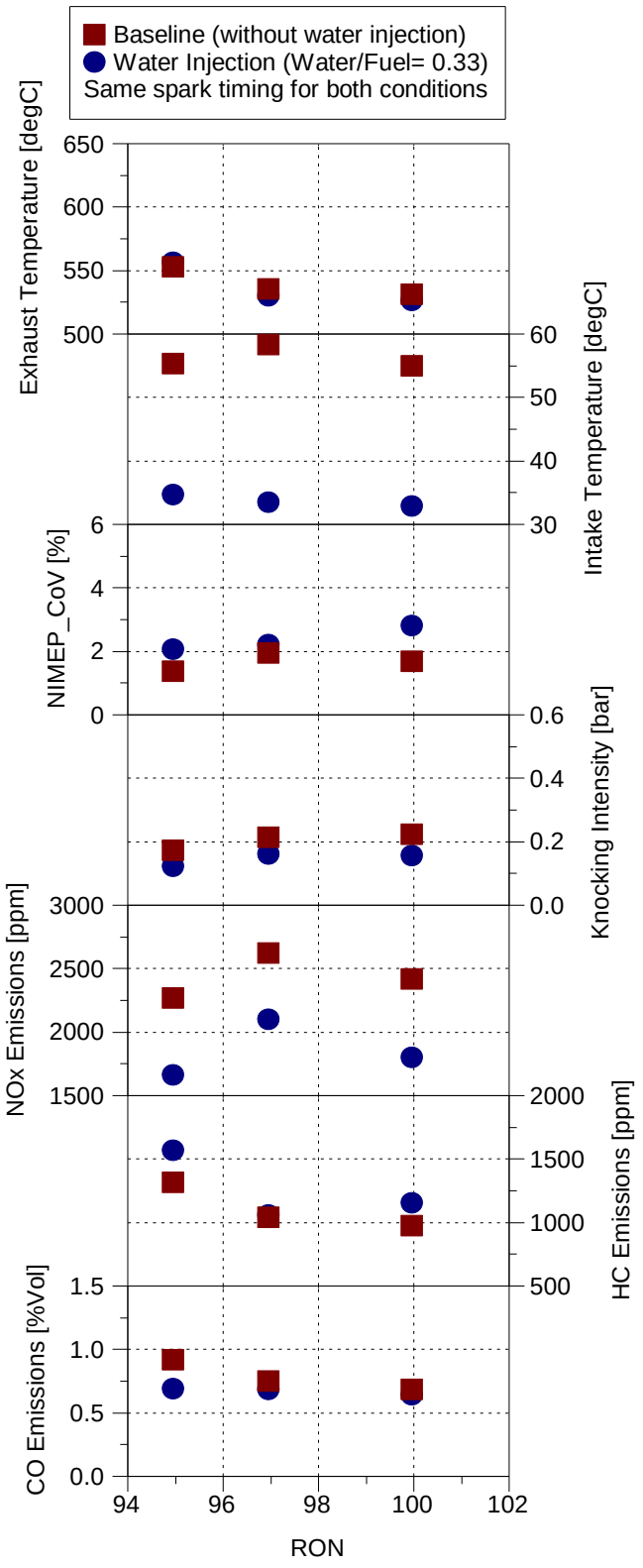

Figure 7-7 Effect of water injection alone without spark advance on combustion and emissions for three fuels at 1000 rpm / 8.83 bar NIMEP

Combustion stability (NIMEP_COV) (Figure 7-7) decreased after injecting a small quantity of water without advancing the spark timing compared to the baseline. The main reason can be the retarded combustion phasing and prolonged flame development angle and combustion duration. Combustion phasing was retarded by around 4 CAD in some cases with water injection. Combustion duration was prolonged by around 3 CAD for water injection cases. These deteriorations in combustion increased the NIMEP variations and led to a lower combustion stability.

As it was expected knocking intensity (Figure 7-7) also decreased with water injection for all three fuels due to the lower peak pressure rise rate and peak in-cylinder pressure. Knocking intensity is an indication of how knock sensitive is the combustion. Values higher than 0.5 shows higher possibility of knock. It was expected that the water injection cases show lower knock intensity due to the increased heat capacity of charge with water injection (higher specific heats of water and increased in-cylinder mass). In addition to increased heat capacity of charge, water injection also provides a cooling effect which decreases the intake air temperature, intake ports and valves.

Figure 7-7 also shows that NO_x emissions decreased with water injection compared to the baseline mainly due to a lower peak in-cylinder temperature at it was also shown in the previous chapter. In addition, peak in-cylinder pressure decreased by water injection when the spark timing was remained constant. Thus, lower peak in-cylinder pressure and temperature are the main contributors to lower NO_x emissions at this condition for all three fuels.

Unburned hydrocarbon emissions increased (Figure 7-7) with water injection compared to the baseline due the dilution effect of water which decreases the in-cylinder temperature during expansion and exhaust strokes and promotes flame quenching. When the injected water enters the cylinder in the liquid phase, significantly decreases the local temperature where the evaporation takes place. This can promote flame quenching which is a source of increased HC emissions. Furthermore, the lower in-cylinder temperature associated with the cooling and dilution effect of water lowers the wall temperature and reduces post-flame oxidation effect during the expansion and exhaust strokes more than that of the baseline without water.

CO emissions were slightly lower with the water injection case compared to the baseline which also can be due to the dilution effect of water and lower in-cylinder temperature during expansion and exhaust strokes as CO is formed in high temperature and fuel-rich areas. Therefore, less hydrocarbons were oxidized to CO.

Figure 7-8 shows the effect of water injection and spark advance on in-cylinder pressure, heat release rate and mass fraction burned history of RON 97 at 1000 rpm / 8.83 bar NIMEP. As can be seen in this figure, combustion timing was retarded (mass fraction burned history), in-cylinder pressure rise after TDC was slower, peak cylinder pressure decreased and heat release was also delayed by adding water to the mixture without spark advance compared to the baseline case. CA50 was delayed by around 2 CAD, combustion duration also increased by around 2 CAD and cylinder pressure dropped by around 2.5 bar.

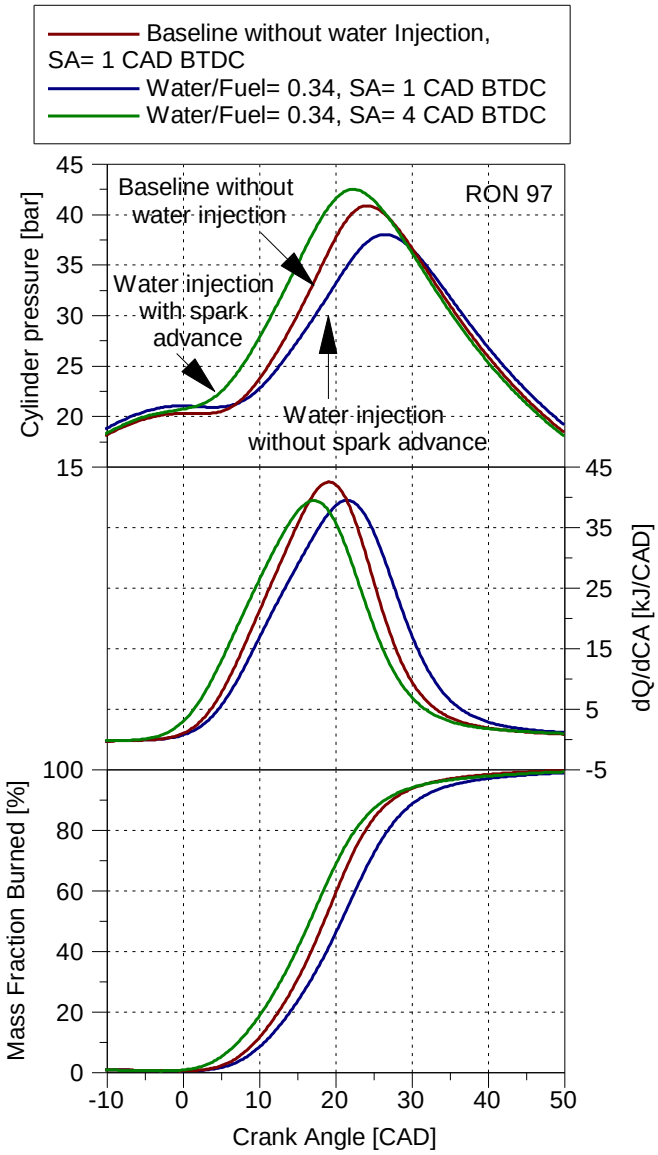

Figure 7-8 Effect of water injection and spark advance on cylinder pressure, heat release and MFB at 1000 rpm / 8.83 bar NIMEP (RON 97)

The injected water in the intake port absorbed the heat from the intake air, valves and ports and acted as an inert gas after vaporization. Hence, combustion timing was retarded and as a results efficiency was reduced when the spark timing remained constant. However, the inert gas effect also created an opportunity or a margin for spark timing to be advanced further. Therefore, combustion timing, heat release and peak cylinder pressure were advanced without occurrence of knock

by injecting the same amount of water and advancing the spark timing simultaneously. This eventually led to an improvement in efficiency. RON 95 and 100 (Figure 6-3) fuels also showed the same behaviour during water injection.

The effect of water injection without spark advance for the three fuels at 2000 rpm / 8.90 bar NIMEP is shown in Figure 7-9 and Figure 7-10. The results show a very similar trend to the previous test point. Adding water to the mixture without advancing the spark timing deteriorates the combustion phasing, duration and efficiency which directly affects the net indicated efficiency for all three fuels. In terms of emissions also similar results were observed. NO_x emissions decreased due to a lower peak in-cylinder pressure and temperature. HC emission were higher due to the flame quenching and lower oxidation during expansion and exhaust strokes.

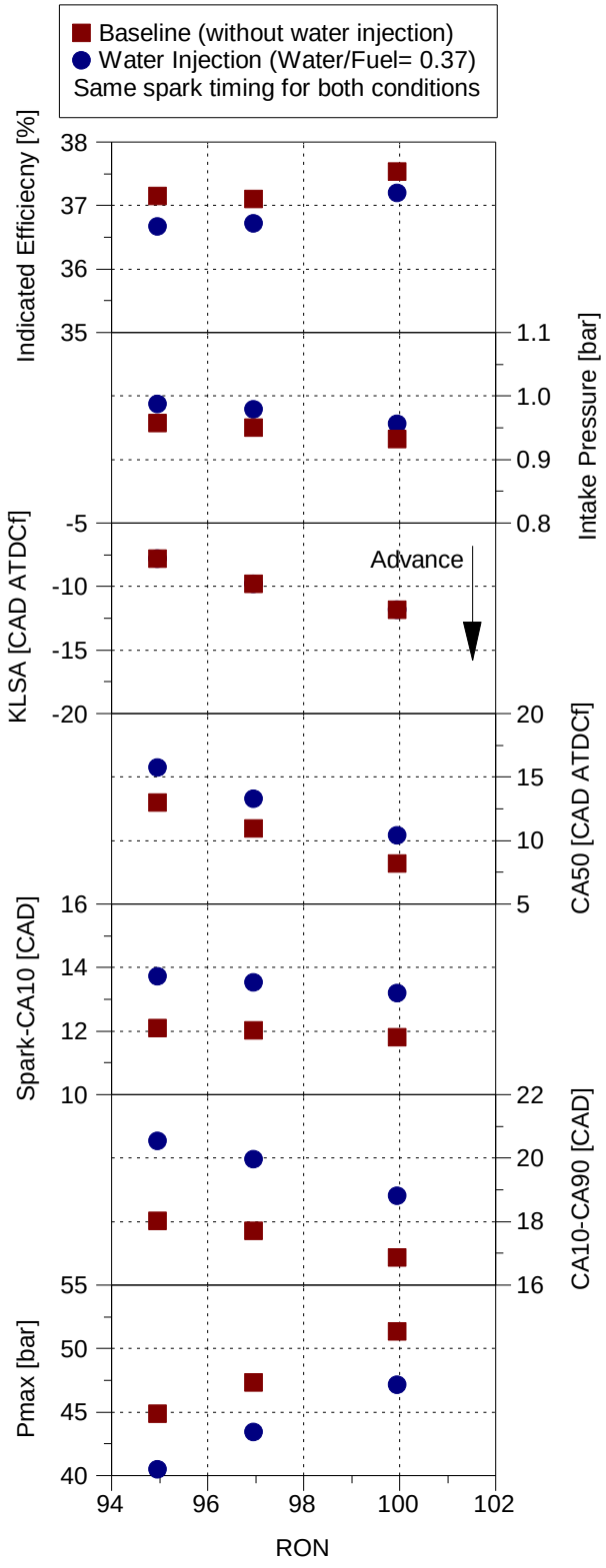

Figure 7-9 Effect of water injection alone without spark advance on efficiency, combustion phasing and duration for three fuels at 2000 rpm / 8.90 bar NIMEP

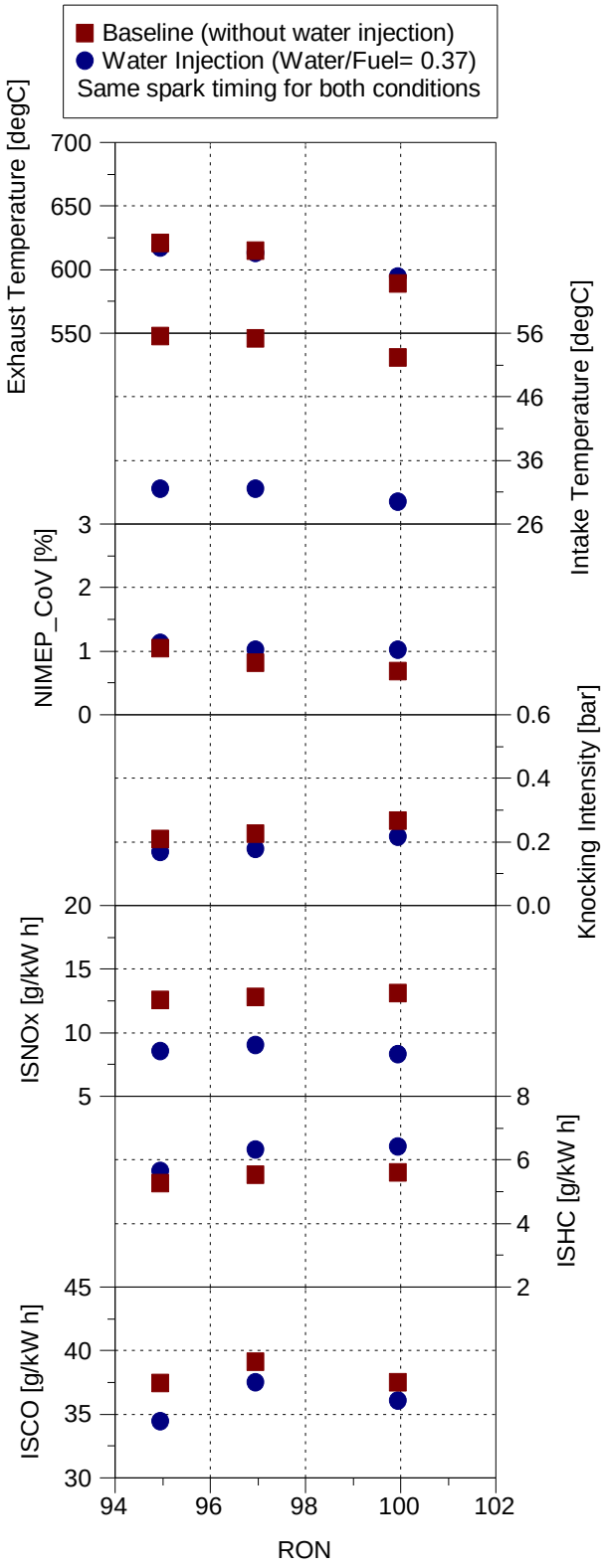

Figure 7-10 Effect of water injection alone without spark advance on combustion and emissions for three fuels at 2000 rpm / 8.90 bar NIMEP

Figure 7-11 shows the effect of the injected water quantity on efficiency and combustion characteristics of the engine at 1000 rpm / 8.83 bar NIMEP for all three fuels. Increasing the injected water mass could increase the knock tolerance and therefore the knock limited spark advance (KLSA) could be advanced further by a maximum of around 15 CAD without knock occurrence for all three fuels. This advancements in spark timings led to improvement in combustion phasing as CA50 was advanced by a maximum of around 10 to 12 CAD for the three cases. Indicated efficiency increased by around 6% for RON 95 and around 4% for RON 97 and 100. This improvement is mainly due to the use of more efficient (advanced) spark timings which shifts the combustion phasing towards the optimum point (CA50 around 8 CAD ATDC).

The indicated efficiency (Figure 7-11) graph also shows that adding 14.76 mg/cycle of water (water/fuel ratio of around 60% or 0.123 g/s) to RON 95 and advancing the spark timing by 6 CAD compared to the baseline can increase the efficiency to the same level achieved with RON 100 without water. Hence, the research octane number of RON 95 fuel was boosted to 100 by addition of water to the intake air. Indicated efficiency obtained from RON 97 and 100 were very similar due to the fact that their combustion phasing (CA50) were very close despite using more advanced spark timings with RON 100.

As the injected water mass ratio was increased to 1.5, indicated efficiency achieved with RON 95 moved closer to the indicated efficiency achieved by the other two fuels and they crossed at water/fuel ratio of around 1.5 (Figure 7-11). Indicated efficiency achieved with RON 95 continued to increase slightly after water ratio of 1.5 whereas there is a slight decrease in indicated efficiency achieved with RON 97 and 100.

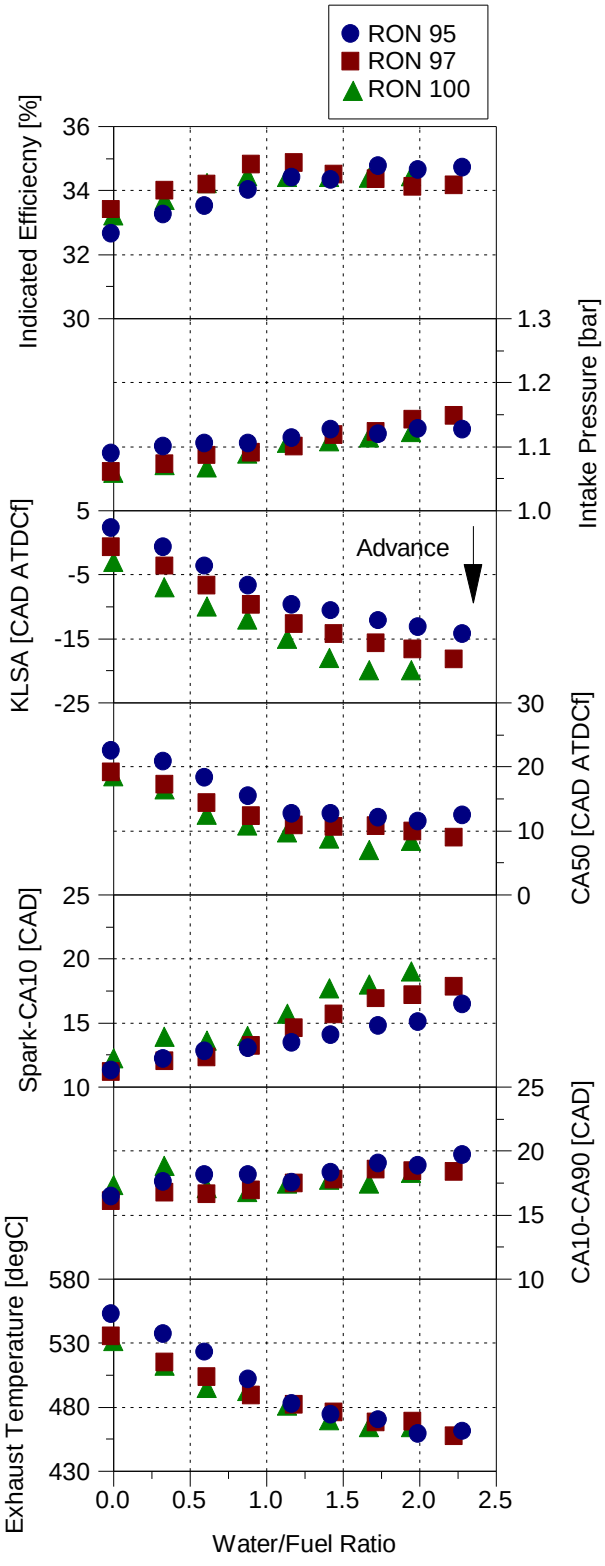

Figure 7-11 Impact of water / fuel ratio sweep on stoichiometric combustion and efficiency at 1000 rpm / 8.83 bar NIMEP for all three fuels

This is due to the fact that combustion phasing with RON 100 and 97 was already very close to optimum (CA50 ~8 CAD ATDC for RON 100 and ~10 CAD ATDC for RON 97) at water/fuel ratio of 1.5, so adding more water could not improve the combustion phasing and in fact had a slight negative effect on flame development angle and combustion duration (Figure 7-11) which were both prolonged. On the other hand, CA50 was around 12 CAD ATDC for RON 95 at water/fuel ratio of around 1.5 and therefore there was still room for improvement in combustion phasing to get closer to CA50 of around 8 CAD ATDC. As the spark timing gets closer to the MBT timing the improvements in combustion phasing and therefore indicated efficiency are less pronounced. The indicated efficiency and CA50 graphs show that when the CA50 is around 12 CAD ATDC, advancing the combustion phasing further does not improve indicated efficiency significantly.

In all three cases as the injected water mass was increased, both flame development angle and combustion duration were prolonged (Figure 7-11), especially with very high water/fuel ratios. Flame development angle increased monotonically by around 7 CAD for all three fuels when comparing the baseline to the maximum water/fuel ratio. Dilution effect of water led to a longer flame kernel initiation and growth period, thus spark-CA10 was increased for all three fuels. Increase in combustion duration, however, was less pronounced (CA10-CA90 only increased around 2 to 3 CAD when comparing the baseline to the maximum water/fuel ratio). Combustion duration of the three fuels was very similar at this test point Adding water and advancing the spark timing initially increased the efficiency by positioning combustion closer to TDC where it is exposed to the high temperature and pressure environment. However, increasing the injected water mass further had a negative effect on combustion and could not improve the

efficiency further. Dilution effect of large quantities of water decreased the air-fuel reactivity which could not be compensated by the more advanced combustion phasing anymore. Therefore, efficiency improvement slowed down in the case of RON 95 or even start to decrease with RON 97 and 100 with excessive amount of water. In addition, too much water also deteriorates the combustion efficiency which can be another reason for lower indicated efficiency with high water / fuel ratios (this will be explained further in Figure 7-13).

Intake pressure is also shown in Figure 7-11, the slight increasing trend in all cases could be due to displacement of some air with the injected water into the intake port. Thus, slightly higher intake pressure was required to compensate for the water displacement. As expected, RON 97 and 100 required slightly lower intake pressure compared to RON 95 due to the more advance spark timings and therefore more advance combustion phasing which was possible when using fuels with higher octane number. As a result, slightly lower intake pressure was required to maintain the same load with higher octane number fuels.

Furthermore, exhaust temperature (Figure 7-11) decreased by a maximum of around 100°C with water injection compared to the baseline for all three fuels mainly due to the advancement in combustion phasing and increased heat capacity of charge. RON 97 and 100 both showed lower exhaust temperatures compared to RON 95 which is also due to the more advance combustion phasing of RON 97 and 100 compared to 95. The lowest exhaust temperature was achieved when using RON 100 as it was expected due to the use of the most advanced spark timings among the three fuels. As it was mentioned in Chapter 6, lower exhaust gas temperature is beneficial especially in turbocharged engines as it eliminates the need for fuel enrichment which is used to suppress knock and

protect the components (turbine and exhaust system) from high temperatures. This can extend the lambda 1 operation area of the engine map. However, excessively low exhaust temperature can reduce the aftertreatment performance.

Figure 7-12 shows the changes in peak in-cylinder pressure, peak in-cylinder pressure rise rate and their corresponding angles as well as the knocking intensity by increasing the injected water mass for all three fuels at the same test point.

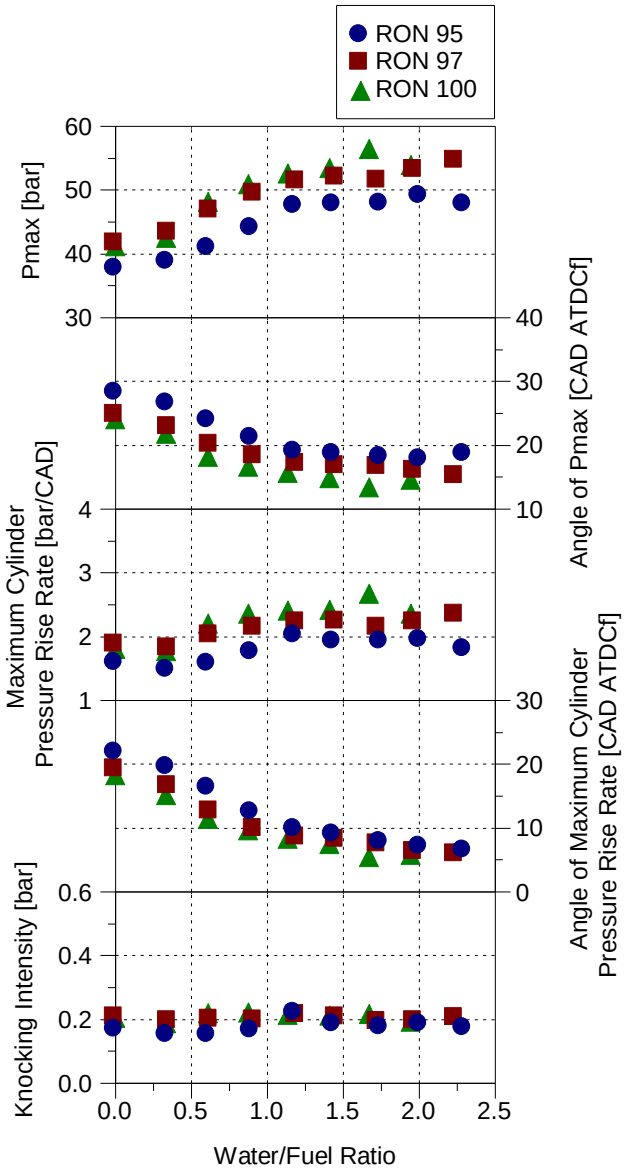

Figure 7-12 Impact of water / fuel ratio sweep on stoichiometric combustion at 1000 rpm / 8.83 bar NIMEP for all three fuels

RON 95 has the lowest peak in-cylinder pressure and also the lowest peak in-cylinder pressure rise rate due to the least advanced spark timing and combustion phasing among the three fuels. Knocking intensity of RON 95 is slightly lower than the other two fuels again due to the least advanced spark timings and lower pressure rise rate.

Impact of water injection on gaseous exhaust emissions and combustion efficiency is shown in Figure 7-13. As can be seen, for all three fuels NO_x emission decreased significantly (around 64% for RON 95 and 97, and around 50% for RON 100 when comparing the baseline to the maximum water/fuel ratio) at the beginning by increasing the injected water mass, but this reduction slowed down gradually and ultimately NO_x emissions stayed the same by increasing the water / fuel ratio beyond 1.5. Lower peak heat release (Figure 7-8 and Figure 7-14) and reduced peak in-cylinder temperature (Figure 7-15) with water injection can be the main reason for lower NO_x emissions compared to the baseline. Dilution effect of water also reduces the flame temperature by increasing the heat capacity of charge which ultimately leads to a reduction in NO_x emissions. NO_x emissions were slightly higher for RON 97 and 100 compared to RON 95 due to the use of more advanced spark timings with higher octane number fuels and therefore higher peak in-cylinder pressures.

Increasing the injected water mass also increased unburned hydrocarbon (UHC) emissions (Figure 7-13) mainly due to the dilution effect of the water. When a large amount of water is injected in the intake port, only part of it evaporates in the intake port before entering the cylinder and the other part could be in the liquid phase. This water enters the cylinder in the liquid phase and decreases the local temperature where the evaporation takes place. This can promote flame

quenching which is a source of increased HC emissions. In addition, post-flame oxidation is also reduced during the late expansion and exhaust strokes with water injection due to the lower peak in-cylinder temperature, another source for increased HC emissions.

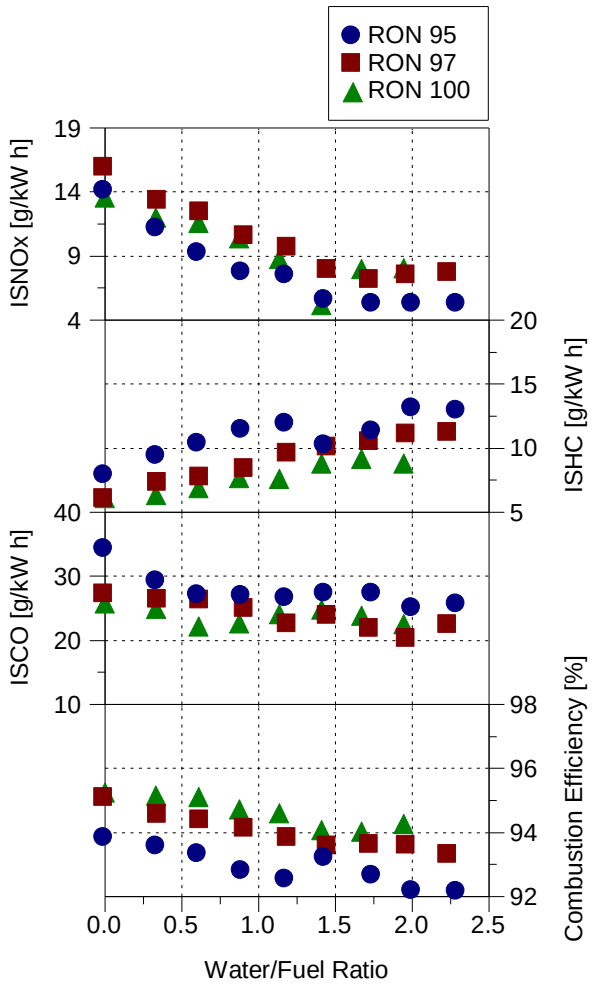

Figure 7-13 Impact of water / fuel ratio sweep on specific exhaust emissions and combustion efficiency at 1000 rpm / 8.83 bar NIMEP

When comparing the three fuels RON 95 produced the highest amount of UHC and RON100 the lowest among the three fuels. This can be due to the difference between the combustion phasing of the three fuels. Higher peak in-cylinder pressure and temperature with RON 100 compared to RON 95 and 97 can result

in higher HC burn up, therefore HC emissions were slightly lower with RON 100. Slightly lower CO emissions also can be due to the dilution effect of water. Increased HC emissions ultimately lead to a lower combustion efficiency. Slightly lower HC and CO emissions led to a higher combustion efficiency with RON 100 compared to the other two fuels.

Figure 7-14 shows the shift of combustion phasing to an optimum position by adding water and advancing the spark timing for RON 95. The graph compares the effect of adding a small quantity of water and the optimized water/fuel ratio with the baseline without water. Improvements in peak in-cylinder pressure and combustion phasing were small when the injected water mass was small due to slight advancement in spark timing. However, as the water/fuel ratio increased to around 1.74, CA50 was advanced by around 10 CAD compared to the baseline. Peak in-cylinder pressure also increased by around 10 bar and shifted towards TDC. Similar shift towards TDC also can be seen in the heat release diagram. Larger amount of water could provide greater cooling for intake air, port and valves, and in the cylinder (some water might enter the cylinder in liquid phase), thus combustion phasing could be advanced more.

At this speed and load combination optimum efficiency (Figure 7-11) was achieved with the water/fuel ratio of around 1.74 for RON 95, 1.20 for RON 97 and 0.88 for RON 100. For RON 95 although maximum efficiency was achieved with water/fuel ratio of around 1.74, the efficiency stayed almost flat from the water ratio of around 1.2 to the maximum water ratio. Peak efficiency occurred with less water for RON 97 and 100 (water / fuel ratio around 0.8) due to lower sensitivity to knock with these higher-octane fuels and therefore spark timings could be more advanced

with the same amount of water. Also, for RON 97 and 100, efficiency became almost flat after reaching its peak with water/fuel ratio of around 0.8.

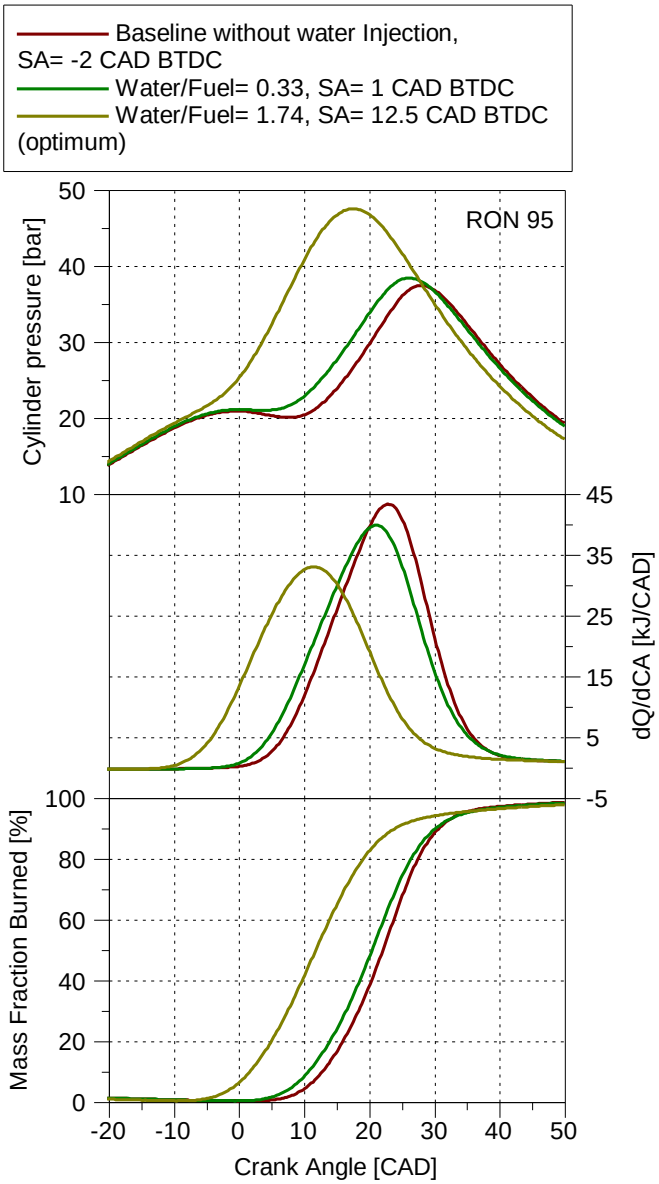

Figure 7-14 Effect of different water / fuel ratios and spark advance on in-cylinder pressure, heat release and MFB at 1000 rpm / 8.83 bar NIMEP (RON 95)

Cylinder temperature against crank angle for two cases, baseline without water injection and with water / fuel ratio of 1.95, is plotted in Figure 7-15. Calculations were performed using the ideal gas law and assuming the mass of residual gas to

be equal to mass of cylinder at the time when exhaust valves just closed (cylinder temperature assumed to be equal to exhaust temperature at this time). Peak cylinder temperature dropped significantly (around 198 K) by adding water to the intake air. This can be the main reason for lower NO_x emissions. In addition, with water injection in-cylinder temperature was around 10 K lower during the compression stroke after the intake valves closure which enabled the use of a more advanced spark timing.

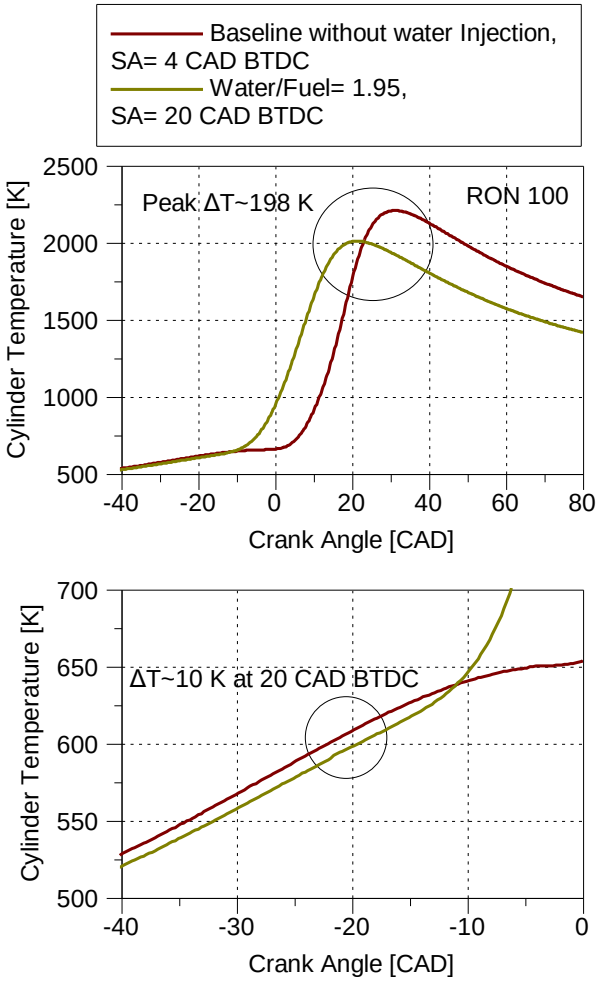

Figure 7-15 Effect of water injection on in-cylinder temperature at 1000 rpm / 8.83 bar NIMEP (RON 100)

Similarly, water injection tests were performed at 2000 rpm / 8.90 bar NIMEP as well for the three fuels. Figure 7-16, Figure 7-17 and Figure 7-18 show the efficiency, combustion characteristics and gaseous emissions during water injection.

Figure 7-16 shows that there was a slight increase in indicated efficiency for RON 95 and 97 when increasing the injected water mass to around 70% of the injected fuel (water/fuel ratio of around 0.7). However, when adding water to the mixture and using RON 100, the efficiency starts to decrease immediately after adding water. The difference between the combustion phasing with these three fuels is the main reason for the difference in efficiency. When using RON 100, CA50 is already around 8 CAD ATDC without adding any water, however, for the other two fuels CA50 was around 10 and 12 CAD ATDC without water injection. Therefore, adding water could help to advance the spark timing for RON 95 and 97 which led to an improvement in efficiency. Whereas for RON 100 adding water only prolonged the initial and the main part of the combustion and did not improve the combustion phasing as it was already optimum (CA50 of around 8 CAD ATDC).

When the water/ fuel ratio is around 0.7 for RON 95, same indicated efficiency as RON 100 without water injection was achieved (Figure 7-16). This shows that adding 15 mg/cycle or 0.25 g/s (water/fuel ratio around 0.7) of water to RON 95 can increase the octane number of this fuel to RON 100. Adding the same amount of water to RON 97 also can boost the octane number of this fuel to RON 100.

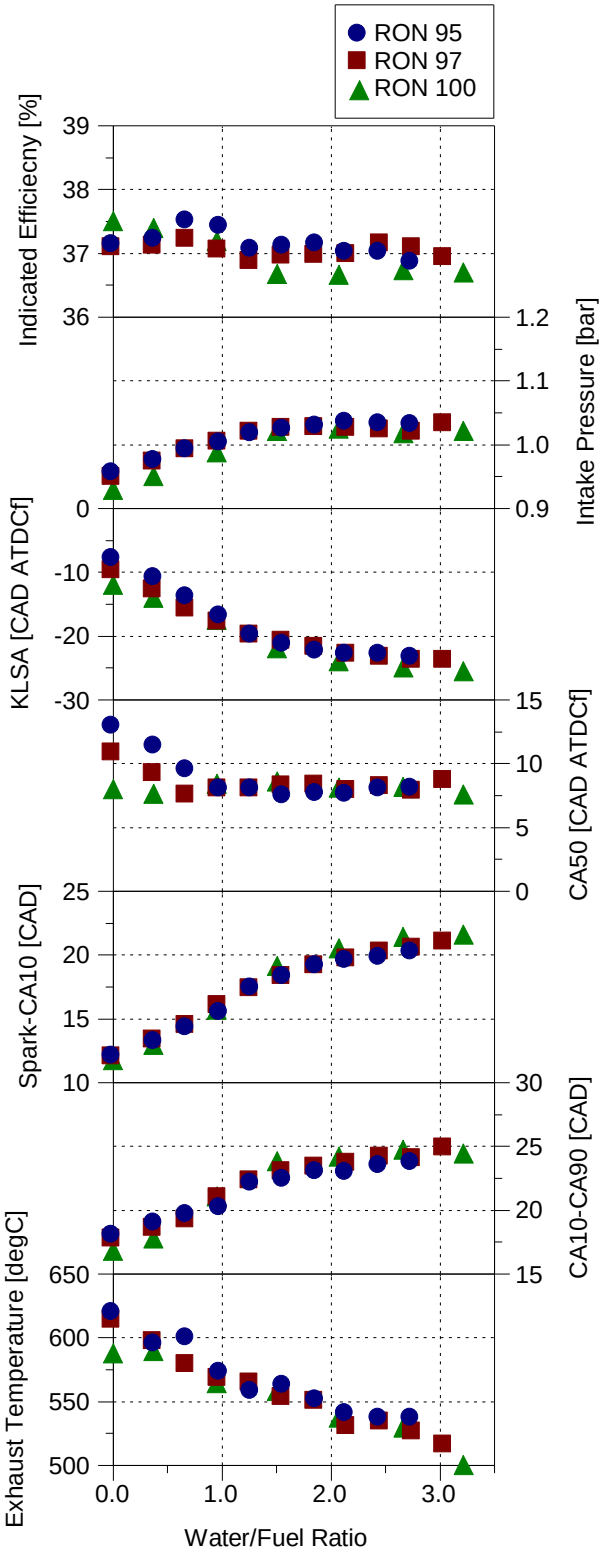

Figure 7-16 Impact of water / fuel ratio sweep on stoichiometric combustion and efficiency at 2000 rpm / 8.90 bar NIMEP for all three fuels

As can be seen in Figure 7-16, flame development angle and combustion duration were both prolonged due to the dilution effect of water as it was also explained for the previous test point. Exhaust temperature decreased due to the advancement of combustion phasing for RON 95 and 97, and more importantly due to the increased heat capacity of charge for RON 100.

At this test point the maximum net indicated efficiency was achieved with the water/fuel ratio of around 0.7 for RON 95 and 97. The maximum efficiency for RON 100 was achieved with no water injection and adding water decreased the efficiency with this fuel. Increasing the injected water mass after this optimum point led to a decrease in efficiency due to the deterioration of combustion duration and combustion efficiency.

Figure 7-17 shows the combustion stability which decreases by increasing the injected water mass at this test point for all three fuels. This was mainly due to the slower combustion which could not be compensated by combustion phasing at this test point. Knocking intensity also clearly decreased since there was not much advancement in combustion phasing and the peak in-cylinder pressure rise rate was almost remained constant throughout the water/fuel ratio range.

Although at this test point indicated efficiency did not improved significantly or there was a slight decrease in efficiency with water injection, NO_x emissions (Figure 7-18) dropped significantly by around 80% for all three fuels. This large reduction in NO_x emissions was mainly due to the dilution effect of water which led to the increased heat capacity of charge and decrease peak in-cylinder temperature as it was shown in Figure 7-15 and also Chapter 6.

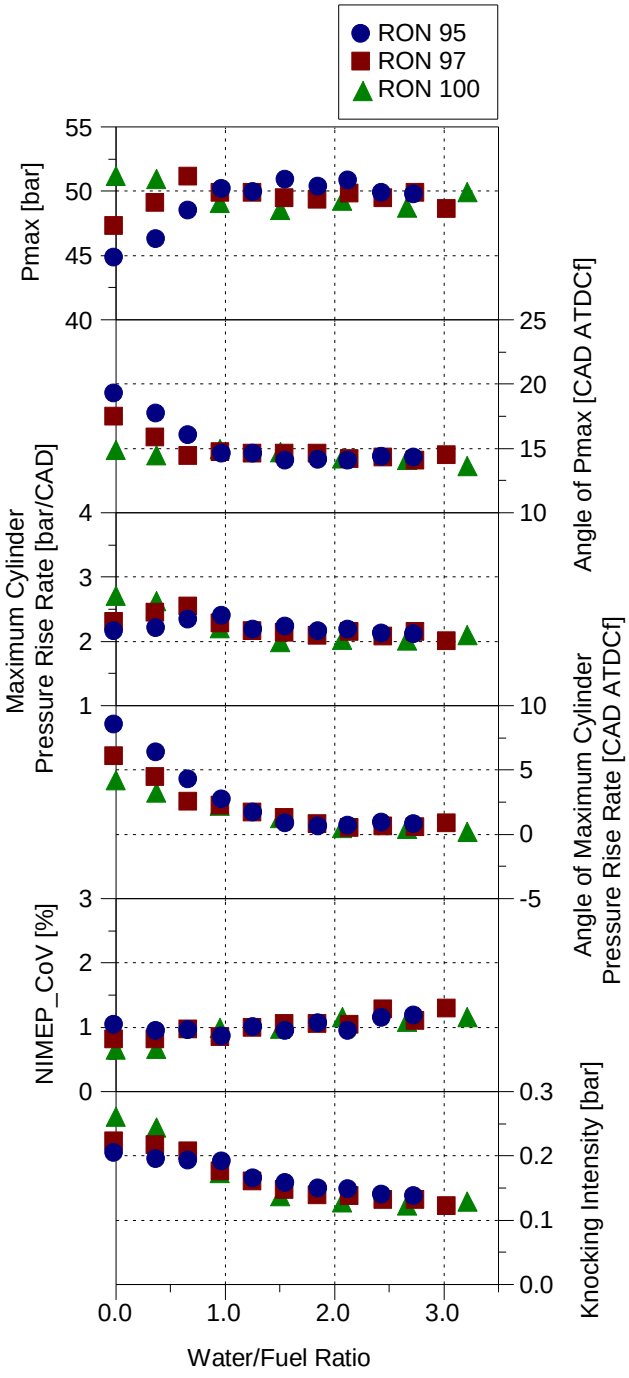

Figure 7-17 Impact of water / fuel ratio sweep on stoichiometric combustion at 2000 rpm / 8.90 bar NIMEP for all three fuels

Figure 7-18 also shows the increase in HC emissions for all three fuels as the injected water mass increase. As it was mentioned earlier this is mainly due to the

dilution effect of water which promotes flame quenching and reduces the post flame oxidation of HC during late expansion stroke and exhaust stroke.

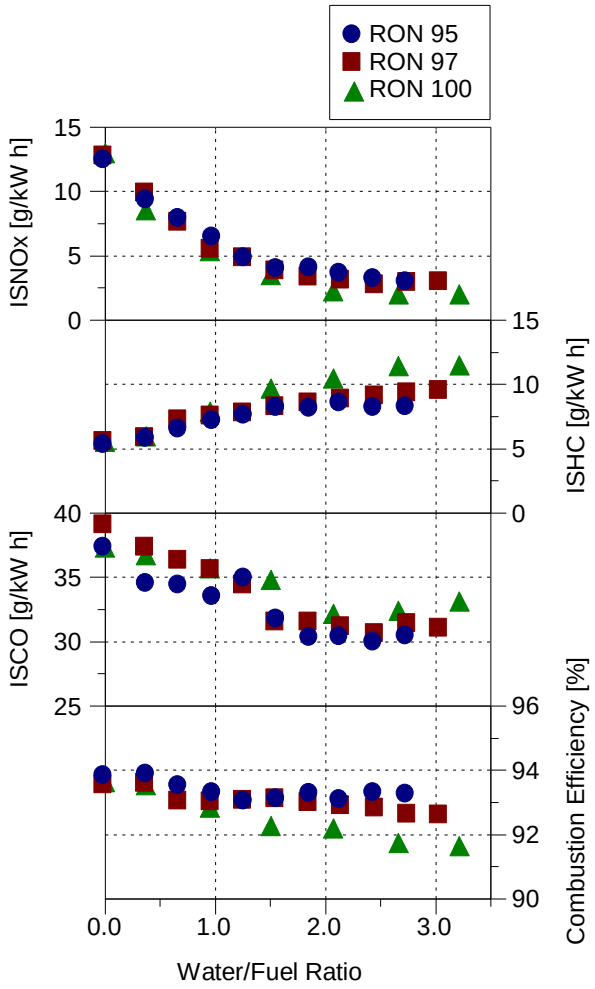

Figure 7-18 Impact of water / fuel ratio sweep on specific exhaust emissions and combustion efficiency at 2000 rpm / 8.90 bar NIMEP

7.3.3 Effects of water injection on gasoline octane number, engine performance and emissions at high-load condition

Since water injection at low speed and medium load was promising and effective in knock mitigation, experiments also were carried out to study the effect of water injection on high load at different speeds under stoichiometric air/fuel ratio for three fuels. The same test procedure as the previous section was followed in this section

for the high load points. Water/fuel ratio sweep, and simultaneous optimization of spark timing were performed. Water/fuel ratio was increased to a maximum level until there was no apparent improvement in efficiency. The maximum water/fuel ratio was slightly more than 3 which was recorded at 3000 rpm / 16.04 bar NIMEP for all three fuels.

Figure 7-19 shows the impact of water injection on efficiency and combustion characteristic for the three fuels at 2000 rpm / 16.04 bar NIMEP. As the injected water mass increased, the knock limited spark timing could be advanced which led to a significant improvement of indicated efficiency. Indicated efficiency increased to a maximum value as the water mass increased due to mitigation of knock. However, increasing the injected water beyond the optimum value could not improve the efficiency further and in some cases, it even led to a decrease in indicated efficiency.

The indicated efficiency graph (Figure 7-19) also shows the relation between the amount of water injected and the octane number of fuel. When the water / fuel ratio is around 0.5, indicated efficiency achieved with RON 95 is almost equal to the indicated efficiency achieved with RON 97 without water. This means, adding around 21 mg of water per cycle (equal to 0.35 g/s or water / fuel ratio of 0.5) to RON 95 can increase the octane number of gasoline from 95 to 97. Increasing the water / fuel ratio further to 0.8 or adding 33 mg/cycle of water to the mixture could increase the octane number of RON 95 even higher to 100. When the water/fuel ratio is around 0.8 the indicated efficiency obtained with RON 95 is almost equal to the indicated efficiency obtained with RON 100 without water. This is important in analysing the effect of water on octane number of gasoline.

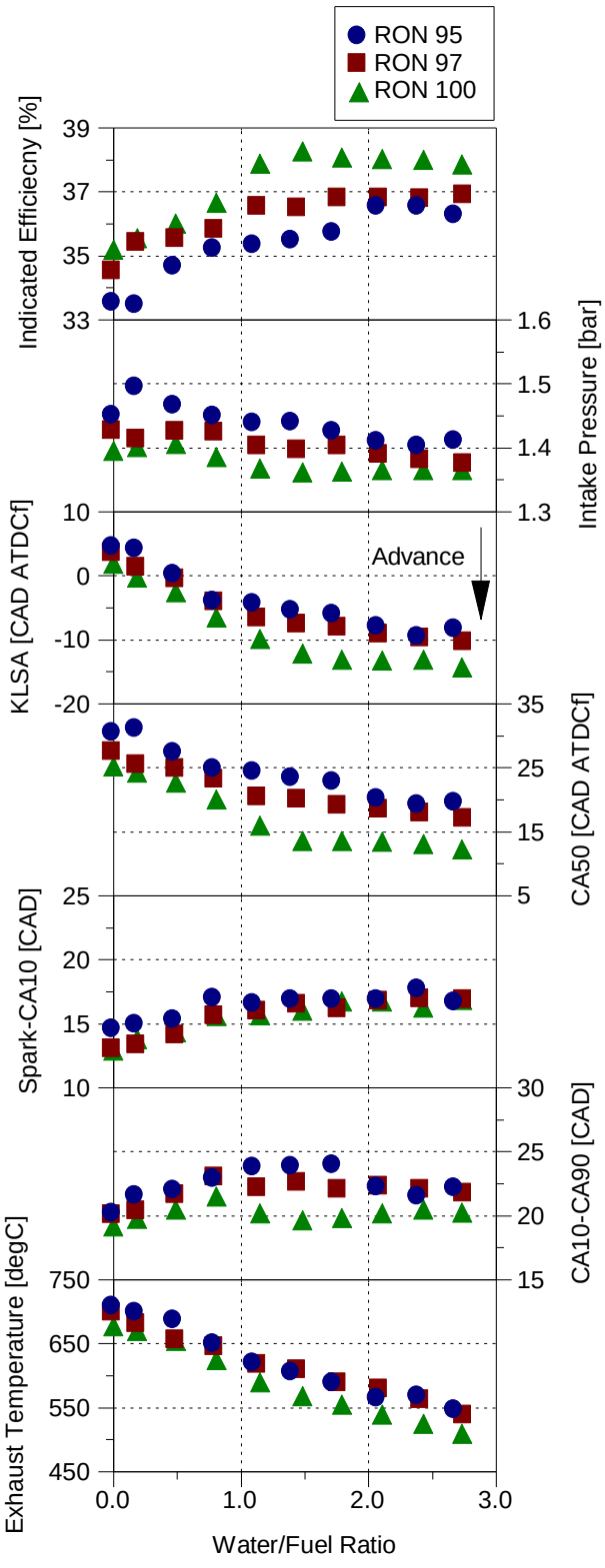

Figure 7-19 Impact of water / fuel ratio sweep on stoichiometric combustion and efficiency at 2000 rpm / 16.04 bar NIMEP

With RON 95 the highest indicated efficiency was slightly more than 36% which was achieved with water/fuel ratio of around 2.1. Increasing the injected water mass further did not improve the efficiency and it stayed almost flat. With RON 97 this almost flat area or maximum efficiency area of the curve is achieved at around water / fuel ratio of 1.8 and stayed almost the same as the water ratio was increased further. Maximum efficiency achieved with RON 97 was around 37%. With RON 100 even less water (water/fuel ratio of around 1.5) was required to reach the maximum efficiency (around 38%). This trend shows that as the octane number of fuel increases, less water is required to obtain the optimum efficiency.

The maximum indicated efficiency for RON 95 is achieved when the water/ fuel ratio is around 2. However, the same efficiency was achieved with RON 97 when the water/fuel ratio is only around 1.2 and also the same efficiency was achieved with RON 100 when water/fuel ratio was only around 0.8.

In all cases, the initial part of the combustion (spark to CA10) prolonged by increasing the water / fuel ratio (Figure 7-19). As it was mentioned in the previous test point, the main reason for this is the dilution effect of water which makes it difficult to initiate and stabilize the flame kernel after spark discharge. Combustion duration also increases slightly by addition of small mass of water at the beginning. For most of these test points spark timing was very close to TDC or after TDC where the piston started to move down and expand. Therefore, the combustion occurred in lower ambient temperatures and pressures as well as cylinder volume expansion. Spark timing could be advance only slightly at the beginning by adding small quantity of water. Thus, the negative effect of charge dilution could not be compensated by the slightly advanced combustion phasing. However, Increasing the water/fuel ratio to around 1.5 decreases the combustion duration slightly again

for all three fuels. This is because there is enough water to cool down the charge enough for a more advanced spark timing. Hence, the effect of advance combustion phasing was more pronounced this time as the combustion phasing was closer to TDC and combustion was exposed to a higher temperature and pressure environment near TDC. Moreover, as the injected water was increased further to its maximum level (water / fuel ratio of around 2.7), combustion duration increased again for RON 95 and 100, and efficiency dropped slightly due to the decreased reactivity of air-fuel mixture with higher dilution effect of water.

In terms of combustion phasing (Figure 7-19), RON 100 shows the most advanced CA50 compared to the other two fuels due to the higher octane number and therefore higher knock tolerance which allowed the use of the most advanced spark timings compared to the other two fuels. This also led to the lower required intake pressure (boost pressure) for RON 100 compared to the other fuels to achieve the same load.

Furthermore, exhaust temperature (Figure 7-19) also decreased significantly by around 150 °C for all three fuels which, as it was explained in the previous section, was due to the more advanced combustion phasing and increased heat capacity of charge. This can eliminate the need for fuel enrichment and extend the operation area under stoichiometric condition as well as reducing the unburned combustion products specifically CO which is high under fuel-rich conditions. RON 100 also shows the lowest exhaust temperature due the most advance combustion phasing among the three fuels.

Figure 7-20 also shows that RON 100 produced the highest peak in-cylinder pressure, the highest peak in-cylinder pressure rise rate and the highest

combustion stability compared to the other two fuels with lower octane numbers. This is also mainly due to the more advance spark timings and therefore more advanced combustion phasing with RON 100. As it was mentioned before faster and earlier combustion of RON 100 led to higher peak in-cylinder pressure and less variations in NIMEP.

Figure 7-21 shows that the unburned HC emissions increased for all three fuels as the injected water mass increased, mainly due to the dilution effect of water. The reason for this can be a decrease in local in-cylinder temperature with water injection which can cause quenching and ultimately increase the HC emissions. NO_x emissions decreased by around 60% for all three fuels mainly due to a lower peak in-cylinder temperature by water injection. CO emissions also decreased for all three fuels to a minimum level then stayed almost constant as the injected water quantity increased. This decrease in CO emissions can be due to the dilution effect of water which resolves the relatively fuel-rich areas (such as the area near the injector tip and spark plug which has a lower local lambda) in the cylinder. Furthermore, there was a slight increase in combustion efficiency for all three fuels when adding a small quantity of water at the beginning (water/fuel ratio around 0.2) due to lower CO emissions. However, Combustion efficiency decreased again soon after increasing the injected water mass due to increased HC emissions.

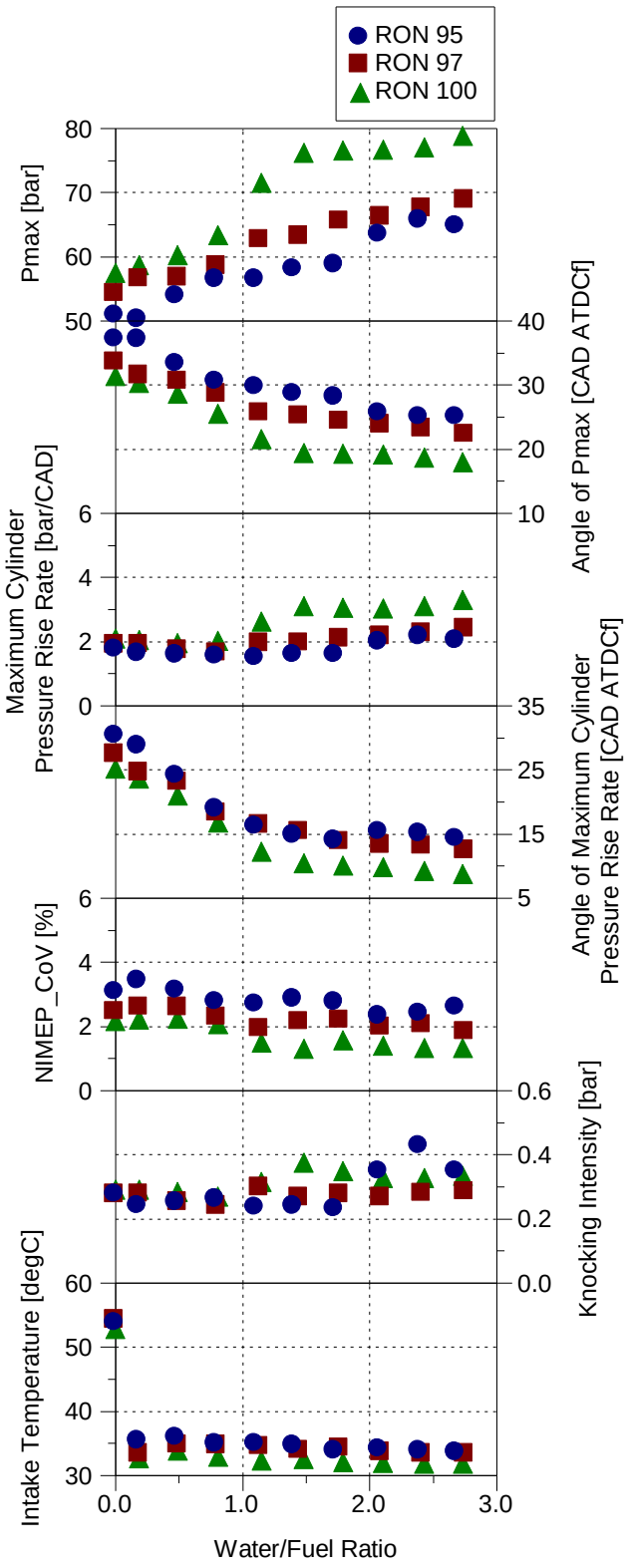

Figure 7-20 Impact of water / fuel ratio sweep on stoichiometric combustion at 2000 rpm / 16.04 bar NIMEP

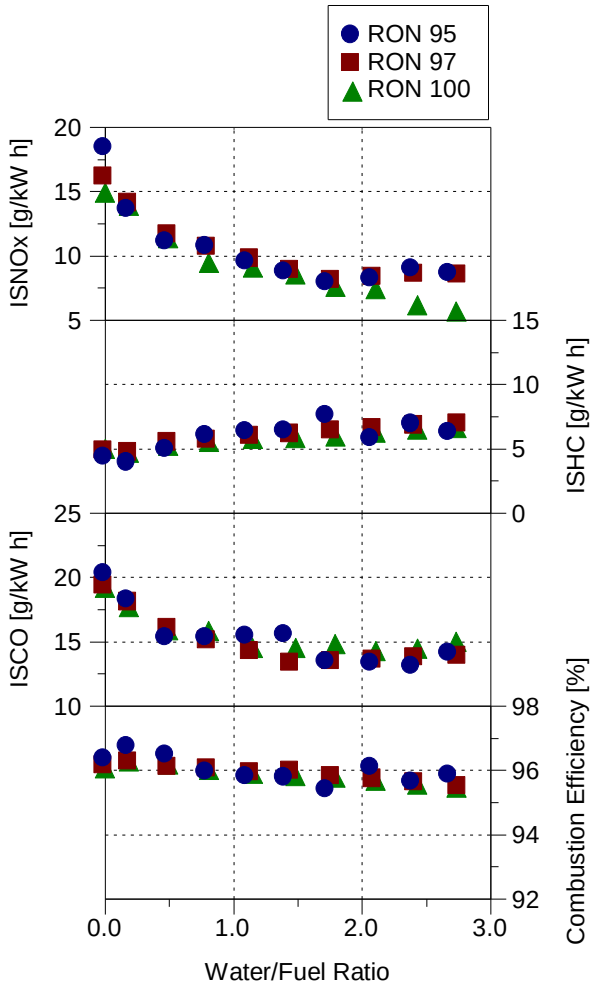

Figure 7-21 Impact of water / fuel ratio sweep on specific exhaust emissions and combustion efficiency at 2000 rpm / 16.04 bar NIMEP

Figure 7-22 shows the impact of small and optimum quantity of water on in-cylinder pressure, heat release and MFB history at 2000 rpm / 16.04 bar NIMEP for RON 100. As the injected water mass increased to the optimum level, peak cylinder pressure increased considerably and shifted towards TDC due to the advancement of the combustion phasing. This shift towards TDC also can be seen in heat release and MFB curves.

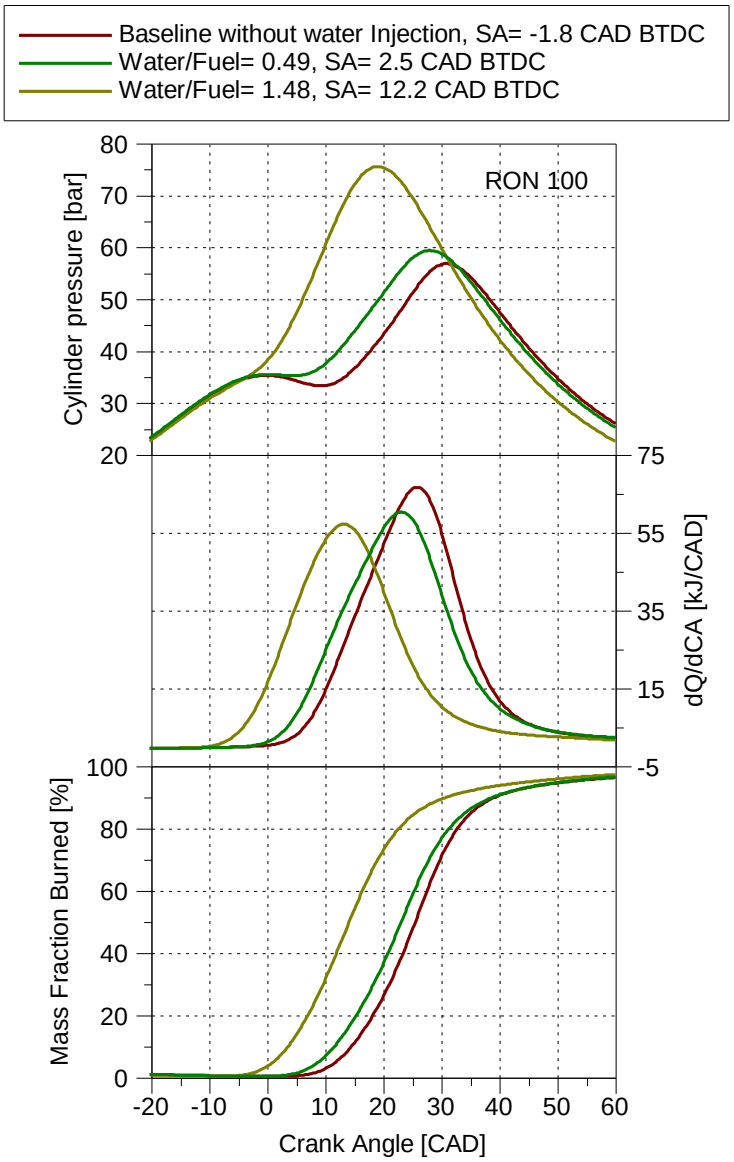

Figure 7-22 Effect of different water/fuel ratios and spark advance on in-cylinder pressure, heat release and MFB at 2000 rpm / 16.04 bar NIMEP (RON 100)

The difference between the in-cylinder temperature of the baseline and the optimum water injection case during the late compression and the early expansion strokes at 2000 rpm / 16.04 bar NIMEP for RON 97 is shown in Figure 7-23. In-cylinder temperature was calculated using the same method which was explained in the previous section. Temperature started to rise earlier in the cycle after the

spark discharge for the water injection case due to a more advanced spark timing and combustion phasing. Water injection decreased the charge temperature and pressure and allow the advancement of spark timing during the compression stroke. In-cylinder temperature was around 40 K lower than the baseline during compression at the time of spark ignition. The injected water increased the heat capacity of the charge and absorbed more heat from the surroundings during compression stroke, therefore in-cylinder temperature was lower. Peak in-cylinder temperature was also significantly lower with water injection (around 260 K), which can be the main reason for lower NO_x emissions.

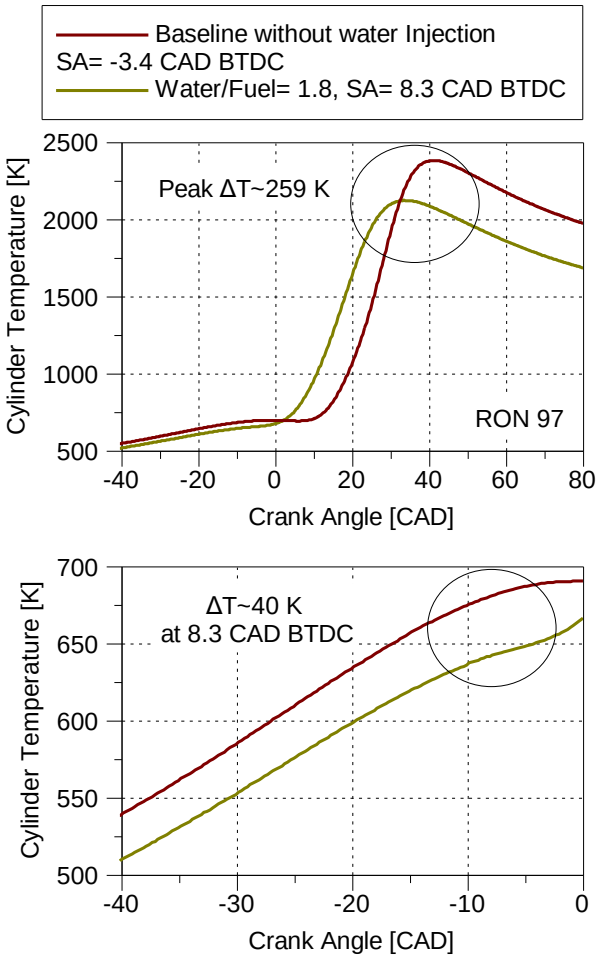

Figure 7-23 Effect of water injection on in-cylinder temperature at 2000 rpm / 16.04 bar NIMEP (RON 97)

Figure 7-24, Figure 7-25 and Figure 7-26 show the effect of water injection on octane number of the fuel, combustion characteristic, efficiency and emissions at 3000 rpm / 16.04 bar NIMEP. At this test point similar results to 2000 rpm / 16.04 bar NIMEP were achieved.

As shown in Figure 7-24, when increasing the water/fuel ratio to around 1 with RON 95, the same efficiency as RON 100 without water can be achieve. Therefore, the octane number of RON 95 can be boosted to RON 100 with the water /fuel ratio of around 1.

When increasing the water/fuel ratio to around 0.5 with RON 95, same efficiency as RON 97 can be achieved without water. Therefore, octane number of RON 95 can be increased to RON 97 with water/fuel ratio of around 0.5.

In addition, octane number of RON 97 can be increased to RON 100 when the water/fuel ratio is around 0.8. The highest indicated efficiency is slightly more than 38% at this point which is achieved using RON 100 with the water/fuel ratio of around 1.8. More advanced spark timings were used with higher octane number fuel of RON 100 which advanced the combustion phasing more than the other two fuels. Combustion was also faster slightly faster with RON 100 at this test point (Figure 7-24).

Furthermore, as can be seen in Figure 7-25, lower exhaust temperature and higher combustion stability was achieved with RON 100 due to the more advanced combustion phasing, increased heat capacity of charge (for lower exhaust temperature) and faster combustion.

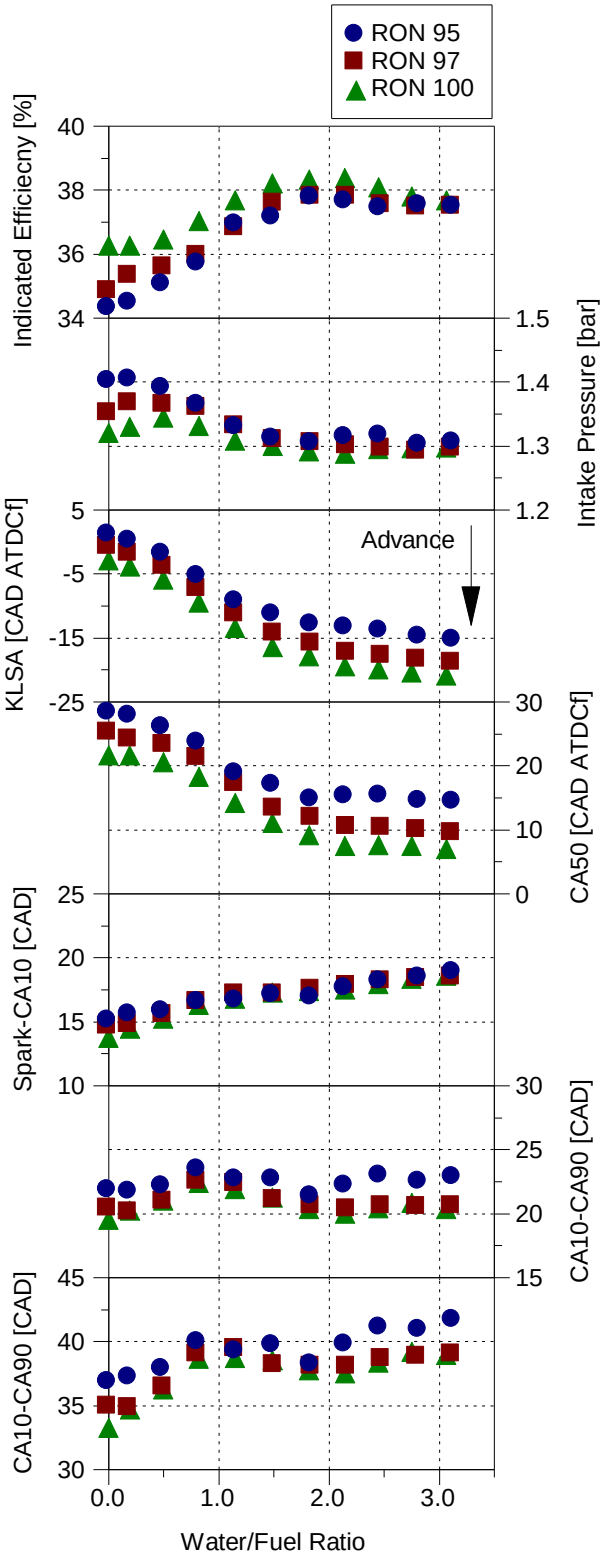

Figure 7-24 Impact of water / fuel ratio sweep on stoichiometric combustion and efficiency at 3000 rpm / 16.04 bar NIMEP

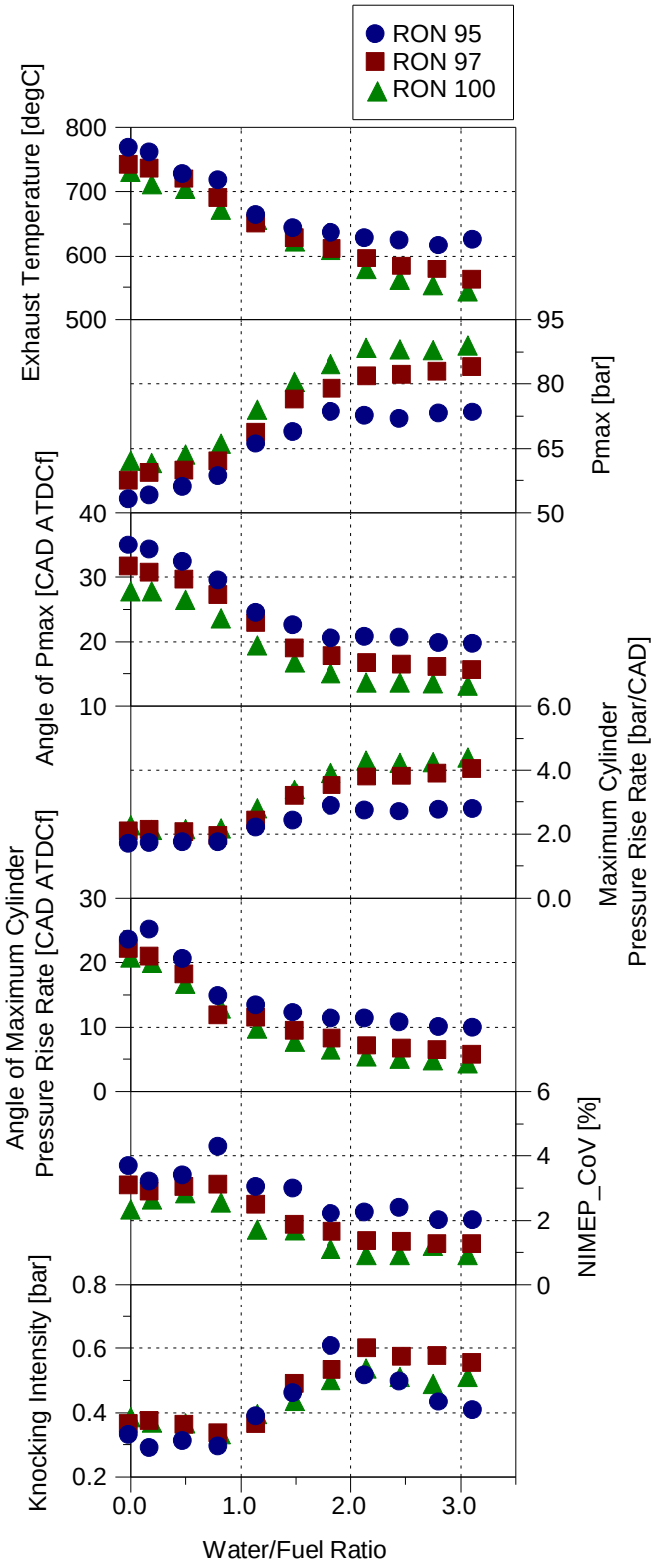

Figure 7-25 Impact of water / fuel ratio sweep on stoichiometric combustion at 3000 rpm / 16.04 bar NIMEP

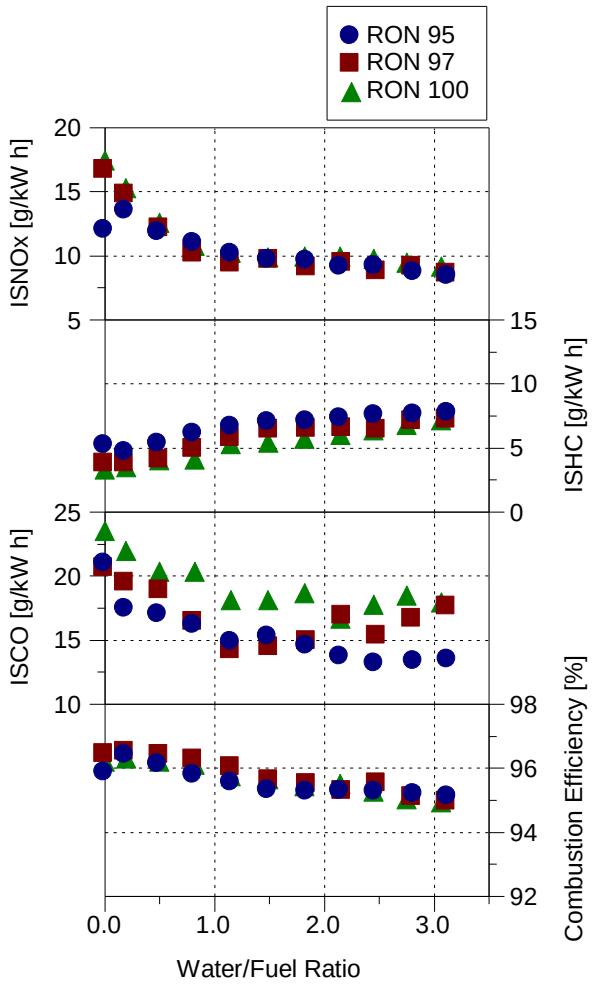

Figure 7-26 Impact of water / fuel ratio sweep on specific exhaust emissions and combustion efficiency at 2000 rpm / 16.04 bar NIMEP

Figure 7-27, Figure 7-28 and Figure 7-29 show another example of water injection and its impact on octane number of gasoline, combustion characteristic, efficiency and emissions at 3000 rpm / 20 bar NIMEP. The effect of adding water and advancing the spark timing was explained in detail for the previous test points in this chapter and the previous chapter. This test point also follows the same trend by increasing the water/fuel ratio in terms of efficiency, combustion characteristic and emissions. At this test point increasing the water/fuel ratio to around 1.3 can boost the octane number of RON 97 to RON 100.

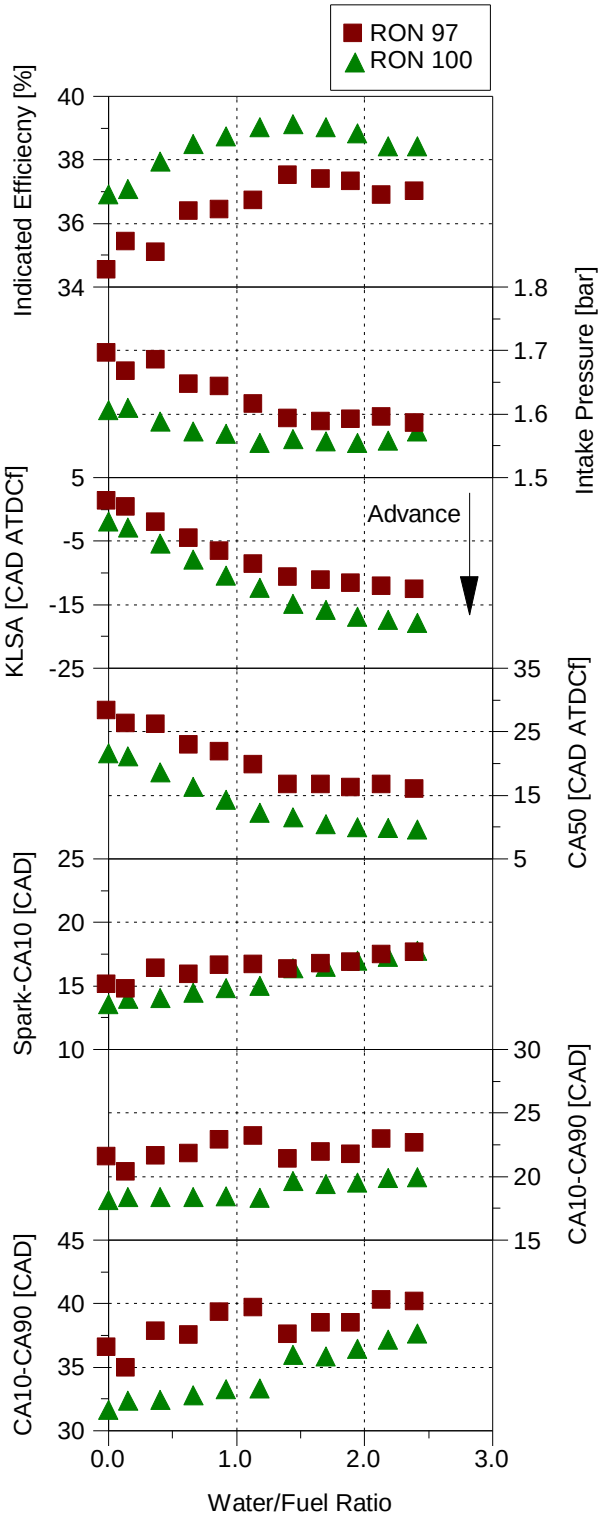

Figure 7-27 Impact of water / fuel ratio sweep on stoichiometric combustion and efficiency at 3000 rpm / 20 bar NIMEP

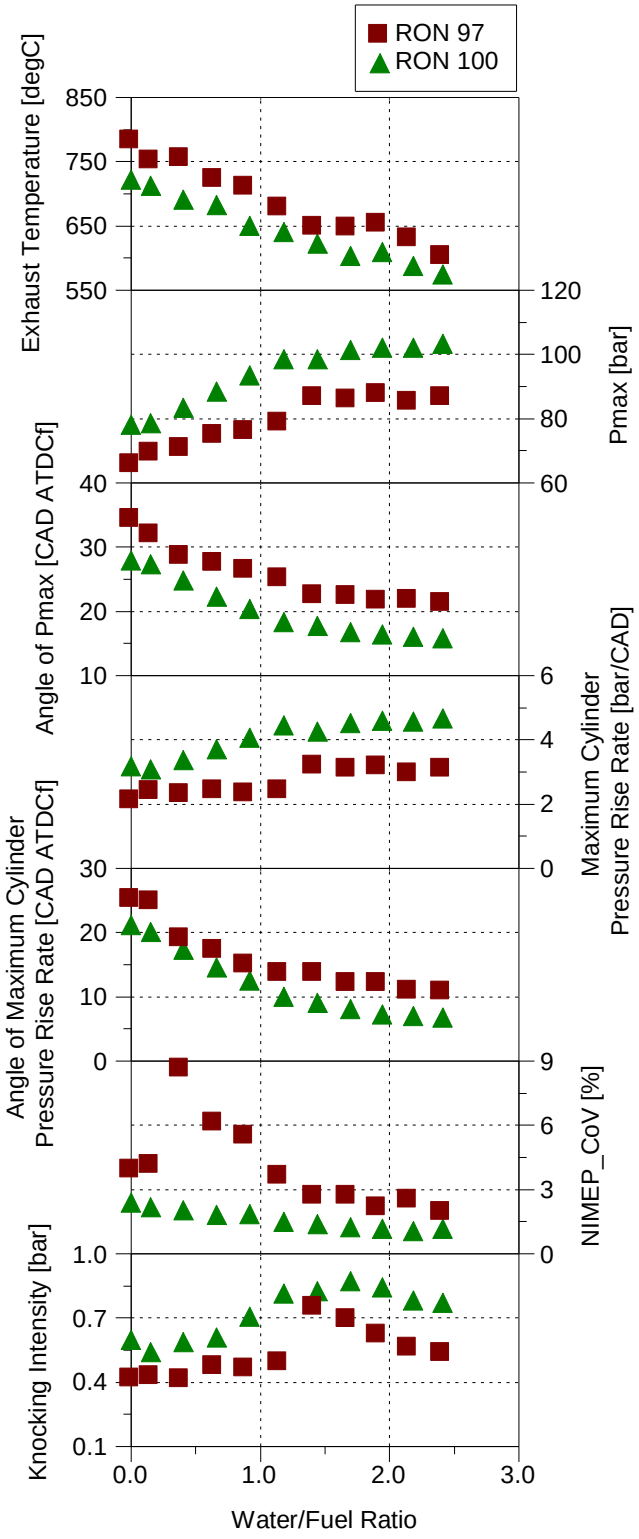

Figure 7-28 Impact of water / fuel ratio sweep on stoichiometric combustion at 3000 rpm / 20 bar NIMEP

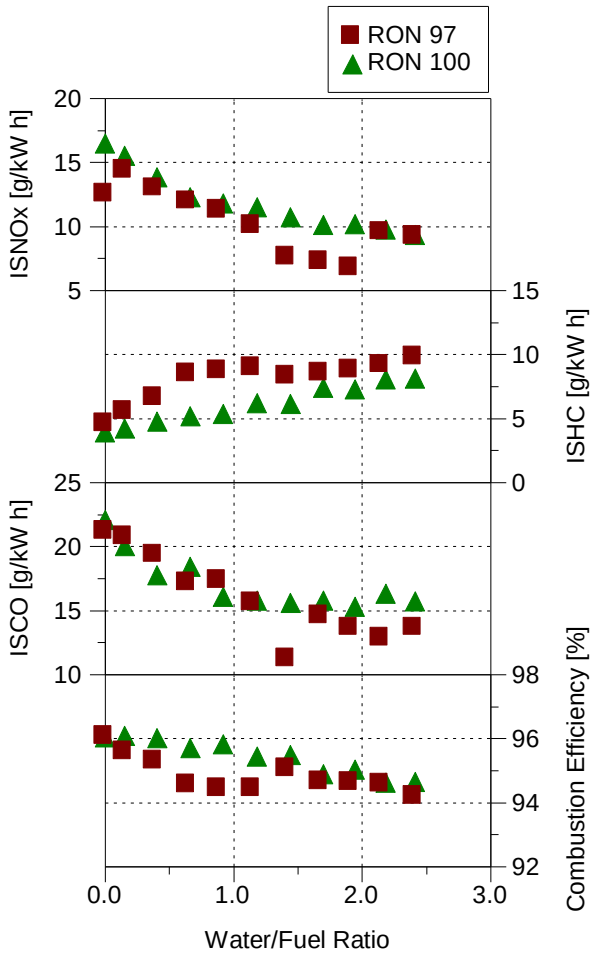

Figure 7-29 Impact of water / fuel ratio sweep on specific exhaust emissions and combustion efficiency at 3000 rpm / 20 bar NIMEP

7.4 Summary

The aim of this chapter was to investigate the impact of intake port water injection on octane number of fuel, performance, fuel consumption and exhaust emission of a boosted downsized single cylinder GDI engine. Gasoline with three research octane number (RON) of 95, 97 and 100 was injected directly into the cylinder, while water was port injected. During these experiments water injection timing and pressure were remained constant at 90 CAD BTDCf and 5 bar respectively. Several steady state points from medium to high load (8.83 to 20 bar NIMEP) and

low to high speed (1000 to 3000 rpm) where the knock start to occur were selected for these experiments. Experiments first began by performing a spark timing sweep without water injection for all the three fuels at each test point in order to find the baseline and check the performance of the engine with each fuel. Then the water/fuel ratio sweep was performed by adding water and increasing the injected water mass until there was no apparent improvement in efficiency for all three fuels. At the same time, spark timing was also adjusted to its most advanced timing. Finally, the data for all three fuels and all the test points were analysed and compared to the baseline without water injection.

The main findings of this chapter reveal that when comparing the results of the three fuels, water injection can virtually increase the RON of fuel, therefore makes it possible to run the engine on a low octane number fuel and achieve higher efficiency by adjusting the water mass in order to increase the octane number of a fuel. This improvement in octane number of gasoline was shown for all the six tests point. However, different amount of water is required at different test points to increase the octane number of fuel to a certain number. This depends on how knock limited the combustion is at that specific test point. Therefore, more water is required at more knock limited test points to increase the octane number of fuel. Adding 33 mg/cycle of water to the mixture can increase the RON of gasoline from 95 to 100 at 2000 rpm / 16.04 bar NIMEP. Octane number of gasoline can be increased from 97 to 100 when the water/ fuel ratio is around 1.2 at 3000 rpm / 20 bar NIMEP.

In addition, at 2000 rpm / 8.90 bar NIMEP water injection could not improve the efficiency significantly since the combustion phasing was close to optimum without

water injection. However, at this point water injection was very effective to decrease the NO_x emissions for all three fuels similar to other 5 test points.

Chapter Eight

Conclusion and Future Work

Chapter 8 Conclusion and Future Work

8.1 Conclusion

In this study extensive engine experiments were performed in order to study the effect of port and direct fuel injection strategies as well as the effect of intake port water injection on a downsized GDI engine.

Port and direct injection strategies including PFI only, DI only, PFI / late DI, PFI / early DI, DI / late DI were investigated. Injection timing sweep were performed for the late DI to find out the optimum injection timing which gives the highest indicated efficiency. In addition, ratio sweep tests were also performed for PFI / DI and DI / DI cases in order to understand the effect of fuel ratio between PFI and DI on combustion and emissions. These strategies were tested under both stoichiometric and lean air/fuel ratios to understand the effect of these injection strategies on lean combustion and its emissions.

The results of these PFI / DI strategies are presented in Chapter 4 and 5 of this thesis which compare the combustion, fuel economy and emissions of the baseline strategy (PFI only and single early DI) to the PFI / late DI and early DI / late DI injection strategies on the boosted DISI gasoline engine. The results show that there is an optimum injection timing for the late DI which directly affects fuel economy and emissions. When using PFI / late DI or early DI / late DI strategy at the stoichiometric air / fuel ratio, the optimum injection timing was found to be 60 CAD BTDC at 1000 and 2000 rpm and 90 CAD BTDC at 3000 rpm for low and mid-high load operating points. When the optimum late DI injection was used, it led to faster flame propagation and reduced tendency to knocking combustion due to the cooling effect of the late DI injection which reduced the in-cylinder

temperature, so the knock limited spark timing could be advanced more, and the combustion process could take place near the TDC for maximum efficiency. Retarding the late DI injection timing from its optimum point increases the under-mixing effect which forms fuel-rich areas and unburned combustion products such as CO and smoke emissions. Therefore, combustion efficiency is lower with the very late DI timings. Advancing the late DI timings increased the charge temperature and knocking tendency, therefore forces the use of less advanced spark timings which has a negative effect on combustion timing and efficiency. Cases with Late DI injection generally have higher CO emissions compared to the baseline due to the late DI injection which led to a formation of fuel-rich areas around the spark plug. In addition, when comparing different late DI timings, UHC emissions tended to be higher as the late DI injection was advanced. PFI / late DI operations produced significantly lower smoke emissions and lower UHC emissions than those with the single early DI injection.

Furthermore, the slope of the compression curve on Log P-Log V diagram also revealed the effect of late DI timings on heat transfer and the charge temperature at the time of ignition right after the late DI injection. Late DI injection ratio greatly affects the mixture temperature and homogeneity. Minimum NISFC was achieved when the late DI ratio was around 40% for both PFI / late DI and early DI / late DI cases at the testing condition. Very low ratios of late DI were not able to provide sufficient cooling effect to decrease the charge temperature. Therefore, combustion timings were retarded, and efficiency was lower. Very high ratios of late DI increased the unburned combustion products such as CO, HC and smoke emissions and result in low combustion efficiency. High ratios of late DI reduced the charge temperature more and result in more advance combustion timings and

reduced exhaust temperature. PFI / late DI and early DI / late DI cases can reduce the fuel consumption significantly compared to baseline PFI only and DI only cases across the lambda range. Strong cooling effect of the late DI injection which affects the heat transfer rate and charge temperature during the late compression stroke is the main reason for higher efficiency at the knock limited points. Lean combustion stability limit was extended from lambda 1.4 to lambda 1.7 with PFI / late DI strategy. Reduced HC and smoke emissions and lower exhaust temperature across the lambda range are the other advantages of this dual injection system.

The second part of the research was focused on the effect of intake port water injection on the engine efficiency and emissions. The experiments include spark timing sweep for the baseline without water injection, water / fuel ratio sweep and spark timing sweep with water injection in order to find out the optimum water / fuel ratio at each test point and its impact on combustion and emissions. The tests were performed at 6 steady state test points which include mid and high-load conditions and represent the conditions at which knocking combustion occur. In addition, these experiments were performed using gasoline with three different research octane numbers of 95, 97 and 100 in order to determine the effective octane number of water injection. The efficacy of water as an anti-knock agent was also evaluated at each test point. The difference between closed intake valve water injection and opened intake valves water injection was investigated in terms of efficiency, combustion, water consumption and emissions.

The results in chapter 6 and 7 revealed that the intake port water injection mitigated the possibility of knock occurrence at medium and high load conditions

when the combustion was knock limited. Hence, spark timing could be advanced further which shifted the combustion phasing to the optimum point and increased the indicated efficiency. Water / fuel ratio was increased to a maximum level until there was no improvement in efficiency. The highest level of water injected was between 200 and 300% of the mass of fuel at various speed and loads. There was a significant improvement in efficiency as the water/fuel ratio increased to its optimum value specially at high load conditions. Improvement in efficiency was mainly due to the cooling effect of the injected water evaporation which reduced the in-cylinder temperature and pressure. Thus, knock sensitivity was reduced and more efficient spark timings could be used which shifted the combustion phasing closer to the optimum point. The improvements in combustion phasing also led to a lower exhaust gas temperature. Increased heat capacity of charge is also another reason for lower exhaust gas temperature with water injection. Lower exhaust gas temperature is beneficial especially in turbocharged engines to protect the turbine and exhaust system and reduces the need for enrichment.

Also, the results revealed that there is an optimum water/fuel ratio for each test point. Increasing the injected water mass further decreased the efficiency and increased the unburned combustion products such as HC emissions. This was mainly due to the prolonged flame development angle and combustion duration, and decreased combustion efficiency with higher HC emissions due to the dilution effect of water. In addition, too much water decreased the in-cylinder pressure after combustion during expansion stroke due to increased heat capacity of charge, thus the net integrated work area of the P-V diagram was reduced.

Improvements in efficiency with water injection were lower at higher engine speed (for example 2000 rpm compared to 3000 rpm). The main reason for this could be the increase in intrinsic knocking tolerance by increasing engine speed as knocking combustion is more likely to happen at low engine speeds.

Comparing the results of the three fuels reveals that water injection can virtually increase the RON of fuel, therefore makes it possible to run on a low octane number fuel and achieve higher efficiency by adjusting the water mass. The results of experiments with RON 95, 97 and 100 show that the effect of water in increasing the octane number of fuel is different at each test point.

Intake port water injection in the opened intake valves showed no or small different compared to the close intake valves injection at most test points. The small differences could be due to the presence of higher percentage of liquid water in the cylinder.

In terms of emission, intake port injection of water is capable of reducing NO_x emissions significantly at all test points mainly due to a lower peak in-cylinder temperature. HC emissions, however, increased with water injection due to the cooling and dilution effect of water which decreased the combustion temperature and promoted flame quenching. Lower in-cylinder temperature also leads to lower cylinder wall temperature and reduces the post-flame oxidation effect during expansion and exhaust strokes. CO emissions were reduced with water injection. Number of particles emitted dropped significantly up to a minimum value by using water injection and more advanced spark timings. Increasing the water / fuel ratio further increased the number of particles again.

8.2 Recommendations for Future Work

More works will be needed to fully explore the potential of the PFI / DI strategies by injecting different fuels through each injector under different load and speed conditions. A combination of fuels with different research octane number and different properties such as low octane number gasoline / high octane number gasoline, gasoline / ethanol, gasoline / diesel and gasoline / CNG can be injected from each injector in order to improve the efficiency and emissions.

In addition, in-cylinder studies of the mixture formation and combustion in an optical engine is required in order to better understand the physical and chemical process involved in the ignition and combustion process of different PFI / DI and DI / DI injection strategies.

Intake port water injection strategy was investigated in this study at medium and high loads. There is a potential to extend the lambda 1 operation area of the engine map with this strategy. Therefore, experiments at high speed and full load test points with and without exhaust back pressure also need to be conducted to show the potential of intake port water injection strategy at the enrichment part of the engine map.

As it was mentioned earlier, in this study fuel was directly injected into the cylinder by DI and water was port injected by PFI. However, direct injection of water can be more effective similar to direct injection of fuel as it is also reported in the literature [188]. With direct injection of water higher cooling effect is expected from the same amount of water compared to port injection. In addition, direct injection of both fuel and water can create a synergy and increase the effectiveness of both

systems [139–141,182]. On the other hand, this leads to a more complex control and calibration process to optimize different parameters such as injection quantity, timing and pressure for both fuel and water. The design of the combustion system with two direct injectors also is another issue which makes the optimization more complex. Water and fuel emulsion or injecting water and fuel mixture also can be recommended for conducting further work on this topic.

Optical visualization and 3D simulation (computational fluid dynamics (CFD)) is another topic for further work on water injection which can be effectively used to better understand the water spray behaviour (targeting, penetration, distribution and vaporization) in the intake port and inside the cylinder. It is worth noting that an alternative ignition system might be required depending on the water injection system in use.

Improvement in the ignition system is also recommended for further investigation which could also enhance the effectiveness of the water injection concept even further by reliably promoting a fast and safe ignition of the in-cylinder mixture which contains air, fuel, residual gas, EGR and water.

Ultimately, investigation of direct water injection strategy such as multiple or split water injection has a potential to improve combustion processes even further by improving the cooling effectiveness of water and helping to avoid water impingement on piston top and cylinder walls.

References

1. Smil, V., “Prime movers of globalization: The history and impact of diesel engines and gas turbines,” *Electron. Green J.* (32):22, 2007, doi:10.1017/S1740022807002331.

2. Zhao, H., “Advanced Direct Injection Combustion Engine Technologies and Development: Gasoline and Gas Engines,” Woodhead Publishing Limited, ISBN 9781845697327, 2010.

3. United Kingdom Parliament, “Clean Air Act, 1956,” 38, 1956.

4. Miller, P. and Solomon, M., “A brief history of Technolgy-Forcing Motor Vehicle Regulations,” *Experientia* 49(5):366–368, 2009, doi:10.1007/BF01923581.

5. MAHLE Powertrain, “MAHLE Powertrain - Open Day Slides,” Northampton, 2018.

6. DieselNet, “Emission Standards-EU: Cars and Light Trucks,” https://www.dieselnet.com/standards/eu/ld.php#test, 2018.

7. International Organization of Motor Vehicle Manufacturers, “Co2,” 9, 2014.

8. SMMT, “New Car CO 2 Report 2016 The 13th report,” 2018.

9. ICCT, “2017 Global update: Light-duty vehicle greenhouse gas and fuel economy standards,” 36, 2017.

10. EEA, “Monitoring CO2 emissions from new passenger cars and vans in 2014,” ISBN 978-92-9213-713-7, 2015, doi:10.2800/214970.

11. Nations, U., “UNECE Regulation 49,” (March 1958), 2013.

12. Environmental Protection Agency, “FEDERAL REGISTER,” 77(199):62623–63200, 2012.

13. European Parliament and Council of the European Union, “Regulation (EC) no. 443/2009,” *Off. J. Eur. Union* 140(1):1–15, 2009, doi:10.1524/zkri.2009.1105.

14. EU Commission, “COMMISSION REGULATION (EU) No 582/2011 of 25 May 2011 - Heavy Duty,” *Off. J. Eur. Union* L 167:1, 2011.

15. European Parliament and Council of the European Union, “REGULATION (EC) No 715/2007 OF THE EUROPEAN PARLIAMENT AND OF THE COUNCIL of 20 June 2007 on type approval of motor vehicles with respect to emissions from light passenger and commercial vehicles (Euro 5 and Euro 6) and on access to vehicle repair and mai,” *Off. J. Eur. Union* L171(December 2006):1–16, 2007, doi:OJEU 29.6.2007 L171.

16. Fraunhofer Institute for Systems and Innovation Research (ISI), “Technologies and incentives to reduce CO2 emissions from passenger cars,” 2010.

17. Automotive Council Technology Group, “Lightweight vehicle and train roadmap Power electronics roadmap Power electronics roadmap vehicle and power Traction motors,” *Automot. Counc. Technol. Gr.*, 2013.

18. Survey, 2016 DuPont Automotive WardsAuto, “Lightweighting Remains Top Focus for Automakers to Meet CAFE Standards,” http://www.dupont.com/industries/automotive/press-release/WardsAuto-

survey-2016.html, 2016.

19. Heywood, J., “Internal Combustion Engine Fundamentals,” McGraw-Hill Education, ISBN 9780070286375, 1988.

20. Pulkrabek, W.W., “Engineering fundamentals of the internal combustion engine,” 411, 1997, doi:10.1017/CBO9781107415324.004.

21. Stone, R., “Introduction to Internal Combustion Engines,” Palgrave Macmillan, ISBN 9781137028297, 2012.

22. Ed, K.R., “Gasoline Engine Management,” ISBN 978-3-658-03963-9, 2015, doi:10.1007/978-3-658-03964-6.

23. Weberbauer, F., Rauscher, M., Kulzer, A., Knopf, M., and Bargende, M., “Generally Applicate Split of Losses for New Combustion Concepts,” *MTZ Mot. Zeitschrift* 66(2):120–124, 2005, doi:10.1007/BF03227253.

24. OECD/IEA, “International Comparison of Light-duty Vehicle Fuel Economy 2005-2015 Ten years of fuel economy benchmarking,” *Int. Energy Agency*, 2017.

25. European Automobile Manufacturers’ Association (ACEA), “New passenger cars market share in Europe by fuel type,” https://www.acea.be/, 2018.

26. ACEA, “New Passenger Car Registrations by Alternative Fuel Type in the European Union,” (September):1–10, 2018.

27. Yuanping, L., “EXPERIMENTAL STUDY OF A MILLER CYCLE BASED APPROACH FOR AN EFFICIENT BOOSTED DOWNSIZED GASOLINE DI ENGINE A thesis submitted for the degree of Doctor of Philosophy by

Yuanping Li Department of Mechanical , Aerospace and Civil Engineering Brunel University," (September), 2017.

28. Cairns, A., "Vehicle Design," *Veh. Des. Lect. Notes, Transm. Part 1* 28, 2013.

29. Richard van Basshuysen, "Gasoline Engine with Direct Injection Processes, Systems, Development, Potentia," 1st ed., Vieweg+Teubner Verlag, ISBN 978-3-8348-0670-3, 2009.

30. Çelik, M.B. and Özdalyan, B., "Gasoline direct injection," *Fuel Inject.* 1–42, 2010.

31. Horie, K., Nishizawa, K., Ogawa, T., Akazaki, S., and Miura, K., "The Development of a High Fuel Economy and High Performance Four-Valve Lean Burn Engine," *SAE Tech. Pap.*, 1992, doi:10.4271/920455.

32. Matsuki, M., Nakano, K., Amemiya, T., Tanabe, Y., Shimizu, D., and Ohmura, I., "Development of a Lean Burn Engine with a Variable Valve Timing Mechanism," *SAE Tech. Pap.* 13, 1996, doi:10.4271/960583.

33. Kühn, M., Abthoff, J., Kemmler, R., and Kaiser, T., "Influence of the Inlet Port and Combustion Chamber Configuration on the Lean-Burn Behaviour of a Spark-Ignition Gasoline Engine," (412), 1996, doi:10.4271/960608.

34. Technical, S.A.E. and Series, P., "Toyota Lean Combustion System -," (412), 1993.

35. Stokes, J., Lake, T.H., and Osborne, R.J., "A Gasoline Engine Concept for Improved Fuel Economy – The Lean Boost System," *SAE Technical Paper*

2000-01-2902, 2000, doi:10.4271/2000-01-2902.

36. Hanabusa, H., Kondo, T., Hashimoto, K., Sono, H., and Furutani, M., “Study on homogeneous lean charge spark ignition combustion,” *SAE/KSAE 2013 International Powertrains, Fuels and Lubricants Meeting, FFL 2013-01-2562*, 2013, doi:10.4271/2013-01-2562.

37. Hanabusa, H., Kondo, T., and Hashimoto, K., “Study on Cyclic Variations of Laminar Flame Speed in Homogeneous Lean charge Spark Ignition Combustion,” *SAE Technical Paper 2016-01-2173*, 2016, doi:10.4271/2016-01-2173.

38. Zhao, F., Lai, M.-C., and Harrington, D.L., “Automotive spark-ignited direct-injection gasoline engines,” *Prog. Energy Combust. Sci.* 25(5):437–562, 1999, doi:http://dx.doi.org/10.1016/S0360-1285(99)00004-0.

39. Schwarz, C., Schünemann, E., Durst, B., Fischer, J., and Witt, A., “Potentials of the Spray-Guided BMW DI Combustion System Reprinted From : SI Combustion and Direct Injection SI Engine Technology,” (724), 2016.

40. Szekely, G. a and Alkidas, A.C., “Combustion Characteristics of a Spray-Guided Direct-Injection Stratified-Charge Engine with a High-Squish Piston Reprinted From : SI Combustion and Direct Injection SI Engine Technology,” *SAE Technical Paper 2005-01-1937*, 2005, doi:10.4271/2005-01-1937.

41. Rohr, F., Peter, S.D., Lox, E., Kögel, M., Müller, W., Sassi, A., Rigaudeau, C., Juste, L., Belot, G., Gélin, P., and Primet, M., “The Impact of Sulfur Poisoning on NOx-Storage Catalysts in Gasoline Applications,” 2005(724), 2005, doi:10.4271/2005-01-1113.

42. Krebs, R., Pott, E., Kreuzer, T.P., Göbel, U., Glück, K., Ag, O.M.G., and Kg, C., “Exhaust Gas Aftertreatment of Volkswagen FSI Fuel Stratified Injection Engines Reprinted From : Advanced Catalysts and Substrates,” (724):2002-01–0346, 2002.

43. Urushihara, T., Yamaguchi, K., Yoshizawa, K., and Itoh, T., “A Study of a Gasoline-fueled Compression Ignition Engine ～ Expansion of HCCI Operation Range Using SI Combustion as a Trigger of Compression Ignition ～,” 2005(724), 2005, doi:10.4271/2005-01-0180.

44. Zhao, H., “HCCI and CAI Engines for the Automotive Industry,” Elsevier Science, ISBN 9781845693541, 2007.

45. U.S. Department of Energy, “HCCI - Homogeneous Charge Compression Ignition,” 2(1):817–826, 2015.

46. Green Car Congress, “GMs HCCI Demonstrator Combines a Set of Enabling Technologies and Strategies for Extending Operating Range - Green Car Congress,” http://www.greencarcongress.com/2009/05/gm-hcci-20090528.html, 2009.

47. Fuerhapter, A., Piock, W.F., and Fraidl, G.K., “CSI - Controlled Auto Ignition – the Best Solution for the Fuel Consumption – Versus Emission Trade-Off ? DIUSP9V8UDPI,” *SAE Int. J. Engines*, 2018.

48. Steiger, W., Stolte, U., Scholz, I., and Schmerbeck, S., “The CCS Combustion System from Volkswagen,” *ATZautotechnology* 8(3):32–37, 2008, doi:10.1007/BF03247037.

49. Yamasaki, Y., Umahashi, S., Uesugi, Y., Ma, Q., and Kaneko, S.,

"Development of Dynamic Models for an HCCI Engine with Exhaust Gas Rebreathing System," 2015.

50. Patrick Schäfer, "Engine Technology | Mazda Unveils Petrol Engine with Homogeneous Compression Ignition | springerprofessional.de," https://www.springerprofessional.de/en/engine-technology/emissions/mazda-unveils-petrol-engine-with-homogeneous-compression-ignitio/13534078, 2017.

51. Green Car Congress, "Mazda announces SKYACTIV-X: gasoline Spark Controlled Compression Ignition - Green Car Congress," http://www.greencarcongress.com/2017/08/20170808-mazda.html, 2017.

52. Königstein, A., Grebe, U.D., Wu, K.-J., and Larsson, P.-I., "Differentiated analysis of downsizing concepts," *MTZ Worldw.* 69(6):4–11, 2008, doi:10.1007/BF03227890.

53. Kratzsch, M. and Günther, M., "Knocking in Gasoline Engines," ISBN 978-3-944976-04-4, 2013.

54. Lang, O., Geiger, J., Habermann, K., and Wittler, M., "Boosting and Direct Injection - Synergies for Future Gasoline Engines Reprinted From : New SI Engine and Component Design 2005," *Engineering* 2005(724), 2005, doi:10.4271/2005-01-1144.

55. Bandel, W., Fraidl, G.K., Kapus, P.E., Sikinger, H., and Cowland, C.N., "The Turbocharged GDI Engine: Boosted Synergies for High Fuel Economy Plus Ultra-low Emission," 2006, doi:10.4271/2006-01-1266.

56. Woflram, P., German, J., Mock, P., Tietge, U., Wolfram, P., German, J.,

Mock, P., and Tietge, U., “Deployment of passenger car technology in Europe and the United States,” (October):1–19, 2016.

57. Wilhelm, H., “Variable Valve Timing Systems on Modern Spark Ignition Engines in Series Productuion and under Development,” *Lect. Budapest Univ. Technol. Econ.*, 2009.

58. Potul, S., Nachnolkar, R., and Bhave, S., “Analysis Of Change In Intake Manifold Length And Development Of Variable Intake System,” *Int. J. Sci. Technol. Res.* 3(5):223–228, 2014.

59. Liter, N. and Engine, I., “A Newly Developed Intelligent Variable Valve Timing System – Continuously Controlled Cam Phasing as Applied to a New 3 Liter Inline 6 Engine,” *SAE Tech. Pap.*, 1996, doi:960579.

60. Leone, T.G., Christenson, E.J., and Stein, R.A., “Comparison of Variable Camshaft Timing Strategies at Part Load,” *SAE Tech. Pap.* (412):960584, 1996, doi:10.4271/960584.

61. Urata, Y., Umiyama, H., Shimizu, K., Fujiyoshi, Y., Sono, H., and Fukuo, K., “A Study of Vehicle Equipped with Non-Throttling S.I. Engine with Early Intake Valve Closing Mechanism,” (412), 1993, doi:10.4271/930820.

62. Kreuter, P., Heuser, P., Reinicke-Murmann, J., Erz, R., Peter, U., and Böcker, O., “Variable Valve Actuation - Switchable and Continuously Variable Valve Lifts,” *SAE Tech. Pap.*, 2003, doi:10.4271/2003-01-0026.

63. Hannibal, W., Flierl, R., Stiegler, L., and Meyer, R., “Overview of current continuously variable valve lift systems for four-stroke spark-ignition engines and the criteria for their design ratings,” *SAE Tech. Pap. Ser.* 2004-01–

12(724), 2004, doi:10.4271/2004-01-1263.

64. Hong, H., Parvate-Patil, G.B., and Gordon, B., “Review and analysis of variable valve timing strategies - eight ways to approach,” *Proc. Inst. Mech. Eng. Part D-Journal Automob. Eng.* 218(D10):1179–1200, 2004.

65. Kreuter, P., Heuser, P., Reinicke-Murmann, J., Erz, R., Stein, P., and Peter, U., “Meta - CVD System An Electro-Mechanical Cylinder and Valve Deactivation System,” *SAE Pap. 2001-01-0240* 2001(724), 2001, doi:10.4271/2001-01-0240.

66. Falkowski, A., McElwee, M., and Bonne, M., “Design and Development of the DaimlerChrysler 5.7L HEMI® Engine Multi-Displacement Cylinder Deactivation System,” *SAE Tech. Pap.* (724):1–12, 2004, doi:10.4271/2004-01-2106.

67. Rebbert, M., Kreusen, G., and Lauer, S., “A New Cylinder Deactivation by FEV and Mahle,” 2008(724), 2008, doi:10.4271/2008-01-1354.

68. Hentschel, W., Block, B., Hovestadt, T., Meyer, H., Ohmstede, G., Richter, V., Stiebels, B., and Winkler, A., “Optical Diagnostics and CFD-Simulations to Support the Combustion Process Development of the Volkswagen FSI® Direct-Injection Gasoline Engine,” (724), 2001, doi:10.4271/2001-01-3648.

69. Neußer, H.-J., Endres, H., and Breuer, M., “New Variable Intake and Mixture Formation System for Multi-Valve SI Engines,” *SAE Tech. Pap.* (412):940449, 1994, doi:10.4271/940449.

70. Roberts, M., “Benefits and challenges of variable compression ratio (VCR),” *SAE Tech. Pap.* (724):03P–227, 2002, doi:10.4271/2003-01-0398.

71. Study of a Gear-Based Variable, (724), 2004.

72. Ferrey, P., Miehe, Y., Constensou, C., and Collee, V., “Potential of a Variable Compression Ratio Gasoline SI Engine with Very High Expansion Ratio and Variable Valve Actuation,” *SAE Int. J. Engines* 7(1):2014-01–1201, 2014, doi:10.4271/2014-01-1201.

73. Pohjalainen, T. and Larmi, M., “Novel Crank Mechanism Increasing Engine Efficiency and Reducing CO2 Emissions,” *SAE Tech. Pap.* 2015-01–1259, 2015, doi:10.4271/2015-01-1259.

74. INFINITI VC-Turbo: The world’s first production-ready variable compression ratio engine - Global Newsroom, https://newsroom.nissan-global.com/releases/infiniti-vc-t-the-worlds-first-production-ready-variable-compression-ratio-engine, 2016.

75. Grandin, B., Angstroem, H.-E., Stalhammar, P., and Olofsson, E., “Knock suppression in a turbocharged SI engine by using cooled EGR,” *SAE Tech. Pap.* (724), 1998, doi:982476.

76. Diana, S., Giglio, V., Iorio, B., and Police, G., “Evaluation of the Effect of EGR on Engine Knock,” *SAE Tech. Pap.* (724):982479, 1998, doi:10.4271/982479.

77. Han, S., “Design and Demonstration of a Spark Ignition Engine Operating in a Stratified-EGR Mode,” 1998(724), 1998, doi:10.4271/980122.

78. Diana, S., Giglio, V., Iorio, B., and Police, G., “A Strategy to Improve the Efficiency of Stoichiometric Spark Ignition Engines,” (412), 1996, doi:10.4271/961953.

79. Alger, T., Chauvet, T., and Dimitrova, Z., “Synergies between High EGR Operation and GDI Systems,” *SAE Int. J. Engines* 1(1):2008-01–0134, 2008, doi:10.4271/2008-01-0134.

80. Chadwell, C., Alger, T., Zuehl, J., and Gukelberger, R., “A Demonstration of Dedicated EGR on a 2.0 L GDI Engine,” *SAE Int. J. Engines* 7(1):2014-01–1190, 2014, doi:10.4271/2014-01-1190.

81. Siokos, K., Koli, R., Prucka, R., Schwanke, J., and Miersch, J., “Assessment of Cooled Low Pressure EGR in a Turbocharged Direct Injection Gasoline Engine,” *SAE Int. J. Engines* 8(4):2015-01–1253, 2015, doi:10.4271/2015-01-1253.

82. New 2.5-liter Direct-injection, Inline 4-cylinder Gasoline Engine | TOYOTA Global Newsroom, https://newsroom.toyota.co.jp/en/powertrain/engine, 2016.

83. Tully, E.J. and Heywood, J.B., “Lean-Burn Characteristics of a Gasoline Engine Enriched with Hydrogen from a Plasmatron Fuel Reformer,” *SAE Pap.* (2003-01–0630), 2003, doi:10.4271/2003-01-0630.

84. Toulson, E., Schock, H.J., and Attard, W.P., “A Review of Pre-Chamber Initiated Jet Ignition Combustion Systems,” 2010, doi:10.4271/2010-01-2263.

85. Dale, J., Checkel, M.D., and Smy, P.R., “Application of high energy ignition systems to engines,” *Prog. Energy Combust. Sci.* 23(5–6):379–398, 1997, doi:10.1016/S0360-1285(97)00011-7.

86. Oppenheim, a K., “Prospects for Combustion in Piston Engines,” (724),

2002, doi:10.4271/2002-01-0999.

87. Attard, W.P. and Blaxill, H., “A Single Fuel Pre-Chamber Jet Ignition Powertrain Achieving High Load, High Efficiency and Near Zero NOx Emissions,” *SAE Int. J. Engines* 5(3):2011-01–2023, 2011, doi:10.4271/2011-01-2023.

88. Attard, W.P., Kohn, J., and Parsons, P., “Ignition Energy Development for a Spark Initiated Combustion System Capable of High Load, High Efficiency and Near Zero NOx Emissions,” *SAE Int. J. Engines* 3(2):2010-32–0088, 2010, doi:10.4271/2010-32-0088.

89. Attard, W.P., Kohn, J., and Parsons, P., “Flame Kernel Development for a Spark Initiated Pre-Chamber Combustion System Capable of High Load, High Efficiency and Near Zero NOx Emissions,” *SAE Int. J. Engines* 3(2), 2010, doi:10.4271/2010-01-2260.

90. Attard, W.P., Kohn, J., and Parsons, P., “A Normally Aspirated Spark Initiated Combustion System Capable of High Load, High Efficiency and Near Zero NOx Emissions in a Modern Vehicle Powertrain,” *SAE Int. J. Engines* 3(2):2010-32–0088, 2010, doi:10.4271/2010-01-2196.

91. Attard, W.P., Fraser, N., Parsons, P., and Toulson, E., “A Turbulent Jet Ignition Pre-Chamber Combustion System for Large Fuel Economy Improvements in a Modern Vehicle Powertrain,” *SAE Int. J. Engines* 3(2):2010-01–1457, 2010, doi:10.4271/2010-01-1457.

92. Alkidas, A.C. and Tahry, S.H. El, “Contributors to the Fuel Economy Advantage of DISI Engines Over PFI Engines,” *SAE Technical Paper 2003-*

01-3101, 2003, doi:10.4271/2003-01-3101.

93. Schumann, F., Sarikoc, F., Buri, S., Kubach, H., and Spicher, U., “Potential of spray-guided gasoline direct injection for reduction of fuel consumption and simultaneous compliance with stricter emissions regulations,” *Int. J. Engine Res.* 14(1):80–91, 2013, doi:10.1177/1468087412451695.

94. Spicher, U., Magar, M., and Hadler, J., “High Pressure Gasoline Direct Injection in Spark Ignition Engines - Efficiency Optimization through Detailed Process Analyses,” *SAE Int. J. Engines* 9(4):2120–2128, 2016, doi:10.4271/2016-01-2244.

95. Ikoma, T., Abe, S., Sonoda, Y., and Suzuki, H., “Development of V-6 3 . 5-liter Engine Adopting New Direct Injection System Reprinted From : SI Combustion and Direct Injection SI Engine Technology,” *SAE Technical Paper 2006-01-1259*, 2016, doi:10.4271/2006-01-1259.

96. Zhu, G., Stuecken, T., Schock, H., and Yang, X., “Combustion Characteristics of a Single-Cylinder Engine Equipped with Gasoline and Ethanol Dual-Fuel Systems,” *SAE Technical Paper 2008-01-1767*, 2008, doi:10.4271/2008-01-1767.

97. Iorio, S. Di, Sementa, P., and Vaglieco, B.M., “Experimental Characterization of an Ethanol DI - Gasoline PFI and Gasoline DI - Gasoline PFI Dual Fuel Small Displacement SI Engine,” *SAE Technical Paper 2015-01-0848*, 2015, doi:10.4271/2015-24-2459.

98. Golzari, R., Li, Y., and Zhao, H., “Impact of Port Fuel Injection and In-Cylinder Fuel Injection Strategies on Gasoline Engine Emissions and Fuel

Economy," *SAE Technical Paper 2016-01-2174*, 2016, doi:10.4271/2016-01-2174.

99. Yang, J. and Anderson, R.W., "Fuel Injection Strategies to Increase Full-Load Torque Output of a Direct-Injection SI Engine," *SAE Technical Paper 980495*, 1998, doi:10.4271/980495.

100. Xu, Z., Zhou, Z., Wu, T., Li, T., Cheng, C., and Yin, H., "Investigations of Smoke Emission , Fuel Dilution and Pre-Ignition in a 2 . 0L Turbo-Charged GDI Engine," *SAE Technical Paper 2016-01-0698*, 2016, doi:10.4271/2016-01-0698.

101. Costa, M., Sorge, U., Merola, S., Irimescu, A., Villetta, M. La, and Rocco, V., "Split injection in a Homogeneous stratified gasoline direct injection engine for high combustion efficiency and low pollutants emission," *Energy* 1–11, 2015, doi:10.1016/j.energy.2016.03.065.

102. Costa, M., Catapano, F., Marseglia, G., Sorge, U., Sementa, P., and Vaglieco, B.M., "Experimental and Numerical Investigation of the Effect of Split Injections on the Performance of a GDI Engine under Lean Operation," *SAE Technical Paper 2015-24-2413*, 2015, doi:10.4271/2015-24-2413.

103. Serras-Pereira, J., Aleiferis, P.G., and Richardson, D., "An experimental database on the effects of single- and split injection strategies on spray formation and spark discharge in an optical direct-injection spark-ignition engine fuelled with gasoline, iso-octane and alcohols," *Int. J. Engine Res.* 16(7):851–896, 2015, doi:10.1177/1468087414554936.

104. Story, O. and Ture, M., "Lean-Burn Stratified Combustion at Gasoline

Engines,” *MTZ Worldw.* 10–17, 2013.

105. Lake, T., Stokes, J., Murphy, R., Osborne, R., and Schamel, A., “Turbocharging Concepts for Downsized DI Gasoline Engines,” *SAE Technical Paper 2004-01-0036*, 2004, doi:10.4271/2004-01-0036.

106. Clark, L.G., Kook, S., Chan, Q.N., and Hawkes, E.R., “Influence of Injection Timing for Split-Injection Strategies on Well-Mixed High-Load Combustion Performance in an Optically Accessible Spark-Ignition Direct-Injection (SIDI) Engine,” *SAE Technical Paper 2017-01-0657*, ISBN 9780646596952, 2017, doi:10.4271/2017-01-0657.

107. Clark, L.G., Kook, S., Chan, Q.N., and Hawkes, E.R., “Multiple Injection Strategy Investigation for Well-Mixed Operation in an Optical Wall-Guided Spark-Ignition Direct- Injection (WG-SIDI) Engine through Flame Shape Analysis,” *SAE Technical Paper 2016-01-2162*, 2016, doi:10.4271/2016-01-2162.

108. Song, J., Kim, T., Jang, J., and Park, S., “Effects of the injection strategy on the mixture formation and combustion characteristics in a DISI (direct injection spark ignition) optical engine,” *Energy* 93:1758–1768, 2015, doi:10.1016/j.energy.2015.10.058.

109. Merola, S.S., Irimescu, A., Tornatore, C., Marchitto, L., and Valentino, G., “Split Injection in a DISI Engine Fuelled with Butanol and Gasoline Analyzed through Integrated Methodologies,” *SAE Int. J. Engines* 8(2):2015-01–0748, 2015, doi:10.4271/2015-01-0748.

110. Wang, Y., Wang, J., Shuai, S., Lei, X., and An, X., “Study of Injection

Strategies of Two-stage Gasoline Direct Injection (TSGDI) Combustion System Reprinted From : SI Combustion and Direct Injection SI Engine Technology," *SAE Technical Paper 2005-01-0107*, 2005, doi:10.4271/2005-01-0107.

111. Imaoka, Y., Shouji, K., Inoue, T., and Noda, T., "A Study of a Multistage Injection Mechanism for Improving the Combustion of Direct-Injection Gasoline Engines," *SAE Int. J. Engines* 8(3):2015-01–0883, 2015, doi:10.4271/2015-01-0883.

112. Fansler, T.D., Reuss, D.L., Sick, V., and Dahms, R.N., "Combustion instability in spray-guided stratified-charge engines: A review," *Int. J Engine Res.* 16(3):260–305, 2015, doi:10.1177/1468087414565675.

113. Zheng, Z., Tian, X., and Zhang, X., "Effects of split injection proportion and the second injection time on the mixture formation in a GDI engine under catalyst heating mode using stratified charge strategy," *Appl. Therm. Eng.* 84:237–245, 2015, doi:10.1016/j.applthermaleng.2015.03.041.

114. Su, J., Xu, M., Yin, P., Gao, Y., and Hung, D., "Particle Number Emissions Reduction Using Multiple Injection Strategies in a Boosted Spark-Ignition Direct-Injection (SIDI) Gasoline Engine," *SAE Int. J. Engines* 8:20–29, 2014, doi:10.4271/2014-01-2845.

115. Schmidt, L., Seabrook, J., Stokes, J., Faizan, M., Zuhdi, A., Begg, S., Heikal, M., and King, J., "Multiple Injection Strategies for Improved Combustion Stability under Stratified Part Load Conditions in a Spray Guided Gasoline Direct Injection (SGDI) Engine," *SAE Technical Paper 2011-01-1228*, 2011,

doi:10.4271/2011-01-1228.

116. Heiduk, T., Kuhn, M., Stichlmeir, M., and Unselt, F., “The new 1.8 l TFSI Engine from Audi part 2: Mixture Formation, Combustion Method and Turbocharging,” *MTZ Worldw. eMagazine* 72(7):58–64, 2011, doi:10.1365/s38313-011-0078-1.

117. Zhuang, Y. and Hong, G., “Investigation to Leveraging Effect of Ethanol Direct Injection (EDI) in a Gasoline Port Injection (GPI) Engine,” *SAE Technical Paper 2013-01-1322*, SAE International, 2013, doi:10.4271/2013-01-1322.

118. Zhuang, Y. and Hong, G., “The Effect of Direct Injection Timing and Pressure on Engine Performance in an Ethanol Direct Injection Plus Gasoline Port Injection (EDI+GPI) SI Engine,” *SAE Technical Paper 2013-01-0892*, 2013, doi:10.4271/2013-01-0892.

119. Zhuang, Y. and Hong, G., “Effects of direct injection timing of ethanol fuel on engine knock and lean burn in a port injection gasoline engine,” *Fuel* 135:27–37, 2014, doi:10.1016/j.fuel.2014.06.028.

120. Kim, N., Cho, S., and Min, K., “A study on the combustion and emission characteristics of an SI engine under full load conditions with ethanol port injection and gasoline direct injection,” *Fuel* 158(2015):725–732, 2015, doi:10.1016/j.fuel.2015.06.025.

121. Kim, N. and Cho, S., “The Efficiency and Emission Characteristics of Dual Fuel Combustion Using Gasoline Direct Injection and Ethanol Port Injection in an SI Engine,” *SAE Technical Paper 2014-01-1208*, 2014,

doi:10.4271/2014-01-1208.

122. Cho, S., Kim, N., Chung, J., and Min, K., “The Effect of Ethanol Injection Strategy on Knock Suppression of the Gasoline / Ethanol Dual Fuel Combustion in a Spark-Ignited Engine,” *SAE Technical Paper 2015-01-0764*, 2015, doi:10.4271/2015-01-0764.

123. Liu, H., Wang, Z., Long, Y., Xiang, S., Wang, J., and Fatouraie, M., “Comparative study on alcohol–gasoline and gasoline–alcohol Dual-Fuel Spark Ignition (DFSI) combustion for engine particle number (PN) reduction,” *Fuel* 159:250–258, 2015, doi:http://doi.org/10.1016/j.fuel.2015.06.059.

124. Liu, H., Wang, Z., Long, Y., Xiang, S., Wang, J., and Wagnon, S.W., “Methanol-gasoline Dual-fuel Spark Ignition (DFSI) combustion with dual-injection for engine particle number (PN) reduction and fuel economy improvement,” *Energy* 89:1010–1017, 2015, doi:10.1016/j.energy.2015.06.051.

125. Iorio, S. Di, Sementa, P., and Vaglieco, B.M., “Experimental Investigation of a Methane-Gasoline Dual-Fuel Combustion in a Small Displacement Optical Engine,” *SAE Technical Paper 2013-24-0046*, 2013, doi:10.4271/2013-24-0046.

126. Iorio, S. Di, Sementa, P., Vaglieco, B.M., and Catapano, F., “An experimental investigation on combustion and engine performance and emissions of a methane-gasoline dual-fuel optical engine,” *SAE Technical Paper 2014-01-1329*, 2014, doi:10.4271/2014-01-1329.

127. Catapano, F., Iorio, S. Di, Sementa, P., and Vaglieco, B.M., “Effects of Ethanol and Gasoline Blending and Dual Fueling on Engine Performance and Emissions .,” *SAE Technical Paper 2015-24-2490*, 2015, doi:10.4271/2015-24-2490.

128. Catapano, F., Iorio, S. Di, Sementa, P., and Vaglieco, B.M., “Experimental Analysis of a Gasoline PFI-Methane DI Dual Fuel and an Air Assisted Combustion of a Transparent Small Displacement SI Engine,” *SAE Technical Paper 2015-24-2459*, 2015, doi:10.4271/2015-24-2459.

129. Biffiger, H. and Soltic, P., “Effects of split port/direct injection of methane and hydrogen in a spark ignition engine,” *Int. J. Hydrogen Energy* 40(4):1994–2003, 2015, doi:10.1016/j.ijhydene.2014.11.122.

130. Viollet, Y., Abdullah, M., Alhajhouje, A., and Chang, J., “Characterization of High Efficiency Octane-On-Demand Fuels Requirement in a Modern Spark Ignition Engine with Dual Injection System,” *SAE Technical Paper 2015-01-1265*, 2015, doi:10.4271/2015-01-1265.

131. Pilla, G., Kumar, R., Laget, O., Francqueville, L. De, Dauphin, R., and Solari, J.-P., “Simulation and Optical Diagnostics to Characterize Low Octane Number Dual Fuel Strategies: a Step Towards the Octane on Demand Engine,” *SAE Int. J. Fuels Lubr.* 9(3), 2016, doi:10.4271/2016-01-2164.

132. Bourhis, G., Solari, J., DAUPHIN, R., and Francqueville, L. De, “Fuel Properties and Engine Injection Configuration Effects on the Octane on Demand Concept for a Dual-Fuel Turbocharged Spark Ignition Engine,” *SAE Technical Paper 2016-01-2307*, ISBN 2016012307, 2016,

doi:10.4271/2016-01-2307.

133. Nande, A.M., Wallner, T., and Naber, J.D., “Influence of Water Injection on Performance and Emissions of a Direct-Injection Hydrogen Research Engine.,” *SAE Technical Paper 2008-01-2377*, 2008, doi:10.4271/2008-01-2377.

134. Younkins, M., Wooldridge, M.S., Boyer, B.A., and Co, F.M., “Port Injection of Water into a DI Hydrogen Engine,” *SAE Technical Paper 2015-01-0861*, 2015, doi:10.4271/2015-01-0861.

135. Younkins, M., Wooldridge, M., and Boyer, B., “Direct In-cylinder Injection of Water into a PI Hydrogen Engine,” *SAE Technical Paper 2013-01-0227*, 2013, doi:10.4271/2013-01-0227.

136. Boretti, A., “Water injection in directly injected turbocharged spark ignition engines,” *Appl. Therm. Eng.* 52(1):62–68, 2013, doi:10.1016/j.applthermaleng.2012.11.016.

137. Kim, J., Park, H., Bae, C., Choi, M., and Kwak, Y., “Effects of water direct injection on the torque enhancement and fuel consumption reduction of a gasoline engine under high-load conditions,” *Int. J. Engine Res.* 17(7):795–808, 2016, doi:10.1177/1468087415613221.

138. Rohit, A., Satpathy, S., Choi, J., Hoard, J., Surnilla, G., and Hakeem, M., “Literature Survey of Water Injection Benefits on Boosted Spark Ignited Engines,” *SAE Tech. Pap.*, 2017, doi:10.4271/2017-01-0658.

139. Hoppe, F., Thewes, M., Seibel, J., Balazs, A., and Scharf, J., “Evaluation of the Potential of Water Injection for Gasoline Engines,” *SAE Int. J. Engines*

10(5):2017-24–0149, 2017, doi:10.4271/2017-24-0149.

140. Thewes, M., Hoppe, F., Baumgarten, H., and Seibel, J., “Water Injection for Gasoline Combustion Systems,” *MTZ Worldw.* 76(2):10–15, 2015, doi:10.1007/s38313-014-1012-0.

141. Hoppe, F., Thewes, M., Baumgarten, H., and Dohmen, J., “Water injection for gasoline engines: Potentials, challenges, and solutions,” *Int. J. Engine Res.* 17(1):86–96, 2016, doi:10.1177/1468087415599867.

142. Daggett, D.L., Ortanderl, S., Eames, D., Snyder, C., and Berton, J., “Water Injection : Disruptive Technology to Reduce Airplane Emissions and Maintenance Costs,” *SAE Tech. Pap. Ser.* 1(3108), 2004.

143. ROWE, M.R. and LADD, G.T., “WATER INJECTION for Aircraft Engines,” *Southern California Section of the SAE*, SAE International, 1946, doi:https://doi.org/10.4271/460192.

144. Olds FAQ -- Jetfire, http://www.442.com/oldsfaq/ofjet.htm, Oct. 2017.

145. Sam Burnett, “Water World,” *Engine Technol. Int.* 14–15, 2016.

146. Bosch WaterBoost, http://www.bosch-mobility-solutions.com/en/highlights/powertrain-and-electrified-mobility/water-injection/, Oct. 2017.

147. Lanzafame, R., “Water Injection Effects In A Single-Cylinder CFR Engine,” *SAE Technical Paper*, 1999.

148. Karagöz, Y., Yüksek, L., Sandalcı, T., and Dalkılıç, A.S., “An experimental investigation on the performance characteristics of a hydroxygen enriched

gasoline engine with water injection," *Int. J. Hydrogen Energy* 40(1):692–702, 2015, doi:10.1016/j.ijhydene.2014.11.013.

149. Morsy, M.H., "Assessment of a direct injection diesel engine fumigated with ethanol/water mixtures," *Energy Convers. Manag.* 94:406–414, 2015, doi:10.1016/j.enconman.2015.01.086.

150. Sahin, Z., Tuti, M., and Durgun, O., "Experimental investigation of the effects of water adding to the intake air on the engine performance and exhaust emissions in a di automotive diesel engine," *Fuel* 115(x):884–895, 2014, doi:10.1016/j.fuel.2012.10.080.

151. Brusca, S., "Water Injection in IC - SI Engines to Control Detonation and to Reduce Pollutant Emissions," *Sae Pap. 2003-01-1912*, 2003, doi:10.4271/2003-01-1912.

152. Iacobacci, A., Marchitto, L., and Valentino, G., "Water Injection to Enhance Performance and Emissions of a Turbocharged Gasoline Engine under High Load Condition," *SAE Int. J. Engines* 10(3):2017-01–0660, 2017, doi:10.4271/2017-01-0660.

153. Worm, J., Naber, J., Duncan, J., Barros, S., and Atkinson, W., "Water Injection as an Enabler for Increased Efficiency at High-Load in a Direct Injected, Boosted, SI Engine," *SAE Int. J. Engines* 10(3):2017-01–0663, 2017, doi:10.4271/2017-01-0663.

154. Tornatore, C., Siano, D., Marchitto, L., Iacobacci, A., Valentino, G., and Bozza, F., "Water Injection: a Technology to Improve Performance and Emissions of Downsized Turbocharged Spark Ignited Engines," *SAE Int. J.*

Engines 10(5):2017-24–0062, 2017, doi:10.4271/2017-24-0062.

155. Bellis, V. De, Bozza, F., Teodosio, L., and Valentino, G., “Experimental and Numerical Study of the Water Injection to Improve the Fuel Economy of a Small Size Turbocharged SI Engine,” *SAE Int. J. Engines* 10:550–561, 2017, doi:10.4271/2017-01-0540.

156. Bozza, F., Bellis, V. De, and Teodosio, L., “Potentials of cooled EGR and water injection for knock resistance and fuel consumption improvements of gasoline engines,” *Appl. Energy* 169:112–125, 2016, doi:10.1016/j.apenergy.2016.01.129.

157. Berni, F., Breda, S., Lugli, M., and Cantore, G., “A numerical investigation on the potentials of water injection to increase knock resistance and reduce fuel consumption in highly downsized GDI engines,” *Energy Procedia* 81:826–835, 2015, doi:10.1016/j.egypro.2015.12.091.

158. Shah, S. and Maiboom, A., “Experimental Study of Inlet Manifold Water Injection on a Common Rail HSDI Automobile Diesel Engine, Compared to EGR with Respect to PM and Nox Emissions and Specific Consumption,” *SAE Tech. Pap.*, 2009, doi:10.4271/2009-01-1439.

159. Hountalas, D.T., Mavropoulos, G.C., and Zannis, T.C., “Comparative Evaluation of EGR, Intake Water Injection and Fuel/Water Emulsion as NOx Reduction Techniques for Heavy Duty Diesel Engines,” *SAE World Congress & Exhibition*, SAE International, 2007, doi:10.4271/2007-01-0120.

160. Hountalas, D.T., Mavropoulos, G.C., Zannis, T.C., and Mamalis, S.D., “Use of Water Emulsion and Intake Water Injection as NOx Reduction Techniques

for Heavy Duty Diesel Engines," 2006(724), 2006, doi:10.4271/2006-01-1414.

161. Nazha, M.A.A., Rajakaruna, H., and Wagstaff, S.A., "The Use of Emulsion , Water Induction and EGR for Controlling Diesel Engine Emissions," *SAE Pap.* 2001-01–19(724), 2001, doi:10.4271/2001-01-1941.

162. Kegl, B. and Pehan, S., "Reduction of Diesel Engine Emissions," (724), 2001.

163. Christensen, M. and Johansson, B., "Homogeneous Charge Compression Ignition with Water Injection," *SAE Tech. Pap.* (724), 1999, doi:10.4271/1999-01-0182.

164. Ishida, M., Ueki, H., and Sakaguchi, D., "Prediction of NOx reduction rate due to port water injection in a di diesel engine," *SAE Tech. Pap.* (412), 1997, doi:10.4271/972961.

165. Psota, M.A., Easley, W.L., Fort, T.H., and Mellor, A.M., "Water Injection Effects on NOx Emissions for Engines Utilizing Diffusion Flame Combustion," (x), 1997, doi:10.4271/971657.

166. Maiboom, A. and Tauzia, X., "NOx and PM emissions reduction on an automotive HSDI Diesel engine with water-in-diesel emulsion and EGR: An experimental study," *Fuel* 90(11):3179–3192, 2011, doi:10.1016/j.fuel.2011.06.014.

167. Kumar, N., Sharma, A., and Vibhanshu, V., "Performance Analyses of Diesel Engine at Different Injection Angles Using Water Diesel Emulsion," *SAE Tech. Pap.* 7, 2013, doi:10.4271/2013-01-2170.

168. Ogawa, H., Shibata, G., Kato, T., Setiapraja, H., and Hara, K., “Combustion Characteristics of Emulsified Blends of Water and Diesel Fuel in a Diesel Engine with Cooled EGR and Pilot Injection,” *SAE Int. J. Fuels Lubr.* 6(3):977–985, 2013, doi:10.4271/2013-32-9022.

169. Subramanian, K.A., “A comparison of water-diesel emulsion and timed injection of water into the intake manifold of a diesel engine for simultaneous control of NO and smoke emissions,” *Energy Convers. Manag.* 52(2):849–857, 2011, doi:10.1016/j.enconman.2010.08.010.

170. Koc, A.B. and Abdullah, M., “Performance and NOx emissions of a diesel engine fueled with biodiesel-diesel-water nanoemulsions,” *Fuel Process. Technol.* 109(x):70–77, 2013, doi:10.1016/j.fuproc.2012.09.039.

171. Murotani, T., Hattori, K., Sato, E., Chryssakis, C., Babajimopoulos, a, and Assanis, D.N., “Simultaneous reduction of NOX and soot in a heavy-duty diesel engine by instantaneous mixing of fuel and water,” *SAE Tech. Pap.* 2007(724), 2007, doi:10.4271/2007-01-0125.

172. Park, J.W., Huh, K.Y., and Lee, J.H., “Reduction of NO , smoke and brake speci c fuel consumption with x optimal injection timing and emulsion ratio of water-emulsi ed diesel,” (April 2000):83–94, 2001.

173. Kohketsu, S., Mori, K., and Sakai, K., “Reduction of Exhaust Emission with New Water Injection System in a Diesel Engine,” (412), 1996.

174. Iwashiro, Y., Tsurushima, T., Nishijima, Y., Asaumi, Y., and Aoyagi, Y., “Fuel Consumption Improvement and Operation Range Expansion in HCCI by Direct Water Injection,” *SAE Tech. Pap.* 2002(724), 2002,

doi:10.4271/2002-01-0105.

175. Kaneko, N., Ando, H., Ogawa, H., and Miyamoto, N., “Expansion of the Operating Range with In-Cylinder Water Injection in a Premixed Charge Compression Ignition Engine,” *SAE Tech. Pap.* 2002-01–17(724), 2002, doi:10.4271/2002-01-1743.

176. Ogawa, H., Miyamoto, N., Kaneko, N., and Ando, H., “Combustion control and operating range expansion in an homogeneous charge compression ignition engine with direct in-cylinder injection of reaction inhibitors,” *Int. J. Engine Res.* 6(4):341–359, 2005, doi:10.1243/146808705x30440.

177. Mingrui, W., Thanh Sa, N., Turkson, R.F., Jinping, L., and Guanlun, G., “Water injection for higher engine performance and lower emissions,” *J. Energy Inst.* 90(2):285–299, 2017, doi:10.1016/j.joei.2015.12.003.

178. Taghavifar, H., Anvari, S., and Parvishi, A., “Benchmarking of water injection in a hydrogen-fueled diesel engine to reduce emissions,” *Int. J. Hydrogen Energy* 42(16):11962–11975, 2017, doi:10.1016/j.ijhydene.2017.02.138.

179. Bhagat, M., Cung, K., Johnson, J., Lee, S.-Y., Naber, J., and Barros, S., “Experimental and Numerical Study of Water Spray Injection at Engine-Relevant Conditions,” 2013, doi:10.4271/2013-01-0250.

180. Gadallah, A.H., Elshenawy, E.A., Elzahaby, A.M., El-salmawy, H.A., and Bawady, A.H., “Effect of In Cylinder Water Injection Strategies on Performance and Emissions of a Hydrogen Fuelled Direct Injection Engine,” *Sae* 4970(2009-01–2684), 2009, doi:10.4271/2009-01-2684.

181. Bedford, F., Rutland, C., Dittrich, P., Raab, A., and Wirbeleit, F., “Effects of

Direct Water Injection on DI Diesel Engine Combustion," *SAE Pap.* 2000-01–29(724):1–10, 2000, doi:2000-01-29.

182. Thewes, D.M., Baumgarten, H., Dohmen, J., Hoppe, D.F., Martin, D., Krieck, S., and Hoppe, D.P., "Gasoline Combustion Systems Beyond 2020," *23rd Aachen Colloq. Automob. Engine Technol. 2014* 267–292, 2014.

183. Hancock, D., Fraser, N., Jeremy, M., Sykes, R., and Blaxill, H., "A new 3 cylinder 1 . 2L advanced downsizing technology demonstrator engine," *SAE Technical Paper 2008-01-0611*, 2008, doi:10.4271/2008-01-0611.

184. Bassett, M., Hall, J., Hibberd, B., Borman, S., Reader, S., Gray, K., and Richards, B., "Heavily Downsized Gasoline Demonstrator," *SAE Int. J. Engines* 9(2):2016-01–0663, 2016, doi:10.4271/2016-01-0663.

185. Hall, J., Bassett, M., Hibberd, B., and Streng, S., "Heavily Downsized Demonstrator Engine Optimised for CNG Operation," *SAE Int. J. Engines* 9(4):2250–2261, 2016, doi:10.4271/2016-01-2363.

186. Bassett, M., Hall, J., Cains, T., Underwood, M., and Wall, R., "Dynamic Downsizing Gasoline Demonstrator," *SAE Int. J. Engines* 10(3):2017-01–0646, 2017, doi:10.4271/2017-01-0646.

187. Bassett, M., Vogler, C., Hall, J., Taylor, J., Cooper, A., and Gray, K., "Analysis of the Hardware Requirements for a Heavily Downsized Gasoline Engine Capable of Whole Map Lambda 1 Operation," *SAE Int.* (lambda 1):1–10, 2018, doi:10.4271/2018-01-0975.Abstract.

188. Anderson, W., Yang, J., Brehob, D.D., Vallance, J.K., and Whiteaker, R.M., "Understanding the Thermodynamics of Direct Injection Spark Ignition (DISI)

Combustion Systems: An Analytical and Experimental Investigation," (412), 1996, doi:10.4271/962018.

189. Lumsden, G., OudeNijeweme, D., Fraser, N., and Blaxill, H., "Development of a Turbocharged Direct Injection Downsizing Demonstrator Engine," *SAE Int. J. Engines* 2(1):1420–1432, 2009, doi:10.4271/2009-01-1503.

190. Li, Y., Zhao, H., Stansfield, P., and Freeland, P., "Synergy between Boost and Valve Timings in a Highly Boosted Direct Injection Gasoline Engine Operating with Miller Cycle Experimental Set-Up," *SAE Technical Paper 2015-01-1262*, 2015, doi:10.4271/2015-01-1262.

191. Zhang, Y., "Experimental investigation of CAI combustion in a two-stroke poppet valve DI engine," 2014.

192. Zhao, H. and Ladommatos, N., "Engine Combustion Instrumentation and Diagnostics," Society of Automotive Engineers, ISBN 9780768006650, 2001.

193. Coates, B., "INVESTIGATION OF ENGINE DESIGN PARAMETERS ON THE EFFICIENCY AND PERFORMANCE OF THE HIGH SPECIFIC POWER DOWNSIZED SI ENGINE," (November), 2012.

194. Randolph, A.L., "Methods of Processing Cylinder-Pressure Transducer Signals to Maximize Data Accuracy," 1990, doi:10.4271/900170.

195. Melo, T.C.C. de, Brito, M.F.M. de, Machado, G.B., and Paiva, C.E.F., "Procedure for Uncertainty of Measurement Determination of Spark Ignition Engine Emission Tests," 2012, doi:10.4271/2012-36-0488.

196. Rao, S., Barros, S., Atkinson, W., Miganakallu, N., and Naber, J.D., “Experimental Investigation of Water Injection Technique in Gasoline Direct Injection Engine,” *Proc. ASME 2017 Intern. Combust. Fall Tech. Conf.* (October):V001T03A013, 2017, doi:10.1115/icef2017-3619.

Appendix

The following figures show the effect of water injection on engine out particulate emissions at medium and high load conditions using gasoline RON 95. 97 and 100. The indicated time at each legend (such as 2ms or 5ms water injection) shows the injection duration of the PFI for water injection. As the injection duration increases the injected water also increases.

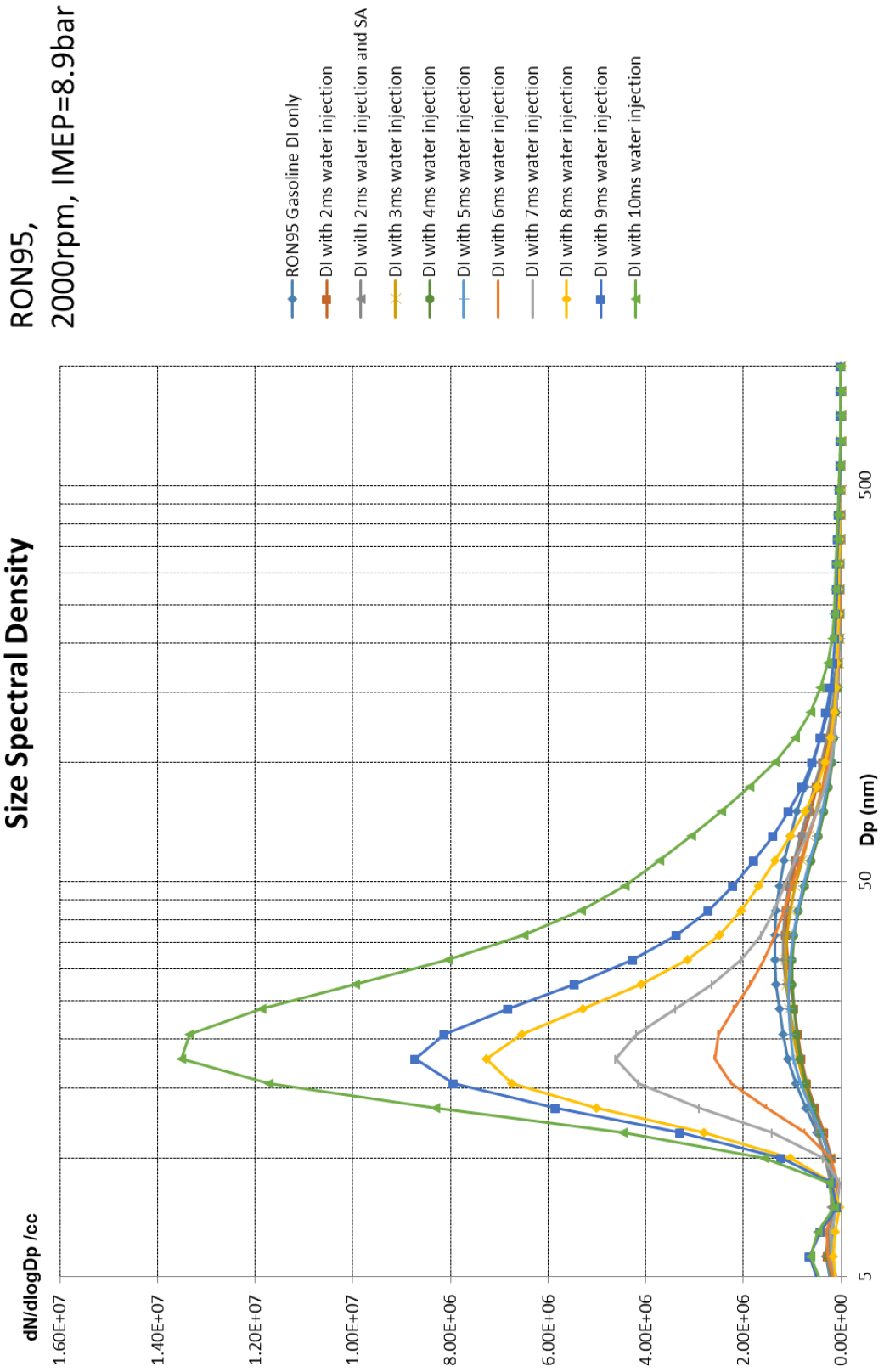

Figure A.0-1 Impact of water injection on particles size and number at 2000 rpm / 8.90 bar NIMEP (RON 95)

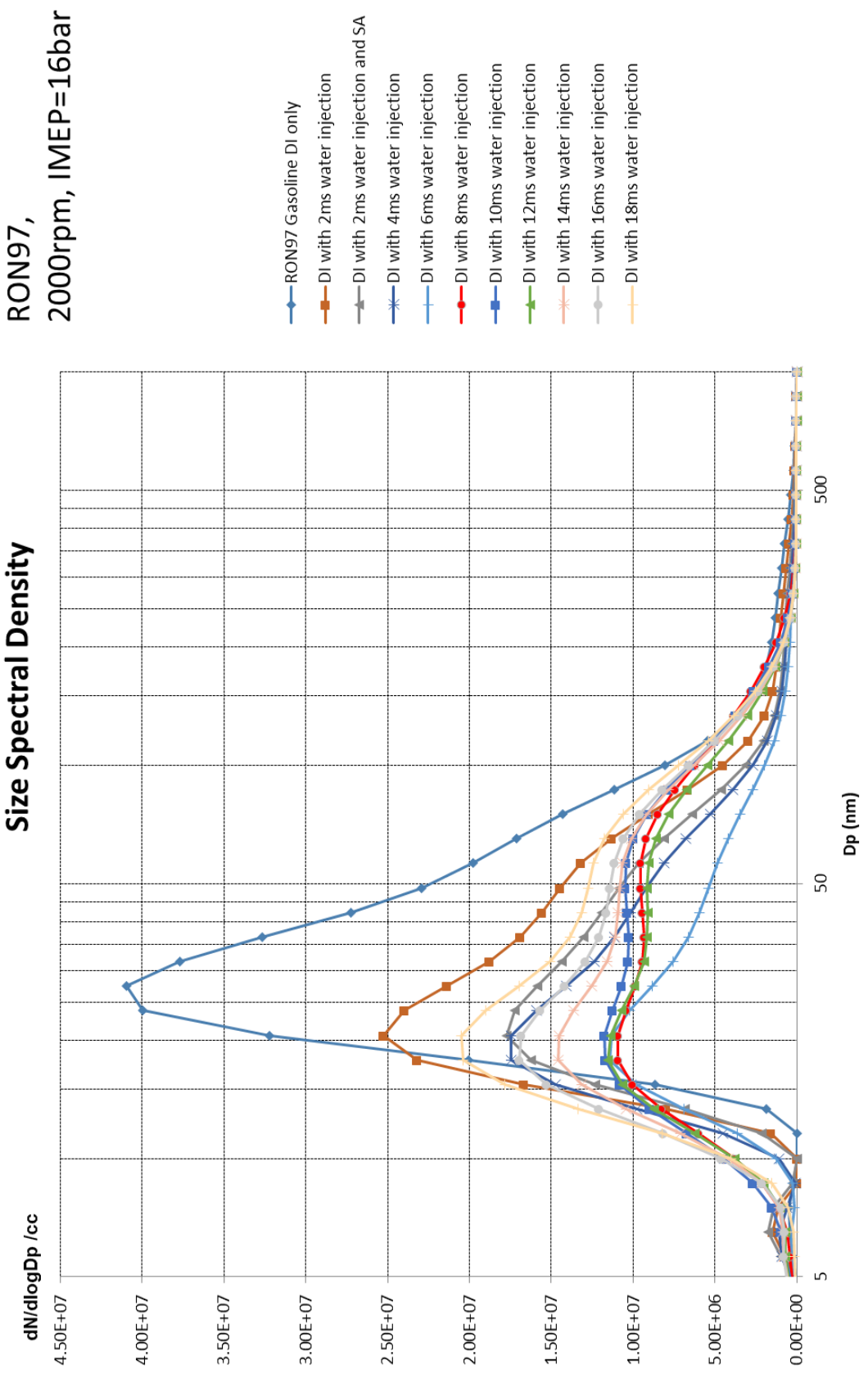

Figure A.0-2 Impact of water injection on particles size and number at 2000 rpm / 16.04 bar NIMEP (RON 97)

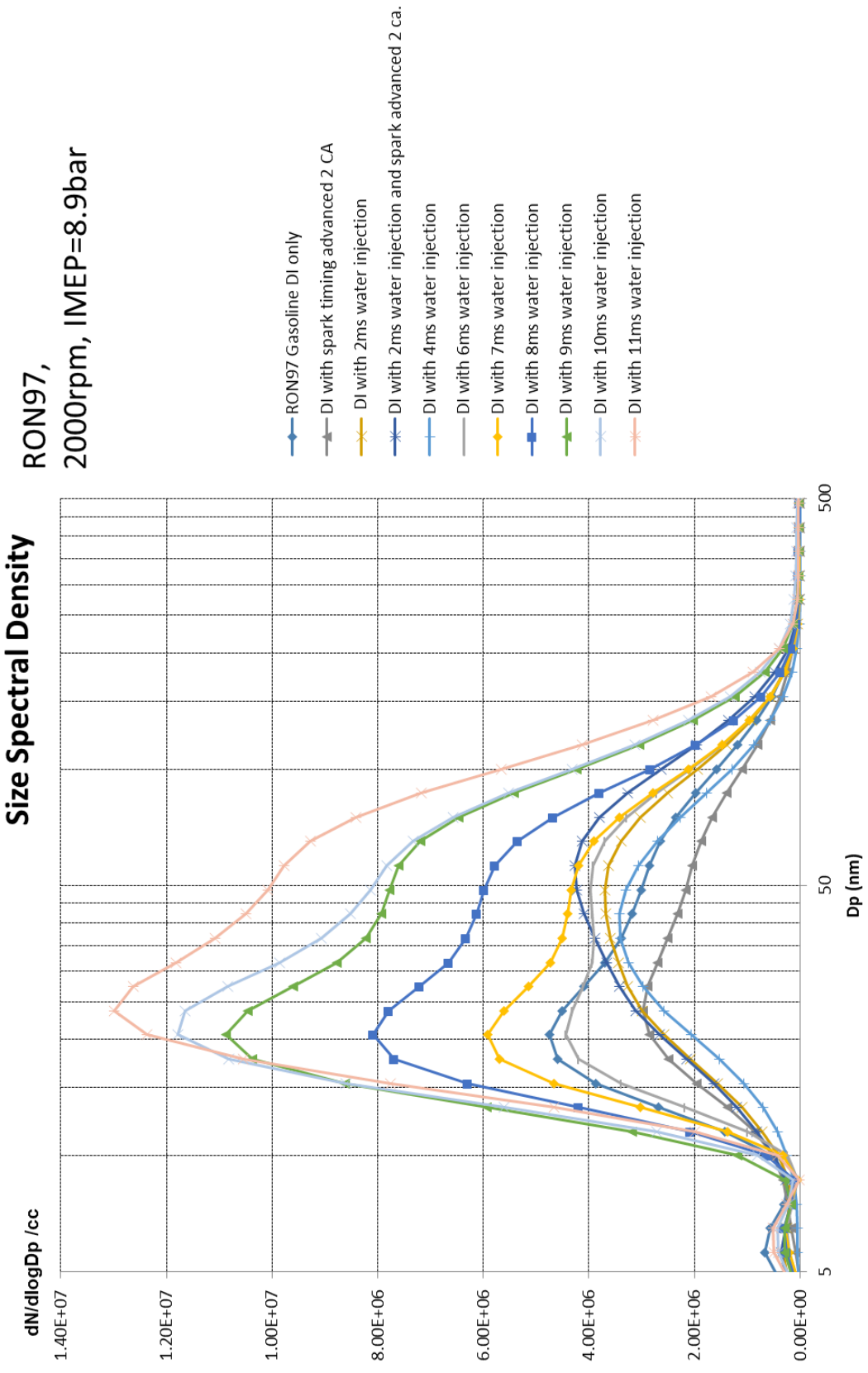

Figure A.0-3 Impact of water injection on particles size and number at 2000 rpm / 8.90 bar NIMEP (RON 97)

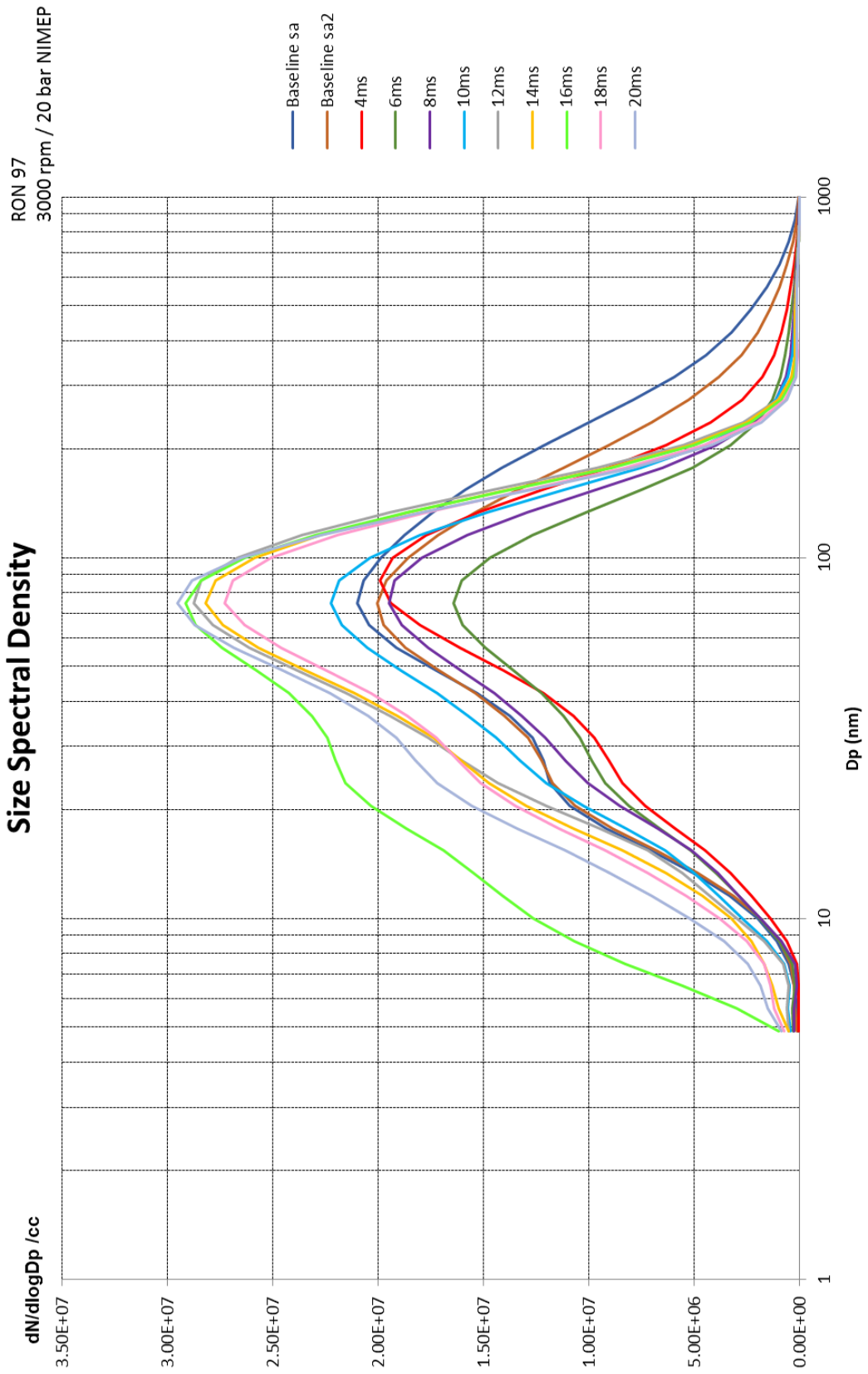

Figure A.0-4 Impact of water injection on particles size and number at 3000 rpm / 20 bar NIMEP (RON 97)

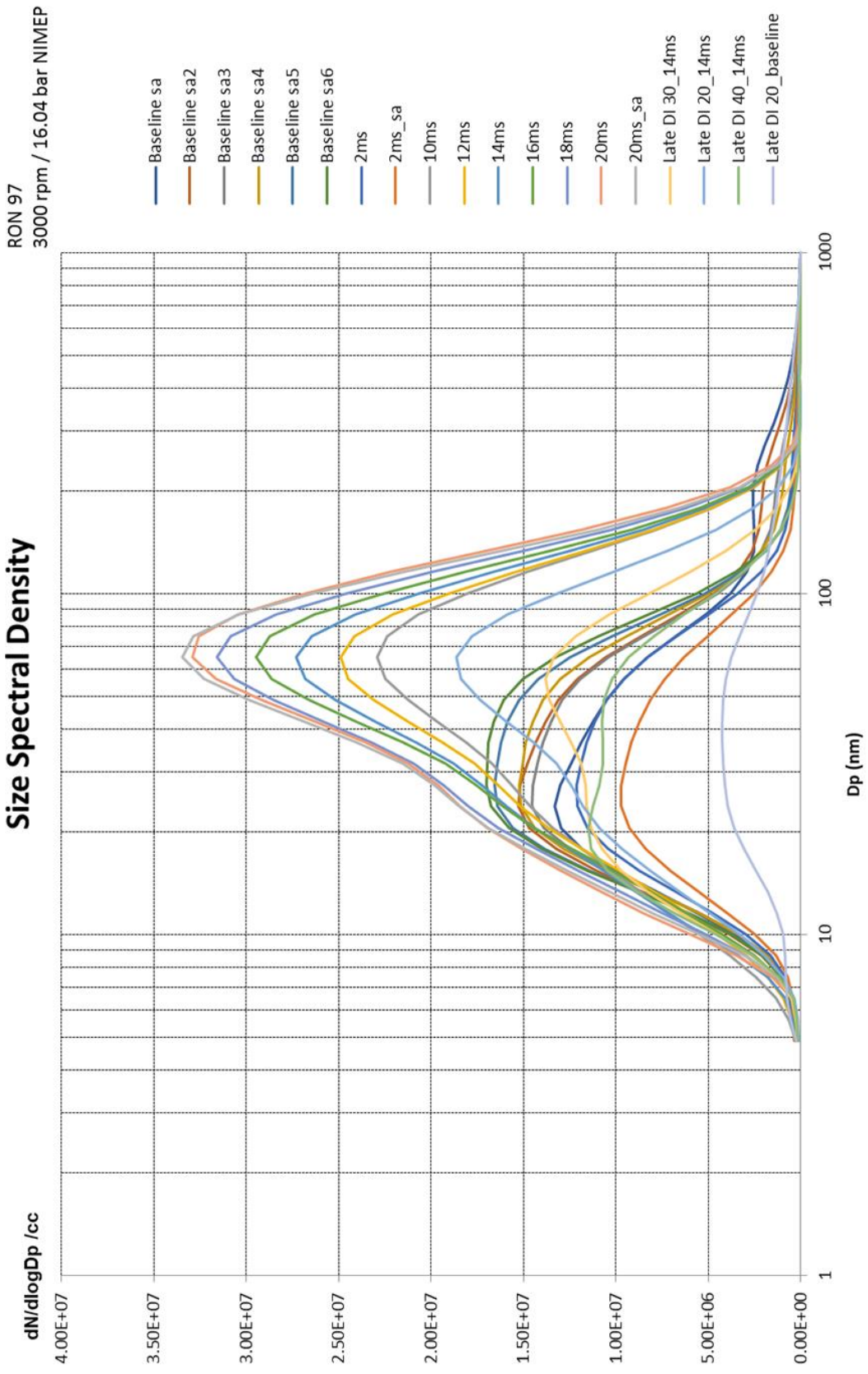

Figure A.0-5 Impact of water injection on particles size and number at 3000 rpm / 16.04 bar NIMEP (RON 97)

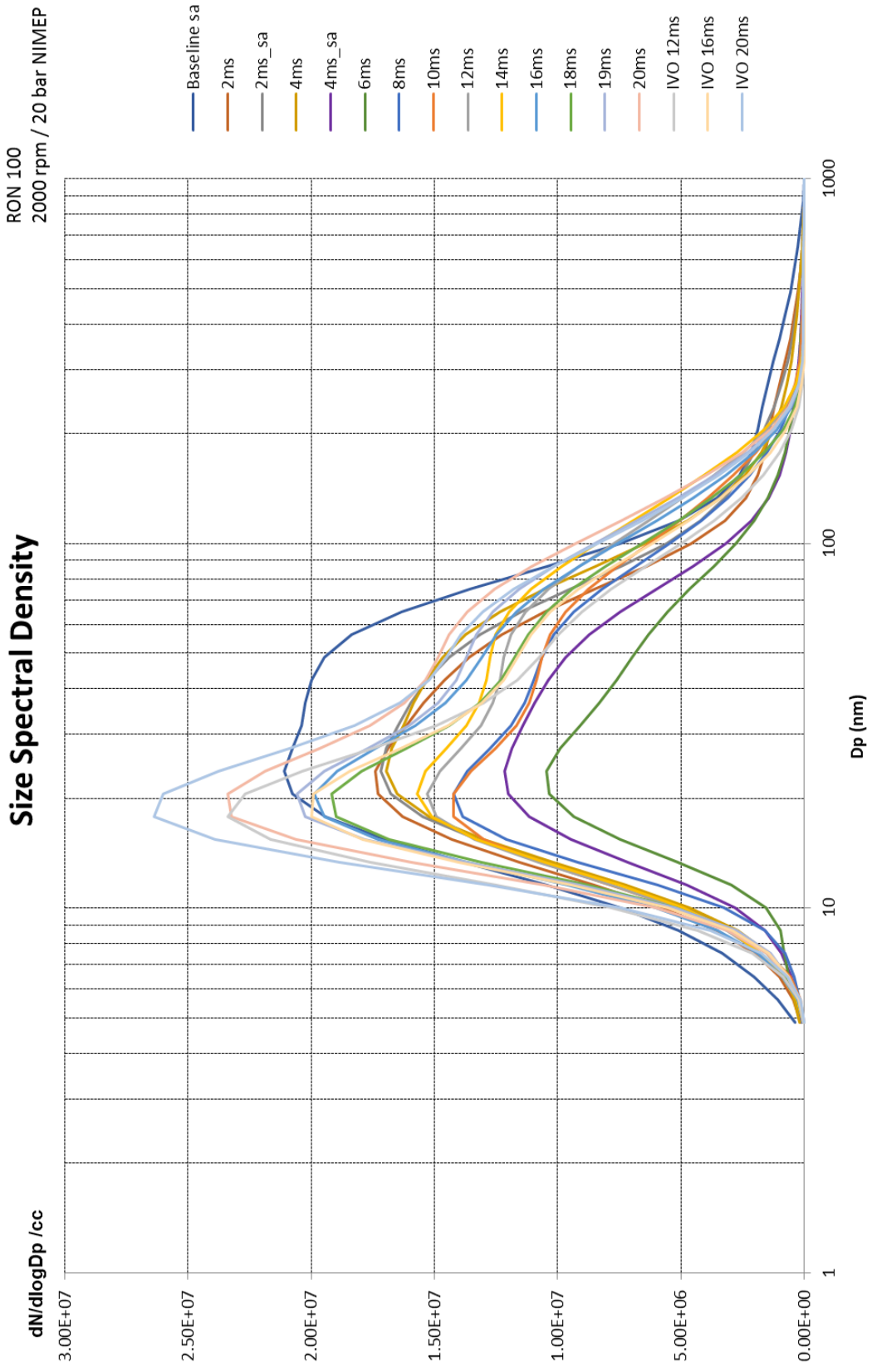

Figure A.0-6 Impact of water injection on particles size and number at 2000 rpm / 20 bar NIMEP (RON 100)

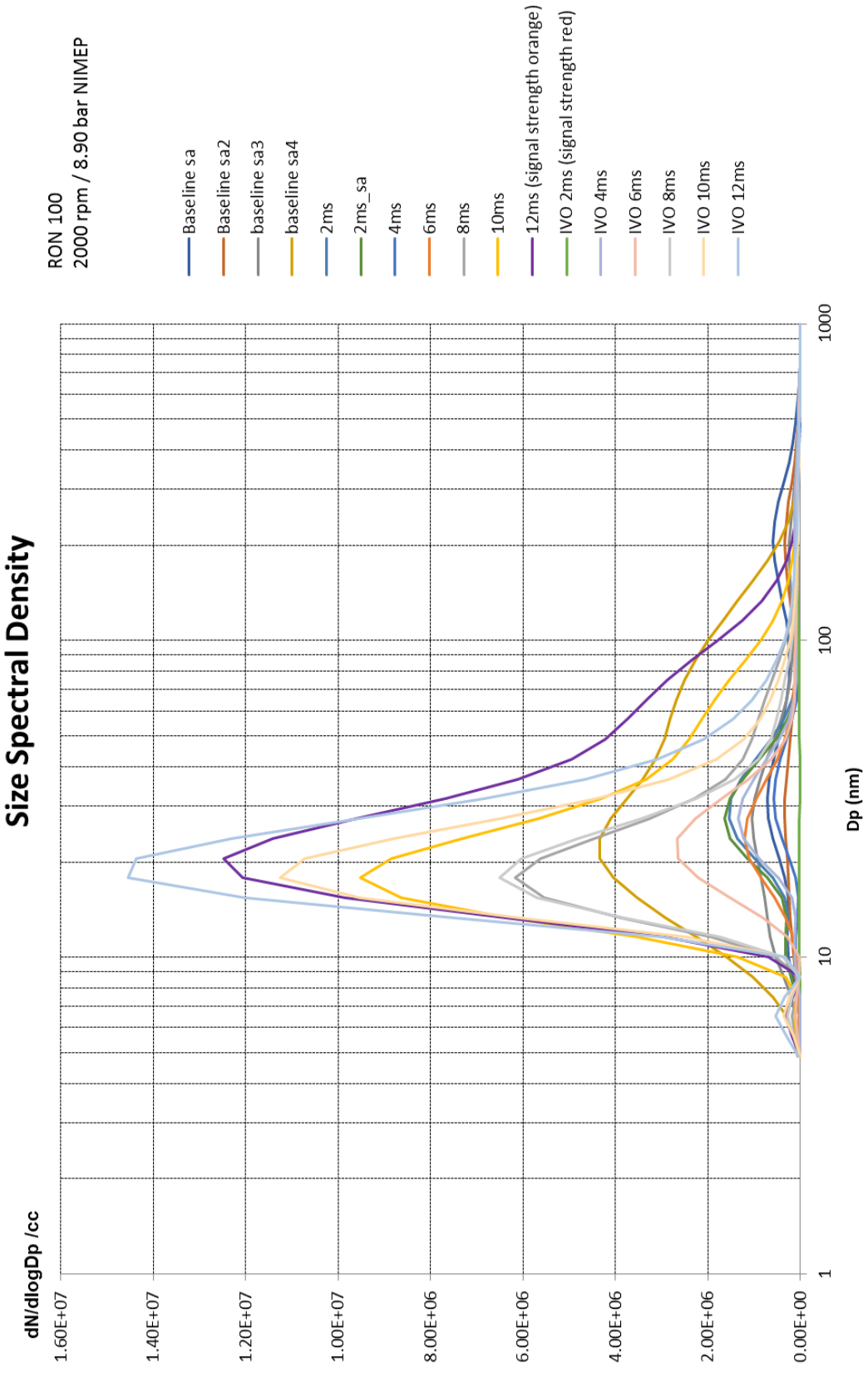

Figure A.0-7 Impact of water injection on particles size and number at 2000 rpm / 8.90 bar NIMEP (RON 100)